Lidar Studies of Middle Atmospheric Density and Temperature Structures over Mount Abu

Som Kumar Sharma

Ph. D. Thesis
April 2009

PHYSICAL RESEARCH LABORATORY
AHMEDABAD – 380 009, INIDA

Lidar Studies of Middle Atmospheric Density and Temperature Structures over Mount Abu

A thesis submitted to

Gujarat University

for the degree of

Doctor of Philosophy in Physics

By

Som Kumar Sharma

Space and Atmospheric Sciences Division
PHYSICAL RESEARCH LABORATORY,
AHMEDABAD - 380 009, INDIA

April 2009

CERTIFICATE

I hereby declare that the work presented in this thesis is original and and done by me. It has not formed the basis for the award of any degree or diploma by any University or Institution.

Som Kumar Sharma

Som Kumar Sharma
(Author)

Certified by :

Shyam Lal

Prof. Shyam Lal
(Thesis Supervisor)
Space and Atmospheric Sciences Division,
Physical Research Laboratory,
Navrangpura, Ahmedabad-380 009,
INDIA

Dedicated

to

Mataji-Pitaji and Arti-Aanshi-Ansh

Contents

Acknowledgements

I am grateful to my thesis advisor Prof. Shyam Lal for his invaluable guidance, support and encouragement. He has been a wonderful thesis mentor and navigator throughout this scientific journey

I am indebted to Prof. Harish Chandra for inducing research aptitude in me since my joining PRL. I am greatly benefited by his vast knowledge, cool, cordial and very affectionate nature. He is not just an advisor, he is a fatherly figure who loves and cares for me from the bottom of his heart.

Help and support received from Dr. Y. B Acharya and Prof. A. Jayaraman in the field of lidar was invaluable This journey of research wouldn't have been so rewarding and wonderful for me without their encouragement, inspiration and guidance. I am indebted to Acharyaji for the help and support I received from him throughout the period, for instruments, field campaigns and during thesis writing Over and above, the concern and affection showered by him, kept me going and motivated throughout this scientific journey.

Prof. H. S. S. Sinha has always been with me during my ups and downs in the field of research. His wonderful organizational skills left a deep impression on me His pleasing personalty, timely suggestions and valuable guidance helped me immensely. Scientific and technical discussions with Mr. R. N. Misra were very fruitful and are acknowledged.

I am grateful to our collaborators Prof Hassan Bencherif (Reunion, France) and Dr. V. Sivakumar (CSIR, South Africa) for thought provoking scientific discussions, suggestions and support during the course of this work Few results in the present study are the outcome of our fruitful scientific collaborative works. Thanks are due to Prof Philippe Keckhut (CNRS, France), and Prof I S. McDermid (USA) for suggestions and providing OHP and Mauna Loa Rayleigh lidar data.

I thank the scientific and technical team members of the HALOE (onboard UARS) and TOMS. HALOE data used in this study were acquired as part of the NASA's Earth-Sun System Division and archived and distributed by the Goddard Earth Sciences (GES) Data and Information Services

Center (DISC) Distributed Active Archive Center (DAAC). Thanks are also due to NOAA-CIRES Climate Diagnostic Center, USA for providing NCEP reanalysis data and Ozone Processing Team of NASA/Goddard Space Flight Center, USA for TOMS ozone data used in this study Team members of ERA-40 data sets are also duly acknowledged.

I am thankful to Dr. David Hooper (Rutherford Appleton Laboratory, UK) for his valuable suggestions and support during initial phase of my research career and for the excellent hospitality during my visit to Oxford.

I am extremely thankful to Prof. R. Sridharan and Prof K N. Iyer for their inspiration, thought provoking scientific discussions and helping me at various levels of my scientific research

I am thankful to former directors of NARL, Prof. P. B. Rao, Prof. A. R. Jain and Prof. D Narayana Rao for their concern, support and encouragement. Thanks are due to Drs. Anandan, Patra, Sarma, Srinivasulu and Bhavanikumar for help during our MST radar/lidar observational campaigns at NARL, Gadanki.

Help and support received from Uma-Sanat Das and family can not be expressed in words. They were always with me during my ups and downs on professional and personal fronts and supported me immensely during this long journey of research. Their suggestions at various stages, really helped me in shaping my thesis. It would have been extremely difficult to sail through without their pleasant company, unconditional support and open discussions on various fronts. I am highly indebted to them, cute Adi and their family.

I am grateful to Prof. Hari Om Vats and his family for unconditional, perineal support and blessings on professional and personal fronts. Since my joining PRL they provided me home away from home and are local guardians for me and my family. Rawat ji, Baliyan ji and their families gave me full strength for carrying out my research work.

I am indebted to PRL's lidar group members (Prof. Harish Chandra, Prof. A. Jayaraman, Dr. Y. B. Acharya and Mr. J. T. Vinchi) for providing me full fledged support and encouragement during lidar observations at Gurushikhar, Mt. Abu.

I am thankful to Dr. G. D. Vyas for teaching me various experimental techniques during my initial phase of research at PRL His calm and composed personality had a deep impact on me.

I am thankful to Prof. Panigrahi, Dr. Rangarajan (Raghu) and Dr Bhas Bapat for their valuable help and suggestions on various fronts and encouragement during this study.

I am grateful to the faculty members of SPA-SC division, Profs. R Sekar, S P Gupta, S. A Haider, K P Subramniam, D. Pallam Raju, S Ramchandran, Drs Bhas Bapat, Varun Sheel, D. Chakrabarty, Mr. S. B. Banerjee, M. B. Dadhania, Narain Dutt, A. P Gohil, R Narayanan, S. Venkatramani, K S. Modh, T. A Rajesh, R P Singh (Jr.), I A. Prajapati and staff memebers Mrs. Manishaben, Ms. Rannaben, Sunilbhai, Pillai (P.K.)and Nathuram Bhai for their full support and cooperation during course of this work. The presence of our division PDFs and research scholars; Uma, Sanat, Bhavesh, Ramya, Amit, Kushwaha, Sumanto, Suchita, Sumita, Arvind, Iman, Chinmaya, Amrendra made my long working hours lively Thanks are due to Mt. Abu observatory staff members (Rajeshbhai, Mathurji, Kothariji, Purohitji, Jainji, Padamji, Patwalji, Narayanji) for their cooperation, help and logistic support during lidar observations at Mt Abu.

Thanks are due to former PRL director Prof. G. S Agarwal and dean Prof. V. B. Sheorey for allowing me to pursue my doctoral work at PRL. My sincere thanks to Prof J N Goswami, Director, PRL, Prof. A K Singhvi, Dean, PRL for their valuable scientific support, inspiration and encouragement. I am grateful to Prof Utpal Sarkar, Chairman, Academic committee and members for critically reviewing my research work, and for their useful suggestions and support. I am thankful to Profs. S. Krishnaswami, A. C. Das, Vijay Kumar, N Bhandari, R. G Rastogi, P. N. Shukla, D. P Dewangan, U. C. Joshi, B G Anand Rao, N. M. Ashok, T. Chandrasekar, R. Ramesh, M M. Sarin, S. V. S Murthy, A. Ambastha, V K B Kota, A. S Joshipura, S. Rindani and Dr. P. Sharma for their concern and support.

I am thankful to Mrs Nishtha Anilkumar for her concern and encouragement along with all staff members of PRL's library for promptly providing me various research articles, books and journals. I acknowledge the timely, generous help provided by Ubale ji and his workshop team, Sanjay Bhai and others in CMD, purchase, stores, accounts and administration during commissioning and functioning of PRL's lidar laboratory at Mt. Abu. I am thankful to Mr. Dholakiaji, Jigar Bhai and all staff members for computational and help in printing of thesis. Thanks to Sudheendranathan bhai and Pillai bhai (N.R.) for help on various administrative works and their concern for my timely completion of thesis.

My special thanks to Mohanty-Srubabati, Hiranmaya-Amrita, Jerry, Nanditaji (USO), Shantanam, Angom, R. P. Singh (Sr.), J. Banerjee and Sunil Singh for their help and cheerful support at PRL

I am thankful to my friends Dipu, Ravi (Bhushan), Navinji, Jyoti, Anil, Deshpande, Alok, Vinay, Kuljeet (Jitti), Subrata, Panda, Brajesh (USO), Vikas, Nirvikar, Tarun(Pant), Prashanta (Daddu), Manish (Naja), Patra (PK), Duli, Lokesh, Sudheer (Vempatik), Kaushik, Sankar, Anil (Pattu), Sunish, Rajneesh, Aalam, Shikha, Shushma, Duli, Neeraj, Prasanta, Santosh, Vachaspati, Sanjeev, Ganguly, Rishi, Yogesh, Gowda, Bindu, Subimal, Satya, Shreyas, Sasadhar, Antra, Vandana and many others. I am indebted to one of the best friends, Dr. P. K. Rajesh for his support on professional and personal fronts throughout my stay in Ahmedabad and he provided unconditional help whenever I needed it. His wife's (Gere) concern and affection to me and my family is duely acknowledged.

My special thanks to Sahrad Bhai, Swaroopda, Awasthiji (IPR), Harsih Gadhavi, Manishaben, Bhartiben and their families for their help and support,

I am thankful to Mrs. Paulineben, Preetiben, Parulben, Vijayaben, Nishthaben, Leelaben, Umaben (Desai), Nandiniben, Ms Jayashree, Meeraben and Shantaben for being very affectionate and helping me directly or indirectly.

My thanks are due to family members of Profs Harish Chandra, Shyam Lal, Acharya, Sinha, Raghu, Jerry and Mohanty for their concern and affection to me and my family.

Dipu-Amrita-Aayusi, Anil-Dipti-Sivangi, Sashi-Abhi-Gayatri, Ramakant-Kirti-Purva-Pujan de-serve special thanks for providing very cheerful, lively and showering affection to me and my family.

I am thankful to my shcool/college/university teachers, Shri B. R. Verma, K. N Tirpathi, Prof. V D Gupta, Drs. Poonam Tondon, Shantanu Rastogi and Alka Mishra and friends: Pankaj, Amit, Anupam, Dinesh, Rajaram for encouragement and pleasant company during those days

I am out of words to express my gratitude toward my **Mataji and Pitaji** Without their constant blessing, inspiring words, research wouldn't have been possible for me. I am wordless to acknowledge love, affection support from my Brothers : Raj Kumar, Vinay and Arun Bhaiya; Bhabhies· Rashmi, Geeta and Aruna Bhabhi Since I joined PRL, Rajkumar Bhaiya and Rashmi Bhabhi never let me feel that I am away from home. They always supported me during high or low moments of this journey. I am thankful to my sisters. Rani, Shashi and Beena didi for their constant support. Innocent smiles of my nieces. Shobha, Sonika, Monika, Akrati (Teenu), Shivi and nephew Aabhas (Chintu) has been a real source of inspiration for me. Playing with them was like recharging battery I am thankful to my in-laws· Mummy-Papaji, sister and brother in-laws. Ashadi+Bhuvaneshji and Neerudi+Shalaishji for help and providmg cheerful company on various occasions.

Last but not least, silent, unconditional love, support and patience of my wife **Arti** were the biggest strength for me, throughout the course of this thesis work. Smiles of my daughter **Aanshi** and son **Ansh** were rejuvenating my energies everyday. I have deprived them of many things as I could not give them sufficient time; my apologies and I promise to spend more quality time with them

Som Sharma

Preface

Lidar is one of the important remote sensing instruments to monitor the structure and dynamics of the atmosphere. A wide range of studies have been carried out on the middle atmospheric structure and dynamics, mostly at mid- and high-latitudes and a few at low-latitudes using various types of Lidars. However, there are very few studies over sub-tropical latitudes (between 20°N to 30°N). Studies in sub-tropical regions are crucial as they bridge the gap between low and mid latitudes and have an imprint of the processes associated with low- and/or mid-latitudes. This thesis presents a comprehensive study of the thermal structure of the upper stratosphere and the mesosphere (30-75 km) over a sub-tropical location, Gurushikhar, Mount Abu (24.5°N, 72.7°E, ~1.7 km above MSL), (henceforth referred to as Mt. Abu) using Rayleigh lidar measurements for approximately 400 nights from 1997 to 2007. The thesis is structured in the following way.

Chapter 1 presents an introduction to the structure and dynamics of the Earth's atmosphere with emphasis on the middle atmospheric processes.

Chapter 2 describes techniques of the atmospheric probing, a brief summary of the scattering and extinction of the light in the atmosphere, the lidar technique, PRL's Nd-YAG laser based Rayleigh lidar system and the method used for lidar data analysis. A brief description of errors in the measurements is also given. An account of other data sets (Satellites, NCEP and ERA-40) which are used in characterizing the observed temperature structure are also described.

Chapter 3 presents results of the temperature structure in the height range of 30 to 75 km over Mt. Abu obtained using PRL's Rayleigh lidar. Aspects of the temperature structure presented include the day-to-day, seasonal, annual and stratopause variability over Mt. Abu. The climatological mean temperature is estimated and discussed. A possible association between ozone and the stratospheric temperature is also studied.

A comparative study of the thermal structure is presented in Chapter 4. The lidar observed temperatures are compared with CIRA-86, MSISE-90 and an Indian low-latitude model. Results are also compared with similar observations at three different locations in the northern hemispheres, viz., Gadanki (13.5°N, 79.2°E), Mauna Loa (19.5°N, 156°W), Observatoire de Haute Provence (OHP) (44°N, 6°E) and a southern hemispheric station, Reunion Island (20.8°S; 55.5°E), to examine hemispheric anomaly, if any, in the sub-tropics. Temperature structures over Mt. Abu are also compared with HALOE (onboard UARS) observed temperatures.

Chapter 5 deals with the event-based studies of some of the interesting geophysical phenomena in the stratosphere and the mesosphere viz., double stratopause, mesospheric temperature inversion, and stratospheric sudden warming. Various characteristics of these and associated operative processes are described through a few case studies. In addition, a detailed statistical study is also carried out. The observed characteristics are compared with the low- and mid-latitudes and discussed in the light of the current understanding of the source mechanisms.

Chapter 6 describes a brief study of the long term temperature trends over Mt. Abu using about 11 years of the Rayleigh lidar data. In view of the increasing anthropogenic activities and their consequent impact on various middle atmospheric geophysical processes, an effort has been made to delineate possible causes for observed temperature trends over Mt. Abu.

Chapter 7, which is the last chapter of the thesis summarizes the results obtained and presents prospects of possible future work on related themes.

CHAPTER 1

Introduction

1.1 The Earth's Atmosphere

The Earth's atmosphere is divided into different regions, based on its composition, temperature structure, etc. On the basis of composition, it is classified into *homosphere* (below ~ 100 km), where the major atmospheric constituents remain well mixed by eddy processes, and the *heterosphere* (above ~ 100 km), where molecular diffusion dominates over mixing by fluid motion, consequently the atmospheric constituents are distributed according to their respective masses. The *turbopause* is the transition region between the homosphere and the heterosphere.

The most familiar nomenclature of the atmosphere is based on its vertical temperature structure. The observed motions (dynamics) in each layer are intimately associated with their temperature structure. These regions are termed as the *troposphere, stratosphere, mesosphere* and *thermosphere* and the regions of transition between them are called the *tropopause, stratopause,* and *mesopause,* respectively. Figure 1.1 shows a mean temperature profile over Mt. Abu, (24.5°N, 72.7°E) based on Mass Spectrometer-Incoherent Scatter Extended (MSISE-90) model. The middle atmosphere is usually considered to be the region between 10 to about 100 km.

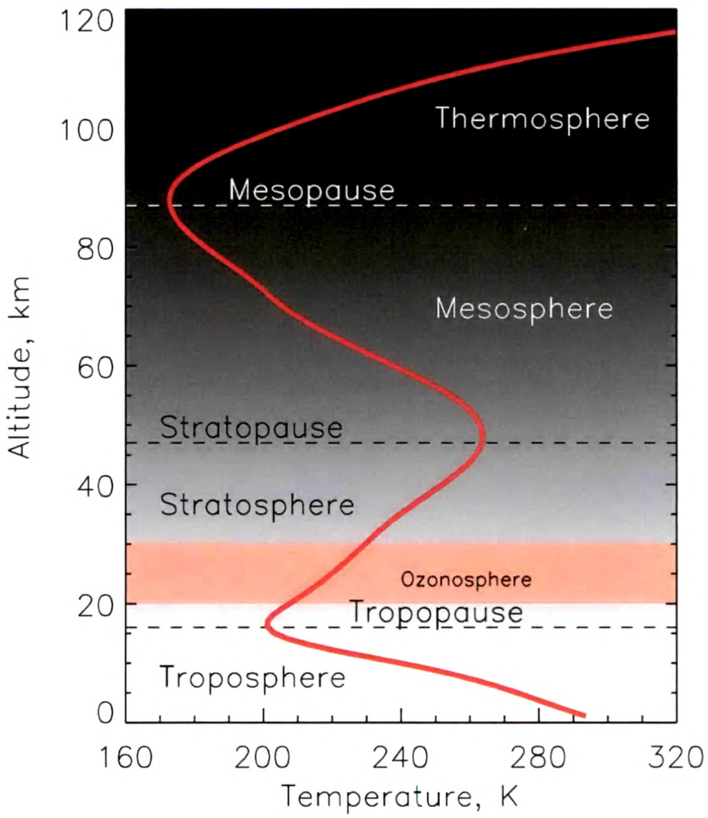

Figure 1.1: *The vertical temperature structure of the Earth's atmosphere over Mt. Abu, based on MSISE-90 model mean temperature.*

The major constituents of the lower and middle atmosphere are molecular nitrogen and oxygen, which together account for $\sim$ 99.02% of the total mass of dry atmosphere. The third most abundant gas is argon, which constitutes to about 0.93% of the mass of the dry atmosphere. The remaining mass (less than $\sim$ 0.1%) is due to atmospheric trace species. The major trace species are water vapor, carbon dioxide, and ozone. Water vapor is highly variable in the lower atmosphere due to the processes of evaporation, condensation and sublimation, while concentrations of water vapor in the stratosphere are very low. Among the major trace species, carbon dioxide is well mixed in most of the middle atmosphere. The most important trace species in the middle atmosphere is ozone, the concentration of which reaches a maximum at around 27 km. The major radiative heat input for the middle atmosphere is due to absorption of the solar ultraviolet (UV) radiation by ozone.

1.2 Pressure Variation in the Atmosphere

The Earth's atmosphere can be assumed to be in hydrostatic equilibrium for most of the processes. The pressure p at an altitude z is then determined by the air mass above that altitude. The air mass can be expressed either as mass density ρ or as number density n times M, where M is the mean molecular weight of air (M$\sim$ 28.97 g.mol^{-1}), which is constant in the homosphere from the ground to $\sim$ 100 km due to strong vertical mixing. The expression relating pressure and density is

$$dp = -g(z)\rho(z)\,dz = -g(z)Mn(z)\,dz \tag{1.1}$$

Combining equation 1.1 with the ideal gas law for pressure, number density, Boltzmann constant k_B and temperature T and integrating over height gives an exponential relationship of decreasing pressure with height which depends on the pressure at the altitude z_o and on the temperature profile of the atmosphere

$$p(z) = p(z_o)exp\left(-\frac{M}{k_B}\int_{zo}^{z}\frac{g(z')}{T(z')}\,dz'\right) \tag{1.2}$$

Assuming an isothermal atmosphere, the above equation simplifies to an exponential relation for the pressure,

$$p(z) = p(z_o)exp\left(-\frac{z-z_o}{H}\right) \tag{1.3}$$

where, scale height $H = \frac{k_B T}{Mg}$ which is the e-folding scale of the pressure. The real pressure profile, however, depends on the altitude-dependence of the scale height which varies between 5 to 8 km in the middle atmosphere [e.g., Dubin et al., 1976]. By analogy it can be shown that the density ρ follows a similar exponential decrease with height. The scale height in the middle atmosphere is $\sim$ 7 km. This implies that pressure and density decrease by an order of magnitude every $\sim$16 km.

Table 1.1: The major radiatively active gases in the Earth's atmosphere [based on Brasseur and Solomon, 1986]

Atmospheric region	IR Cooling	UV heating
Troposphere	H_2O, CO_2	H_2O
Stratosphere	CO_2, O_3	O_3
Mesosphere	CO_2, O_3	O_2, O_3
Thermosphere	CO_2, O, NO	O_2

1.3 Temperature Variation in the Atmosphere

Temperature is one of the important physical quantities that determines the general state of the Earth's atmosphere. The temperature structure of the Earth's atmosphere is shown in Figure 1.1. The mean temperature structure of the atmosphere is determined by a combination of adiabatic heating and cooling in vertical motions, heating through absorption of solar UV radiation, radiative cooling at infrared (IR) wavelengths, and the heat conduction. The major radiatively active gaseous components in the Earths's atmosphere are given in Table 1.1. Their concentrations vary with height and the net radiative contribution is warming in the troposphere and cooling in the stratosphere and mesosphere.

1.3.1 Troposphere

The troposphere is the lowest part of the Earth's atmosphere. There is a decrease in temperature with height from $\sim$ 300 K at the ground to about 210 K at the tropopause at low latitudes (Figure 1.1). The average lapse rate in the troposphere is about 6.0 K/km, although there can be a wide range of values at individual locations. This temperature structure leads to strong convection and mixing, which characterizes the region. Aerosols, solids and liquids are removed from the troposphere quickly due to scavenging and precipitation. There is a change in the observed lapse rate at $\sim$ 15-16 km (over a sub-tropical location). The decrease in temperature with height ceases, and gradually temperature increases with height. This temperature inversion has the effect of limiting the transfer of air upwards. This transition region is called as the tropopause, and its height is variable in space and time. At the equator, where there is a large amount of radiative heating and convective activity, tropopause is located at a height of around 17 km, while at the cooler polar regions it is as low as $\sim$ 8 km. There is a decrease in the amount of water vapor with increasing height, while ozone concentrations may increase by an order of magnitude. At low-latitudes, sporadic breaks can occur in the tropopause and air may be exchanged between the troposphere and the stratosphere. At these tropopause breaks, water vapor can enter the stratosphere and dry ozone-rich air may intrude into the low-latitude troposphere.

1.3.2 Stratosphere

The stratosphere extends from the tropopause to about 50 km where temperatures reach a maximum mean value of around 270 K (Figure 1.1). The air density in the stratosphere is considerably less than that in the troposphere, and even a limited absorption of solar radiation by atoms and molecules will produce a large increase in temperature. Much of this heating is due to absorption of the solar UV radiation by ozone. This part of the atmosphere is characterized by little vertical mixing, due to the positive temperature gradient. It is essential to know the stratospheric heat budget to understand its temperature, which is primarily governed by the absorption of solar UV radiation by ozone and emission of IR radiation by carbon dioxide, ozone and water vapor. Stratospheric temperatures are essential for the study of minor species abundances, and their transport as well as to the characterization of stratospheric general circulations [e.g., Christopher et al., 1999]. The temperature in the lower polar stratosphere in winter is also variable, particularly in the northern hemisphere. Occasionally, polar regions exhibit a rapid increase in temperature of several tens of degrees Kelvin which lasts for a few days. These events are termed Stratospheric Sudden Warming (SSW), and may persist for several weeks. Depending on the strength and ambient geophysical conditions, these SSWs can propagate down to low latitude [e.g., Sivakumar et al., 2006]. SSW events are accompanied by a weakening of the stratospheric westerly winds, and in some cases this reduction may be severe. Furthermore, on few occasions two stratopause levels are noted, a feature which is termed as double stratopause. Detailed study of the SSW and double stratopause phenomena over Mt. Abu is presented in Chapter 5.

1.3.3 Mesosphere

Above the stratopause, the atmosphere exhibits another decrease in temperature with height up to the mesopause around 85 km. As seen in Figure 1.1, mean temperature can reach a minimum of around 185 K at these heights. As is the case in the troposphere, vertical air motions are not strongly impeded. The lowest temperatures in the entire atmosphere are found at the mesopause during the summer at high latitudes and can be as low as $\sim$ 130 K. In summer, thin noctilucent cloud layers occur occasionally in the upper mesosphere over the polar regions. These are most prominent at twilight, when illuminated by sunlight while the lower atmosphere is still dark. This is the region in which an important phenomena of mesospheric temperature inversion (MTI) takes place. Observed characteristics of MTIs over Mt. Abu are presented and described in Chapter 5.

1.3.4 Thermosphere

Above the mesosphere, temperature increases monotonically and this region is called as thermosphere. Atmospheric constituents in the thermosphere are not homogenously mixed. They are distributed according to their molecular weights. The highest temperature in the atmosphere is in the thermosphere $\sim$ 2000 K (varies with the solar activity). Intense solar radiation with wavelengths between 100 and 200 nm is absorbed between 85 and 100 km in the thermosphere by molecular oxygen (O_2), while radiation with wavelengths shorter than 100 nm is absorbed above 100 km.

1.4 Stability of the Atmosphere

It is well known fact that warm air rises, and cold air sinks. This is because warm air is less dense than cold air. In the troposphere, it is almost always the case that colder air overlays warmer air. The warm air is heated at the surface and it rises up. Under the right conditions, water vapor condenses out of the air and forms clouds. Stability of the atmosphere is very crucial in describing various dynamical features of the atmosphere and is generally governed by the thermal structure.

1.4.1 Static Stability

The stratospheric temperature increases with altitude and hence warmer air overlays colder air. This temperature structure impedes convection in the stratosphere. If we displace an air parcel to a higher altitude in the stratosphere, it would be colder than its surroundings. Cold air is more dense than warm air, and the parcel would sink back to its original location, though it would overshoot slightly because of its momentum. After overshooting, it would drop to a location where it would be warmer than its surroundings. Warm air is less dense than cold air, and the parcel would rise back to its original location, though it would once again overshoot slightly. This process would continue in a series of vertical oscillations about some equilibrium altitude if the parcel density and the ambient air density are the same. Such oscillations of air are observed and are major cause for generation of the waves in the atmosphere. These oscillations typically have a period of ~ 40 seconds and ~ 70 seconds in the stratosphere and troposphere, respectively. The faster oscillation in the stratosphere occurs because the air in the stratosphere gets warmer with altitude. It indicates that the air has greater static stability or greater buoyancy in the stratosphere. The greater stability in the stratosphere is the major reason for impeded vertical motions and hence it is stably stratified. A schematic of these motions is depicted in Figure 1.2.

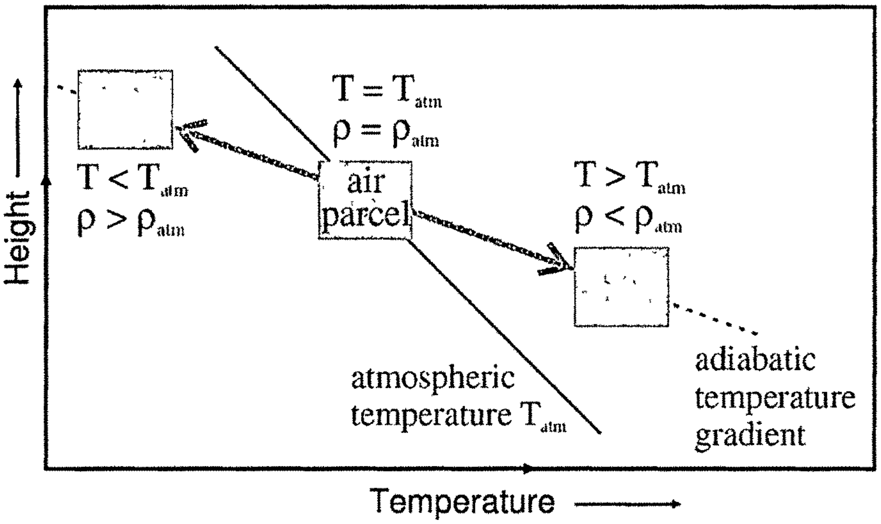

Figure 1.2: Schematic of air parcel movements and buoyancy oscillations in the atmosphere under different conditions of the atmosphere (source Andrews et al., 1987).

1.4.2 Brunt-Väisälä Frequency

The Brunt-Väisälä or natural frequency N, is a measure of the stability of the atmosphere. It represents the frequency of adiabatic oscillation for a fluid parcel displaced vertically from it's equilibrium position in a stably stratified atmosphere. If the effects of humidity are ignored, the Brunt-Vaisäla frequency can be expressed as

$$N^2 = \left(\frac{g}{\Theta}\right)\left(\frac{d\Theta}{dz}\right) \tag{1.4}$$

[Gill, 1982] where g represents the acceleration due to gravity, and Θ is the potential temperature which is is given by

$$\Theta(z) = T(z)\left[\frac{1000}{p(z)}\right]^{1-\frac{1}{\gamma}} \tag{1.5}$$

where γ is the ratio of specific heats at constant pressure c_p and constant volume c_v, respectively ($\gamma = \frac{c_p}{c_v} = 0.286$).

The potential temperature is defined as that temperature which a parcel of dry air at a temperature T and a pressure p would have if it were expanded or compressed adiabatically to the reference pressure of 1000 mb. In an atmosphere in which Θ is constant with height, the temperature at any height will be that which leads by adiabatic ascent or descent to the same value of temperature at 1000 mb. The atmosphere is then said to be in a state of convective equilibrium, and a vertically displaced air parcel will be heated or cooled adiabatically to the same temperature as its surroundings.

Therefore, if the potential temperature increases with height, the atmosphere is stable, and a vertically displaced parcel of air will be subject to restoring forces which will tend to return the parcel to its equilibrium position. In this way, the parcel will oscillate about its equilibrium position with a frequency N. If there is a decrease with height of potential temperature, then the atmosphere is said to be convectively unstable, with a vertically displaced air parcel continuing to move away from the equilibrium position.

1.4.3 Isentropic Surfaces

Surfaces along which the entropy and potential temperature of air are constant are known as isentropic surfaces (IS). Potential temperature becomes very large at higher altitudes in the stratosphere, hence it is difficult to move air upward or downward. Stratospheric air tends to remain on an isentropic surface for many days. Consequently, vertical motions are very small. An added advantage of using isentropic surfaces is that there is a little air motion through such surfaces, since thermodynamic processes in the atmosphere are approximately adiabatic. IS are extremely useful in describing atmospheric parameters as atmospheric variables tend to be better correlated along an isentropic surface than on a constant pressure surface. Furthermore, the vertical spacing between IS is a measure of the static stability. Convergence (divergence) between two isentropic surfaces decreases (increases) the static stability in the layer.

1.5 General Circulation of the Middle Atmosphere

The general circulation in the atmosphere is a very complex interplay of many different external and internal forcings that act as drivers for the wind and circulation systems. The overall circulation in the stratosphere and mesosphere is driven primarily by the differential heating due to the absorption of solar UV radiation in the ozone layer and the emission of infrared radiation out into space from ozone, carbon dioxide and water vapor. The heat transport term includes the local temperature changes produced by the air motion, known as dynamical heating or cooling. The meridional circulation which balances the differential heating is termed as the diabatic heating. At the solstices, this takes the form of a rising motion near the summer pole, a meridional flow into the winter hemisphere and a sinking motion near the winter pole. This flow is influenced by the Coriolis torque, producing zonal westerlies in the winter hemisphere and easterlies in the summer hemisphere. During equinoxes the heating is greatest at the equator, while there is cooling at the poles. A weak diabatic circulation then occurs, with rising in the equatorial region and a meridional poleward winds in both hemispheres. This leads to weak westerly zonal winds in both the hemispheres.

The mean zonal winds for solstice conditions are shown in Figure 1.3. They are mainly driven by the difference in solar absorption between the equator and the poles. The summer (winter) stratosphere and mesosphere are sunlit for more (less) hours each day at the poles than at the equator. Therefore, they should be warmer (colder) at the poles compared to the equator. Through the thermal wind relation this induces an equator-ward (pole-ward) flow in the summer (winter) hemisphere [e.g., Holton, 1992]. Deflected by the Coriolis force, this forms the westward (eastward) jet in the summer (winter) stratosphere and mesosphere. Holton, [1983] described the role of gravity waves breaking in the general circulations of the middle atmosphere. The vertical and meridional flow forms the so-called diabatic circulation and is shown in Figure 1.4 [based on Andrews et al., 1987].

In the lower middle atmosphere, the jets are westerly in both summer and winter hemispheres, and the winter jet is approximately twice as strong as the summer jet. At higher levels ($\sim$ 60-70 km) the jets are westerly in winter and easterly in summer, and the jet stream is again observed to be stronger in the winter hemisphere. The globally averaged temperature in the stratosphere and mesosphere is approximately in radiative equilibrium, although eddy motions can cause significant local departures, particularly in the winter stratosphere. While the uniform

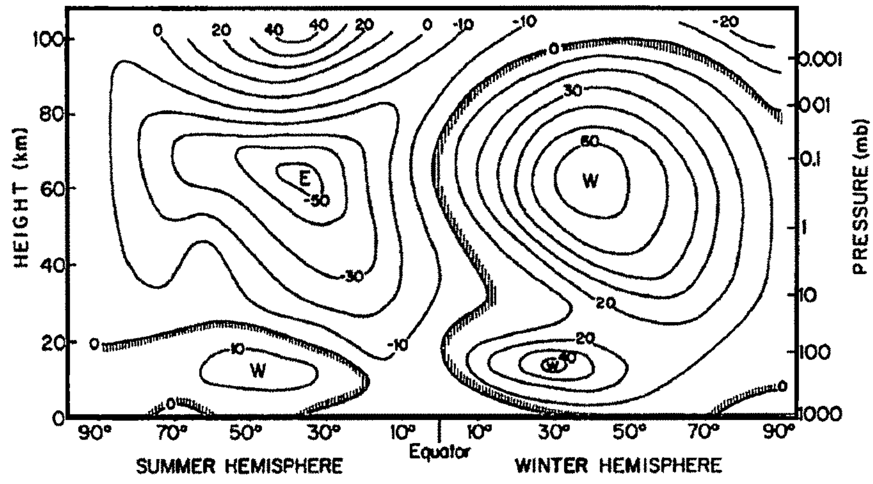

Figure 1.3: Mean zonal wind at solstice. Note the closure of the mesospheric jets in the mesopause region. The middle atmosphere westward summer jet ($u < 0$) is weaker than the eastward winter jet ($u > 0$) and is closed at a lower altitude. E and W denotes easterly and westerly jets, respectively. (Andrews et al., 1987).

decrease of temperature from the summer pole to the winter pole in the $\sim$ 30-60 km height range is as expected from radiative considerations alone, there are several observed features which cannot be explained on this basis. Firstly, in winter the temperature is seen to increase in the lower stratosphere from the tropics to mid-latitudes. Secondly, the temperature gradient is reversed at heights above about 50-60 km, and temperatures are seen to decrease steadily from the winter to the summer pole. Such effects are due to a major role played by certain dynamical processes (propagation of Gravity Waves (GW), Planetary waves (PW), and their interaction with mean circulation) in establishing the temperature structure.

1.6 Waves in the Atmosphere

An understanding of the Earth's atmosphere requires information on fluid dynamics, radiative transfer and photochemistry. Each of these areas is the subject of a great deal of current investigation, and there is a growing awareness of the importance of the interactions between them. An important atmospheric phenomenon

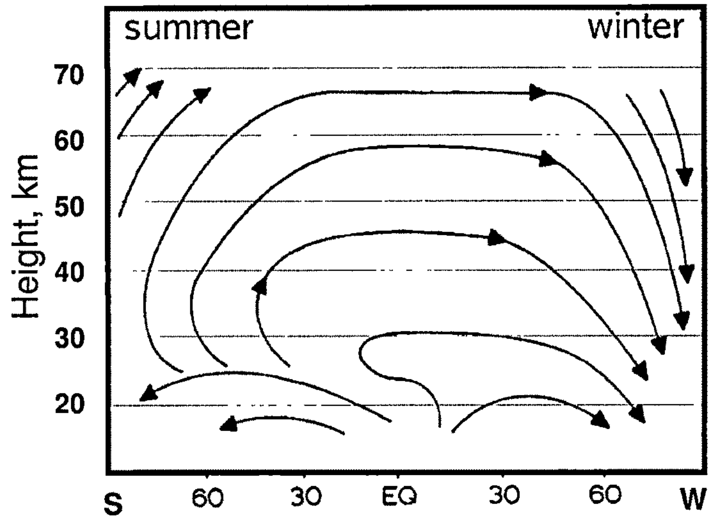

Figure 1.4: Streamlines of the diabatic meridional circulation. S and W denote summer and winter poles, respectively. (based on Andrews et al., 1987).

for transferring momentum and energy in the atmosphere are waves. The atmosphere has unique quality to sustain many wave-like motions with a variety of space and time scales ranging from slow moving planetary waves to much faster and smaller gravity waves. Such waves can provide a means whereby one region of the atmosphere can influence other regions at large distances. These waves also influence the large scale flow patterns in the atmosphere and the transport of atmospheric gases due to large scale circulation and small scale diffusion. These waves play an important role in the troposphere/stratosphere/mesosphere and are also a potential candidate for asymmetries in the polar vortex, occurrence of Stratospheric Sudden Warming (SSW), Mesospheric Temperature Inversions (MTI) and occurrence of double stratopause. Waves are also responsible for the forcing of the QBO and the control of the mean meridional circulation.

Atmospheric waves are one of the main elements in coupling process in the atmosphere. Wave sources are mostly located in the troposphere and these are excited by convection, weather systems, geostrophic adjustment, and due to orographic forcing. By transporting momentum from lower to high altitudes wave dynamics couple the different altitude, regimes in the Earth's atmosphere. The

Figure 1.5: *A picturesque imprint of gravity waves in the cloud structures.*

wave breaking plays an important role in the vertical temperature structure of the atmosphere (for example, the cold summer mesopause at high latitudes, where the lowest temperatures in the Earth's atmosphere are observed, in spite that the sun never sets).

The interaction of waves with the mean flow is quantitatively not well understood. In particular, the forcing of waves by convection and the parametrization of GWs are major sources of uncertainty in atmospheric modeling and climate prediction. The important wave types for atmospheric dynamics are: mid- and high-latitude planetary waves, equatorial PWs modes, GWs, and tides.

1.6.1 Gravity Waves

The class of wave motion, known as internal gravity waves, has in recent years been recognized as playing a major role in determining the structure and general circulation of the middle atmosphere. Figure 1.5 shows a picturesque view of the gravity waves seen in clouds in the troposphere. It is the ability of GWs to transport and deposit momentum and energy vertically that helps to modify the simple radiative equilibrium model of the atmosphere to give a closer agreement with the observed distributions of temperatures and winds.

GWs in the mountain ranges have been studied as early as in the 1940s [e.g., Scorer, 1949]. Hines, [1960] proposed that these kind of waves also occur higher up in the atmosphere. Lindzen, [1981] was the first to show that GWs were able to transport momentum and energy vertically and deposit them at higher levels through the process of gravity wave saturation. For those gravity waves, which propagate through the stratosphere without significant damping, the energy density is approximately constant with height. This requires that the horizontal velocity amplitude should increase, due to the decrease in atmospheric density with height. GW amplitudes may be small in the lower atmosphere compared to other motions, but in the stratosphere and mesosphere they become increasingly significant.

Depending on their propagation, GWs are classified as surface waves (waves on lakes, oceans etc.) or internal waves, inside a fluid, either in the atmosphere or inside lakes, oceans [e.g., Wiegand and Carmack, 1986; Nash and Moum, 2005]. At the long scale end of the internal wave spectrum, the Coriolis force has to be included in the mathematical description of the waves. These waves are then called inertio-gravity waves [Andrews et al., 1987]. These inertio-gravity waves propagate up into the stratosphere and mesosphere where they break and dissipate. This implies a force on the large-scale flow where the breaking or dissipation takes place.

Since gravity waves play an important role in driving the large-scale circulation system of the atmosphere, they have to be included in the current climate models [e.g., Becker and Fritts, 2006; Fritts and Alexander, 2003; and references therein]. Usually some parametrization scheme is used in these model [e.g., Lindzen and Forbes, 1983; Kim et al., 2003] for computational reasons but recently the direct numerical simulation of gravity waves has become feasible [e.g., Fritts and Alexander, 2003; Becker and Fritts, 2006].

GWs are observed with many different instruments including lidars, radars and spectrometers both from the ground and from the space by satellite instruments. Stratospheric wind system works as a gravity wave filter by favoring the propagation of different GWs during different seasons. An eastward stratospheric wind allows the westward propagating GWs and vice versa [e.g., Baldwin and Dunkerton, 2001; Fritts and Alexander, 2003; Meriwether and Gerrard, 2004 and reference therein].

Breaking of Gravity Waves

The upward propagating gravity waves increase in amplitude according to $\rho^{-1/2}$, where ρ is atmospheric density. As the amplitude grows, the temperature perturbation of the background state gets larger as well. When the temperature gradient of the modulated background state approaches the adiabatic temperature gradient, the Brunt-Väisälä frequency (Equation 1.4) approaches zero which implies that the atmosphere gets unstable and buoyant oscillations are no longer possible. The upward propagating gravity waves are said to be breaking at this level due to static or convective instability. A simple model proposed by Lindzen, [1981] assumes that the gravity wave amplitude will be saturated above the breaking level [Andrews et al., 1987]. Depending on the background atmosphere, the amplitude will no longer increase exponentially or even start to decrease with height. Even when the atmosphere is statically stable ($N^2 > 0$), GWs may break when the vertical wind shear becomes too large. This is called dynamical or shear instability and occurs when the Richardson number R_i, given in equation 1.6 is less than the threshold for the onset of turbulence.

$$R_i = \left[\frac{N^2}{(\frac{\partial u}{\partial z})^2 + (\frac{\partial v}{\partial z})^2}\right] < \frac{1}{4} \tag{1.6}$$

The role of this Kelvin-Helmholtz instability in gravity wave breaking has been described by Fritts and Rastogi, [1985], who discussed the limit of 1/4 which is a mean value that may be both larger or smaller for a particular wave depending on its horizontal wavelength and the background wind profile. Achatz [2007] found that turbulence also occurs at larger Richardson numbers for short term GWs. The excess energy and momentum of the breaking of GWs are transferred to smaller scales, consequently creating atmospheric turbulence [e.g., Zink and Vincent, 2004 and reference therein]. Finally, it ends up as drag on the background flow (up to 100 ms^{-1}/day) and heating/cooling (up to 6 K/day) of the atmosphere [e.g., Alexander and Dunkerton, 1999; Becker and Fritts, 2006]. Recently, Fritts et al., [2006] have reviewed the influence of GWs on the middle atmosphere in much more detail.

1.6.2 Planetary Waves

A set of global-scale waves called planetary waves playing an important role in formation of the zonal mean state and circulation exists in the lower and middle atmosphere. Their source mostly lies in the lower atmosphere and are excited by flow over topography, by latent heat release, or through the nonlinear evolution of the tropospheric eddies in the troposphere [e.g., Scinocca and Haynes, 1998], and then propagate up from the troposphere into the stratosphere and mesosphere.

Planetary waves (PW) are responsible for the longer-period variability in the middle atmosphere such as the quasi-biennial oscillation (QBO) in the tropics, sudden stratospheric warmings (SSW), vacillations of the mean flow at extra-tropical latitudes, etc. Some of the PWs can be identified as the well-known normal atmospheric modes, which correspond to free oscillations of the terrestrial atmosphere [e.g., Volland, 1988] modified by the background wind and temperature.

Planetary scale waves are a very important component of the general circulation of both the lower and middle atmosphere. PWs in middle atmosphere can interact strongly with mean zonal and meridional circulation and thus play a crucial role in heat, momentum, and constituents balance [Geller, 1992]. The dynamics of the middle atmosphere in winter is dominated by PWs of large amplitudes. Among the most important are quasi stationary Rossby waves, which propagate upward from troposphere. Rossby waves are very strong and highly variable during winter months. Due to the dominant forcing of stratospheric PWs, the winter stratosphere (with eastward flow around the pole) is much more disturbed than the summer stratosphere (with westward flow around the pole) and the disturbances in the winter stratosphere tend to have much larger scales than in the troposphere

Another class of PWs are the traveling normal modes also known as free modes. These waves modulate the atmosphere up to large distances. PWs corresponding to the natural modes of variability of the Earth's atmosphere commonly have periods of around 2, 5, 10 and 16 days. In general, these waves do no transport momentum but interact with waves and with mean zonal flow. Wave-wave interaction plays a vital role in deciphering dynamics of the middle atmosphere. Waves also contribute significantly to the atmospheric variabilities of the different temporal and spatial scales [e.g., Pancheva et al., 2008 and reference therein].

1.6.3 Equatorial Waves

Equatorial planetary scale waves are a special case of wave modes trapped at low latitudes. They can be either symmetric or anti-symmetric with respect to the equator and they can propagate either eastward (e.g., Kelvin waves) or westward (equatorial Rossby waves or Rossby-gravity waves). Together with mesoscale gravity waves they are the main drivers of the quasi-biennial oscillation (QBO) of the zonal wind in the tropics. Therefore, they are also relevant for the stability of the subtropical mixing barrier (which is more stable during QBO easterly wind phases) and thereby for mixing processes between troposphere and stratosphere by meridional transports. Temperature modulations due to equatorial waves can also play an important role in the dehydration of the tropical tropopause region.

1.7 Ozone in the Earth's Middle Atmosphere

Ozone plays a very important role in the Earth's atmosphere. In troposphere, it belongs to the family of the trace gases and also acts as one of the atmospheric pollutants. Most of the solar UV radiation between wavelengths of about 240 and 290 nm is absorbed in the middle atmosphere. UV radiation in the wavelength range 290 to 320 nm is biologically active and may modify or even destroy the human DNA. The middle atmosphere is greatly influenced by the heating that

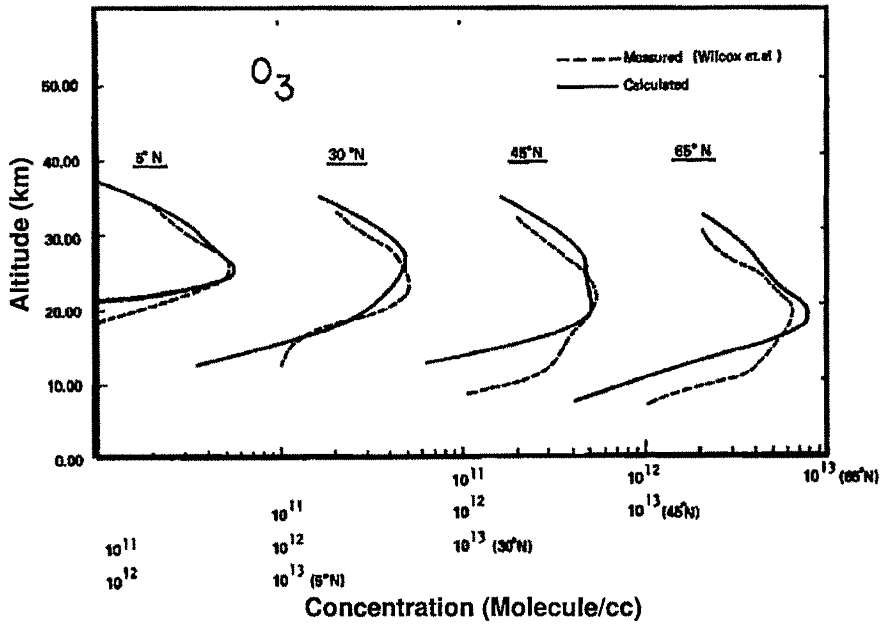

Figure 1.6: Observed and calculated vertical distribution of ozone as a function of latitudes in the northern hemisphere for mid-spring. This figure is reproduced from Miller et al., 1981

follows absorption by ozone of UV and visible radiation.

The influence of ozone on middle atmospheric temperature is very complex. Heating effect of UV radiation is major cause for the increasing temperature in the stratosphere. On the other hand, thermal IR (9.6 μm) emission from ozone leads to heat loss in the upper stratosphere [e.g., Wayne, 2000 and reference therein]. Ozone densities are low enough at these altitudes for the system to be optically thin and for IR radiation escapes from the atmosphere rather than being retained in it. Typical ozone density profiles (observed and calculated) at different latitudes are shown in Figure 1.6. It is to be noted that the peak in ozone concentration is at the higher height in the subtropical latitude (at 30°N, which is latitudinally close to the location of Mt. Abu, 24.5°N) rather than over low- and high-latitudes. Furthermore, variation in stratospheric ozone affects surface UV irradiance and supply of ozone to the troposphere, which may have a significant effect on tropospheric ozone concentrations also [e.g., Zeng and Pyle, 2003].

1.8 Objective and Scope of the Present Work

Middle atmosphere is an important part of the Earth's atmosphere but relatively less understood, as there have not been many observational techniques to explore it continuously for long periods. Middle atmospheric temperature structure has imprints of radiative, dynamical and chemical processes and offers a valuable means to study these processes and their interdependence [e.g., Singh et al., 1996]. Recent attention to the middle atmosphere was focused on the long-term climate change due to the greenhouse effect which is responsible for warming in the lower atmosphere and cooling in the middle atmosphere, along with the issues of ozone variabilities. The circulation of the middle atmospheric system determines the residence lifetime of minor species in the stratosphere that impacts the structure of the ozone layer. The temperature of the middle atmosphere above 30 km has been studied for more than two decades using Lidars [e.g., Hauchecorne and Chanin, 1980; Labitzke, 1980; Barnett and Corney, 1985; Hauchecorne et al., 1991; Clancy et al., 1994; Meriwether et al., 1994; Gobbi et al., 1995; Thomas et al., 1996; Namboothiri et al., 1999; Remsberg et al., 2002; Innis et al., 2006 and references therein]. These studies are mostly confined to mid- and high- latitudes except few studies [Sivakumar et al., 2003; Kishore Kumar et al., 2008] at Indian low latitudes and recently by Li et al., [2008] over Mauna Loa (19.5°N, 155.6°W).

In the sub-tropical region (specially in the 20°N to 30°N), there is no systematic study of middle atmospheric thermal structure so far. Many important scientific questions remain unanswered due to lack of observational input from these regions [McDermid, 1996; Keckhut et al., 2001; Randel, et al., 2004]. Few of them are, (i) is this region more influenced by middle atmospheric processes or by low latitude processes [Keckhut et al., 2004]? (ii) what type of dynamical features (GWs and PWs) are prevailing over these latitudes [Li et al., 2008]? (iii) how strongly are the polar and mid latitudes phenomena impacting this region and what are the time scales of the impact? (iv) imprint of GWs and PWs on the thermal structure, (v) is there any long term temperature trend that exists in the middle atmosphere? (vi) what are the intra-hemispheric differences in the sub-tropical middle atmosphere? etc. As of today, most of the above mentioned important scientific issues are still not properly addressed in the sub-tropical region.

In order to address a few of the above raised scientific issues, a lidar system was installed at Gurushikhar, Mt. Abu by Physical Research Laboratory (PRL) to carry out systematic studies on middle atmosphere thermal structure and dynamics over a sub-tropical Indian location for the first time. In this thesis, the results from a comprehensive study on temperature structure and dynamics of the middle atmosphere mainly in the stratosphere-mesosphere (30-75 km), over Mt. Abu are presented. A study of long term temperature trends in the Earth's middle atmosphere has also been made using the lidar data collected on more than 400 nights from 1997 to 2007. The climatology of the middle atmosphere temperature, including day to day variations, seasonal variations and inter-annual variations is presented and compared with satellite measurements and also with empirical models. Observed climatological features are compared with similar observations made at other mid and low latitude stations in the northern and southern hemispheres. There are interesting geophysical features in the middle atmospheric thermal structure viz., occurrence of double stratopause, MTI, and SSW. These features were reported mainly from mid- and high-latitude locations. In this study various aspects of these features are addressed for a sub-tropical location and a detailed description of their characteristics and source mechanisms have been presented and discussed. The results are compared with that of the low and mid-latitude locations. Long term temperature trends are also compared with the satellite observations over Mt. Abu. A study of different processes which are responsible for altering thermal structure, along with its possible association with ozone has also been studied and presented in this thesis. A study of the possible implication of the observed long term temperature trend has been described. A detailed comparative study with different empirical models revealed significant difference between observed and model predicted thermal structure. These empirical models do not reproduce features observed at sub-tropical latitudes mainly due to lack of observational input from these regions. This study of the thermal structure over Mt. Abu will play an important role in unraveling important scientific issues of coupling between different regions. In addition, a comparative study with different locations, viz., Gadanki (13.5°N; 79.2°E), Mauna Loa (19.5°N; 156°W), Observatoire de Haute Provence, OHP (44°N; 6°E) in the northern hemisphere and Reunion Island (20.8°S; 55.5°E)] in the southern hemisphere, will be valuable in interpreting the influence of high-, mid- and low- latitude features over sub-tropical regions (especially between 20°N and 30°N). Furthermore, the present study over a sub-tropical location may serve as a valuable bridge in addressing scientific issues of latitudinal coupling between the low- and mid- latitude processes and in improving model predictability for the less explored regions.

CHAPTER 2

Techniques, Instrumentation and Data

The lidar system used for the present work is located at Gurushikhar, Mt. Abu (24.5°N, 72.7°E), near the PRL's infrared (IR) observatory, in the Aravalli range of the mountains. It is a range of mountains in the western part of India, running $\sim$ 450 km from northeast to southwest across Rajasthan state. The highest peak, rising to $\sim$ 5653 feet ($\sim$ 1.7 km) from mean sea level, is Gurushikhar situated near the southwestern extremity of the range. Location of Mt. Abu is shown on a topographic map of India in Figure 2.1.

2.1 Techniques of the Middle Atmospheric Probing

There are broadly two types of atmospheric probing techniques (a) in-situ (balloon, rocket etc.), and (b) remote sensing (radar, lidar, optical and radio telescopes, etc.)

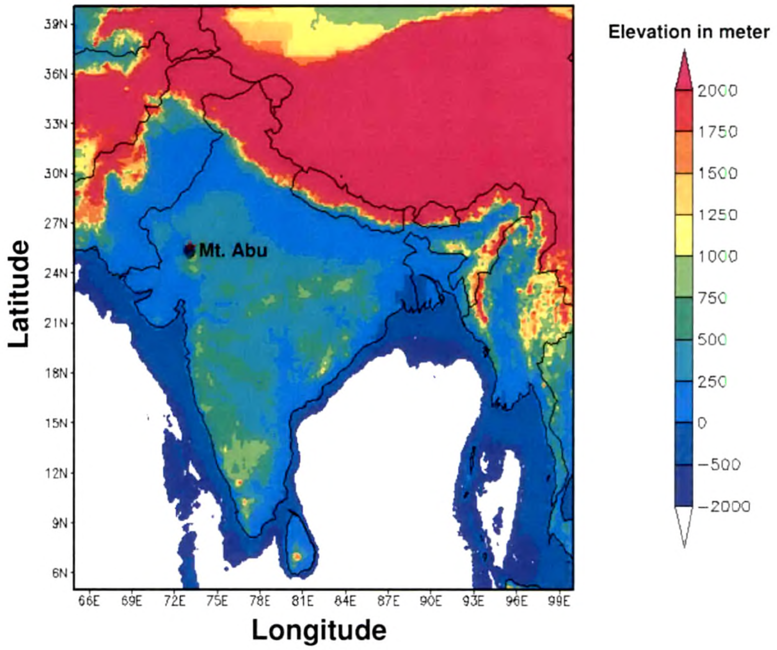

Figure 2.1: *Location of Mt. Abu on the topographic map of India, showing the hilly terrain near to the observatory.*

2.1.1 In-situ Techniques

2.1.1.1 Balloon

Balloon-borne measurements are very effective for the study of the vertical distribution of trace gases, aerosols and temperature profiles in the middle atmosphere with good vertical resolution. Balloons use thermistor/capacitive transducer for the measurement of atmospheric temperature. Several balloon-borne studies of trace gases, ion conductivities, dynamics in the lower and middle atmosphere in the Indian tropical and sub-tropical regions were carried out [e.g., Thomas and Bhattacharya, 1980; Nagpal, 1988; Lal et al., 1989, 1994, Chakrabarty et al., 1994; Patra et al., 2000; Gupta, 2000]. However, the upper height coverage of the balloon-borne sensors is limited to $\sim$ 35–40 km.

2.1.1.2 *Rocket*

Rocket provides very good altitude coverage with remarkable vertical resolution. Measurement of the neutral density, temperature and pressure were carried out by rocket-borne probes viz., Pitot tube [Ainsworth et al., 1961], falling spheres [Wright, 1969], thermistors [Ballard and Rofe, 1969]. An excellent review of these techniques can be found in Heath et al., [1974]. Using a variety of rocket borne sensors several studies on middle atmospheric composition, temperature and dynamics were carried out [e.g., Lal et al., 1979; Raghavarao et al., 1990; Sinha, 1992; Subbaraya et al., 1994a; Chandra et al., 2008; Das et al., 2009 and reference therein]. Major shortcomings of the rockets are that they are expensive and only a snap shot of the atmospheric feature under investigation is obtained. Therefore, long term continuous atmospheric surveillance is not feasible using rocket borne sensors.

2.1.2 Remote Sensing Techniques

Remote sensing is a technique for observing/monitoring a process or object without physical contact with the object under observation. Optical and radio telescopes, cameras, radars, lidars etc. are various types of remote sensing devices. Basically, there are two types of remote sensors to probe the atmosphere- (a) active sensors, and (b) passive sensors. Active sensors provide their own energy source for illumination viz., radar, lidar, sodar, sonar etc. Advantages of active sensors include the ability to make measurements regardless of the time of day or season. Remote sensing systems which measure energy that is naturally available are called passive sensors viz., Sun-photometers, radio telescopes, etc.

2.1.2.1 *Satellite*

Satellite borne instruments are very efficient tools for global coverage and quasi-continuous probing of the atmosphere. For obtaining vertical profile, solar occultation technique is exploited. This technique involves the measurements of the attenuated solar radiation, reaching to satellite after passing through the Earth's atmosphere along an almost horizontal path Measurement at successive satellite

3077

positions corresponding to the ray traversing the atmosphere at different heights can provide a vertical profile of the absorbing constituent and that can be used to derive required physical parameter viz., density, temperature, etc [e.g., Venketswaran et al., 1961; Rawcliff et al., 1963]. Satellite observations revolutionized the era of the atmospheric probing with the galaxy of instruments on-board and with their remarkable coverage [e.g., Dudhia et al., 1993; Leblanc et al., 1995; Randel et al., 1995; Patra et al., 2003 and references therein]. However, these are also limited by poor vertical resolution, limited number of passes over a given location and cloud covers [Leblanc and Hauchecorne, 1997].

2.1.2.2 MST Radar

Mesopshere-Stratosphere-Troposphere (MST) radars are good for the study of variety of atmospheric processes with good vertical and temporal resolution. Temperature can be derived upto $\sim$ 20-25 km using MST radar data. Radar observed vertical velocities are subjected to fast fourier transform analysis to obtain Brunt-Vaisala frequency, from which the temperature profile is obtained [e.g., Revathy et al., 1996]. But MST radars are also blind to 30–60 km height range due to absence or very weak turbulence, which is the main scatterer, in this altitude region [e.g., Woodman and Guillen, 1974; Balsley and Gage, 1980].

2.1.2.3 Lidar

LIght Detection *A*nd *R*anging *(LIDAR)* emerges as a very good tool for ground based long term middle atmospheric probing with very good vertical and temporal resolution. Lidar operations are mostly done at night and are limited by weather condition.

It was first suggested by Synge, [1930] that the scattering of light from a searchlight beam could be utilized to determine the atmospheric density. The field of lidar was revolutionized by invention of the first pulsed laser by Maiman [1960], and it became an ideal light source for the lidar operation. The introduction of these new lasers meant that spectrally narrower filters could be used at the receiver. This, coupled with small beam divergence resulted in a reduction in the background noise level by several orders of magnitude. In addition, a pulsed source meant that the transmitter and receiver could be co-located in a monostatic arrangement, with the range at which the backscattered signal originated was determined by the time delay between the transmitted and received signals. The subsequent introduction of Q-switching led to high power short laser pulses, improving the range achieved and the spatial resolution.

Atmospheric measurements using this method were first made by Fiocco and Smullin, [1963], who observed scattering from above 30 km. Laser radar technique operates on a principle similar to that of normal radar. Over the past few decades, Rayleigh lidar has emerged as a powerful method for studying the middle atmosphere, and early results were presented by Hauchecorne and Chanin, [1980]. The Rayleigh lidar method has also been used to extract temperature for the stratosphere and mesosphere [Measures, 1984]. The height range (30–60 km) in the atmosphere observed by Rayleigh lidar is one which is relatively inaccessible to other techniques.

The strength of the lidar technique is that it is capable of making continuous measurements of lower and middle atmospheric parameters with good temporal and spatial resolutions. Lidars are used in a variety of applications in the field of atmospheric sciences employing different scattering/absorption mechanisms. On the basis of different scattering/absorption mechanisms, lidars are of various types e.g., Rayleigh lidar, Raman lidar, Differential Absorbtion Lidar (DIAL), etc. A Nd-YAG laser based Rayleigh-Mie backscatter lidar was developed at PRL and operated for the study of aerosols and temperature over Ahmedabad (23°N) [Jayaraman et al., 1995a, b; Jayaraman et al., 1996]. Bencherif et al., [1996] developed a lidar for the atmospheric probing over Reunion Island (20.8°S, 55.5°E). In the following section a brief description of different types of scattering mechanisms are presented.

2.2 Scattering of Light in the Atmosphere

In the atmosphere, a light beam suffers a loss of energy due to two mechanisms: scattering and absorption. This loss is termed as attenuation or extinction. In absorption, the light is lost to gases or particles, and its energy contributes to the internal energy of the atoms or molecules. Scattering, which is caused by atmospheric gases and particles results in the loss of light from its original direction.

There are two broad types of scatterings which have been utilized in lidar studies of the atmosphere and these are termed elastic and inelastic. Elastic processes refer to those in which there is no change of frequency/wavelength, and include Rayleigh, Mie, and resonance scattering. Inelastic processes involve a change in the frequency /wavelength between the incident and scattered light and are limited in their applications; these include Raman and fluorescence scatter.

In the following sections, two assumptions are made. The first is that the scattering particles are far enough away from each other such that the light scattered from one particle is unaffected by that from the others (independent scattering). The second is that the photon is scattered only once (single scattering) rather than two or more times, as in the case of multiple scattering.

2.2.1 Elastic Scattering

Elastic scattering refers to scattering in which there is no change in wavelength between the incident and the scattered light. The most important parameter for elastic scattering is the ratio of size of the scattering particles to the wavelength of the incident light.

2.2.1.1 *Rayleigh Scattering*

Lord Rayleigh, [1890], demonstrated for the first time that the scattering of light by air molecules is responsible for the blue color of the sky. Rayleigh scattering occurs when the dimensions of the scattering particles are much smaller than the wavelength of the incident light, and the frequency of the radiation does not correspond to a specific electronic transition. The backscatter cross-section has a λ^{-4} dependence and the mechanism is only effective for particles with radii $\leq$ 0 03λ [e.g., Cerny and Sechrist, 1980]. This latter condition is satisfied by the atmospheric molecules.

Rayleigh Scattering Cross-section

The Rayleigh scatter cross-section is defined as the total energy scattered by a particle in all directions. Stratton, [1941] showed that for an incident wave of unit intensity, the scattered intensity at a distance r from the scatterer is given by

$$I = \frac{16\pi^4 a^6}{r^2\lambda^4}\left(\frac{n^2-1}{n^2+2}\right)^2 \sin^2(\psi) \tag{2.1}$$

where n is the relative refractive index (the ratio of the scatterers' refractive index to that of the surroundings).

Rayleigh scattering cross section is obtained by integrating (2.1) over a sphere for an incident beam of unit intensity and is given by

$$\sigma_R = \frac{128\pi^5 a^6}{3\lambda^4}\left(\frac{n^2-1}{n^2+2}\right)^2 \tag{2.2}$$

The differential Rayleigh backscattering cross-section is the probability of scattering in the backward direction per unit solid angle ($\theta = \pi, \psi = \pi/2$);

$$\frac{d\sigma_R^{(\theta=\pi)}}{d\Omega} = \sigma_R^{\pi} = \frac{16\pi^4 a^6}{\lambda^4}\left(\frac{n^2-1}{n^2+2}\right)^2 \tag{2.3}$$

Hence, from (2.2) and (2.3):

$$\sigma_R = \frac{8\pi}{3}\sigma_R^{\pi} \tag{2.4}$$

For a mixture of gases present in the atmosphere below 100 km, Collis and Russell [1976] have indicated that the differential Rayleigh backscattering cross-section is

$$\sigma_R^{\pi}(\lambda) = 5.45\times\left(\frac{550}{\lambda}\right)^4 \times 10^{-32}\ \mathrm{m^2 sr^{-1}} \tag{2.5}$$

where λ is the laser light wavelength in nm.

This shows the λ^{-4} wavelength dependence of the elastic scattering cross section characteristics of Rayleigh scattering and neglects the effects of atmospheric dispersion. If this effect is taken into account, the exponential factor changes from -4 to -4.09 [Elterman, 1968], corresponding to a change in the cross section of less than 3%. Shardanand and Rao, [1977] have shown that this relation (2.5) holds for a number of gases over the visible wavelength range. For the laser wavelength of λ 532 nm employed in this study, σ_R^{π} is given by:

$$\sigma_R^\pi = 6.24\times10^{-32}\ \mathrm{m^2sr^{-1}} \tag{2.6}$$

The total intensity scattered by a volume of gas is the sum of the scattered intensities from each scatterer within the volume. If all scatterers are considered to be identical, then the total scattered intensity is described by the volume molecular scattering coefficient, $\alpha_{m,s}$,

$$\alpha_{m,s} = N_m\sigma_R \tag{2.7}$$

where N_m is the number of gas molecules per unit volume.

The volume molecular backscatter coefficient β_m^π is similarly defined as

$$\beta_m^\pi \equiv N_m\sigma_R^\pi \tag{2.8}$$

With σ_R^π known, a measurement of β_m^π can be used to determine atmospheric density using (2.8).

Hence, for pure molecular scattering, the Rayleigh backscatter coefficient is a constant multiple of the Rayleigh molecular scatter coefficient:

$$\beta_m^\pi = \frac{3}{8\pi}\alpha_{m,s} \tag{2.9}$$

The total volume backscatter coefficient β_T^π, is the sum of both the molecular and the particulate components,

$$\beta_T^\pi = \beta_m^\pi + \beta_p^\pi \tag{2.10}$$

Above the stratospheric aerosol layer (height > 25 km, under normal conditions) this term is dominated by the molecular component.

Modern Rayleigh lidars typically have a maximum range of around 90 km, while the lowest height for pure Rayleigh scatter depends on the maximum height of the aerosol layer in the stratosphere (~30 km). Measurements of the Rayleigh backscatter in this height interval can be used to derive vertical profiles of molecular density, pressure, and temperature.

2.2 1.2 *Mie Scattering*

As the size of the particles increases beyond the Rayleigh limit, the differential scattering cross-section becomes a complicated function. This form of scattering is characterized by a large differential backscatter cross-section and a very pronounced component of forward scattering. Mie (1908) developed a full treatment for the diffraction of a plane monochromatic wave by a homogeneous sphere situated in a homogeneous medium. His method was based on electromagnetic theory, and has been discussed in detail by several authors [e.g., Kerker, 1969; Liou, 1980, 2002].

2.2.1.3 *Resonance Scattering*

Resonance scattering is sometimes referred to as atomic or resonance fluorescence. It occurs when the frequency of the incident laser light corresponds to a specific transition of an atomic or molecular species, and results in an enhancement of the scattering cross-section. Collisional quenching by other constituents may result in a small signal; hence the technique is best applied to studies of some of the trace constituents in the upper atmosphere [Clemesha, 1984]. The use of tunable dye lasers has made it possible to observe scattering from neutral and ionized metal species from between ~ 80 and ~ 100 km.

2.2.2 Inelastic Scattering

Inelastic scattering refers to scattering mechanisms which produce a change in wavelength of the incident radiation, due to transitions within the scattering molecules. These interactions have also been utilized for lidar studies of the Earth's atmosphere.

2.2.2.1 *Raman Scattering*

Raman scattering involves a change in frequency between the incident and the scattered radiation characteristic of the stationary states of the scattering molecular species, regardless of the illuminating wavelength. As compared to the Rayleigh scattering, the Raman cross-sections are a few orders of magnitude smaller. This technique has a large potential for atmospheric studies, as the scattered signal can be clearly distinguished from that due to other scattering particles, and it does not require a tunable laser. If the scattered wave is examined spectrally, a series of sidebands shifted up and down in frequency by equal amounts are observed. The lower frequency components are due to the molecule gaining energy from the incident light, and are termed Stokes lines. Conversely, the higher frequency component represents a net loss of energy from the molecule to the radiation, and these lines are called the anti-Stokes lines. Raman lidar techniques have been effectively used in measurements for atmospheric temperature, water vapor and aerosols [e.g., Whiteman et al., 1992; Girolamo et al., 2004 and references therein]

Measurement of the Raman scattered signal selected by the use of suitable filters has thus proved to be a useful tool for atmospheric studies, although the weak returns do limit the height coverage. The frequency shift is unique to the scattering species, and the intensity of the scattered signal is proportional to the concentration of the scattering molecules. Hence, this method has also been employed to monitor atmospheric constituents [e.g., Inaba, 1976; Melfi et al., 1997; Whiteman and Melfi, 1999].

Using rotational Raman returns from molecular nitrogen and oxygen, it is possible to derive temperature profiles for height ranges in the lower troposphere. These returns are free from aerosol backscatter, and the ratio of the intensities of two different parts of the received Stokes spectra are approximately proportional to the atmospheric temperature [e.g., Mitev, 1984].

2.2.2.2 *Fluorescence Scattering*

Fluorescence scattering arises from the spontaneous emission of a photon following the excitation an excited state by the absorption of the incident radiation at a frequency which lies within a given absorption line or band of an atomic or molecular species. These excited states decay by the emission of a photon to different levels. As for resonance scattering, this form of inelastic scattering is better achieved in a tunable laser. Although it has a large differential backscatter cross-section ($\sim 10^{-20}$ m^2 sr^{-1}), collisional quenching often substantially reduces the received signal, even at stratospheric heights. This method has been employed for balloon-borne observations of OH fluorescence [Heaps and McGee, 1983, 1985]. This technique was shown to be useful for stratospheric temperature measurements.

2.2.2.3 Differential Absorption

Differential absorption is a method which provides a high sensitivity combined with good spatial resolution for measuring a particular atmospheric constituent. The idea was first suggested by Schotland, [1966] for evaluating the water vapor content in the atmosphere. He termed the technique Differential Absorption of Scattered Energy (DASE). It has subsequently been termed as *DI*fferential *A*bsorption *L*idar (*DIAL*).

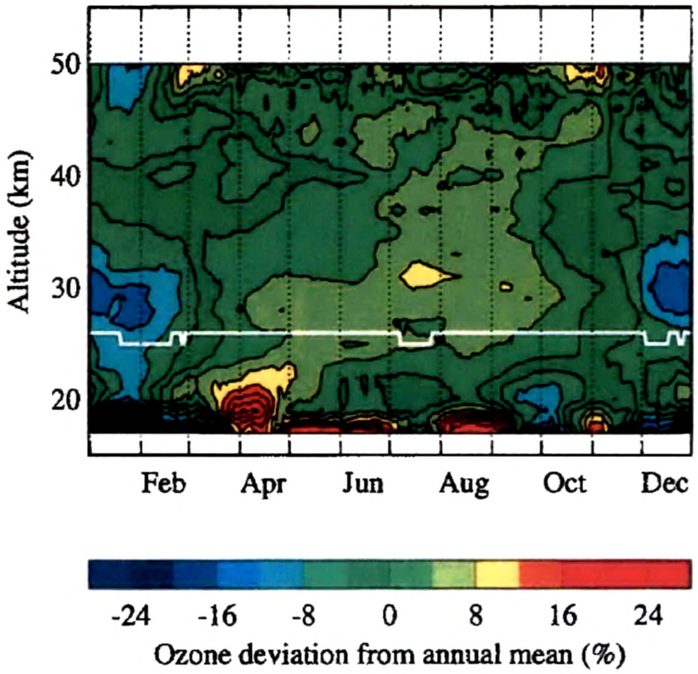

Figure 2.2: *Ozone number density deviation (observed by DIAL technique) from annual mean (in percent) over Mouna loa (1993-1999 reduced to a single composite year) as a function of altitude and month of the year. The contour interval is 4% (from Leblanc et al., 2000).*

The technique involves a comparison of the backscattered radiation when the laser is tuned close to an absorption line of the molecule of interest, with that received when it is tuned to lie in the wing of the line. Both radiations are returned by Rayleigh and possibly Mie scatter, and these data are then used to examine the contribution of molecular absorption to the extinction of the received signal. It has mainly been applied to water vapor studies in the lower troposphere, and ozone measurements in the upper stratosphere [e.g., Megie and Pelon, 1983; McDermid et al., 1995a; Grant et al., 1998]. Figure 2.2 shows a contour plot of ozone climatology using DIAL over Mauna Loa during 1993–1999. The ozone concentrations were lower during winter months in the altitude region of $\sim$ 30 km [Leblanc and McDermid, 2000]. Association between ozone and stratospheric temperature over Mt. Abu are described in chapter 3. Important scattering/absorption cross-sections and their respective applications in different atmospheric height regions are given in Table 2.1.

Table 2.1: *Comparison of optical interaction processes applicable to laser remote sensing methods in the atmosphere (source, Hinkley, 1976)*

Technique	Cross-section, $\frac{d\sigma}{d\Omega}$ $[cm^2/sr]$	Applications in the atmosphere
Rayleigh scattering	about 10^{-26}	Density/Temperature (above $\sim$ 30 km)
Mie scattering	about 10^{-8} to 10^{-26}	Aerosols/clouds etc. (below $\sim$ 30 km)
Raman scattering	about 10^{-29}	N_2, CO_2, H_2O, Temperature etc. (upto $\sim$ 15-20 km)
Absorption	about 10^{-20}	Trace species, O_3, CO_2, H_2O etc. (upto $\sim$ 50 km)
Fluorescence	about 10^{-26}	Trace species mainly NO_2, SO_2 (upto $\sim$ 5 km)

2.3 Attenuation and Absorption

A loss of energy is also caused by the absorption of light by gases and particles. The total volume extinction coefficient (α) is given as

$$\alpha = \alpha_{m,s} + \alpha_{m,a} + \alpha_{p,s} + \alpha_{p,a} \tag{2.11}$$

[e.g., Collis and Russell, 1976], where m, p, s, a represent molecular (gaseous), particulate, scattering and absorption, respectively. This represents the fraction by which the flux of energy in the direction of propagation per unit volume of the atmosphere is reduced.

For molecules, the scattering component ($\alpha_{m,s}$) is dominated by elastic scattering as the size of the molecules is small compared to the laser light wavelength and is given by equation 2.7.

The molecular absorption coefficient ($\alpha_{m,a}$) is strongly wavelength dependent. Atmospheric molecules absorb strongly at specific wavelengths when the photon energy corresponds to an energy level transition of the electrons in an atom or molecule. For laser radiation close to such wavelengths, this effect dominates α. However, these wavelengths are mainly found in the ultra-violet (λ <300 nm) and infra-red (λ >900 nm) regions of the electromagnetic spectrum. In the visible region, scattering is the main cause of molecular attenuation. The only atmospheric molecular component which absorbs light at the laser wavelength used in this study (532 nm) is ozone [Liou, 1980, 2002]. The volume molecular absorption coefficient ($\alpha_{m,a}$) may therefore be considered as being solely due to ozone

$$\alpha_{m,a} = N_{O_3}\sigma_{O_3} \tag{2.12}$$

where N_{O_3} is the ozone number density, and σ_{O_3} is the ozone absorption cross-section. Hence, for a Rayleigh scattered laser pulse,

$$\alpha = \alpha_{m,s} + \alpha_{m,a_{O_3}} \tag{2.13}$$

In the case of particles, the volume particulate extinction coefficient (α_p) is

$$\alpha_p = \sum_{\imath}^{N} \left(\alpha_{p,s} + \alpha_{p,a}\right)_{\imath} \tag{2.14}$$

This represents the sum of all contributions of $\alpha_{p,s}$ and $\alpha_{p,a}$ for each of the $\imath$ species in the atmosphere. Each particle species has its own characteristic size distribution, number density and refractive index. Estimates of α_p are therefore difficult to make. For particles, the effect of particle shape on the attenuation ($\alpha_{p,s}$ and $\alpha_{p,a}$) terms is not as marked as that on the corresponding backscatter coefficient β_p^{π}, and such attenuating particles may, therefore, be considered as being spherical.

The volume particulate extinction and backscattering coefficients are related by

$$\alpha_p^{\pi} = k\beta_p \tag{2.15}$$

Figure 2.3: *A panoramic view of PRL's IR observatory and the atmospheric sciences laboratory at Gurushikhar, Mt. Abu.*

(Pinnick, 1980), where k is the attenuation to backscatter ratio.

2.4 PRL's Lidar System

PRL's lidar system is located at a hill top, Gurushikhar at Mt. Abu. The prime objective of operating the lidar at a hill station was to explore middle atmosphere up to the highest possible altitude. Mt. Abu has very little light pollution and is relatively cloud free. In addition, surrounding hill terrain provides an opportunity to explore the orographically generated dynamical features. A panoramic view of PRL's IR observatory at Gurushikhar is shown in Figure 2.3. The inside view of the lidar laboratory along with Atmospheric Sciences Laboratory building is shown in Figure 2.4.

Regular lidar measurements for temperature studies were started at Mt. Abu with a 90 cm telescope in November 1997 and the lidar was normally operated

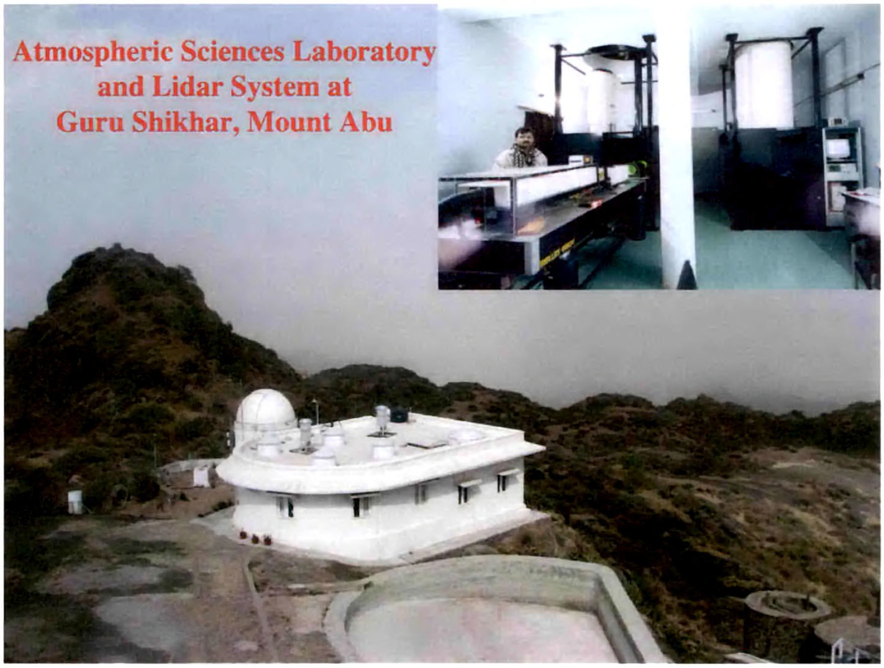

Figure 2.4: *Atmospheric Sciences Laboratory at Mt. Abu with lidar laboratory shown in the inset.*

for about 5-10 nights each month around new moon period. Temperature profiles can be derived up to 70–75 km altitude with an integration time varying from one hour to six hours, depending upon the system status and local weather conditions. During the monsoon period, (mid June to mid September) regular measurements were not possible and only a few nights of observations could be made during June and September.

2.4.1 System Block Diagram

The block diagram of the lidar system is shown in Figure 2.5. It consists of a Nd-YAG laser, a beam expander and a beam steering mirror, comprising the transmitting section. The receiver consists of a Cassegrain telescope and a photomultiplier tube (PMT) which is connected to a photon counting system. The transmitting and receiving optics are non-coaxial, being separated by a distance of ~ 1.5 m. Thus the backscattered signals are not seen by the telescope until the transmitted beam

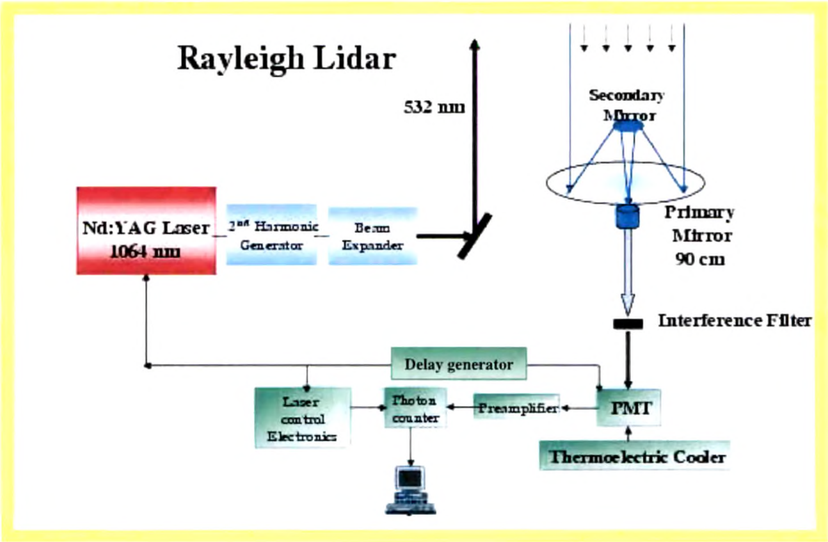

Figure 2.5: Block diagram of the PRL's Rayleigh lidar system.

is fully inside the telescope's field of view, that is beyound $\sim$ 400 m in the present setup. The signal received from the lower heights is very strong, therefore it is necessary to use a gated PMT or a mechanical shutter to avoid saturation induced effects in PMT from the large backscattered signal from lower heights. The receiving section is separated from the rest of the laser transmitting gadgets by using black panels. The laser beam passes through pipes to protect users from exposure to hazardous laser radiations inside the laboratory. This also serves to prevent light from the transmission section reaching the receiving units. Detailed specifications of the lidar system are presented in Table 2.2.

2.4.2 Transmitting System

2.4.2.1 Laser

The first laser system pumped with the flash lamp was a Q-switched ruby laser, later it has been implemented in other lasers (as Nd-YAG laser). Use of solid-state lasers are popular in the atmospheric lidars due to their ruggedness, long life, less maintenance and reasonably good efficiency (e.g., Nd:YAG laser). Nowadays, with

Table 2.2: Major specifications of the lidar system operational at Mt. Abu.

Lidar system	Specification
Laser	
Type	Nd:YAG (581C-10 Quantel, France)
Average Power	4.4 Watt at 532 nm
Energy per pulse	440 mJ at 532 nm
Pulse repetition rate	10 Hz (Maximum)
Pulse width	7 ns
Beam Divergence	0.6 mrad
Telescope	
Telescope type	Cassegrain
Effective focal length	737 cm
Diameter (Primary mirror)	90 cm
Diameter (Secondary mirror)	25 cm
Field of view	1 mrad
Power aperture product	2.6 Wm^{-2}
Optics	
Interference filter	
Central wavelength	532 nm
Filter bandwidth	1 nm
Transmittance	20%
Photomultiplier	9813A (Electron Tubes, UK)
Mode of operation	Photon counting mode
Dark counts	$\sim$ 300 counts/sec at 20° C
Signal processer	
Type	SR430 Stanford Research Systems, USA
Bin width	640 ns ($\sim$ 96 m)

diode array pumping, efficiencies up to $\sim$ 10%- 20% have also been achieved.

The laser used in PRL's lidar is Q-switched Nd-YAG laser (581C-10, Quantel, France). It has two main parts, the optical heads and the power supply. These are connected by cables, wires and hoses running through an umbilical. In addition to energizing the optical heads, the laser power supply provides all logical functions necessary to operate the laser, and cooling device to dissipate the heat generated in the optical heads by the operation of flashlamps. A remote control box is provided for smooth/safe operation of the laser.

The fundamental wavelength of the Nd-YAG laser is in the infrared region, at 1064 nm. It employs highly deuterated (99%) KDP crystals for 2^{nd} and 3^{rd} harmonic generation of radiation at 532 nm and 355 nm, respectively. The crystals are mounted on a mechanical holder and oriented along a horizontal plane and can be tuned separately using thumb wheels for maximum power output. The output signal strength is stabilized (less than 3% fluctuations from pulse to pulse) over hours of operation using temperature controllers. In order to synchronize the signal detection with laser firing, a synchronization pulse of 15 volts is derived from Q-switch for triggering the time delay generator, PMT gating circuit and the photon counter. The laser output at 532 nm and 355 nm, share same output port. However, they have an angular separation which enables the use of two separate reflectors, which reflect more than 99% at both the wavelengths. In the present study, laser radiation at wavelength of 532 nm (2^{nd} harmonic of Nd-YAG laser) was used. The fundamental wavelength of 1064 nm was not used for measurements due to its reduced degree of Rayleigh scattering, and also because of the low quantum efficiency of photomultipliers in this part of the electromagnetic spectrum. The third harmonic of 355 nm would be Rayleigh scattered more efficiently, but was not used for this work primarily because of the lower power output from the laser, the less efficiency of the filters and the increased absorption of this wavelength by ozone.

For the present study, maximum available laser repetition rate of 10 Hz was used. The individual pulses were of 7 ns duration, corresponding to a pulse length of 1.05 m. Such short pulses can provide a very good height resolution which is one of the important features of the lidar technique. The highly monochromatic nature of the transmitted laser light permits us to use narrow band width filters at the receiver end to reject background light, thereby improving the signal-to-noise ratio.

2.4.2.2 *Beam Expander*

The output laser beam was passed through a beam expander. The Laser Beam Expander (LBX) consist of afocal, de-centered pupil and Dall-Kirkham telescope. The primary mirror is a de-centered section of a concave ellipsoid and the secondary mirror is a convex sphere. The unexpanded input beam enters the unit through an aperture located adjacent to the primary mirror mounting plate, at the rear end of the housing. The diameter of this aperture is oversized with respect to the diameter of the input beam. The collimated input beam strikes the convex sphere and diverges to fill the concave primary mirror, which acts as the system aperture stop. The primary mirror re-collimates the wave, and the expanded beam then exits through an oversized aperture at the front of the unit. The beam expander is pre-aligned such that the input and the output beams are parallel to each other, and the input beam is centered at the entrance aperture. The surface accuracy of mirrors is about $\lambda/20$ at 532 nm. The full angle of output beam divergence due to errors in alignment is less than 8 micro-radian. This LBX is combined to form an expanding telescope with a magnifying factor of 10, which reduces the beam divergence from 0.6 mrad to 0.06 mrad. This further increases the altitude coverage of the laser beam and in turn improves the signal to noise ratio of the observed photon counts.

2.4.2.3 *Beam Steering Mirror*

The laser beam is transmitted into the atmosphere vertically with the help of a 6″ diameter, 45° incidence beam steering mirror, having ultra-hard dielectric coating, high density. This reflecting mirror is kept on a two-axis mounting which allows fine adjustment of the mirror, while aligning the lidar system.

2.4.3 Receiving System

The main components of the receiver system are telescope, photomultiplier and photon counting system.

2.4.3.1 *Telescope*

A Cassegrain telescope is deployed for collecting laser induced backscattered signal from different altitudes. It has a front-silvered parabolic primary mirror of 90 cm diameter and a secondary mirror of 25 cm diameter with effective focal length of 737 cm. Though this is basically a light collector, it has been shown that good optical quality mirrors are highly desirable for such studies [e.g., Hauchecorne and Chanin, 1980]. The backscattered radiation collected by primary mirror and after reflecting from the secondary mirror, is sent to the aperture of the photomultiplier assembly through an interference filter.

2.4.3.2 *Filter Wheel Assembly*

There is a filter wheel assembly in which four interference filters can be deployed. For the present study a filter, having central wavelength at 532 nm, is used for receiving Rayleigh backscattered signal.

2.4.3.3 *Photomultiplier Tube*

The photomultiplier tube (PMT) used is 9813A (Electron Tubes, UK) with 52 mm diameter (46 mm effective cathode diameter). It is a 14 stage gated tube with a fused silica front window and is cooled to about − 25 °C by a thermoelectric cooling device. It is of the type which is used in fast photon counting. The quantum efficiency is 9% at wavelength of 532 nm.

Intensity of the observed backscattered signal is very high from lower heights and requires shutting off the detector mechanically or electronically to avoid intense exposure of the PMT. In the present system gating of PMT is used. Therefore, appropriate delay was introduced by a delay counter (which can produce delay up to 999 μs in steps of 1 μs). The main purpose was to protect the PMT from overloading due to large backscattered signal from the lower regions of the atmosphere. A delay of 150 μs which corresponds to $\sim$ 22.5 km has been used in the present study (for the Rayleigh mode). The light then was allowed to pass through an optical interference filter with central wavelength at 532 nm and bandwidth of 1 nm (full width at half maximum). The maximum transmission was about 20% at 532 nm.

All detection instruments used for counting have a dead time or recovery time [Evans, 1955]. The dead time represents the time between the receiving system counting one pulse, and recovering to be ready for the next one. For very high count rates, this may lead to incorrect counting, as a portion of the real signal arrives before the receiving system is ready to count again and consequently is not detected. The receiving system dead time is 100 ns in the present setup. This was calculated in the following manner. If the system recovery time is t_r and total n pulses arrive from the photomultiplier, then the fraction of time during which the system is dead is nt_r. Hence the fraction of time during which the system is active is $1\text{-}nt_r$ which is the fraction of the true number of events, n_o, that the system can actually count,

$$\frac{n}{n_o} = 1 - nt_r \tag{2.16}$$

As n_o increases, the observed count rate n rises uniformly and approaches the value of $n_{max} = 1/t_r$ asymptotically.

2.4.3.4 *Amplifier-Discriminator*

The amplifier-discriminator is used to interface the PMT with the counting equipment. It generates a single output pulse of defined width and amplitude for every input pulse exceeding a set threshold voltage. Its role is to ensure that genuine signal pulses are counted. It is also used to convert the varied signal pulses from the photomultiplier into pulses of approximately uniform amplitude and width.

However, the PMT also produces noise counts which need to be disregarded. Some of these originate further down the dynode chain and so are amplified less, leading to smaller pulses than those generated by genuine backscattered signal. This sets a lower limit, eliminating the majority of the noise counts, as well as any background electrical noise.

2.4.3.5 *Signal Induced Noise*

It is also possible that noise is generated by the mechanism of Signal Induced Noise (SIN) in the photomultiplier. It has been noted [e.g., Pettifer, 1975; Acharya et al., 2004] that the signals themselves can induce an increase in the dark count of the photomultiplier. This need not be an overloading effect, as it exists for small and large counts and is proportional to the number of signals detected. One further source of noise pulses is the ion after-pulse mechanism, due to the gas inside the photomultiplier tube. Electrons ionize the gas, and these ions are attracted to the sides of the tube leading to a larger than normal pulse occurring approximately 1-2 ms after the actual count pulse. Such pulses only constitute less than 1% of the total counts, and are taken care of at the discriminator, to prevent these being counted. The number of system noise counts are minimized by the discriminator and hence have little effect on the derived density/temperature profile.

2.4.3.6 *Counting System*

A multichannel photon analyzer (SR430) manufactured by Stanford Research System has been deployed for photon counting. It is a multichannel scaler and counts incoming pulses in successive time bins. A trigger starts a record of up to 32,704 time bins. The bin width is programmable from 5 ns to 10.5 ms. This offers flexibility to choose the desired vertical resolution. In the present study a bin width of 640 ns, which corresponds to vertical resolution of 96 m, has been used throughout the observation period, 1997-2007.

A software has been developed to control the SR430 to run and collect the photon counts profile in automatic mode. In a given raw data profile there are two columns. First column represents the bin number and other has the total number of photon counts collected in each bin during an integration period of 5/10 minutes. This raw data profile is then used for further calculation of density and temperature.

2.5 Operational Procedure

While setting up the lidar system, utmost care has been taken in the alignment of both the laser and the telescope. Prior to actual lidar observation sessions, all the necessary system checkups and proper alignments were made. It was ensured that the transmitted beam intersected with the receiver field of view at the desired height. A pre-set program of SR430 is used for recording the counts received in each height channel for a given number of laser shots and height resolution. In this study we have used mostly 3000/6000 laser shots (5/10 minutes profile) with an altitude resolution of 96 m which corresponds to bin width of 640 ns. All the alignments and system performance checkups were carried out during the observations whenever the need was felt to do so.

2.5.1 Alignment of the System

For maximum collection efficiency the transmitted beam should lie fully in the field of view of the telescope in the region of the atmosphere to be investigated. The alignment of the system was carried out in two steps. Firstly, alignment was done using simple mechanical alignment techniques. Afterward, the backscattered signal from 600 laser shots were examined in the height range of 30 to 80 km. This value was then maximized using the fine adjustment of the beam steering mirror.

As mentioned earlier, the gating of PMT is done for initial delay of 150 μs, which corresponds to $\sim$ 22.5 km . This also represents the lowest height above which density/temperature can be derived with high degree of confidence (free from possible contamination due to Mie scattering from stratospheric aerosols).

2.6 Lidar Data and Method of Analysis

In this study, lidar data for about 10 years, 1997-2007, collected at Mt. Abu have been used. Observations were taken during the new moon period of every month, for about 5-10 nights (limited by local weather and seeing conditions). Monthly distribution of the observations over Mt. Abu is given in Table 2.3. In order to analyze the lidar data, it was first necessary to transfer the photon count files from the SR430 to the PC. SR430 records data in binary format. While transferring data from SR430 to a PC, a program is used to convert data from binary to ASCII format.

Table 2.3: Statistics of monthly observation over Mt. Abu during 1997-2007, including the observations during INDOEX campaigns, 1998-1999

Year	Sep	Oct	Nov	Dec	Jan	Feb	Mar	Apr	May	Jun	Total Nights
1997	0	4	3	5	0	0	0	0	0	0	**12**
1998	0	3	5	4	4	11	22	0	0	0	**49**
1999	0	0	0	0	4	19	8	5	0	0	**36**
2000	1	0	7	7	0	5	6	8	4	4	**42**
2001	4	10	8	7	5	3	5	6	5	0	**53**
2002	7	4	3	5	8	6	4	5	6	6	**54**
2003	7	6	5	6	8	6	5	5	3	4	**55**
2004	4	3	5	5	8	7	5	7	7	0	**51**
2005	0	5	9	6	7	6	4	9	3	0	**49**
2006	1	6	6	7	6	5	4	4	4	0	**43**
2007	2	3	4	6	7	2	3	5	4	0	**36**
Total	**26**	**44**	**55**	**58**	**57**	**70**	**66**	**54**	**36**	**14**	**480**

This further facilitates checking the quality of data, on line, and gives an option to correct the system parameters/alignments if required. Before the data are analyzed to yield values of density and temperature in the height range of 30 to 75 km, these are corrected for background noise, dead time and range.

2.6.1 Lidar Equation

The theoretical basis of the Rayleigh lidar technique is relatively straightforward. Monochromatic laser pulses are transmitted vertically into the atmosphere and variation of the backscattered signal with height provides information on atmospheric structure. Further reduction of the background 'sky noise' is possible due to the highly collimated transmitted beam, which allows a narrow receiver field of view to be used. For studies of molecular density using Rayleigh scattering, the laser wavelength selected is one which is away from any atmospheric absorption bands or resonance lines.

The basic scattering lidar equation can be derived, with the following assumptions:

i) The photons which are scattered out of the volume of air being investigated have suffered only one scattering event before leaving the volume (absence of multiple scattering).

ii) The scattering is incoherent.

iii) The detector response time t_D must satisfy the equation

$$\Delta h \gg \frac{ct_D}{2} \tag{2.17}$$

so that the height region Δh can be resolved unambiguously.

iv) The laser pulse itself should be of proper shape; for truncated pulses, a small correction is necessary [Measures, 1984].

If the above mentioned conditions are satisfied, then the intensity of the beam at a height z is given by equation

$$I_o = \frac{N_o \Pi}{tz^2 \Omega} \tag{2.18}$$

where N_o is the number of photons contained in a solid angle Ω steradian from a square pulse of t seconds duration, and Π represents the transmissivity, defined by.

$$\Pi = \frac{I}{I_o} = exp\left(-\int_0^z \alpha(z)\, dz\right) \tag{2.19}$$

according to the Beer-Brouger-Lambert law. When a beam of light of wavelength λ travels through the atmosphere, it is attenuated exponentially according to

$$I = I_o exp(-\alpha z) \tag{2.20}$$

where I represents the intensity after traveling a distance z, and I_o is the incident intensity at z=0. The volume extinction coefficient α is assumed to be constant over the distance z.

The backscatter intensity from the volume dV is then given by

$$I^{\pi} = I_o \left(\beta_m^{\pi} + \beta_p^{\pi}\right) \tag{2.21}$$

Where, β_m^{π} is the volume molecular backscatter coefficient and β_p^{π} is volume particulate backscatter coefficient.

Combining (2.18) and (2.21) gives the number of photons backscattered per second per unit steradian from a height z as

$$N(z) = \frac{N_o \Pi}{t z^2 \Omega} \left(\beta_m^{\pi} + \beta_p^{\pi}\right) dV \tag{2.22}$$

If A is the effective surface area of the receiving mirror, then the solid angle subtended at a height z by the receiver is

$$\Omega_z = \frac{A}{z^2} \tag{2.23}$$

and the scattering volume dV is

$$dV = z^2 \Omega \, dz \tag{2.24}$$

At the receiver, the photons have again passed through the atmosphere of transmissivity Π, and the power backscattered from the scattering volume dV into the receiver field of view A/z^2 is

$$P_r(z) = \frac{P_o \Pi^2}{t z^2 \Omega} \left(\frac{A}{z^2}\right) \left(\beta_m^{\pi} + \beta_p^{\pi}\right) dV \tag{2.25}$$

which may be written as

$$P_r(z) = \frac{P_o \Pi^2 A}{t z^2} \left(\beta_m^{\pi} + \beta_p^{\pi}\right) dz \tag{2.26}$$

For a laser pulse of duration t, and with the speed of light denoted by c, the pulse length is ct and

$$dz = \frac{ct}{2} \tag{2.27}$$

The quantity $(ct/2)$ is termed the 'effective pulse length', and is the interval from which signals are received at any instant. This is half the distance covered by the light pulse in time t, as the pulse must travel a two-way path. For a reception time of t_D, (corresponding to a scattering height region $dz = (ct_D/2)$), the power received per unit time into the field of view of the receiver is

$$P_r(z) = \frac{P_o \Pi^2 A}{tz^2} \left(\frac{ct_D}{2} \right) (\beta_m^\pi + \beta_p^\pi) \quad (2.28)$$

Also, if the detection system has an efficiency Q, which includes a geometrical factor for the system, and a factor describing the detector efficiency, (both of which may be wavelength dependent), then (2.28) becomes

$$P_r(z) = \frac{P_o A Q}{tz^2} \left(\frac{ct_D}{2} \right) (\beta_m^\pi + \beta_p^\pi) \Pi^2 \quad (2.29)$$

Therefore, using equations (2.13) and (2.19) for Π, and assuming that there is no contribution from Mie backscatter or absorption by particles, this becomes

$$P_r(z) = \frac{P_o A Q}{z^2} \left(\frac{ct_D}{2} \right) (\beta_m^\pi) \, exp \left(-2 \int \left(\alpha_{m,s} + \alpha_{m,a_{O_3}} \right) dz \right) \quad (2.30)$$

Rigorous derivations of the generalized lidar equation for elastic backscatter have been presented by several authors in different forms [e.g., Kent and Wright, 1970; Measures, 1984; Thomas, 1987]. Equation (2 30) represents the basis for the present analysis. Provided that the received signal is due solely to Rayleigh backscatter, it is then proportional to the molecular density. If the atmosphere is assumed to obey the perfect gas law and to be in hydrostatic equilibrium, then atmospheric temperatures may also be derived.

The method used in this derivation follows that of Chanin and Hauchecorne [1981]. The atmospheric density at the center of an atmospheric layer which is 96 m thick is given by

$$\rho(z_i) = \frac{M(z_i)}{M(z_o)} FA(C(z_i) - N) z_i^2 \quad (2.31)$$

where $M(z_i)$ and $M(z_o)$ are the mean molecular weights at height z_i and the ground level z_o respectively. These are taken to be equal in the height range studied, due to the constant mixing ratio. The integrated photon count is given by $C(z_i)$, and N is the background noise photon count (consisting of the photomultiplier dark count and the sky background); both are corrected for the system dead time. The term F

3077

is a factor which takes into account the attenuation of the laser beam by Rayleigh scattering and absorption by atmospheric ozone and A is normalization constant.

From the derived density profile, the atmospheric pressure can be calculated. The pressure $P\left(z_i - \Delta z/2\right)$ at the bottom of each successive layer, descending in height, is given by

$$P\left(z_i - \frac{\Delta z}{2}\right) = P\left(z_i + \frac{\Delta z}{2}\right) + \rho(z_i)g(z_i)\Delta z \qquad (2.32)$$

For the first calculation, $P\left(z_i + \Delta z/2\right) = P_m\left(z_i + \Delta z/2\right)$ (i.e. equal to the model pressure at the maximum useable height). The profile is then calculated downwards, with the pressure at the top of a layer being set equal to the pressure at the bottom of the layer above (i.e. $P\left(z_{i-1} + \Delta z/2\right) = P\left(z_i - \Delta z/2\right)$)

The temperature of each layer may then be calculated from

$$T(z_i) = \frac{M(z_i)g(z_i)\Delta z}{R\log_e(P(z_i - \Delta z/2)/P(z_i + \Delta z/2)} \qquad (2.33)$$

where M is mean molecular weight of the neutral atmosphere and R represents the universal gas constant.

The use of a model pressure at the upper height limit does introduce a systematic error in the derived pressure and temperature profiles. This error, however, decreases rapidly with decreasing height due to the exponential growth of density. Although the values of density derived are relative, the temperature values themselves are absolute. There may be some errors in the derived temperature at the uppermost levels due to the assumed model pressure values up to the maximum of two scale heights $\sim$ 10-12 km. Therefore, in present study temperature profiles, only up to the altitude of 70 to 75 km are used for the fitted value of pressure at 85 km.

2.6.2 Dead-time Correction

Dead-time correction was applied to each sample of the backscattered signal. The greatest effect on the received signal occurred at the lower heights (near 30 km) where the backscattered signal count rate was the highest. Consequently, it would be more likely that the backscattered signal arrived during the dead time of the system, and was undetected. At greater heights, the count rate decreased and virtually all of the backscattered signal was detected. Prior to density/temperature calculations, all profiles were corrected for the dead-time.

2.6.3 System Noise/Background Signal Correction

It was also necessary to correct the data for systematic noise, which was present in each height channel. This was independent of range, possibly time varying, and had several possible origins. One source was 'sky noise' such as the light from the moon, stars and unavoidable stray lights near the observatory. Spurious counts could also have arisen from the electrical equipment used, and thermal noise from the photomultiplier. The contribution of the total systematic noise to the recorded signal was estimated by calculating the mean number of counts for the top 100 height channels where there were only noise counts. These mean number of counts were then subtracted from the counts in all the height channels to be used in the subsequent data analysis.

2.6.4 Rayleigh and Ozone Attenuation

It was also necessary to take into account the effects of Rayleigh and ozone attenuation on both the transmitted and the backscattered signals through the height range studied. The total increase in the received signal over this height range (30-80 km) was less than 1% due to Rayleigh and ozone attenuation and hence had negligible effect on calculated temperature profiles.

2.6.5 Range-corrected Profile

The range corrected profile is defined as the total number of counts for a given height channel multiplied by the square of the height to which the height channel corresponds, and (under several basic assumptions) is proportional to the atmospheric neutral air density. An example of the raw data on 24 March 2001, along with range corrected profiles at 96 m and 480 m range resolutions are shown in Figure 2.6. The variation of the range corrected profile for the observation session

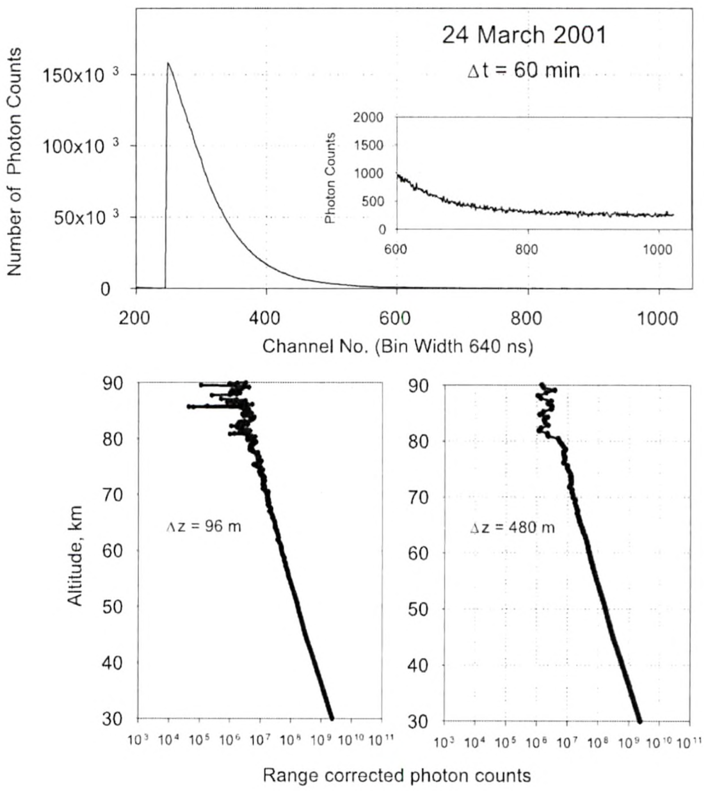

Figure 2.6: An example of raw-data (upper panel) and range corrected signals at 96 m and 480 m range resolution (lower panel) over Mt. Abu on 24 March 2001. To have better feel of the signal from higher heights, the raw data from range bins 600 to 1064 are also shown on inflated scale along Y axis.

on the night of 22 October 2001 is shown in Figure 2.7. This particular recording session consisted of 12 consecutive 10 minute profiles. On this occasion, delay generator for PMT gating was adjusted such that the signal from the lower height of up to approximately 22.5 km was not amplified by PMT. In each case, the individual samples were corrected for counter resets and the system dead time. The total profile itself has been smoothed over 480 m (5 range bins) in the vertical direction to reduce the small scale variability and finally a 5 point running average is applied to the temperature profiles. Relative atmospheric density is derived under the assumption that the atmosphere obeys the perfect gas law, is in hydrostatic equilibrium, and that the returns are due only to Rayleigh scattering from

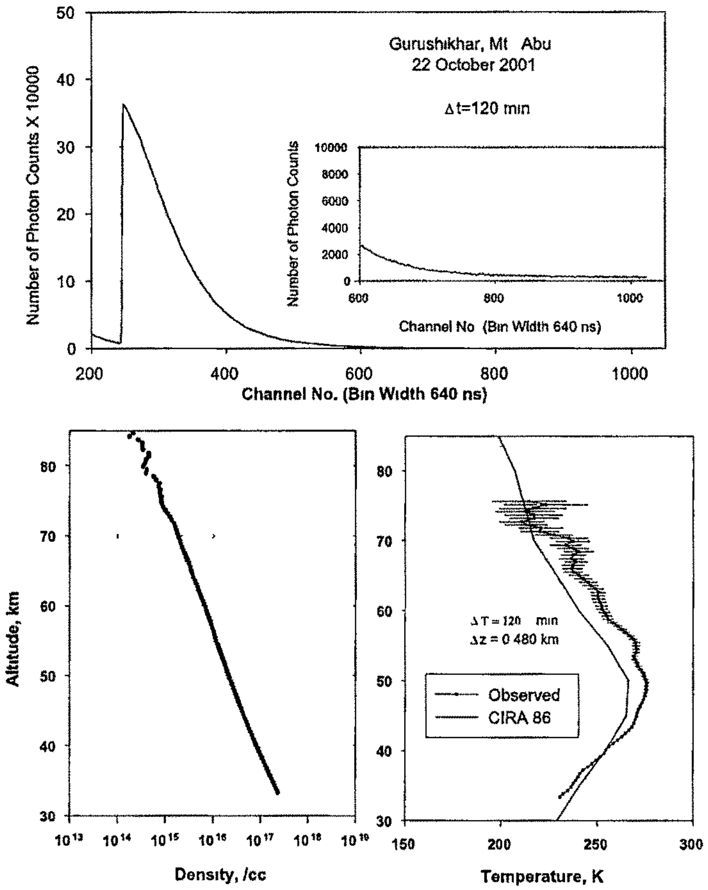

Figure 2.7: An example of raw-data, density and temperature observed over Mt. Abu on 22 October 2001. To have better feel of the signal from higher heights, in the inset the raw data from range bins 600 to 1064 are also shown on inflated scale along Y axis.

molecules. This is represented by an approximately linear section between 30 and 75 km which represents the decrease of neutral air density with height. The mean background noise signal was calculated from the top 100 height channels (i.e. 90 to 100 km), and subtracted from the counts recorded in all the lower height channels used in the analysis.

The corresponding density and temperature profiles derived for the total observation session are also shown in Figure 2.7. The data were fitted at both the upper and lower height limits to model pressure values taken from the CIRA-86 reference model atmosphere, interpolated for Gurushikhar's latitude and for the particular month. The model values are also indicated in the figures, and it can be seen that there is an agreement between these and the lidar derived values. The density and temperature profiles used in this study were derived from the raw data using a C-language based program. The method followed in the present study is similar to that of Chanin and Hauchecorne [1980, 1984].

2.6.6 Selection of the Upper Height Limit

The upper height at which the data were fitted to the model could be varied depending on the level at which the signal to noise ratio is good. The fitting height had a small effect on the derived density profile due to the model values used, although the derived pressure and temperature profiles were more sensitive to such changes. Generally, these values converged at heights below $\sim$ 10 km at which the upper level pressure was fitted. This represented the height at which the value of the fitted pressure became negligible compared with the derived pressure. It was typically found that the received signal was dominated by noise for heights greater than $\sim$ 75-80 km, and this level was adopted as the upper height limit for the subsequent derivation of the profiles of density and temperature from the data.

2.7 Errors in Lidar Measurements

Photon count rate in lidars closely follows a Poisson distribution. Hence, in each height channel, the number of counts recorded has a counting error derivable from Poisson statistics. For a Poisson distribution, one standard deviation is equal to the square root of the total number of counts for that height channel. This allows an estimate to be made of the error in the derived values of density and temperature. As the number of counts detected obeys the inverse-square law, the proportional error is largest at greater heights from where the total number of received counts is relatively small. The derivation of the errors in the measured density and temperature from the lidar data follows that of Hauchecorne and Chanin [1980].

The relative uncertainty on the density measurements is given by

$$\frac{\Delta\rho}{\rho} = \frac{\Delta N_L(z)}{N_L(z) - B(z)} \tag{2.34}$$

where N_L is the signal from an altitude z, $B(z)$ is the total background signal due to the dark current (the signal generated within the system itself) and the sky background. The total background signal is estimated from the uppermost heights at which the signal is dominated by the noise. If $B(z)$is negligible, then it corresponds to $(\Delta N_L/N_L)$ or $(N_L)^{-1/2}$

It can then be shown that the derived temperature has a statistical standard error of

$$\frac{\delta T(z_i)}{T(z_i)} = \frac{\delta \log(1+X)}{\log(1+X)} = \frac{\delta X}{(1+X)\log(1+X)} \tag{2.35}$$

where

$$X = \frac{\rho(z_i)g(z_i)\Delta z}{P(z_i + \Delta z/2)} \tag{2.36}$$

$$\left(\frac{\delta X}{X}\right)^2 = \left(\frac{\delta\rho(z_i)}{\rho(z_i)}\right)^2 + \left(\frac{\delta P(z_i + \Delta z/2)}{P(z_i + \Delta z/2)}\right)^2 \tag{2.37}$$

and

$$\delta P(z_i + \Delta z/2)^2 = \sum\nolimits_{j=i+1}^{n} \left(g(z_j)\delta\rho(z_j)\Delta z\right)^2 + \left(\delta P_m(z_n + \Delta z/2)\right)^2 \tag{2.38}$$

At the top of the profile, the uncertainty in the model fitted pressure is assumed to be around 15%. The effect of model fitted pressure, on the temperature uncertainty, decreases rapidly with altitude, and is less than 1% at 10-12 km from the top of the height range [Hauchecorne and Chanin, 1980; Ferrare et al., 1995]. Sivakumar et al., [2003] have also shown that the standard error associated with the temperature measurement at Gadanki is $\sim$ 15 K at the top reference level of 90 km and decreases exponentially to $\sim$ 1 K at 50 km.

The accuracy of the density and temperature measurements depends upon the number of photons $N(z)$ received from the height range Δz during the time Δt. It therefore varies as $(N(z))^{1/2}$ or $(\Delta t \Delta z)^{1/2}$, and will depend on the time and space resolutions required; these will vary with the problem to be studied. For long period and large scale phenomena, Δt and Δz can be large, although for smaller scale rapidly varying features, these should be as small as possible. A study was

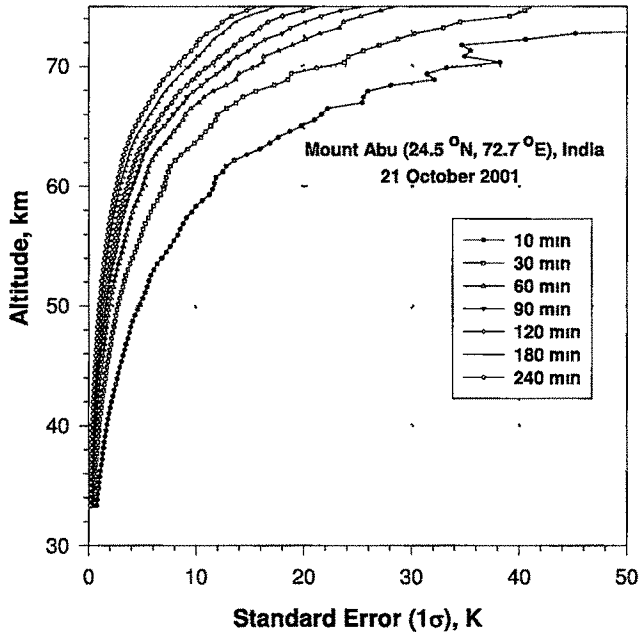

Figure 2.8: Error variation with altitude and time integration.

made on the errors in derived density and temperature as a function of data length and bin width. The performance of the system for different integration times is shown in Figure 2.8, derived from the observed data on 21 October 2001. These data correspond to a vertical resolution of $\sim$ 480 m. Temperature profiles were obtained from this data set using different data lengths corresponding to 10, 30, 60, 90, 120, 180, and 240 minutes. As the integration time is increased, the errors are seen to decrease. For a 10 minute data, typical uncertainties in the derived densities (temperatures) are 0.7% ($\sim$ 2.0 K) at 40 km, 1.6% ($\sim$ 5.0 K) at 50 km, 4.2% ($\sim$ 12 K) at 60 km, and 15% ($\sim$ 35 K) at 70 km. These are significantly reduced as the duration of the observation session is increased. The values for the total observation session (of about 240 minutes) are 0.1% ($\sim$ 0.26 K), 0.3% ($\sim$ 1.0 K), 0.8% ($\sim$ 2.0 K) and 2.3% ($\sim$ 7.0 K) for heights of 40, 50, 60, and 70 km, respectively. A detailed estimate of errors is also given in Table 2.4.

Table 2.4: Error variation in temperature derivation with altitude and different integration times.

Height (km)	Standard Error (K)		
	1 Hour Integration	2 Hour Integration	4 Hour Integration
35	0.5	0.3	0.1
40	0.8	0.5	0.3
45	1.2	0.9	0.5
50	2.1	1.2	1.0
55	4.3	2.1	1.8
60	5.8	2.9	2.3
65	6.3	3.5	2.9
70	12.0	4.5	3.2
75	27.0	21.0	15.0

2.8 Satellite Based, NCEP and ERA-40 Data Sets

In addition to the lidar data, satellite based temperature, total column ozone measurements and National Centers for Environmental Prediction-National Center for Atmospheric Research (NCEP - NCAR), and European Center for Medium-Range Weather Forecasts (ECMWF) Re- Analysis (ERA-40) data sets have also been used in the present study.

2.8.1 Temperature Data from HALOE onboard UARS

Upper Atmosphere Research Satellite (UARS) equipped with 10 instruments onboard for the Earth's atmospheric probing was launched using space shuttle Discovery in 1991 [e.g., Reber et al., 1993]. It orbited at an altitude of 576 km with an orbital inclination of 57° and was in operation till 2005. It measured temperature, ozone, chemical compounds which affect ozone chemistry and processes along with the winds and the energy input from the Sun in the stratosphere-mesosphere and in the lower thermosphere. One of the important instruments onboard UARS was the Halogen Occultation Experiment (HALOE). The basic scientific goal of

HALOE was to provide global scale data on temperature, odd chlorine (ClOy), odd nitrogen (NOy), odd hydrogen (HOy) etc., compounds needed to study the chemistry and dynamics of the middle atmosphere [Russell et al., 1993]. It employs the principle of satellite solar occultation and a technique of absorption of solar energy in selected spectral bands. The HALOE instrument includes broadband and gas filter channels covering the spectral range from 2.45 micrometer to 10.04 micrometer as described by Russell et al., [1993]. All together, these measurements are very useful for unraveling the role of the upper atmosphere in the Earth's climate and in its variability. Detailed discussions related to the validity of HALOE data can be found in a number of papers [e.g., Russell et al., 1993; Hervig et al., 1996; Singh et al., 1996].

In the present study, HALOE temperature data from 1991-2005 have been used for the satellite passes near ($\pm 5°$) to the lidar site at Mt. Abu.

2.8.2 Ozone Data from TOMS

Total Ozone Mapping Spectrometer (TOMS) onboard Nimbus-7 and Meteor-3 provided global measurements oftotal column ozone on a daily basis and together provide a complete data set of daily ozone from November 1978-December 1994. After an eighteen month period when the program had no on-orbit capability, ADEOS TOMS was launched on August 17, 1996 and provided data until June 29, 1997. Earth Probe TOMS was launched on July 2, 1996 to provide supplemental measurements, but was boosted to a higher orbit to replace the failed ADEOS. Earth Probe continues to provide near real-time data. Total column ozone data over Mt. Abu during 1997-2001 are utilized to investigate a possible association between observed temperature and ozone.

2.8.3 NCEP and ERA-40 Data Sets

The National Center for Environmental Prediction-National Center for Atmospheric Research (NCEP–NCAR) reanalysis data set providing the temperature and wind information from ground to lower stratosphere at intervals of about 2.5 $\times$ 2.5 latitude and longitude resolution [e.g., Kistler, et al., 2001]. Along with NCEP data, European Center for Medium-Range Weather Forecasts (ECMWF) Re- Analysis (ERA-40) data sets [Kallberg, et al., 2004, Uppala et al., 2005] have also been used in characterizing the event based phenomena double stratopause, stratospheric sudden warming. NCEP wind at different pressure levels have also been used in interpretation of the observed temperature features.

CHAPTER 3

Temperature Climatology over Mt. Abu

Atmospheric temperature is an important parameter for the study of various geophysical processes and has crucial imprint of radiative, dynamical and chemical behavior of the atmosphere. Its monitoring offers a valuable means to study the rate of chemical reactions and a variety of atmospheric phenomena and their interdependence [Singh et al., 1996]. In addition, climatological study of the middle atmospheric temperature is indispensable for empirical studies of climate and its variability, and also necessary for constraining the behavior of numerical models. Temperature measurements of the middle atmosphere above 30 km started using in-situ rocket measurements in 1950's and later by remote sensing and satellite experiments. The first comprehensive climatologies for the middle atmosphere were the 1964 and 1972 COSPAR International Reference Atmospheres (CIRA), which were based largely on single station balloon and rocket data. An updated version of CIRA in 1986 (CIRA-86) included early satellite observations of the stratosphere and mesosphere and has served as a community standard since that time. The rockets provide good vertical resolution and coverage but have problems of accuracy beyond 60-70 km due to the rarefaction of the atmosphere. The number of rocket soundings is also limited by the high cost of launches. Falling spheres are used to obtain temperature from density measurements up to 90 km [Schmidlin, 1981] but these also were not done on a regular basis. Satellite experiments are good for a global coverage of the temperature field but have poor vertical resolution and are limited by number of passes over a given location. The upper stratosphere is covered by the Stratospheric Sounding Unit (SSU), [Miller et al., 1980] but with a poor vertical resolution. The mesospheric temperature has been measured by infrared limb sounders from 1975 to 1982: Pressure Modulated Radiometer (PMR), [Curtis et al., 1974], Selective Chopper Radiometer (SCR) [Ellis et al., 1973], Limb Infrared Mesospheric Sounder [Gille et al., 1984] and Stratosphere and Mesosphere Sounder (SMS) [Drummond et al., 1980].

Labitzke, [1980], initiated a detailed analysis on climatology of the temperature structure of the stratosphere and mesosphere. The SME satellite data provided the vertical profile of temperature with height resolution of the order of 4 km, which is better than that of the PMR and SCR data used for CIRA-86. Mesospheric temperature climatology has been presented by Clancy and Rusch, [1989] from global observations of UV limb radiances from the Solar Mesosphere Explorer (SME) for the period 1982-1986. Barnett and Corney, [1985] studied the climatology of the middle atmospheric temperature using PMR data from 1975 to 1978 and this became the base of the new CIRA-86. It gives a reasonably good representation of the latitudinal, longitudinal and seasonal variations of the temperature. However, the short-term, inter-annual variability and 11-year solar cycle effects were not taken into consideration in bringing up the empirical model, which is unable to represent, sub-tropical and tropical latitudes properly, due to lack of observational input from these regions.

There are a number of techniques (described in Chapter 1) involving spaceborne and ground based instruments for middle atmosphere temperature measurements. The Rayleigh lidar provides continuous measurements of density and temperature with high temporal and height resolutions over a height range of 30 to 90 km. It is capable of obtaining temperature profiles with a good vertical resolution and thus enables the study of temporal evolution of the temperature at many time scales, from fractions of an hour to years and decades.

The climatology of mid-latitude middle atmospheric temperature was given for the first time by Hauchecorne et al., [1991] using Rayleigh lidars from two stations in France. Gobbi et al., [1995] have studied the middle atmospheric temperature variability using lidar measurements over a mid-latitude station, Frascati (42°N, 13°E). Temperature fields from troposphere to mesosphere employing Rayleigh and Raman techniques were studied by various groups [e.g., Keckhut et al., 1990; Hauchecorne et al., 1992; Gross et al., 1997 and reference therein]. Alpers et al., [2004] presented, for the first time, time-resolved temperature profiles in the altitude range from the planetary boundary layer up to the lower thermosphere ($\sim$ 1–105 km) at a mid-latitude station, Kuhlungsborn, Germany (54°N, 12°E). Namboothiri et al., [1999] compared the lidar measured temperature profiles with rocket and satellite measured profiles and also with CIRA-86 model and found that the lidar profiles were in agreement with the rocket and satellite measurements and the model. Remsberg et al., [2002] presented a comparison of HALOE temperature measurements with lidar and inflatable falling sphere measurements. For tropical latitudes, the measurements were limited to only a few rocket observations [e.g., Lal et al., 1979; Subbaraya and Lal, 1980; Mohankumar, 1994 and reference therein] and lidar measurements [e.g., Parameswaran et al., 2000]. Sivakumar et al. [2003] brought out a comprehensive middle atmospheric temperature climatology using Rayleigh lidar measurements from 1998 to 2001 over a tropical Indian location, Gadanki. In addition, temperatures measured using ground based lidar have also been used to validate various remote sensing instruments viz., Microwave Limb Sounder (MLS), HALOE on board UARS [e.g., Fishbein et al., 1996; Gill et al., 1996; Hervig et al., 1996; Remsberg et al., 2002]. Recently, Sica et al., [2008] have made use of temperature (from ground-based and space-borne) measurements to validate Atmospheric Chemistry Experiment (ACE) measurements.

The climatology of the middle atmospheric temperature has been studied over the past two decades over different locations using various remote sensing experiments around the globe [Barnett and Corney, 1985; Chanin et al., 1985; Clancy and Rusch, 1989; Hauchecorne et al., 1991; Wang et al., 1992; Clancy et al., 1994; Lambeth and Callis, 1994; Whiteway and Carswell, 1994; Wild et al., 1995; Thomas et al., 1996; Keckhut et al., 1996; Wickwar et al., 1997; Burris et al., 1998; LeBlanc et al., 1998; Chen et al., 2000; Bencherif et al., 2000; Gardner et al. 2001; Nee et al., 2002;

Sivakumar et al., 2003; She et al., 2003; Randel et al., 2004; Argall et al., 2007; Li et al., 2008]. Among the high latitude studies, Gobbi et al.,[1991] illustrated the evidence for denitrification in the Antarctic spring stratosphere using lidar and temperature measurements. In another interesting study, Donfrancesco et al., [1996] presented lidar observations of stratospheric temperatures above McMurdo Station (78°S, 167°E) at Antarctica. Detailed temperature records in the arctic middle atmosphere were presented by Duck et al., [2000]. Recently, a Rayleigh lidar based comprehensive temperature climatology at ALOMAR (69°N), highlighting importance of temperature measurements in the polar region, was presented by Schoch et al., [2008]. Earlier, Klekociuk et al., [2003] also reported the middle atmospheric temperature structures over Antarctica using the Rayleigh lidar.

In addition the imprint of dynamical and radiative features of the middle atmosphere temperature plays vital role in the Earth's ozone budget (due to temperature sensitive rate constants of ozone chemistry), which is an important and crucial gas to be monitored in the atmosphere [e.g., Lal, 1981; Subbaraya and Lal, 1981; Naja and Lal, 1996; Leblanc et al., 2001; Sahu and Lal, 2006; Erying et al., 2007]. Therefore, by studying temperature, we can unravel various aspects of ozone and its chemistry which plays pivotal role in deciding stratospheric temperatures [e.g., Fortuin and Kelder, 1998; Michelson et al., 1998; Shepherd, 2003; Steinbrecht et al., 2003; Hare et al., 2004; Keckhut et al., 2004]. Nevertheless, recent attention focused on the long term climate change, increased concentration of greenhouse gases possibly due to increased anthropogenic activities in the lower atmosphere and their imprint in the middle atmosphere. The circulation of the middle atmosphere system determines the residence lifetime of minor species in the atmosphere and their impacts on the structure of the ozone layer in the stratosphere [e.g., Karoly, 2003].

Despite many observations and simulation studies (based on the input, mostly from high- and mid-latitudes), in the middle atmosphere, the quantitative information from tropical and sub-tropical latitudes and coupling between various geophysical processes is still not fully understood. Therefore, quantifying and understanding the underlying process associated with subtropical region is an important step and is likely to contribute in improving numerical models [e.g., Randel et al., 2004].

In view of the above mentioned scientific issues, there is a pressing need to monitor middle atmospheric temperature with high temporal and spatial resolution by having well distributed network of lidars and other instruments. In the past, most of the lidar studies were limited to mid- and high-latitude stations and few in tropical latitudes and very few from sub-tropical region. There are no systematic long term temperature measurements reported from sub-tropical latitudes in India. Rayleigh lidar, located at Mt. Abu (an Indian sub-tropical station) is operational and has collected data for about 60 nights per year since 1997 (described in Chapter 2). Temperature climatology based on observations during 1997 to 2001, is presented.

3.1 Observations and Data Analysis

The Lidar was operated in Rayleigh mode for about 5 to 10 nights in each month around new Moon except during the monsoon season. Photon counts integrated for 5/10 minutes were stored in each data file. The total number of nights of operation in different months during which good quality data were obtained is given in Table 2.3 Data are available for more than total 20 nights for most of the months and about 10 nights each in May, June and September. No measurements could be made during the months of July and August due to cloudy sky condition. Off-line data processing involves adding the photon counts of 5 range bins to give effective range bins of 480 m each. A five point linear running mean was applied to further smooth the photon count profile. The background noise was removed at this stage, by estimating the average photon counts above 90 km, which was subtracted from each bin. Range correction was then applied and the density values are were obtained from the range corrected photon count profile. The pressure value from CIRA-86 model [Fleming et al., 1990] was fitted at 85 km to derive the temperature profile. The uncertainty in model pressure at top of the profile is about 10-15 %. Its contribution to derived temperature decreases rapidly and becomes less than 2% at about 12 km from the top [Hauchecorne and Chanin, 1980]. Finally, the measurement error in temperature (1 σ) was computed. The temperature profile was derived from the relative density profile following the method described in

Chapter 2. The derived temperature profile up to 75 km, along with the error (one sigma level) is shown in Figure 3.1. A study was made on the error in derived temperature as a function of data length and range width. The data sequence of 4 hour was made during the night of October 21, 2001. Temperature profiles were obtained from this data set using different data lengths corresponding to 10, 30, 60, 90, 120, 180 and 240 minutes. Figure 3.1 also shows the variation of the error with altitude for different data lengths. The error for 10 minutes of data length varies from 1 K at 40 km to more than 30 K at 70 km. For a data length of 30 minutes, these vary from about 0.5 K at 40 km to 20 K at 70 km. The errors vary from less than 0.5 K at 40 km to 15 K at 70 km for 60 minutes of data length and from less than 0.5 K at 40 km and 11 K at 70 km for 120 minutes of data length. For studying climatology, data has been used from 1997–2001 and for detailed comparative study (presented in next Chapter 4) data from other available stations during this period was also used.

3.2 Accuracy

Though, a detailed description of error is given in Chapter 2, here we present these very briefly in the context of climatological features of the thermal structure. Errors affecting the measurements may be divided into two parts, the statistical errors and systematic errors. It is rather easy to evaluate statistical errors due to the photon counting. For the climatological study, average nighttime profiles with $\sim$ 480 meter vertical resolution were used, and integrated for 2 to 4 hours, yielded temperature with errors less than 1 K in 30–50 km region and less than 5 K in 50–70 km region.

Variations of error in the derived temperature with increasing integration time using lidar data of 21 October 2001 is shown in Figure 3.1 . Source of systematic errors is optics and electronics of the system, which are very difficult to evaluate. In order to estimate these errors, temperature profiles obtained simultaneously at the two lidar sites during 65 nights were been compared by Hauchecorne et al., [1991]. At all altitudes, between 30 and 80 km, this difference has been found to be less than 2 K. Neither a facility of rocketsonde nor other lidar is available near

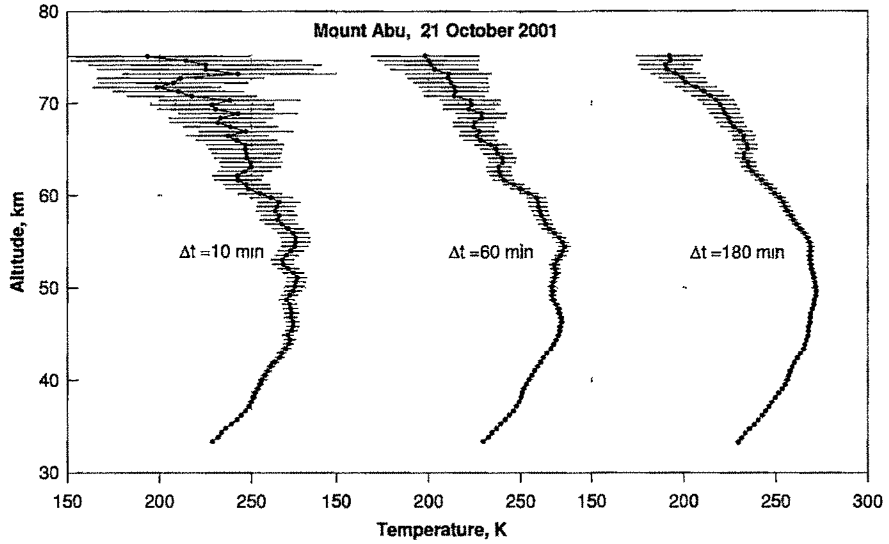

Figure 3.1: *Effect of temporal integration on error in observed temperatures is shown for 10, 60 and 180 minute observations.*

to the present lidar observation site at Mt. Abu, hence in this study also we have considered systematic error of similar magnitude (< 2 K).

3.3 Results

3.3.1 Observed Mean Temperature over Mt. Abu

Mean temperature profiles have been computed from the observed nightly mean temperature variation over Mt. Abu. The mean monthly temperature climatology based on the entire data for about five years is shown in Figure 3.2. The contour shows the mean temperature as a function of month and altitude, from September to May. The number of observations are less in September due to extended monsoon period during most of the years, while no measurements were possible during July and August due to the monsoon season as mentioned earlier. Temperature values do not show prominent variability up to $\sim$ 40 km from September to May. Nevertheless at $\sim$35 km, temperature in March is less ($\sim$ 235 K) as compared to the other months. Similarly, at 40 km lower temperature is recorded during Jan-

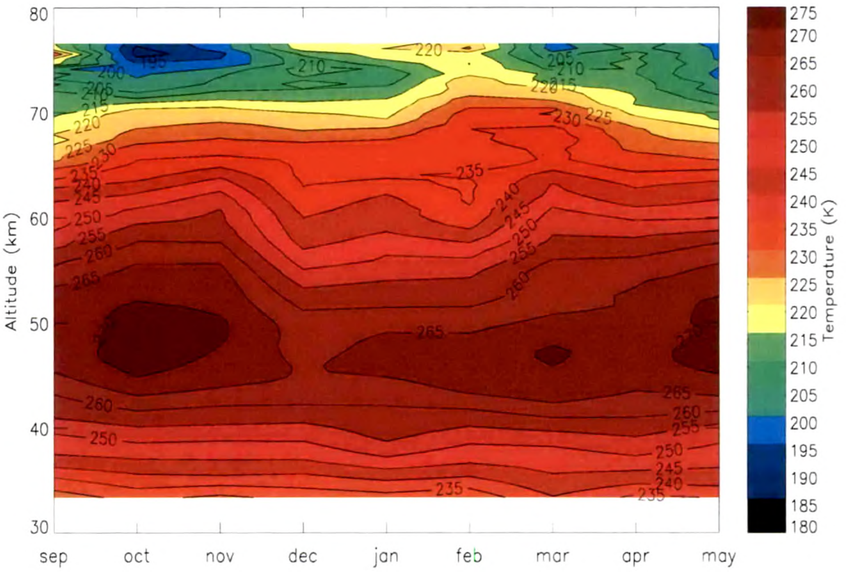

Figure 3.2: *Mean temperature climatology (1997-2001) over Gurushikhar, Mt. Abu.*

uary. During vernal and autumn equinoxes, September-October and March-April, respectively, warm temperature ($\sim$270 K) pools have been found. Interestingly, vernal equinoctial warming is temporally and spatially localized. Though, autumn equinoctial warming pool is bit extended with maximum during March. Another maximum $\sim$ 270 K is again seen during May . The coolest stratopause is seen during local winter months and minimum temperature is noted during December. It should be noted that we have not considered the days of major Stratospheric Sudden Warming (SSW) in climatological temperatures described in this section.

Mesospheric temperatures also show a semi-annual oscillation (SAO) which is stronger and very clear at $\sim$ 60 km. From 55 to 70 km, maximum temperature is observed during October and March with a minimum during local winter (December-January). Above 70 km minimum temperatures were observed during the equinoctial ($\sim$ 195 K) months with a maximum during February ($\sim$ 220 K). As above 70 km the signal to noise ratio is poor and errors in temperature measurements are more than 10 K, any variability or observed changes in theses altitudes

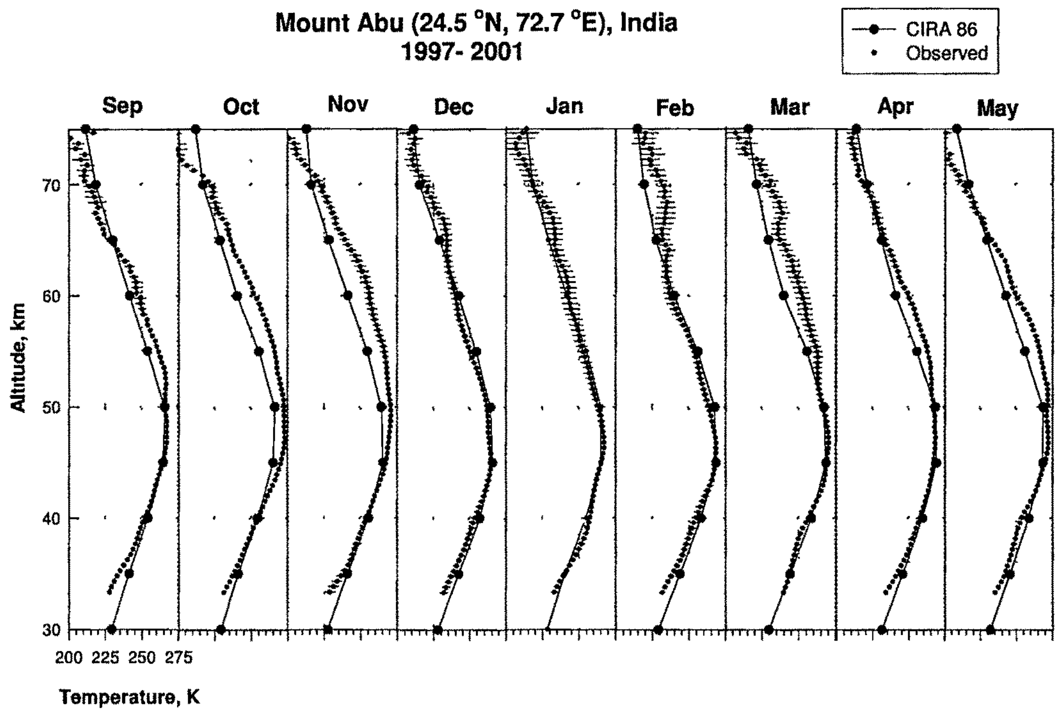

Figure 3.3: Month to month temperature variability over Mt. Abu.

may not be statistically significant if it is less that 10-12 K. Higher temperatures are observed during February–March in the altitude region 65-72 km. This is due to frequent occurrence of Mesospheric Temperature Inversion (MTI) during these months. Occurrence of MTI and their characteristics are discussed in Chapter 5. Observed temperature climatology over Mt. Abu has been compared, with satellite data, model and similar observations from other stations, in the next chapter. Line plots of the mean monthly temperatures are shown in Figure 3.3 along with CIRA-86 temperatures.

3.3.2 Day to Day Variability

Daily temperature profiles during the months of January, May and October during 2001, are shown in Figure 3.4 to study day to day variability. Selected months, January, May and October, represent winter, summer and equinox, respectively.

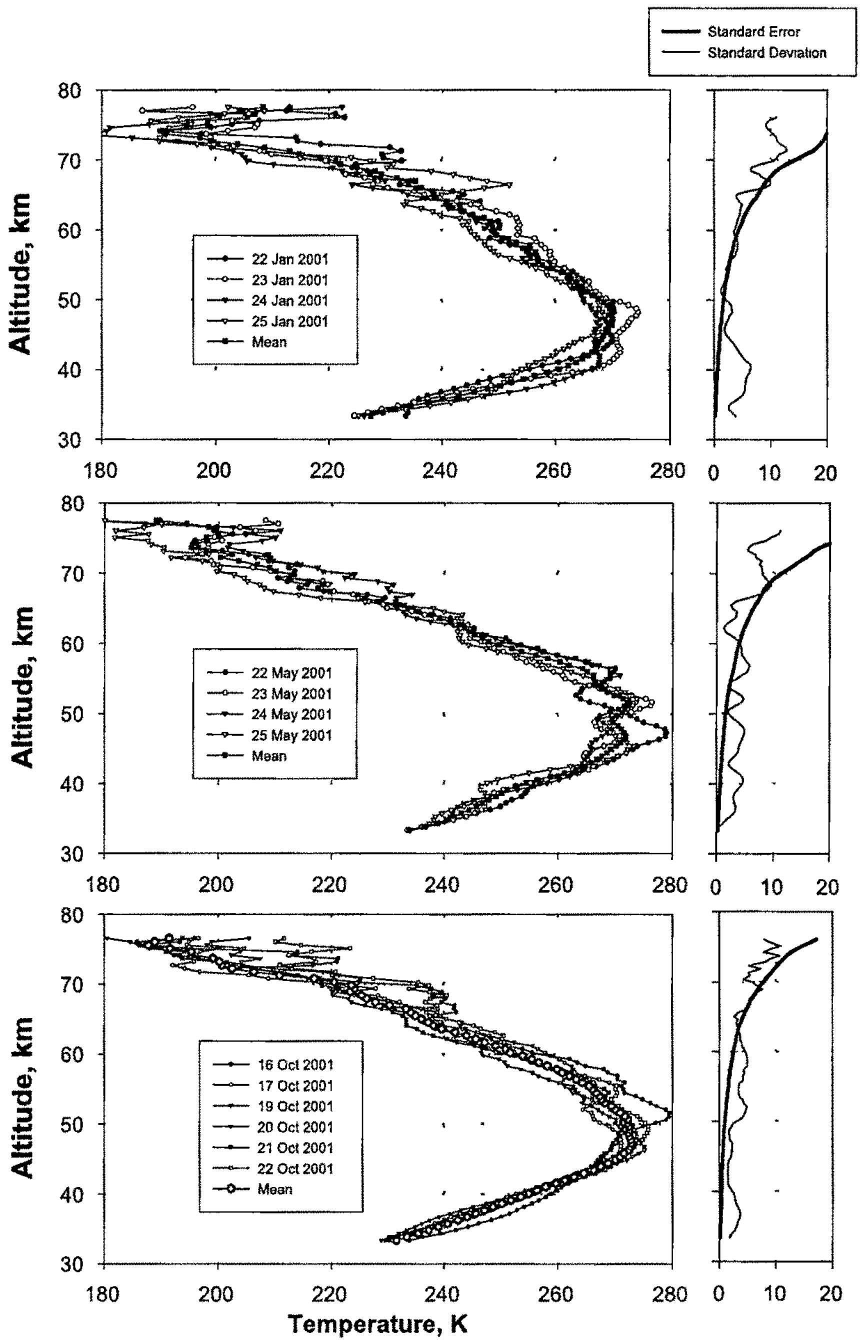

Figure 3.4: Day to day temperature variability during different months over Mt Abu.

Top panel of Figure 3.4 shows temperature profiles on each of the four nights of 22-25 January 2001 and a mean profile of all four nights. The geophysical variability (described by the standard deviation of the measured values) and the standard errors in measurement are also plotted in the side panel as a function of altitude. The temperature values are relatively higher on 23 January as compared to other days. Increased Planetary Waves and Gravity Waves activity during northern hemisphere winter [Gobbi et al., 1995; Shepherd, 2007] are mainly contributing to these observed changes. Temperature profiles for four nights from 22 to 25 May 2001 and the mean monthly profile of May 2001 are shown in the middle panel of Figure 3.4. Signatures of gravity waves are clearly noticed on each of the four nights. The standard deviation is within 2-5 K below 65 km and about 10 K above 65 km. However, in view of the error being more than the standard deviation above 65 km, this may not be considered significant. In the bottom panel of Figure 3.4, temperature profiles are shown for the nights of 16, 17, 19-22 October 2001 and the monthly mean profile. The standard deviation again varies between 2 K and 10 K with lowest values in the region of 40-50 km. Below 60 km, the standard errors in measurements are less than the standard deviation, whereas above 70 km, the errors in measurements are greater than the standard deviation. The altitude variation of the standard deviation for January 2001 shows high values around 40 km (7 K) and 70 km (10 K) with a minimum around 51-52 km (1K). The standard deviation during May 2001 shows fluctuations between 3 and 5 K up to 65 km and a peak at 68 km (10 K). The altitude variation of the standard deviation for the month of October 201 shows peaks around 37 km (4 K), 52 km (5 K) and 69 km (8 K) with low values of 1-2 K between 41 and 49 km. The regions of minimum variability in January is between 50-60 km and during the October month the variability is minimum in 40-50 km height range. Similar day to day variability has been reported from lidar observations over a mid-latitude station, Aberystwyth (52.4°N, 4.1°W) [Jenkins et al., 1987] and short term variabilities have been reported by Hauchecorne et al., [1991] over Observatoire de Haute Provence (OHP)(44°N, 6°E).

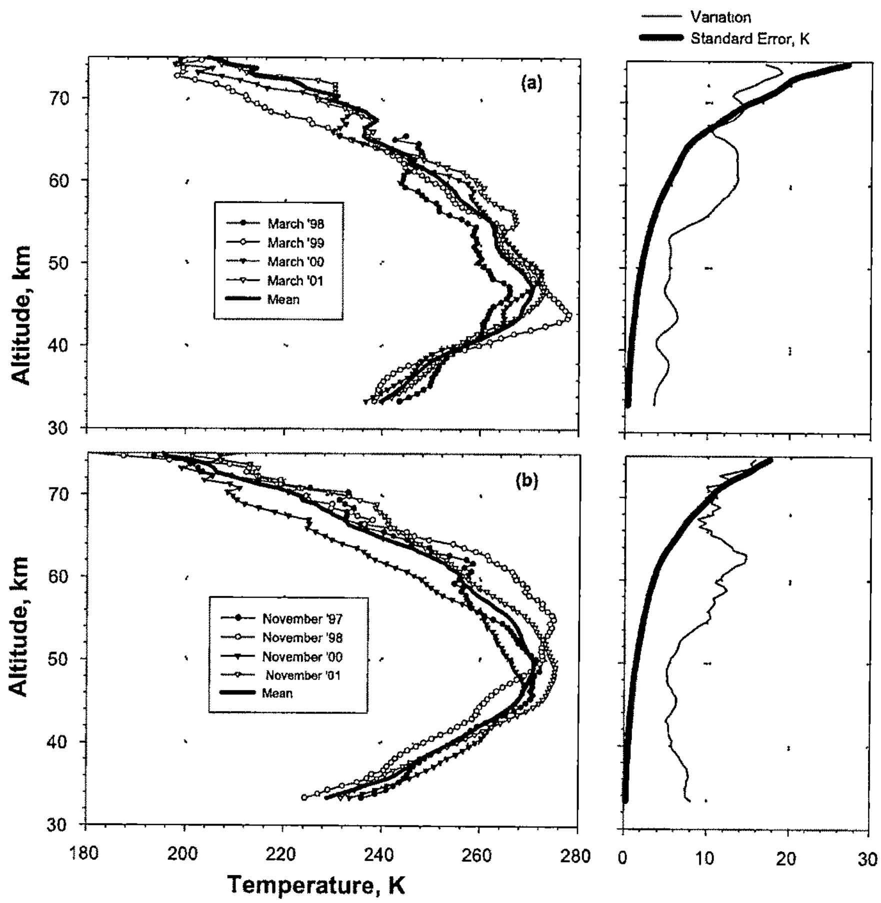

Figure 3.5: Year to year temperature variability over Mt. Abu.

3.3.3 Interannual Variability

Mean monthly temperature profiles have been estimated for different years to examine the interannual variability in the thermal structure. Top panel of Figure 3.5 shows the mean monthly profiles for the month of March during the years 1998 to 2001. The standard errors in measurement and the standard deviation are also shown in the side panels. The standard deviation is least (4 K) around 40-42 km and values close to 5 K at altitudes below 53 km. The standard deviation values show a peak of 14 K between 60 and 67 km. Higher values are seen above 70 km but the errors are larger there. Similar plots for the month of November for the years 1997 to 1998 and 2000 to 2001 are shown in the bottom panel of Fig-

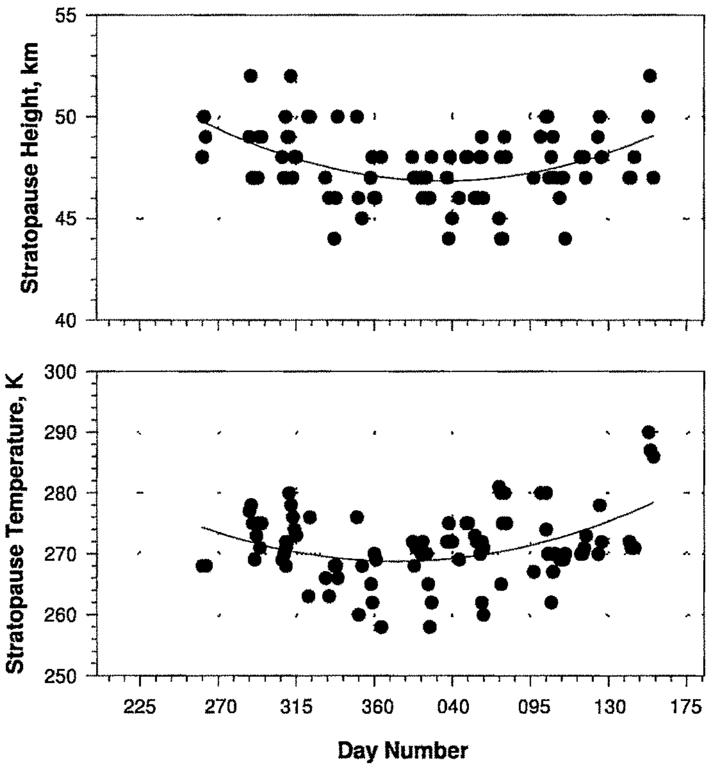

Figure 3.6: Observed stratopause height and temperature variability over Mt Abu.

ure 3.5. Year to year variability is very prominent above 50 km. The variability is least around 40-50 km with a value of 5 K. It is found that the region of minimum interannual variability lies near the height of stratopause for most of the months. Standard deviation values are 15 K at 35 km and 62 km. The standard error exceeds standard deviation values above 70 km. Thus the results of Figure 3.5 clearly indicate a trend of lower variability in the region 40-50 km.

3.3.4 Stratopause Height and Temperature Variability

The stratopause temperature and altitude level are derived from each individual profile of the observed temperature to study the stratopause variations in detail. The scatter plots of the stratopause height and the stratopause temperature for the period 1997–2001 are shown in Figure 3.6. There is a clear indication of an

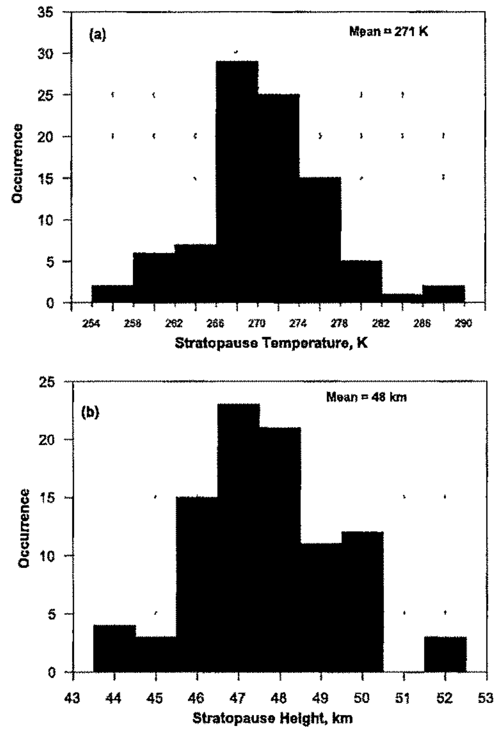

Figure 3.7: *Histogram showing stratopause variability over Mt. Abu.*

annual variation in both the stratopause temperature and height showing lowest values during winter months indicating a trend of maximum during local summer months. There is a significant day to day variability and for any month the difference between minimum and maximum values is about 15 K in temperature and about 5 km in the altitude of stratopause.

Different temperatures and heights of the stratopause occurrences are shown in Figure 3.7 in the form of histogram. The temperature varies between 254 and 290 K with 95% of values between 258 and 282 K. The mean value of the stratopause temperature is 271 K with standard deviation of 5.7 K. The stratopause height varies between 44 and 52 km with a mean value of 48 km and standard deviation of 1.7 km.

3.3.5 Stratospheric Temperature and its Association with Ozone

Stratosphere and mesosphere have an entirely different thermal structure (positive temperature gradient in the stratosphere and negative in the mesosphere). Therefore, associated geophysical processes in these regions are also different. Stratosphere is very stratified and less turbulent due to its stable thermal structure and mesosphere is turbulent due to negative temperature gradient. Stratospheric processes are strongly coupled with the stratospheric ozone due to maximum ozone in this region (at about 27 km). In order to quantify stratospheric processes, the study of ozone, its association with temperature, and their interdependence, is indispensable. Stratospheric thermal structure has strong imprint of ozone and it is steered by the heating caused by UV absorption by the stratospheric ozone [Robock, 1996; Cagnazzo et al., 2006]. Column averaged lidar observed temperature from 30-50 km is shown in the top panel of Figure 3.8.

Columnar ozone density from Total Ozone Mapping Spectrometer (TOMS) along with lidar observed temperatures over Mt. Abu have been used for the study of association between temperature and ozone during 1997-2001. Monthly mean values of the columnar ozone are plotted in the middle panel of Figure 3.8. A scatter plot of ozone and lidar temperatures shows good correlation with a correlation coefficient of 0.61 as can be seen in the bottom panel of Figure 3.8. This further strengthens the fact that ozone plays a very vital role in stratospheric thermal structure over a sub-tropical location also [e.g. Leblanc et al., 1997; Shepherd, 2007]. The stratospheric temperature is mainly governed by concentration of ozone as ozone absorbs solar UV radiation. And temperature affects ozone concentration, as in its formation and or loss reactions rate are temperature sensitive. Therefore, ozone and temperature are highly interdependent in the middle atmosphere.

However, the column averaged temperature has oscillatory behavior and small deviations of few degrees are also noted. These differences in variations are attributed to different observational platforms, resolutions and over and above the local processes which are mostly dynamically driven. Recently, Pawson et al., [2008] explored link between the stratospheric thermal structure and the ozone distribution using chemistry-climate model (CCM). They validated ozone and tem-

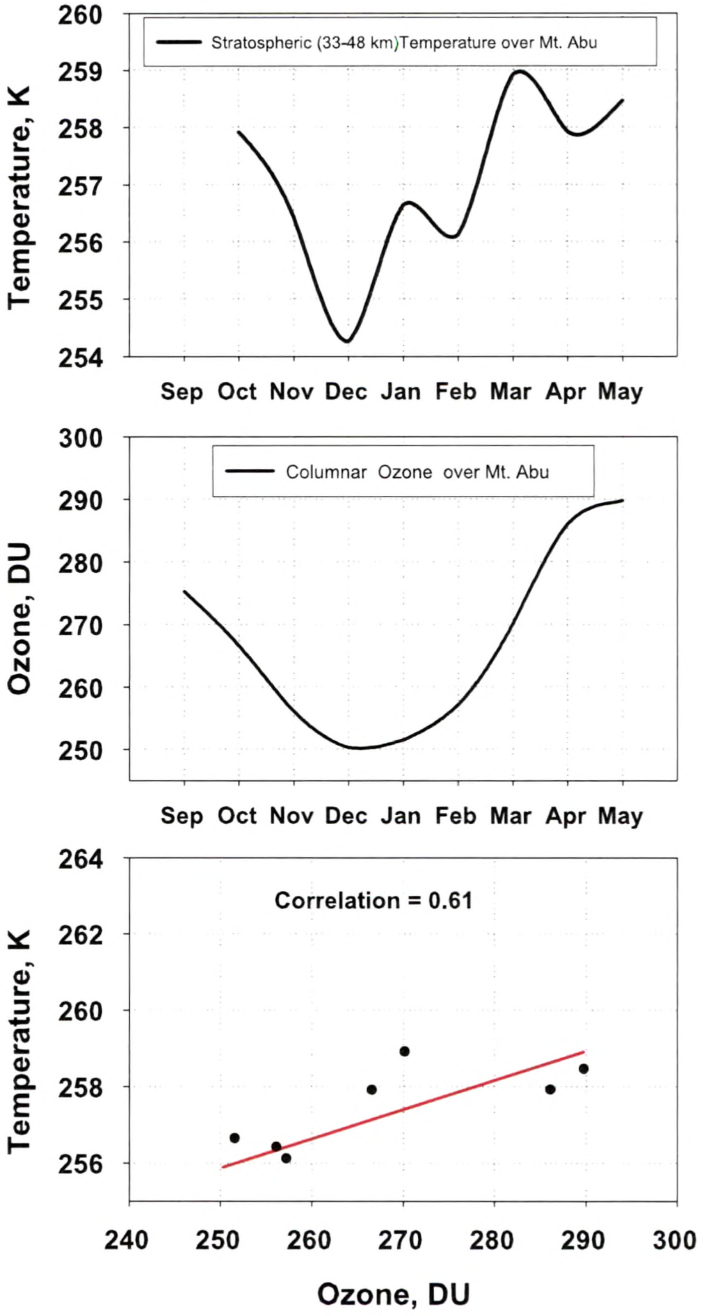

Figure 3.8: *Stratospheric temperature and column averaged ozone over Mt. Abu. Correlation between stratospheric temperature and ozone is shown in bottom panel.*

perature fields using estimates based on observations. Their ozone-change experiments revealed that the thermal structures of the general circulation model (GCM) and CCM respond in a similar manner to ozone differences between 1980 and 2000. The total ozone concentrations are low ($\sim$ 250 DU) in the tropical and subtropical regions. Therefore, ozone concentrations are highly sensitive to the changes in the temperature and vice versa. Additional description of ozone and temperature is presented in Chapter 6.

3.3.6 Monthly Temperature Deviations over Mt. Abu

For a detailed quantitative scenario of monthly temperature variations, temperature differences from the annual mean temperature are given in Table 3.1. Temperatures are shown at every five km between 35-70 km covering months from September to May. Minimum temperature was found in the month of December at an altitude of about 55 km and the maximum temperature in March at an altitude of about 70 km. It is to be noted that in this altitude range measurement errors are also high.

Table 3.1: Monthly temperature deviations over Mt. Abu.

Height (km)	Sep	Oct	Nov	Dec	Jan	Feb	Mar	Apr	May
35	-5.2	-1.3	-1.3	-1.5	1.1	-0.6	4.2	2.2	2.4
40	-2.9	-0.2	-0.8	-1.5	2.5	-0.3	1.7	2.5	-1.0
45	-2.7	3.1	0.1	-3.2	-1.7	0.3	1.7	-0.3	2.7
50	-0.6	5.4	3.9	-4.9	-3.8	-3.9	-0.7	-0.1	4.8
55	0.8	6.2	6.2	-10.3	-7.5	-7.0	2.3	2.8	6.2
60	-0.5	4.8	8.9	-7.1	-4.3	-10.6	5.0	1.7	2.1
65	-6.7	2.1	5.1	0.4	-0.1	-1.9	3.3	-0.9	-1.2
70	-8.9	0.9	1.3	-1.7	-2.1	10.8	11.2	-2.5	-9.1

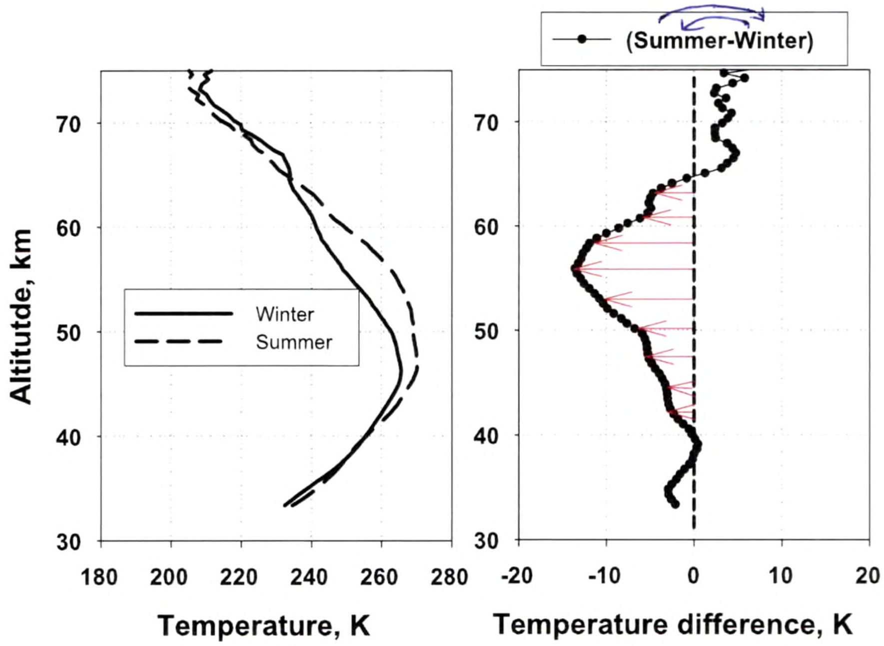

Figure 3.9: Winter and summer time temperature differences observed over Mt. Abu.

3.4 Winter and Summer-time Differences in Temperature

The wave activity is significantly different in the northern and southern hemispheres and also has prominent seasonal differences [Chen et al, 2002; Chen and Li, 2007 and reference therein]. In the northern hemisphere, wave activity is different during summer and winter months as planetary wave activity is stronger during winter months than during summer months. Fluctuations of the northern hemisphere atmospheric circulation are usually characterized by large-amplitude stationary waves [Branstator, 1984; Ting et al., 1996].

Apart from effects of ozone on the thermal structure, waves are the second major source of temperature variability in the stratosphere and in the mesosphere. During winter months planetary wave activity is very strong and while propagating from lower to middle atmosphere, it modulates atmospheric temperature structure. For studying temperature differences for local winter and summer months over Mt. Abu, data are averaged for winter (December-February) and summer (April-June) months. Vertical structure of temperature during winter and summer is shown in Figure 3.9. It is found that there is a strong cooling during winter months, with a maximum magnitude of about 12 K at an altitude of about 55 km. Errors in the derived temperature are $\sim$ 1 K in this altitude region. Therefore, observed difference in the thermal structure during winter and summer is significant and these are in agreement with the earlier mid-latitude observations [Keckhut et al., 1996] and model results. Observed cooling over Mt. Abu during winter is in line with the observed seasonal variation of ozone reported over a sub-tropical location Mauna Loa and has been shown in Figure 2.2 [Leblanc et al., 2000]. Another interesting feature noted is that there are two low temperature regions (Figure 3.10). First minimum temperature is in the month of December and second minimum is in the month of February. The heights of cold temperature pools are also different; second cool pool in February occurs at slightly higher height ($\sim$ 60 km) than the December cool pool ($\sim$ 55 km). This type of modulation is possible due to enhanced planetary wave activity in winter months. Though, events of SSW are observed during winter months, it was expected there will be warming episodes, but on the contrary we noted significant cooling. It should be noted that only few very strong SSW events have affected temperature structure of sub-tropical latitudes. Detailed study of SSW is presented in Chapter 5.

3.5 Middle Atmospheric Heating and Cooling Rates over Mt. Abu

The middle atmosphere heating and cooling rates are described in this section. Deviations from the annual mean temperature profile for each month have been estimated and a height versus months contour plot of the monthly mean deviations are shown in Figure 3.10. There is a very clear cold temperature pool with two eyes type of structure during December and February as mentioned earlier. Although there is warmer temperature during equinoxes, warm temperature pools observed during both the equinoctial months (vernal and autumn), are showing

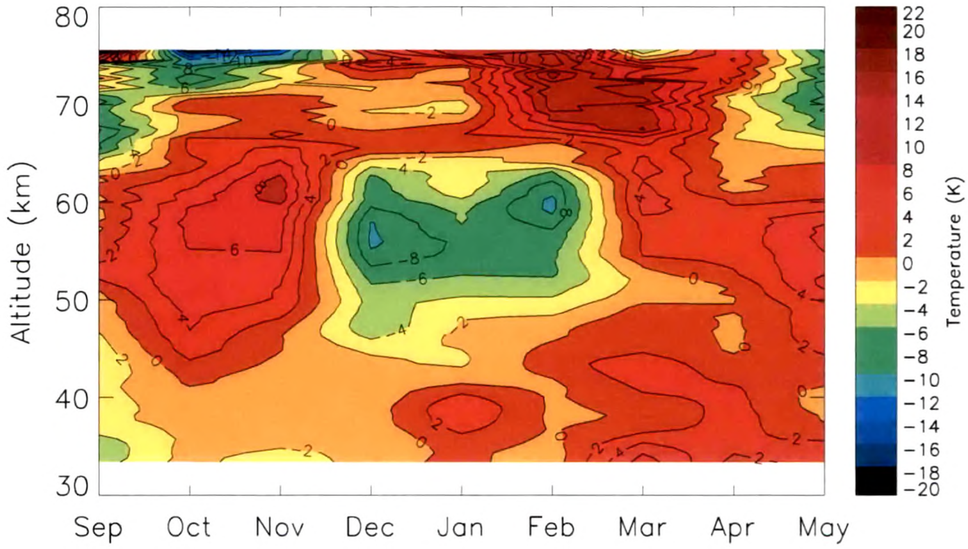

Figure 3.10: *Monthly temperature deviation from mean temperature observed over Mt. Abu.*

entirely different features. During vernal equinox, there is very strong gradient in the temperature showing upward trend with heating rate of about 2.5 K/month. Inception of warm pool is in the month of October at 45 km and has upward trend and disappears by end of the November. In contrast, during autumn there is a downward trend of warm temperature pool. It first appears in the mesosphere at height of about 72 km and then recedes downward upto the altitude of 45 km in the stratosphere. It may reach further down in altitude during June and July but observations are not possible due to local monsoon. The rate of cooling (from March to May) is about 1 K/month and has tendency of downward propagation, from mesosphere to down upto the stratosphere. These features have been observed first time in the temperature climatology over a sub-tropical location. These results are further compared , contrasted and discussed with model, satellite and observations at other locations in the next chapter.

3.6 Discussion

Temperature climatology gives important new insights in the middle atmosphere as highlighted by all previous middle atmospheric temperature climatologies. A dominant annual cycle is observed at mid-latitudes and a semiannual cycle is dominant at lower latitudes. But behavior over a sub-tropical location is still not clear due to lack of systematic observations in these region.

In the present study, we found signature of quasi annual cycle with minimum temperature during winter and higher temperature during both the equinoxes. The observed downward propagating temperature behavior in the mesosphere points out the dominant wave driven pattern, in contrast with the vertically stationary behavior observed below 45-50 km. Over Mt. Abu the dominant semiannual cycle is modulated by the northern mid-latitude annual cycle, thus contributing, together with the seasonally asymmetric SAO, to the first warm-cold cycle (equinox and winter) being stronger than the second (winter and equinox). Similar finding has been reported from the Lidar observations at Mauna Loa another sub-tropical, high altitude station in the northern hemisphere. Maximum variability in the mesosphere is observed in winter over Mt. Abu which is due to a) maximum planetary wave activity in winter and b) due to the occurrence of the mesospheric temperature inversions. Observed statistics and characteristics of mesospheric temperature inversions over Mt. Abu are presented in Chapter 5.

In the stratosphere also, variability is strong during winter months over Mt. Abu, possibly due to dominance of gravity waves of orographic origin (Mt. Abu is located in hilly terrain, shown in Figure 2.1) and stronger planetary waves. Leblanc et al., [1998] showed latitudinal gradient in temperature with decreasing variability from the mid-latitude to the lower latitudes. Observed variabilities over Mt. Abu are in reasonable agreement with findings of Leblanc et al., [1998]. Instead of steady cooling and warming in the stratosphere and mesosphere (as predicted by the vertically and temporally smoothed CIRA-86 model), some short periods of strong cooling and warming are observed. Systematic departures from the CIRA-86 model were observed which are in agreement with the similar results of previous comparisons [e.g., Hauchecorne et al., 1991; Clancy et al., 1994; Sivakumar et al., 2003].

Detailed comparison of the observed thermal structure with models is presented in next chapter. Above Mauna Loa, it is more likely that most of the observed departure in the middle and upper mesosphere is related to tidal effects and/or the mesopause thermal SAO. The amplitudes of 1-5 K was predicted by tidal models [e.g., Hagan et al., 1995]. The climatology presented in this chapter was obtained using composite temperature profiles from five years of measurements. A non negligible interannual variability may disturb the temperature field from year to year. However, the features already observed in previous climatologies [e.g., Hauchecorn et al., 1991; Hood et al., 1993] remain small compared to the seasonal variations. A study on temperature trends (11-year solar cycle) over Mt. Abu is presented in Chapter 6.

Stratospheric cooling and warming are associated with the concentration of ozone and CO_2 [Wang et al., 1992; Ramaswamy et al., 2001; references therein]. In the present study also a reasonable correlation is found (R^2=0.61) in observed stratospheric temperature and total column ozone over Mt. Abu. Observed temperature cooling during the months of December and January is also in agreement with the the climatology presented by Randel et al., [2004]. We found admixture of tropical and mid-latitude processes in the observed temperature features over Mt. Abu. Huang et al., [2005] reported that there is circumstantial evidence that the stratospheric temperature oscillations (heating or cooling) could be driven by the meridional winds, which in turn could be generated by wave generation and interaction and concluded with a statement, "more definite conclusion, however, must await simultaneous coordinated temperature and wind measurement at common altitudes". However, it is worth noticing that two maxima appearing in the 54-65 km during April–May and September–November over Mt. Abu are in corroboration with the secondary maxima in gravity wave activity observed by Gobbi et al., [1995] in the mid-latitudes. Part of the variability of monthly averages and climatology over Mt. Abu can be explained by mesoscale fluctuations with temporal and spatial scales long enough and not filtered out on single observation session during a night. gravity waves are primarily responsible for these short-scale and short-term fluctuations [Wilson et al., 1990]. This is mainly due to natural day to day variability of gravity wave activity induced by changes in low level forcing and mean winds [e.g., Gobbi et al. 1995].

Observations over Mt. Abu revealed that the average height of stratopause is $\sim$ 48 km which is in agrement with observed mean height of stratopause at Gadanki [Sivakumar et al., 2003] and with rocket measurements from Trivandrum [e.g., Mohankumar, 1994]. The spread in stratopause height is about 9 km over Mt Abu, which is in reasonable agreement with mid-latitudes, the spread has a maximum of about 12 km in winter and $\sim$6 km in summer. Observed stratopause temperatures over Mt. Abu are higher than those are at Gadanki [Sharma et al., 2006]. This is attributed to the higher orographically generated gravity waves, which propagate upwards and have significant contribution in causing double stratopause and higher temperatures.

The use of such a complete climatology is important for many purposes such as providing a reference atmosphere for models, validation of satellite based instruments, an overall comprehension of the strongly coupled lower-middle-upper atmosphere, etc. To this date, only a few instruments can provide such good quality long term temperature data. With the recent and future development of many ground-based lidars at many latitudes in India, a more complete climatology of the middle atmospheric temperature in the low and sub-tropical latitude should be available in the coming years based on larger data base.

3.7 Summary

Temperature climatology has been established using data from Nd-YAG laser based Rayleigh Lidar over Guru Shikhar, Mt. Abu. In this study the temperature structure in the altitude region of 30-75 km at sub-tropical latitude is investigated in detail. Day to day variability is less than about 5 K for altitudes below 50 km and up to 10 K around 70 km. The variability is the least around 40-50 km. The mean values of the stratopause level and temperature are found to be 48 km and 271 K, respectively over the measurement site. Seasonal variation of the temperature below 60 km shows equinoctial and summer maxima whereas above 70 km, winter maximum with equinoctial minima are seen. The year to year variability is less than 10 K below 50 km and up to 20 K above 50 km. The variability is also least around 40-45 km. The stratopause level varies between 44 and 52 km with a mean value of 48 km. The stratopause temperature varies between 260 and 280 K with a mean value of 271 K. Both the stratopause height and temperature are lowest during winter months. Significant difference in winter and summer temperatures is found; winter is about 12 K cooler than the summer in the height range of 45-65 km. A cold winter pool is found in altitude region of about 45-60 km and in both the equinoxes warm temperature pool with upward and downward propagating tendencies are also observed. Good correlation with total column ozone and stratospheric temperature is found over Mt. Abu. It is to be noted that temperature climatology over Mt. Abu is in closer agreement to the climatological features of mid-latitude rather than low latitude.

CHAPTER 4

Thermal Structure over Mt. Abu: Comparison with Models and Other Observations

Thermal structure observed over Mt. Abu is compared with empirical model temperatures, satellite observations and also with lidar observations over other locations and is presented in detail in this chapter. One of the major objectives of this comparative study is to address the issue of how adequately the models represent the thermal structure over sub-tropical latitudes. In addition, comparison with similar observations over other locations will provide a clear view of the middle atmospheric processes operative in the sub-tropical locations and their association with tropical and mid-latitude processes. In view of very sparse lidar observations in this region, present study will play a very important role in understanding the intricacies involved in sub-tropical processes and their latitudinal coupling with other regions.

Empirical models of the stratosphere, mesosphere and thermosphere are indispensable tools used by middle and upper atmospheric research communities. These are used for data analysis, initialization of detailed physics-based models, and mission and instrument design also. Two empirical models namely CIRA-86, MSISE-90 are very important and are being extensively used by middle atmospheric research community. Concrete basis for COSPAR International Reference Atmosphere-86 (CIRA-86) model was laid by Barnett and Corney, [1985]. They reported, middle atmospheric climatology using Pressure Modulated Radiometer (PMR) and Selective Chopper Radiometer (SCR) data for the period of 1975–1978. The results became backbone for CIRA-86 model, which provides a good reference model for latitudinal, longitudinal and seasonal variations in the middle atmospheric temperature and other atmospheric parameters. But it was unable to reproduce variability of short-term and long-term fluctuations at higher altitudes (above 60 km). Clancy and Rusch, [1989] improved the CIRA-86 on the basis of global observations of UV Limb radiances from the SME satellite data for the period of 1982-1986. Another empirical model used in this study is Mass Spectrometer - Incoherent Scatter Extended (MSISE-90) model [Hedin, 1991]. This is an empirical model for the temperature and composition of the atmosphere at heights between 0 and 700 km. Spectrometer data from various satellites and incoherent scatter radar data from several sites form the basis of the MSISE model. In addition to CIRA-86 and MSISE-90, Indian low latitude model [Sasi and Sengupta, 1979; 1986; Sasi, 1994] have also been used in this study. Indian low latitude model is largely based on the radiosonde measurements at Minicoy (8.3°N, 73.2°E), Trivandrum (8.5°N, 76.9°E), Port Blair (11.7°N, 92.7°E) and Chennai ((13.1°N, 78.4°E), and the M-100 weekly rocket flights from Thumba (Trivandrum).

Lidar observed temperatures over Mt. Abu are also compared with satellite observations (HALOE onboard UARS) over and near to the lidar location. There are very few lidar stations operational in the tropical and sub-tropical regions for sufficiently long period to yield temperature climatology. Therefore, in addition to comparison with model results and satellite observations, temperature climatology over Mt. Abu is also compared with the lidar observations over following four locations in the tropical, sub-tropical and mid-latitude region in the northern and southern hemisphere viz., Gadanki, Mauna Loa , Observatoire de Haute Provence, OHP and Reunion Island. This will further facilitate in understanding latitudinal coupling of middle atmospheric processes on a global scale.

4.1 Data and Methodology

Lidar data over Mt. Abu collected from 1997 and the temperature data obtained during 1997 to 2001 are utilized for comparative study. In addition, a comparative study of temperature structures over Mt. Abu and Gadanki during March, April and May 2002–2004 is also presented. HALOE (onboard UARS) data have been used for the satellite passes in $5 \times 5°$ latitude-longitude grid of the lidar location at Mt. Abu. For comparison with other locations, we have used data available at Network for the Detection of Atmospheric Composition Change (NDACC) web site and for few stations, published data have also been used. It should be noted that, as for as possible, other stations, data have also been taken for same/similar period while comparing or contrasting the observed features.

4.2 Comparison with Empirical Models

For comparison with the models, monthly mean temperature profiles have been computed from the available temperature profiles over Mt. Abu.

4.2.1 Comparison with CIRA-86

CIRA-86 model profiles have been taken for the location of 25°N. Figure 4.1 shows the contour maps of the temperature structure obtained from lidar observations and CIRA-86 model. There does not seem to be significant change in the temperature values with month below about 45 km in either the observed or model values. Small but significant deviations are seen below 35 km for almost all the months. The observed temperature values are qualitatively in agreement with CIRA-86 model values between 30 to 65 km during the months of December, January and February. For other months, values match below 50 km but are up to 10-15 K higher than the CIRA-86 model values at altitudes of 50-70 km. The differences are largest during equinoxes. Another noticeable difference is in the stratopause region. Lidar temperatures exhibit significant month to month variability in 40-55 km, but CIRA-86 does not show these features.

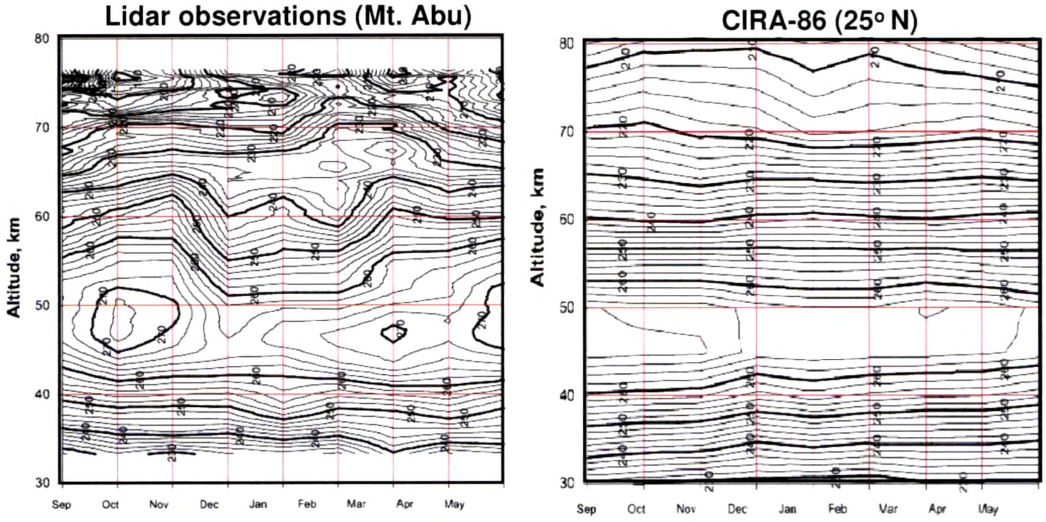

Figure 4.1: Mean annual temperature climatology over Mt. Abu and CIRA-86 model temperature from September to May.)

The contours of the difference between the observed temperature and the CIRA-86 values are shown in Figure 4.2. Below 50 km the differences are less than 5 K. The difference is high around 60 km with values about 15 K during October–November and 10 K during March. Another peak in temperature difference (> 10 K) is noticed during May. The differences are again high above 70 km during equinoctial months; in these altitude region (> 70 km) errors are also large.

Similar but less pronounced deviations were reported from lidar observations over Gadanki [Sivakumar et al., 2003]. Observed stratopause values are slightly higher than the CIRA-86 values and are highest for the equinoctial months of October and March–May as described by model also. Between 50 and 65 km, comparatively larger change with season is seen in the observed values with equinoctial maxima. Above 70 km the model shows winter maximum and summer minimum. The observed values indicate the trend for higher values for January–February. To have a quantitative view of the difference between observed and CIRA-86 model temperatures in the height range of 35–70 at every 5 km are given in Table 4.1. Near 75 km difference is very large (upto about 24 K) and it is attributed to the higher occurrence of Mesospheric Temperature Inversion (MTI) at these altitudes during

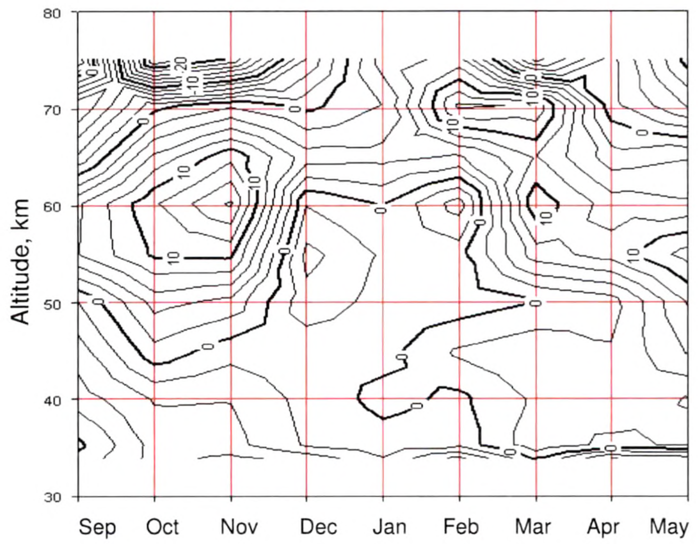

Figure 4.2: *Contours of difference between observed and CIRA-86 model temperature over Mt. Abu.*

winter months. Detailed study of MTI over Mt. Abu is presented in Chapter 5.

Systematic departures from the CIRA-86 model were observed which is similar to the previous comparisons at mid-latitude [Hauchecorne et al., 1991; Clancy et al., 1994]. In particular, cold temperatures in the CIRA-86 model lead to a large difference of more than 12 K around 70–75 km compared to lidar results. This could be due to an overestimation of non-local thermodynamic equilibrium effects in the computation of the CIRA-86 temperatures [e.g., Lawrence and Randel, 1996] and also non consideration of occurrence of Sudden Stratospheric Warming (SSW) and Mesospheric Temperature Inversion (MTI). On an annual basis CIRA-86 temperatures seem to be too warm around 55–60 km and too cold between 60 and 75 km. Using too cold CIRA-86 temperatures at 80–90 km for initialization can lead to temperature errors at the very top of the Rayleigh lidar profiles. In this context the model needs to be improved by using more observational input from sub-tropical locations.

Table 4.1: Temperature difference between lidar and CIRA-86 model temperature over Mt. Abu

Height (km)	Sep	Oct	Nov	Dec	Jan	Feb	Mar	Apr	May
35	-10.5	-5.2	-4.7	-1.7	-0.9	-1.3	3.3	1.4	2.4
40	-7.1	-3.8	-3.9	-1.3	0.7	-0.5	2.4	3.5	1.9
45	-5.1	1.3	-1.3	-0.6	-0.7	2.4	3.6	2.2	6.2
50	-1.9	4.8	3.4	-3.3	-1.3	-1.3	-0.1	1.1	8.2
55	5.8	10.3	10.5	-4.7	-1.7	-0.8	7.1	8.9	12.9
60	5.6	11.7	16.3	-1.9	0.2	-5.0	11.4	6.9	6.3
65	-3.6	6.5	11.5	4.9	4.7	3.7	8.2	2.9	3.8
70	-9.9	-0.8	1.8	-0.6	2.1	14.4	13.7	-1.3	-6.2
75	5.7	-24.1	-19.7	-5.8	5.0	6.7	-8.9	-1.3	-10.9

4.2.2 Comparison with MSISE-90

Figure 4.3 show the difference between lidar observed temperatures and MSISE-90 model temperatures. Model temperatures are taken for 15 of every month over the location of Mt. Abu. There are significant differences in observed and MSISE-90 temperatures. Observed temperatures are lower than the model temperatures during winter months (Dec-Jan-Feb) upto 60–65 km. Observed temperatures during equinoxes are higher than the model. During October and April observed temperatures are cooler by about 10–14 K at an altitude of 60 km. Considering estimation errors at these altitudes (less than 10 K), these are considered significant. Large positive difference is noted in the altitude range 70–75 km from MSISE-90 model, similar to the difference noted with CIRA-86 and it is again attributed to the occurrence of MTIs at these altitudes. Month wise (Sep to May) quantitative difference from 35–75 km at every 5 km is given in Table 4.2. It is found that MSISE-90 model temperatures are more closer to the lidar observed temperature than the CIRA-86 model temperatures.

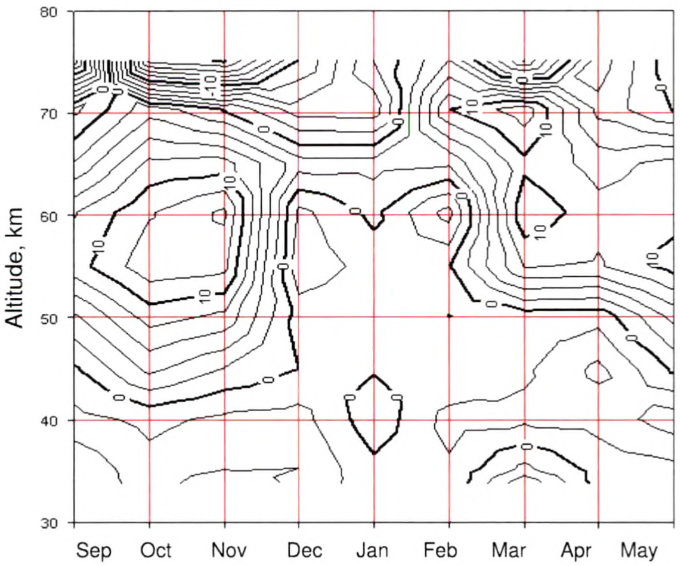

Figure 4.3: *Contour of difference between observed and MSISE-90 model temperature.*

Table 4.2: *Temperature difference between observed and MSISE-90 model temperatures*

Height (km)	Sep	Oct	Nov	Dec	Jan	Feb	Mar	Apr	May
35	-1.5	-0.9	2.4	-1.7	-0.5	-4.0	-3.9	-2.7	-5.5
40	-5.1	-2.7	-2.6	-2.7	1.3	-2.8	-2.5	-1.4	-2.7
45	0.3	-4.5	-1.6	-0.1	-0.2	-0.1	1.8	4.5	-0.4
50	4.8	-1.2	-0.8	-2.0	-0.2	-0.9	7.6	9.0	3.7
55	10.9	7.8	8.1	-0.2	-1.2	-3.4	12.7	13.3	9.1
60	9.2	8.7	11.6	-4.8	0.5	-2.6	14.4	11.8	7.8
65	8.6	7.3	9.5	2.4	2.7	2.9	8.9	8.5	2.1
70	-0.1	3.4	13.2	9.9	-5.3	-5.1	-0.1	3.2	-2.5
75	-1.5	5.1	-8.1	4.0	-2.0	-10.0	-20.3	-18.6	15.0

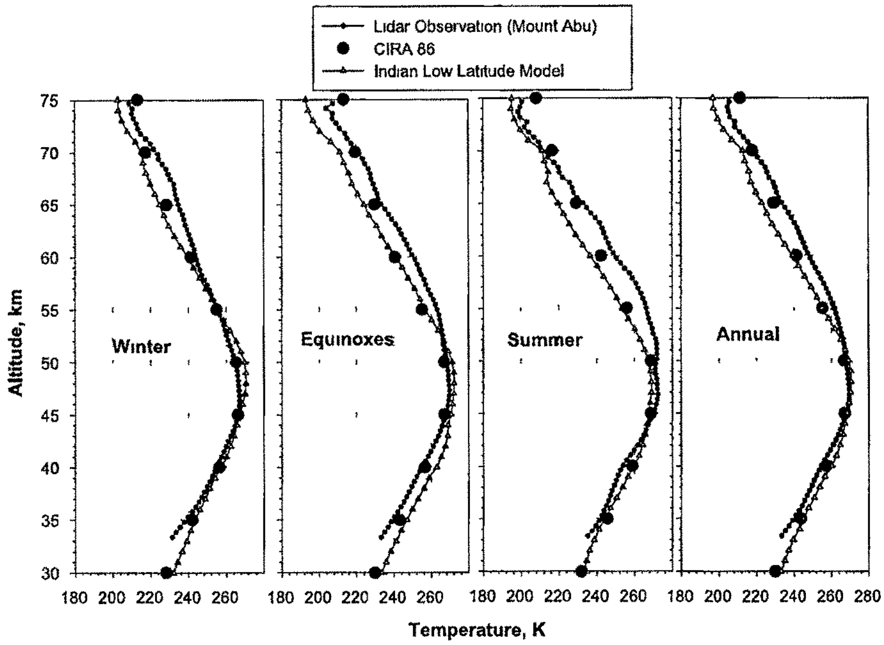

Figure 4.4: *Altitude profiles of the seasonal and annual mean temperature obtained from lidar. Indian Low latitude model and CIRA-86 model temperatures are also shown in the figure.*

4.2.3 Comparison with Indian Low Latitude Model

A reference atmosphere model for low latitudes over the Indian region was made using the radiosonde measurements at Minicoy, Trivandrum, Port Blair and Chennai and the M-100 weekly rocket flights from Thumba (Trivandrum) [Sasi and Sengupta, 1979; Sasi, 1994]. Figure 4.4 shows a comparison of the annual mean and seasonal mean temperature profiles over Mt. Abu with Indian low latitude model. Seasonally averaged CIRA-86 model temperatures are also shown in figure. The three seasons viz., winter (November to February), equinoxes (March, April and September, October) and summer (May to June) are used in the comparison. Up to the stratopause level the observed values over Mt. Abu are lower than the low latitude model by a few Kelvin. However, above 50 km, the observed values over Mt. Abu are higher than the low latitude model by up to 15 K. Below 50 km the observed annual mean values are in close agreement with CIRA-86.

The observed temperatures are higher (by $\sim$ 7 K) between 50 and 70 km. Examination of the observed profiles for different seasons reveals a reasonable agreement below 60 km during winter, but the observed temperatures are more than the model temperatures by up to 7 K between 60 and 70 km. During equinoxes and summer, close agreement is seen below 50 km and observed values are higher by upto 10 K between 50 and 70 km. Temperature in the upper stratosphere shows equinoctial maxima and above 70 km a winter maximum. Seasonal variation in the stratosphere is mainly produced by ozone heating by solar ultraviolet flux. Seasonal dependence in the breaking of gravity waves and tides in the upper mesosphere may be source for large seasonal variation in temperature above 70 km. In the region of upper stratosphere equinoctial maxima occur in temperature while in the mesosphere (70–80 km) a maximum occurs in winter with equinoctial minima. Observed difference over Mt. Abu with low latitude model could be due to latitudinal differences also.

4.3 Comparison with Satellite Observations

Figures 4.5(a), (b) show contours of temperature climatology (from Sep to May) based on lidar and satellite observations ($5 \times 5°$ latitude-longitude grid) over Mt. Abu. Qualitatively, the lidar observed temperatures are similar to the satellite temperatures but there are significant quantitative differences. Mean height of the stratopause is similar (about 48 km) from both platforms, but significant difference (up to 10K) is noted in mean stratopause temperature. Spread in stratopause height is more (in the height range of 42–53 km) in lidar than in the satellite data (in the height range of 46–52 km). Figures 4.5(c), (d) show the monthly deviation from the mean temperature from lidar and satellite. In the lidar derived temperature deviations, a very strong winter cold temperature pool (about -10 K) is observed in the altitude range of 50–65 km is observed, which is not revealed by satellite observations. A very weak (about -2K) cooling is noted at lower altitudes (35–48 km) during the month of January and February in the satellite observations. The signature of warming during equinoctial months is also clearly seen in the lidar observations but this feature is not delineated in the satellite observations over the same location. This is attributed to the coarser resolution of the satellite ob-

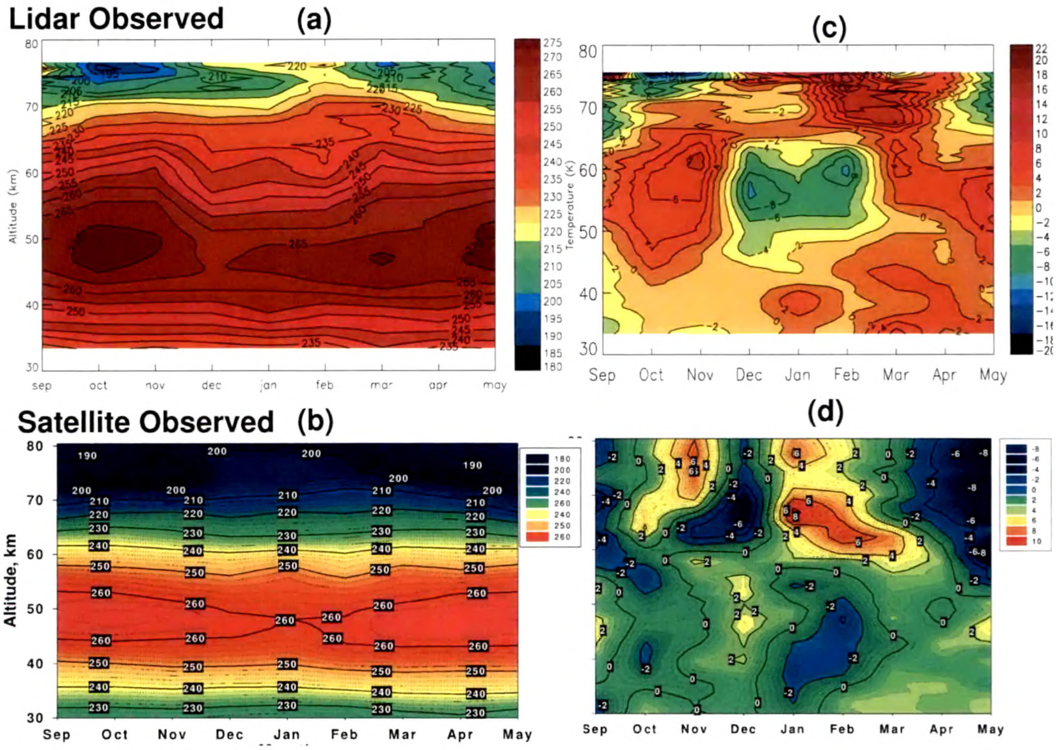

Figure 4.5: *Contour plots of monthly mean temperature over Mt. Abu (Height vs months) from (a) lidar and (b) Satellite (HALOE, onboard UARS). Similar contour plots for deviations from mean temperature over Mt. Abu (c) from lidar and (d) from Satellite (HALOE, onboard UARS).*

servations. It could also be due to differences in the observation timings; lidar observations are mostly during first half of night and satellite profiles are during sunrise and sunset times.

For day-to-day comparison between lidar and satellite observed temperatures, altitude profiles for the nights of 12, 13 April 1999 are shown in Figure 4.6. The trend of the temperature profiles is found similar for both, lidar and HALOE, but the wave type perturbations seen in lidar profile are not delineated in HALOE temperature profiles. The maximum, difference between the lidar and HALOE temperatures are found to be more than 10 K. A significant deviation is seen in the shape of the profile in the height range of 70–75 km, which is due to the MTI and discussed in detail in Chapter 5. The lidar and HALOE profiles are thus exhibiting similar trend, but the dynamical features seen in the lidar temperature are

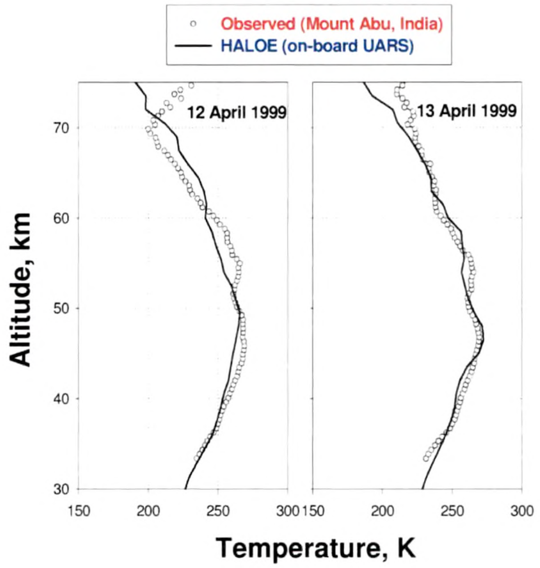

Figure 4.6: Altitude profiles of the daily mean temperature observed from lidar and HALOE during February 1998 and April 1999 over Mt. Abu.

smoothed out in the HALOE observations.

4.4 Comparison with Observations over Other Stations

Temperature structures observed over Mt. Abu are compared with similar Rayleigh lidar based observations over other locations in the northern hemisphere viz., Gadanki, Mauna Loa, OHP and Reunion Island in the southern hemisphere. Major specifications of the lidar systems at other locations along with Mt. Abu are given in Table 4.3.

4.4.1 Comparison with Observations over Gadanki

Gadanki is an Indian tropical location having Indian MST Radar and co-located Rayleigh lidar is operational since 1998. A comparative study using lidar data at both the stations has been done. Apart from climatological comparison, few coordinated lidar observational campaigns over Mt. Abu and Gadanki were also

Table 4.3: Major Specifications of the lidar system at Mt. Abu and at other locations.

Specification	Mt. Abu	Gadanki	Mauna Loa	OHP	Reunion
Location	24.5°N	13.5°N	19.1°N	44.0°N	21.5°S
Laser	Nd-YAG	Nd-YAG	Nd-YAG	Nd-YAG	Nd-YAG
Wavelength	532nm	532nm	532nm	532nm	532nm
Energy /pulse	300mJ	300mJ	350mJ	400mJ	300mJ
Repetition rate	10 Hz	20 Hz	20 Hz	50 Hz	10 Hz
Pulse width	7ns	10ns	10ns	10ns	10ns
Telescope	90cm	75cm	60cm	102cm	75cm
Altitude range, km	30-80	30-80	30-90	30-90	30-80
Vertical Resolution	96m	300m	300 m	100m	300m
Integration time (hours)	1-5	1-6	1-8	1-10	1-5

conducted and important findings are presented in this section.

Monthly-mean temperature profiles are computed from the data collected during four year period from 1998 to 2001 (having data for common period) and shown in Figure 4.7. Due to limitations of observations during rainy seasons, we have chosen March, May, September and November months to represent, vernal equinox, summer, autumnal equinox and winter, respectively. The figure also shows CIRA-86 and MSISE-90 model temperatures for comparison. The mean profiles are within the standard deviations for the heights below 50 km, whereas, the Mt. Abu temperature are warmer by 4–8 K above 50 km. Relatively, Gadanki mean profiles show higher values of standard deviations as comparison to Mt. Abu profiles. In comparison to other months, September profiles show closer agreement between the two stations. But, the models revealed warmer temperature below 50 km and colder temperature above 50 km. Apart from the September month, the models (MSISE-90 and CIRA-86) are found to be fairly in agreement with the observed profiles, except in the mesospheric temperature inversion region of 70–80 km, for which significant deviations are noted. Both the models are close to the lidar observations for the height ranges from 55 to 65 km, and above 65 km, the MSISE-90 is close to lidar observations than CIRA-86. In the height range of 70–80 km, significant deviations of the models from lidar measurements are found.

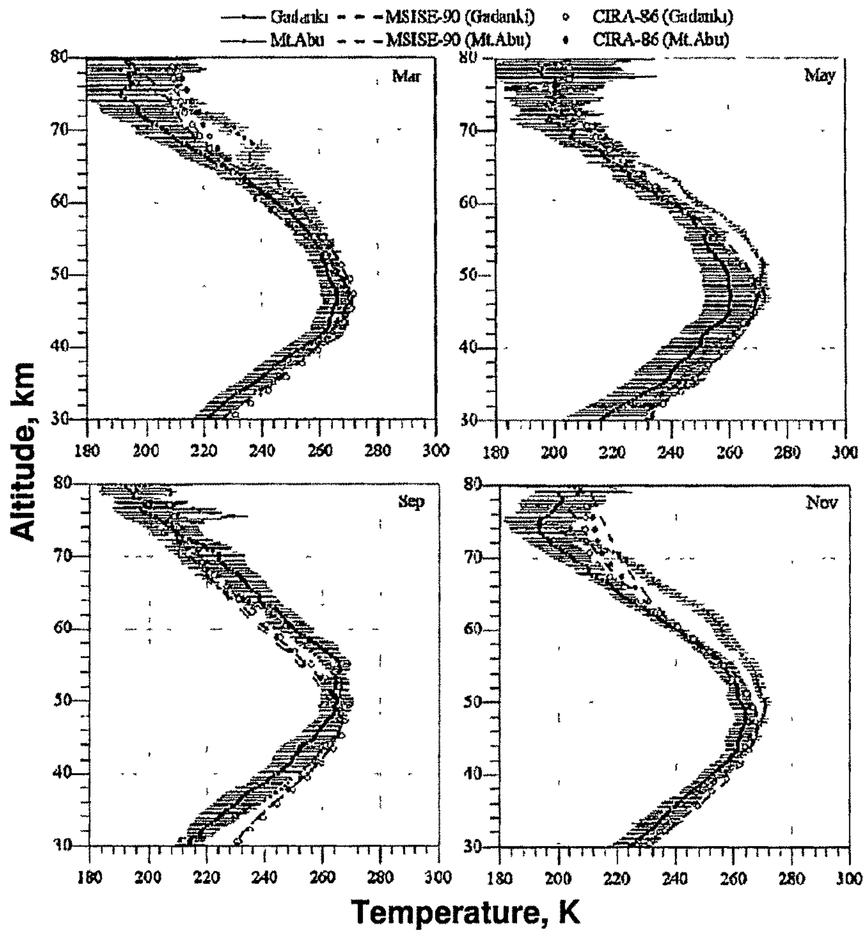

Figure 4.7: Monthly mean temperature profiles obtained for Mt. Abu and Gadanki, for the months of March, May, September and November obtained from the four years (1998–2001). CIRA-86 and MSISE-90 model temperatures are also shown for comparison

Coordinated lidar observations were made during March–May 2004 over Mt. Abu and Gadanki. Figure 4.8 show the temperature profiles observed during 19–21 March 2004 over both the locations. Mean monthly average temperature profiles for the previous years 2002 and 2003 and from CIRA-86 model are also shown in the figure. The temperature structure differs significantly from night to night over both the locations. This study has revealed the following interesting results.

- A maximum temperature of about 250 K is observed at an altitude of 60 km,

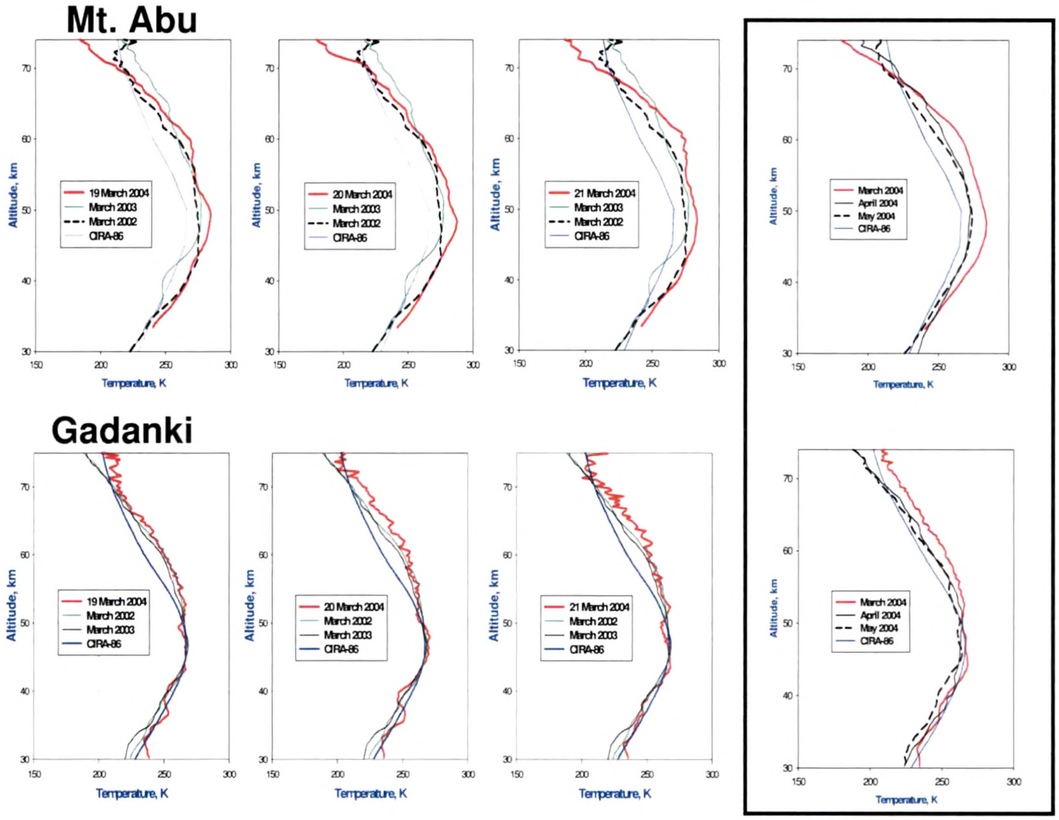

Figure 4.8: *Temperature profiles observed during 19–21 March 2004 at Mt. Abu and Gadanki. Monthly mean temperature profiles of March 2002, 2003 along with CIRA-86 model profiles are also shown. Average temperature profiles of March–May 2004 (Campaign period) are shown in the box for both the stations.*

which is found to be 10 K higher than the model temperature over both the locations.

• Over Mt. Abu a warming is observed in the upper stratosphere, but similar feature is not seen over Gadanki during March 2004.

• In the month of April 2004, the trends of observed temperature are in general agreeing with the model temperature over both the stations. However, on few occasions warming of about 8 K (compared to Model temperatures) are recorded in the height range of 55 to 65 km.

• During May 2004, the temperature structures above the stratopause, at both the stations do not show the signature of warming, which is in contrast to the temperature recorded during the month of March 2004.

Table 4.4: Differences in the observed nightly mean temperatures (in the height 35–70 km, at every 5 km) from Mt. Abu and Gadanki during March–May 2004. Standard errors in the temperature estimation are also given in the table

Height (km)	March 2004	April 2004	May 2004	Standard Error
35	8	9	8	0.2
40	12	4	13	0.5
45	18	9	8	0.8
50	22	8	9	1.5
55	17	11	10	3.0
60	15	14	11	4.0
65	6	15	8	8.0
70	-7	11	6	10.0

More quantitative estimates of the temperature differences along with the standard errors are presented in Table 4.4. Maximum temperature difference of 22 K is found at 50 km in March. Considering the errors of < 5 K in this altitude region the observed differences are very significant. The minimum temperature difference of 4 K has been found at 40 km during April. Observed temperature differences above 60 km may not be very significant whenever these are less than or comparable to 8 K, which is order of the estimation errors in this altitude region.

Figure 4.9 shows a wave type structure with a period of 2–3 days in the temperatures at different altitudes over both the locations during the period of coordinated observations. Day to day temperature modulation is more pronounced at Gadanki, a low latitude location, which is possibly more affected by equatorial waves [e.g., Parameswaran et al., 2005]. Observed day to day difference in the thermal structure are plausible due to their locations. Mt. Abu is located in sub-tropics, over a hill top, and Gadanki is in tropics.

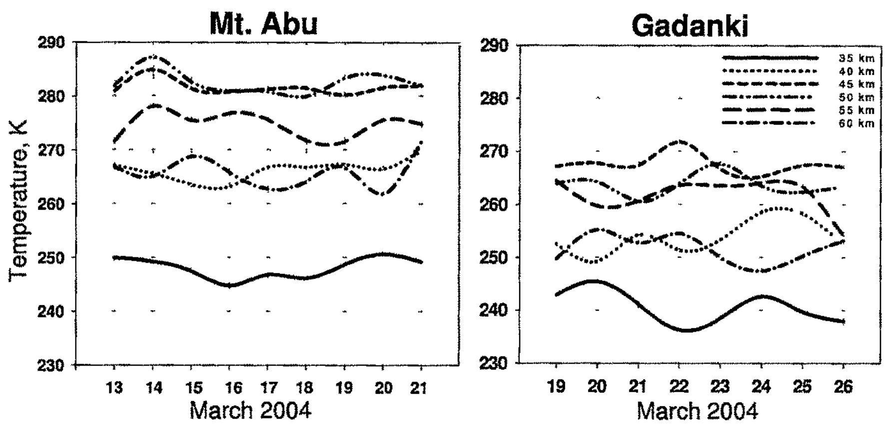

Figure 4.9: Day to day temperature variations at fixed altitudes (at every 5 km, from 35–60 km) over Mt Abu and Gadanki.

4.4.2 Comparison with Observations over Mauna Loa

Rayleigh and Raman lidar is operational at Mauna Loa (19.5°N, 155.6°W) to retrieve temperature in the altitude range between 15 and 90 km [McDermid et al., 1995; Leblanc et al., 1998]. Figure 4.10 shows temperature climatology over Mauna Loa, OHP and Gadanki, along with climatology over Mt. Abu. Though, Mt. Abu and Mauna Loa represent sub-tropical regions, features observed over Mt. Abu are different from that over Mauna Loa. Minimum stratopause temperature over Mt. Abu is found in December, but Mauna Loa showed minimum in July. Spread in the stratopause height is more over Mt. Abu than over Mauna Loa. General features of temperature structure below and above the stratopause are also different over both the locations. Mauna Loa is close to the tropical region, hence it is constantly under influence of tropical process which is clearly evident from the comparison between Mauna Loa with the Indian tropical location Gadanki as shown in Figure 4.10.

4.4.3 Comparison with Observations over OHP

Climatological temperature over OHP is also shown in Figure 4.10 along with other locations. The data used for the construction of the Mt. Abu and OHP cli-

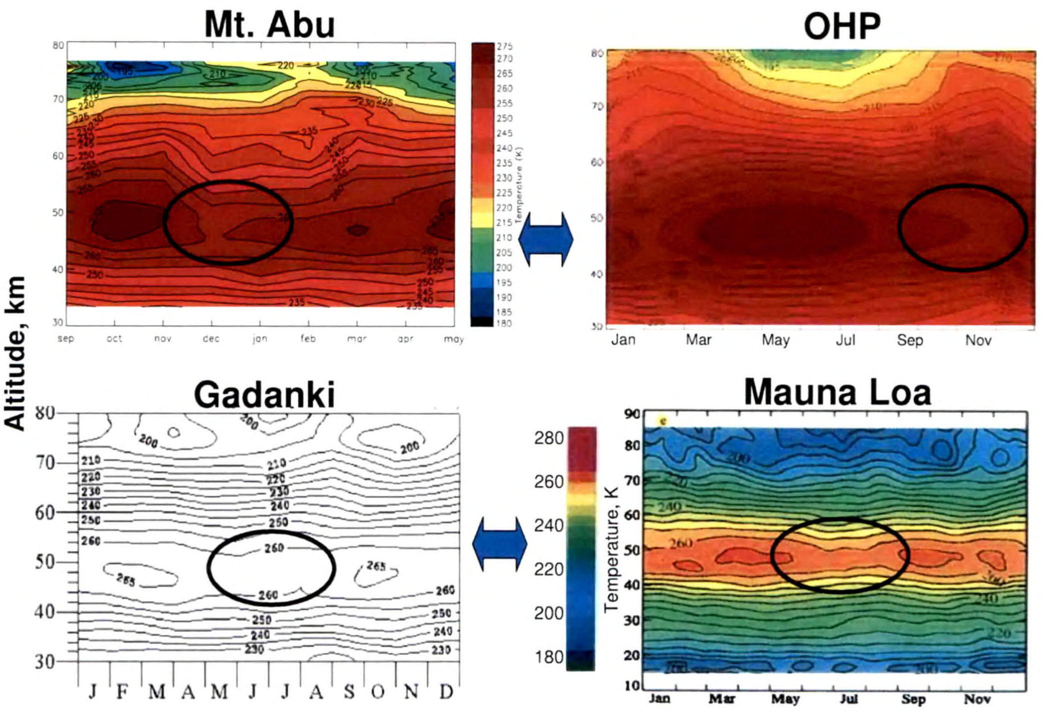

Figure 4.10: Rayleigh lidar observed temperature climatology over Mt. Abu, Observatoire de Haute Provence (OHP), Gadanki and Mauna Loa. Black circles are highlighting observed similarities in thermal structures over Mt. Abu and OHP (upper panels), Gadanki and Mauna Loa (lower panels). These are reproduced from Chandra et al., 2005; McDermid et al., 2004; and Sivakumar et al., 2003.

matologies are for the same period; method of temperature derivation and system parameters are similar over both the stations (Table 4.3). On comparing the climatology over Mt Abu, a sub-tropical location, and over OHP, a mid latitude location, remarkable similarity is found in the temperature structures. Coolest stratopause is seen during winter months over both the locations. It is interesting to note that the spread in the stratopause is large over both the locations. Another remarkable similarity noted is cold winter temperature and warmer temperature during equinoctial months. Observed similarities in the temperature structure have been marked by black circles in Figure 4.10. Furthermore, the observed similarities are very interesting as both the stations are in latitudinally different regions. Both the stations are in hilly terrain, OHP is close to the Alps and Mt. Abu is in the Aravali hill range. Strong similarities found in the middle atmospheric temperature fields over these two locations are indicative of the prominent influence of mid-latitude processes over sub-tropical region. Contribution of orographically induced wave activity (gravity and planetary waves) over both the locations cannot be ruled out.

4.4.4 Comparison with Observations over Reunion Island

Northern and southern hemispheres are having different characteristics due to different habitat and physical processes in these regions. Northern hemisphere contains more than 90% of world's population and anthropogenic effects are very strong. Southern hemisphere is relatively cleaner and dynamical features are different than in the northern hemisphere. Temperature structure over Mt. Abu is compared with temperature observed over Reunion Island which is a sub-tropical southern hemispheric French station to study the effect of different hemispheres in the middle atmosphere. Monthly mean temperature profiles for the months of March 2000 and November 2000 over the two locations are shown in Figure 4.11. These temperature profiles are in agreement except for the region above about 60–70 km for the month of March 2000. Temperature values observed over Mt. Abu are higher than the values over Reunion by about 15 K in the height region 65–70 km. During the month of November, Reunion values are higher than the Mt. Abu values by similar amount. However, considering the seasonal difference (due to different hemispheres) and difference in occurrence of MTI, the temperature values over Mt. Abu are close to the temperature values over Reunion, a sub-tropical stations of similar latitudes in the southern hemisphere.

4.5 Discussion

Temperature morphology revealed by Rayleigh lidar measurements over Mt. Abu in the height range of 30–75 km is compared with the empirical models, satellite observations and with similar observations over other locations in the northern and southern hemispheres.

The lidar observed monthly mean temperature profiles are significantly different than the the empirical models viz. MSISE-90, CIRA-86 and Indian low lati-

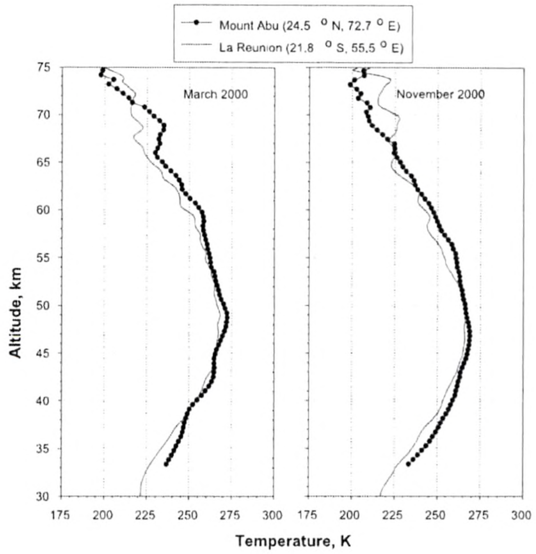

Figure 4.11: Comparision with lidar observations over Reunion Island during March and November

tude. Differences are large in the height range of 65–75 km. Among the models, MSISE-90 temperatures were found close to lidar observations (deviations < 6 K). Significant deviations of the models from lidar measurements are associated with occurrence of MTI in this height of 65–75 km. Deviations with respect to CIRA-86 and the Indian low latitude model are found to be within 10 K. In particular, cold temperatures in the CIRA-86 model lead to a large difference (upto 15 K) around 60–70 km compared to lidar results, possibly due to less observational input from low latitudes and non-LTE effects in the computation of the CIRA-86 temperatures [Lawrence and Randel, 1996; Chandra at al., 2005]. On an annual basis CIRA-86 seems to be too warm around 55–60 km, and cold between 60 and 75 km.

The maximum deviations with respect to all the three models are found in the height range of 55–70 km. The climatological study on mesospheric temperature by Clancy et al., [1994] has revealed very low mesospheric temperature in the height range of 70–80 km and the major cause for the observed cooling was attributed to the doubling CO_2 at these heights. The middle atmospheric temperature structure is known to display significant annual and semi-annual oscillations. Lambeth and Callis [1994] have reported from the satellite data that these annual and semi-annual oscillations are of significant magnitude in the mesosphere and SAO in the stratosphere. The ISAMS and HALOE satellite measurements also reveal evidence of significant annual oscillation at mesospheric heights. The Rayleigh lidar measurements over France by Hauchecorne et al., [1991] showed that the temperature variation near 65 km follows SAO with maxima occurring just after the equinoxes. The stratospheric temperatures, however, showed maximum near the summer solstice and minimum just before winter solstice. Similar to the mid-latitude behavior, the present sub-tropical observations reveal evidence of annual oscillation in the variation of stratopause temperature with maxima in the equinoxes and minima during the winter months.

As presented in Chapter 3, a reasonably good correlation was found in observed temperature and ozone. Similar to this, other groups [e.g , Wang et al., 1992; Ramaswamy et al., 2001] also showed that the stratospheric warming and cooling effects are due to changes in the ozone and CO_2 concentrations. Additional sources that could contribute to the the observed differences are occurrence of SSW and MTI and sharp adiabatic lapse rates above and below the height of the warming events [e.g., Whiteway and Carswell, 1994, 1995; Whiteway et al., 1997; Duck et al., 1998]. The stratospheric warming events were observed over mid- and high-latitudes most frequently during the month of February [Whiteway and Carswell, 1994;Whiteway et al., 1995; Gobbi et al., 1995; Namboothiri et al., 1996; Whiteway et al., 1997; Duck et al., 1998]. It is confirmed from the present observations that these events occur at tropical and sub-tropical latitudes as well Their occurrence characteristics and detailed features are presented in Chapter 5.

Comparison of the lidar observed temperatures over Mt. Abu with satellite measurements (HALOE) reveled that there are eloquent differences in the temperature structures obtained from two different techniques and platforms. In general, features are alike but, in particular, short time and small scale features are not sen in the satellite observations; they are mostly averaged out due to poor vertical resolution. Event based phenomena are mostly missed through satellite due to limited number of passes over a given location. There are many observations and related middle atmospheric temperature studies [Russell et al., 1993; Hervig et al., 1996;

Remsberg et al., 2002] highlighting strong and weak areas of satellite observations.

Detailed comparative study of temperatures over Mt. Abu revealed distinct features from similar lidar observations over other locations. Temperature structures over Mt. Abu are warmer during winter months (March–April) than the temperature over Gadanki. According to Holten and Alexander (2000), in the winter stratosphere, the observed latitudinal temperature gradient is much weaker than the radiative equilibrium gradient; the zonal winds in this region of the atmosphere tend to be much weaker than those that would be in thermal wind balance with the equilibrium temperature distribution. Planetary waves in the northern winter stratosphere may amplify dramatically over short period of time, and produce rapid meridional transport, which leads to rapid deceleration of the mean zonal flow and accompanying sudden stratospheric warming in the high- and mid-latitude regions could propagate up to tropical latitudes[Sivakumar et al., 2004]. Warmings of a less intense nature can occur throughout winter in both the hemispheres and lead to episodic pulses in the meridional transport.

Nee et al., [2002] showed that the observed temperatures at Gadanki are higher than the temperature observed by UARS and reported maximum difference in the stratopause region. In the present study also, we found maximum difference (up to ~ 22 K) is in the stratopause region. Sivakumar et al., [2004] have reported a case study of a stratopause warming of ~ 18 K with respect to winter mean temperature obtained using lidar data at Gadanki. During the month of May, observed differences are less, as local processes are different during summer months over these two locations. Prominent gravity wave and planetary wave activities [Sivakumar et al., 2006; Kishore et al., 2006] are also equally imperative in modifying thermal structures in the low latitude region. As mentioned above, these are the plausible causes for the higher temperatures recorded during winter months. Over and above the contributions of the local dynamical processes operative in the equatorial middle atmosphere cannot be ruled out. It is found that the features observed over Mauna Loa are similar to Gadanki and features of Mt. Abu are more correlated to the mid-latitude observations over OHP. The results presented here are first of its kind in the Indian sub-tropical region. Further, scientific issues will be resolved better by longer period of simultaneous measurements at both the locations, which are planned in near future.

4.6 Summary

Temperature climatology revealed by Rayleigh lidar measurements over Mt. Abu in the height range of 30–80 km is compared with the empirical models, satellite observations and with the similar observation over other locations in the northern and southern hemispheres. Significant differences are found from three models used in the present study. Inspite of the observed differences with all models, quantitatively, lidar measurements are found closer to the MSISE-90 model than CIRA-86 and Indian low latitude models. The temperature profiles obtained from lidar and satellite (HALOE onboard UARS) are qualitatively in agreement but quantitatively there are significant differences. The dynamical features seen in the lidar data, are not revealed by HALOE observations; possibly these are smoothed out in the HALOE data due to poor vertical resolution. It is found that the temperature morphology over a sub-tropical location (between 20–30°N) is very similar to the mid-latitude station. Various middle atmospheric features pertaining to mid latitude are also found in the temperature observations over Mt. Abu. It is to be noted that features are significantly different from the features observed over low latitudes. This is the first lidar based detailed study over Mt. Abu which brought out important features in the upper stratospheric and mesospheric temperature structure using a large database.

CHAPTER 5

Double Stratopause, Mesospheric Temperature Inversion & Stratospheric Sudden Warming over Mt. Abu

There are a few very interesting geophysical phenomena taking place in the middle atmosphere viz., Double Stratopause Structure, Mesospheric Temperature Inversion (MTI), and Stratospheric Sudden Warming (SSW). There are various scientific issues and aspects of these phenomena, which are yet to be understood thoroughly viz., occurrence time, height, magnitude, location, etc. and most importantly, their capability and strength to affect the mean state of the stratosphere and mesosphere. These are also a potential source to modulate general circulation of the middle atmosphere. Detailed investigation of these specific phenomena over different regions are indispensable for understanding the middle atmospheric dynamics and associated variabilities at varying time scales.

Though, there are quite a few studies from mid and high latitudes, tropical and sub-tropical region are highly under-represented due to non availability of the observations. Above mentioned unresolved scientific issues, related to these events, call for more systematic and better spatially and temporally resolved observations. Proper modeling of these events, also demands more observational input from different locations in general and from tropical and sub-tropical locations in particular. In this chapter, these phenomena are studied using lidar and satellite data over Mt. Abu (representing sub-tropical region) and findings are compared with similar observations from other locations.

5.1 Double Stratopause Structure

The Earth's atmosphere is characterized by thermal layers showing alternatively negative and positive temperature gradients. The stratopause is a transition section that separates stratosphere and mesosphere. It is usually located in the height region of 45 km to 55 km, throughout the globe. Changes in the stratopause and stratosphere could occur due to different propagating atmospheric waves and also due to the presence of radiative chemical constituents viz., ozone and other trace gases [Singh et al., 1996]. The above sources also play a significant role in modifying the thermal structure at, above and below the stratopause region (mesosphere and stratosphere)

Gupta et al. [1978] reported the presence of double stratopause over Thumba (8.3°N; 76 5°E) using rocket measurements. They found that the occurrences of double stratopauses is about 20% and the separation between two stratopause altitudes is about 10 km. Using satellite data, Hitchman et al., [1989] revealed the occurrence of separated stratopauses in both the hemispheres and reported more prominent and persistent double stratopause during winter months. By using a 2-D model, they suggested that the gravity waves could account for the observed splitting of stratopause by driving circulation in the winter hemisphere. Allen et al., [1997] presented the double peak structure in the temperature profiles using Microwave Limb Sounder (MLS) data, and found that one is occurring in the stratosphere and other in the lower mesosphere.

In addition to the above measurements, few lidar stations over the globe have reported the occurrence of double stratopause [e.g. Hauchecorne et al., 1991; Leblanc and Hauchecorne, 1997; Sivakumar et al., 2003; Chandra et al., 2005]. Except for the above mentioned sporadic studies, there are no systematic studies. Climatological and statistical information on double stratopause is also not available.

The present study focuses on detailed features of the occurrence of double

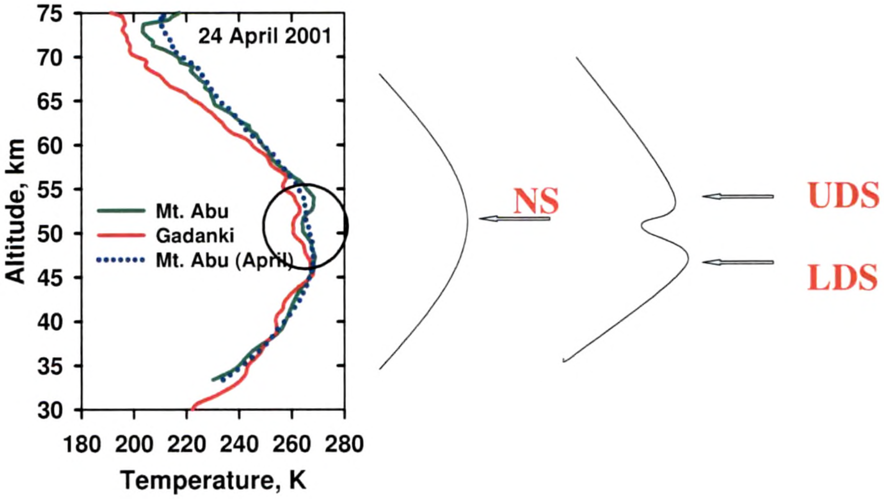

Figure 5.1: Height profiles of temperature illustrating the special features of double stratopause structure observed Gadanki and Mt. Abu for the night of April 24, 2001. Monthly mean profile of April 2001 is also shown by blue dots. Right side of the figure is an artistic view which depicts a sketch for Normal Stratopause (NS), Upper Double Stratopause (UDS) and, Lower Double Stratopause (LDS).

stratopause in the middle atmospheric temperature profiles in the height range of 40-60 km over Mt. Abu using data from 1998 to 2001. These finding are compared with the similar Rayleigh lidar observations at tropical and mid-latitude locations, Gadanki and Observatoire de Haute Provence (OHP), respectively. The seasonal (winter and summer) statistical characteristics of double stratopause over these locations have been investigated in detail. Plausible mechanisms of their generation are also investigated and discussed in terms of wave activity (gravity waves and planetary waves).

5.1.1 Results and Discussion

The daily mean temperature profiles are used to identify the double stratopause occurrence. The heights of occurrences of Normal Stratopause (NS), Upper Double Stratopause (UDS), and Lower Double Stratopause (LDS) are noted from individual profiles, using which the monthly occurrence percentage is estimated. Finally, seasonal (winter and summer) occurrence statistics is prepared for all the three stations.

Figure 5.1 shows typical height profiles of temperature illustrating the double stratopause observed over Gadanki and Mt. Abu on the night of April 24, 2001. Monthly mean profile of April (1997-2001) over Mt. Abu is also shown by blue dots. The separation between LDS and UDS on 24 April 2001 is about 8 km and temperature changes are of the order of 5 K.

Figure 5.2 contains more examples of the observed double stratopause over Mt. Abu during different months and years. An interesting feature which emerges from these is that, UDS and LDS are asymmetric (having different width and deviations from NS) on few occasions viz., 13 April 1999, 22 May 2000, and 11 November 2001. In contrast, few UDS and LDS, elicits remarkable symmetry with respect to NS as seen on 3 May 2000, 6 April 2000 and 23 December, 2000. This observed feature is attributed to the fact that possibly two or more waves, having different characteristics, are responsible for inducing double stratopause along with other radiative and chemical processes. In Figure 5.3, typical profiles of double stratopause over Gadanki, Mt. Abu and OHP are shown. It is found that double stratopause at Mt. Abu and OHP are quite similar. Separation between UDS and LDS is less (about 8 km), in contrast to Gadanki (about 10 km). Magnitude of temperature modulation is also less over Mt. Abu and OHP than over Gadanki.

The percentage occurrence of double stratopause represents the ratio between the number of double stratopause and the total number of observations during 1998–2001. The overall percentage of occurrence shows that it is maximum for Gadanki (63%) followed by OHP (44%) and Mt. Abu (42%). The percentage of occurrences during summer and winter are found to be about 68 and 44, 45 and 58, 40 and 42 for Gadanki, Mt.Abu and OHP, respectively. It indicates a higher percentage of occurrences in summer than in winter for all the three sites. It further elucidates that the prevalence of double stratopause in the temperature profiles is irrespective of place and season, hence reasonable to state that this phenomenon is a global one. The frequency distribution of heights of occurrence of NS, LDS and UDS is obtained by grouping the data in terms of summer and winter seasons irrespective of the years. The observed mean stratopause height for NS, LDS and UDS for summer and winter season is tabulated in Table 5.1

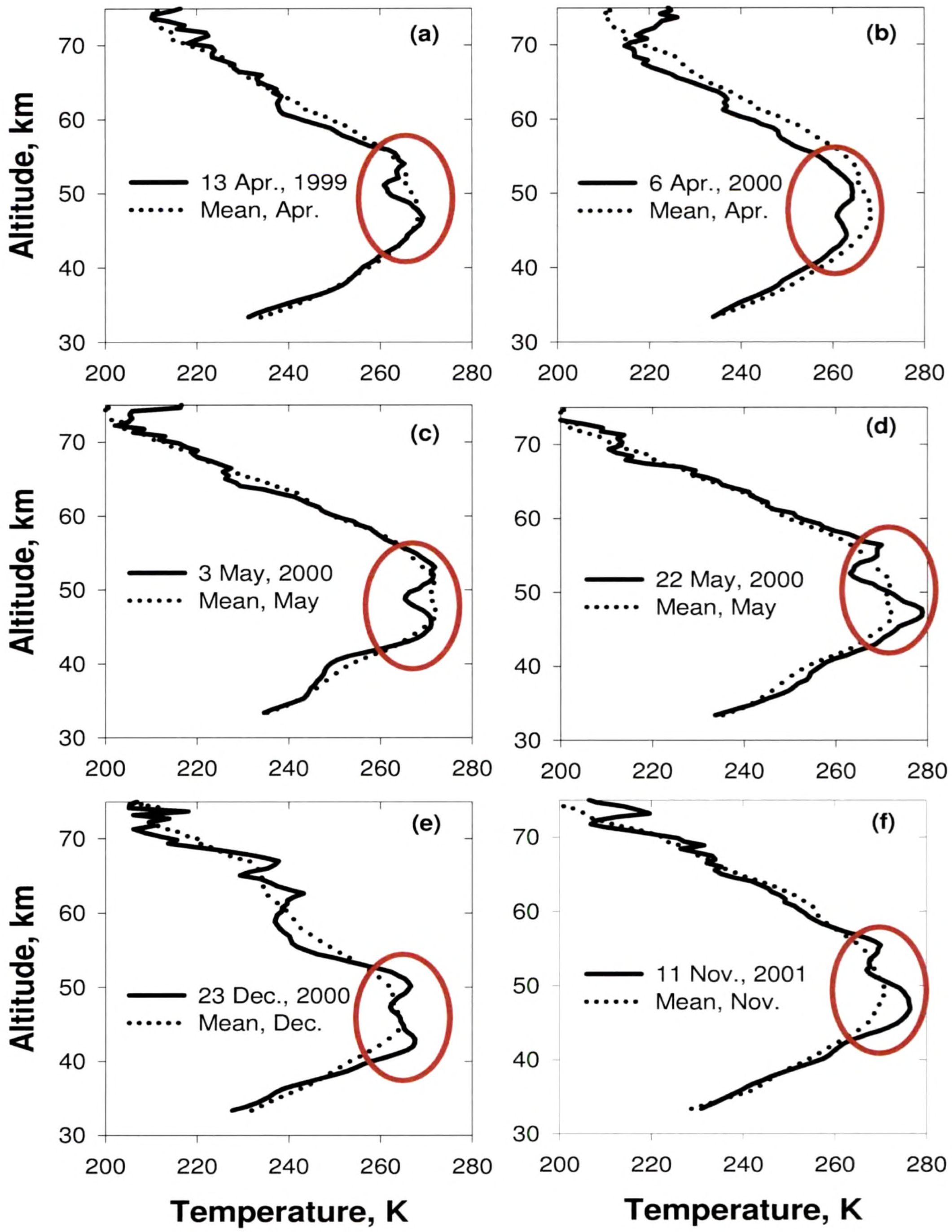

Figure 5.2: *Height profiles of temperature illustrating few typical examples of double stratopause structure observed over Mt. Abu during different months and years (a) 13 April 1999, (b) 6 April 2000, (c) 3 May 2000, (d) 22 May 2000, (e) 23 Dec 2000, and (f) 11 November 2001. Monthly mean profiles of corresponding months are also shown by dots. Regions of occurrence of double stratopause are encircled.*

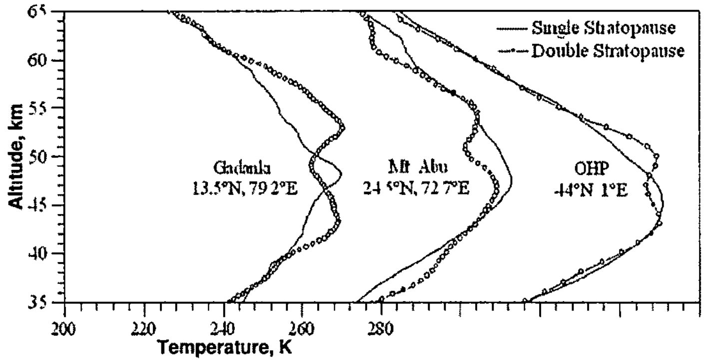

Figure 5.3: *Typical temperature profiles showing the single and double stratopause structure over Gadanki, Mt. Abu and OHP (observed on different dates). The successive profiles are shifted by 40 K.*

Table 5.1: *Mean values of height (km) of Normal Stratopause (NS), Lower Double Stratopause (LDS) and Upper Double Stratopause (UDS) for all the three stations during summer and winter.*

Station	Summer			Winter		
	NS	LDS	UDS	NS	LDS	UDS
Mt. Abu (24.5°N, 72.7°E)	48.1	46.5	53.0	47.3	46.8	49.2
OHP (44°N, 6°E)	48.0	46.5	51.4	47.4	45.5	50.9
Gadanki (13.5°N, 79.2°E)	47.0	45.6	49.8	48.6	46.5	51.0

Figure 5.4, Figure 5.5 and Figure 5.6 show frequency distribution of the LDS, NS and UDS obtained by lidar observations from 1998 to 2001 over Mt. Abu, OHP and Gadanki during summer and winter, respectively. LDS, NS and UDS heights follow the Gaussian distribution, varying from 38 km to 57 km. Distributions of NS, LDS and UDS, ranges within 43-55 km, 37-53 km and 47-57 km and 41-59 km, 41-55 km and 43-59 km, with mean heights at 48, 46 and 53 km and at 47, 46 and 49 km, respectively, for summer and winter over Mt. Abu. NS, LDS and UDS distributions are in the range of 40-56 km, 40-54 km and 43-57 km and 37-57 km, 39-53 km and 39-57 km during summer and winter, respectively, with their corresponding mean values at about 47, 45 and 49 km and at 48, 46 and 51 km, for Gadanki. In case of OHP, the NS, LDS and UDS distributions are within 41-56 km, 41-55 km and 41-57 km and 37-60 km, 37-55 km and 41-59 km with mean heights at about 48, 46 and 51 km and at about 47, 45 and 51 km, for summer and

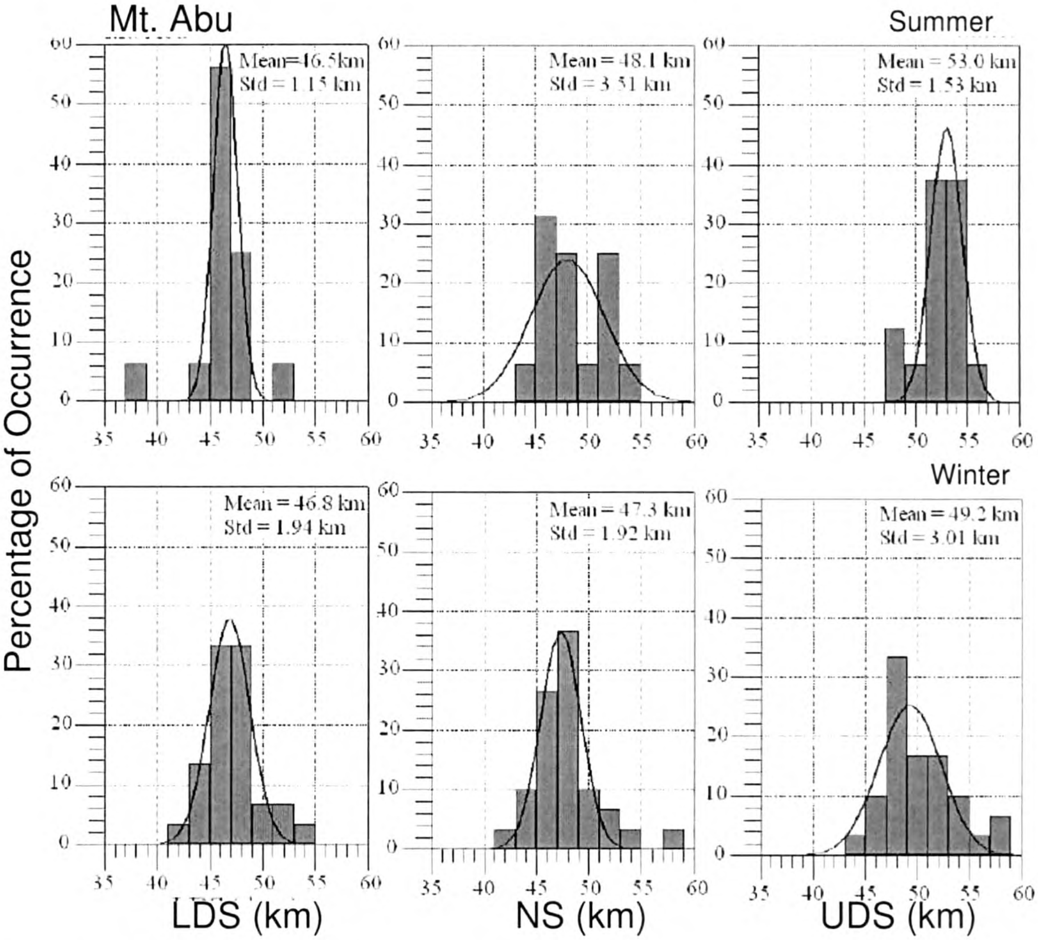

Figure 5.4: *Frequency distribution of the level of lower double stratopause, normal stratopause and level of upper double stratopause obtained by lidar observations from 1998 to 2001 over Mt. Abu during summer (top panel) and winter (bottom panel).*

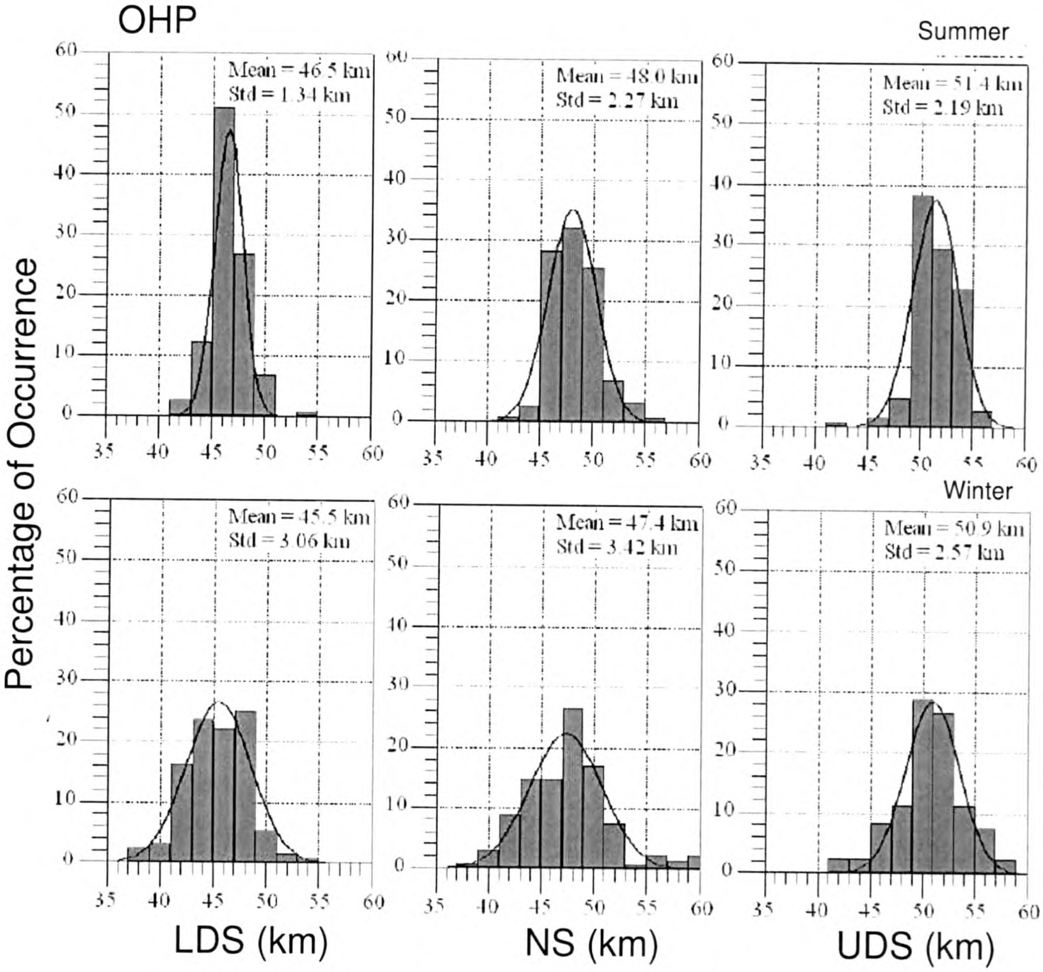

Figure 5.5: *Same as Figure 5.4, but for OHP.*

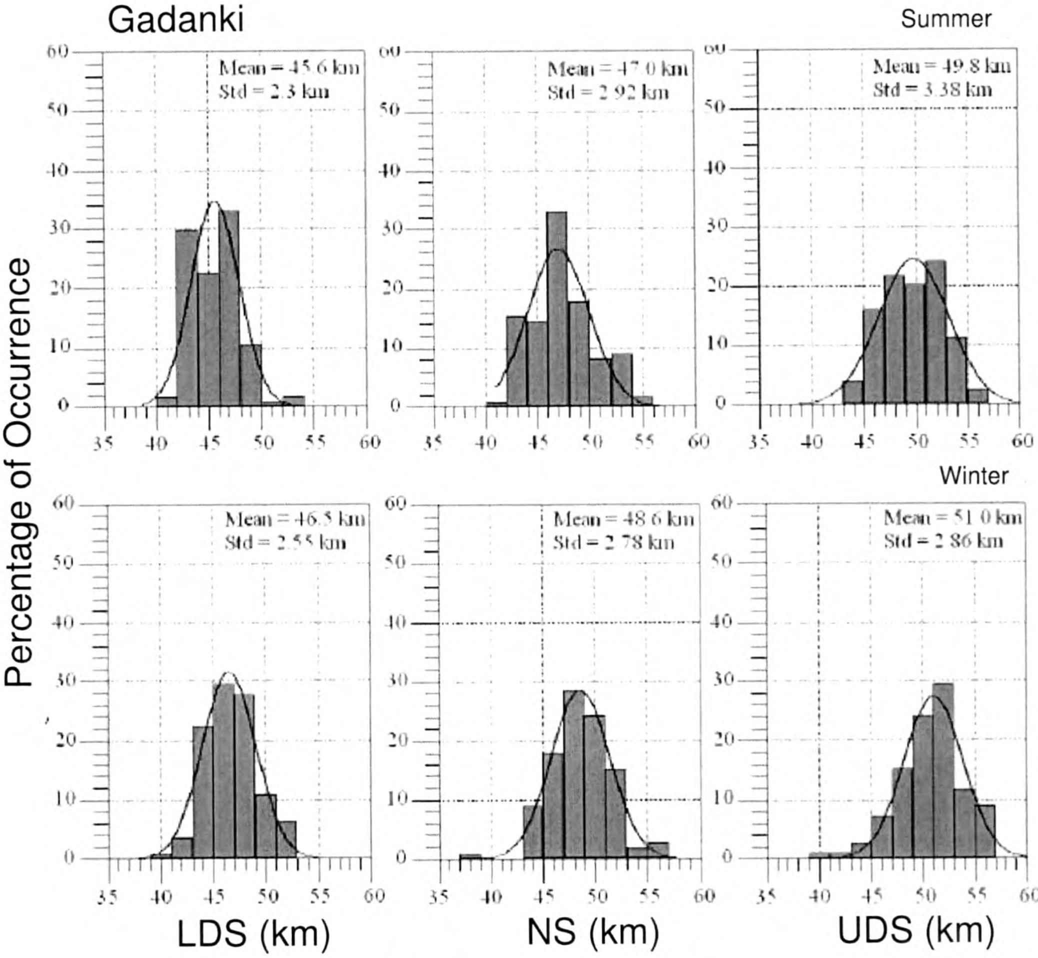

Figure 5.6: *Same as Figure 5.4, but for Gadanki.*

winter, respectively. Mean heights of occurrence of NS, LDS and UDS are higher in summer than in winter for Mt. Abu and OHP and the reverse feature is found for Gadanki (i.e., higher in winter than in summer). It is interesting to note that over all mean percentage of occurrence of double stratopause and the mean heights of occurrence of NS, LDS and UDS are found to be nearly identical for Mt. Abu and OHP.

In previous chapter also, it was very noticeably brought out from the temperature climatology that the features observed over Mt. Abu were similar to mid-latitudes rather than low-latitudes. Interestingly, this study of double stratopause also revealed very similar features in the their characteristics over Mt. Abu and OHP. Furthermore, seasonal distribution of occurrence (winter and summer) over Mt. Abu and OHP is also found to be very similar.

5.1.1.1 *Wave Activity as a Possible Generation Mechanism for Double Stratopause*

Above mentioned statistical description suggests that the presence of double stratopause is not highly dependent on time and location. It is a reasonably well established fact that the perturbations in stratosphere-mesosphere temperature profiles are either due to propagating atmospheric waves or due to compositional changes in radiative chemical constituents. The changes due to chemical constituents do not occur suddenly and do not disappear in a short period of time. Hence, the propagating atmospheric waves could be the main component of causative mechanism which is altering the temperature structure in the stratopause region and can induce the double stratopause.

As the continuous data series at Mt. Abu for longer period is not available during this period, the role of gravity waves and planetary waves activity is explored for OHP and Gadanki only. The wave activity is examined by using quasi-continuous and simultaneous 40-days of lidar observations over OHP and Gadanki, from 18 January 1999 to 28 February 1999. Few data gaps have been filled by linear interpolation. Statistical study of double stratopause demonstrated that the overall and seasonal occurrence of double stratopause over Mt. Abu and OHP is remarkably similar. Furthermore, observed features are well correlated over both the locations. As statistical characteristics are very similar over Mt. Abu and OHP, it is, therefore, envisaged that wave features revealed through quasi continuous data of OHP may also elicit similar behavior over Mt. Abu. It can be mentioned at this juncture that OHP and Mt. Abu have similar topography; OHP is close to Alps hills range and Mt. Abu is in the Aravalli range of mountains. Therefore, it is very likely that wave activity of orographic origin over both the locations have similar characteristics and hence could be responsible for the observed identical behavior of double stratopause.

5.1.1.2 *Role of Gravity Wave and Planetary Wave Activity*

Gravity waves, which commonly propagate from troposphere to mesosphere, might be one of the source mechanisms to perturb the stratopause region, where GW may break and transfer their energy. In this section, we explore the role of GW activity in generating the double stratopause for Gadanki and OHP. The GW associated potential energy (PE) is a parameter which demonstrates the strength of GW and the atmospheric stability. Assuming that the GW perturbation could contribute to the double stratopause, the GW associated PE are computed at both LDS and UDS height regions over Gadanki and OHP. It is calculated by assuming that the atmospheric density perturbations are similar to that of temperature [e.g. Wilson et al., 1991a, b; Whiteway and Carswell, 1994] and following the expression given by Wilson et al., [1991a]

$$PE = \frac{1}{2}\left(\frac{g}{N}\right)^2\left(\frac{T'}{T_o}\right)^2 \tag{5.1}$$

where, T' represents the temperature perturbation evaluated as the difference between temperature profile, T_o, and a third order polynomial fit to it, and N is the Brunt-Vaisala frequency obtained from the following expression,

$$N^2 = \frac{g}{\Theta}\left(\frac{d\Theta}{dz}\right) \tag{5.2}$$

The height profile of PE is computed for 30 to 70 km height range, by following the above expression. The mean PE for LDS and UDS height regions over Gadanki and OHP are then computed and are presented in Figure 5.7a. For Gadanki and

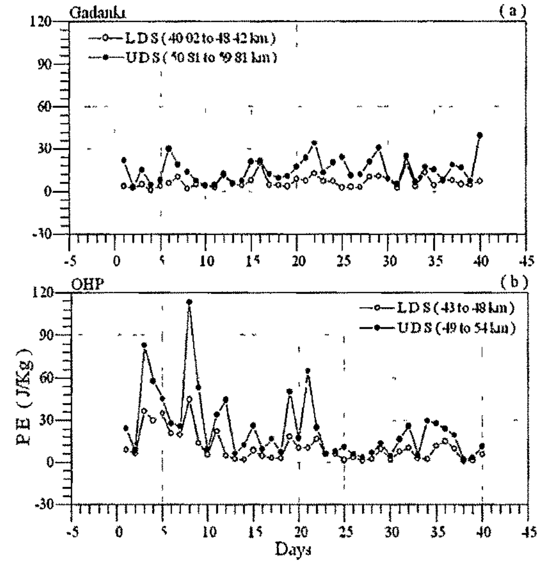

Figure 5.7: Estimated mean potential energy for LDS and UDS height region for the continuous 40-days lidar observations (a) over Gadanki and, (b) over OHP.

OHP, the LDS and UDS height region ranges from 40 km to 49 km and from about 51 km to 60 km, respectively. Similarly, the mean PE is computed for OHP over LDS height region from 43 km to 48 km and over UDS height region from 49 km to 54 km, and shown in Figure 5.7b. As expected, the amplitude of GWs associated PE increases with height; the calculated mean PE displays a higher value for UDS than LDS. The day-to-day variation of PE for LDS and UDS are similar over both stations. The mean value of PE for OHP is higher than that of Gadanki. A correlation analysis is performed between PE values and UDS-LDS heights. The results obtained for Gadanki and OHP show a higher correlation with PE for UDS than for LDS. It suggests that the GW could be a potential cause for the observed UDS structures. It will be very interesting to investigate the possible correlation between UDS and the occurrence of mesospheric temperature inversion (MTI) in future studies.

Moreover, the estimated PE is found to be higher for OHP than for Gadanki which is in agreement with the earlier results showing a maximum GW activity during winter at OHP [Wilson et al., 1991b] and during summer and equinox at

Gadanki [Sivakumar et al., 2006]. It is worth noting that the dominant GW activity may be one of the main sources to contribute for the UDS occurrences.

PWs also contribute to the variability and dynamical changes in the middle atmosphere. A possible role of PW activity in generating the double stratopause is also explored. Continuous wavelet transform (cwt) is applied to the quasi-continuous 40-day lidar observations. The wavelet spectral technique extracts wave parameters into a good time-frequency resolution in comparison with FFT. Generally, FFT is used where there is a fixed window width (like dynamic spectra), whereas the width of the wavelet depends on scale of interest (frequency). In addition, the narrow-broader wavelet allows high-low frequency (small-large time scale) components to be better resolved in time. As the Morlet wavelet has a well-defined relationship between its scales and the Fourier periods [e.g. Malinga and Poole, 2002], the same technique has been used to extract the dominant PW modes. It is subjected to the temperature differences derived by subtracting the 40-day mean temperature profile from the individual daily temperature values. PW amplitudes for the height region from 30 km to 70 km are computed and examined for the periodicity of PW from 5 to 25 days. The examined altitude range are 40-49 km and 51-60 km, corresponding to LDS and UDS height regions over Gadanki. The obtained PW amplitude is shown in Figure 5.8. It is clear from the figure that the wave activity is stronger in the LDS height region than in the UDS. It shows a periodicity of 13-20 days observed over the 40-days observational period, with maximum amplitude from 13^{th} to 37^{th} day. Also, there are small period waves of 8-10 days in the first 15 days and 5-7 days at the end of observation period (from 35 to 40), but their amplitudes are weaker than for PW with period of 13-20 days.

With regard to UDS region, it shows smaller amplitudes for the 10-13 days wave starting on the 10th day and further a 6-7 days time-localized (15^{th}-25^{th}) with slightly weaker amplitude. Similar analysis has been performed for OHP observations to examine the PW activity. Figure 5.9 shows the extracted mean PW amplitude for the LDS and UDS region, i.e., from 43 to 48 km and from 49 to 54 km. The figure shows a 20-25 day wave in the LDS region. In the UDS region, PW amplitudes are weaker than those obtained in the LDS region. The UDS region shows two quasi-persistent 15-20 day waves and a localized 7-8 days wave. This

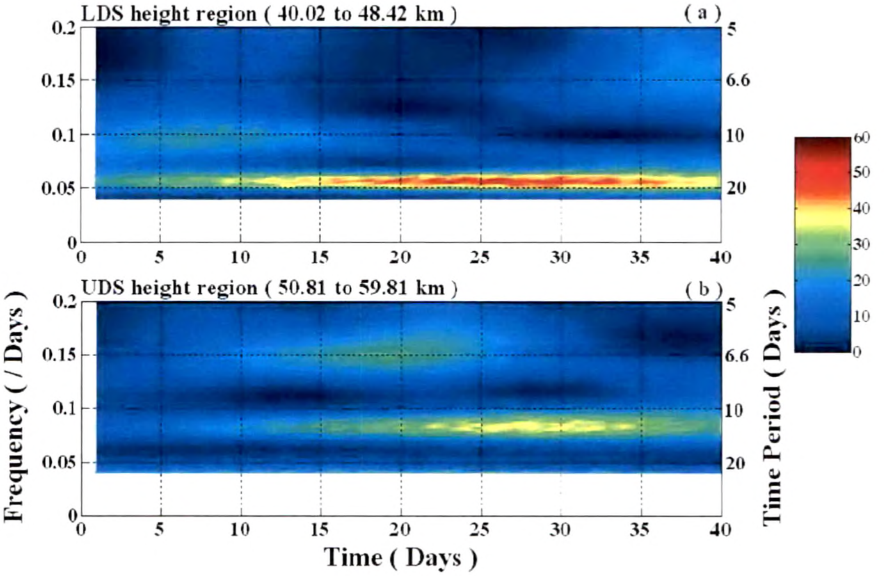

Figure 5.8: *The estimated mean planetary wave amplitude obtained for the LDS and UDS height regions over Gadanki.*

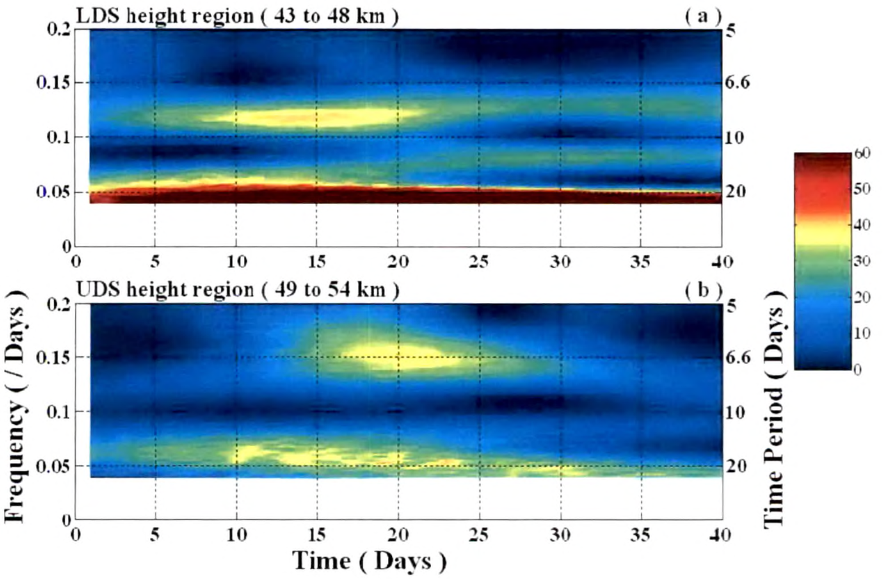

Figure 5.9: *Same as Figure 5.8 but for OHP.*

result shows that PW amplitudes are higher in LDS than in UDS height region. It suggests that the PW could be responsible for LDS at both stations (Gadanki and OHP). In addition, the PW amplitude is observed to be higher over mid-latitudes (OHP) than over tropics (Gadanki). This is in agreement with the fact that PW are generated over high and mid latitude with equator-ward trajectories, and amplitudes are smaller in the sub-tropics and tropics [Barnett and Labitzke, 1990].

5.2 Mesospheric Temperature Inversion

Mesospheric Temperature Inversions (MTIs) are regions of sharp positive temperature gradient in the mesosphere, i.e. regions of increasing temperature with height, which stand out in the mesosphere where normally the temperature decreases with height. They were first reported from rocket borne temperature measurements over mid-latitudes [Schmidlin, 1976]. MTIs are regularly observed at low- and mid-latitudes having good occurrence rates and seasonal dependence [e.g. Hauchecorne et al., 1987; Leblanc et al., 1995, Sivakumar et al., 2001]. MTIs are rather rare at high latitudes [Cutler et al., 2001; Leblanc and Hauchecorne, 1997]. Satellite observations show that these layers are a mesoscale phenomenon that can cover extended regions and persist for hours [Clancy et al., 1994; Leblanc et al., 1995]. Fadnavis and Beig, [2004, 2007] reported HALOE based observations of MTIs and linked their occurrence to chemical heating and thunderstorm activity.

Causative mechanism for MTI has been a subject of debate since their first detection. Many different sources for the formation of MTIs have been suggested including breaking of gravity waves [e.g. Hauchecorne and Maillard, 1990; Meriwether and Gardner, 2000; Liu and Meriwether , 2004], gravity wave tidal wave interactions [e.g. Sica et al., 2002], breaking of planetary Rossby waves and chemical heating [Meriwether and Mlynczak, 1995]. Combining radar observations with lidar temperature observations, a possible link between MTIs and polar mesospheric winter echoes were reported by Thomas et al., [1996].

Using a two-dimensional model, and combining mesosphere photochemistry with the dynamical transport of long-lived species, it was shown that the region of 80-95 km may be heated by as much as 3 to 10 K/d, which is of the same order as that due to the dissipation of gravity waves [Fritts and vanZandt, 1993]. Meriwether and Gerrard, [2004] described two types of MTIs (upper and lower MTIs) and suggested their formation mechanism. They suggested that upper MTIs propagate downward over timescales similar to that of tidal waves. Liu et al., [2000] showed in a model study that breaking of gravity waves can warm the air sufficiently for the formation of MTI if the static stability of the mesosphere had been decreased by a tidal wave.

Leblanc and Hauchecorne, [1997] presented a detailed climatology of the MTI using an extensive data set covering the years 1981-1993 from two lidars located in the south of France and observations from two satellite experiments, ISAMS (Improved Stratospheric And Mesospheric Sounder) and HALOE (on board UARS). They reported development of a mid-latitude belt of strong inversions ($\sim$40 K) in the height range of 70-75 km during winter and a lower latitude belt of strong inversions over 80-85 km occurring a few weeks after the equinoxes.

Sivakumar et al., [2001] presented a detailed morphological study of MTI over an Indian tropical station, Gadanki using Rayleigh lidar data. Recently, Sica et al., [2007], presented lidar observed MTI over Ontario (42.9°N, 81.4°W) and proposed a simple theory of their occurrence and used Canadian Middle Atmospheric Model (CMAM) to quantify the statistics of inversions. Sridharan et al., [2008] presented few case studies of MTI over Gadanki using lidar observation and MF radar measured winds and showed the interaction between waves and tides in the occurrence of MTI.

The present study is based on about 250 nights of Rayleigh lidar observations of the middle atmospheric thermal structure made at Mt. Abu, using data from 1997 to 2003. The observed features are also compared with other low and mid-latitudes observations of MTI. In addition, satellite (HALOE onboard UARS) observation from and nearby passes to lidar locations also have been used.

5.2.1 Criteria for Detection of MTI

The primary criterion for detection of an inversion layer is its amplitude. The difference between the maximum temperature and minimum temperature is known as the amplitude of inversion layer. The altitude where temperature becomes minimum and then starts increasing is known as the bottom altitude of the inversion layer. The altitude where temperature becomes maximum and then again as usual starts decreasing is known as the top (peak) altitude of the inversion layer. The thickness of MTI is the difference between the altitudes, at the top and at the bottom of inversion layer. The thicknesses and amplitudes of MTI are noted for each day. As the error in the temperature around the level of inversion is ~4-8 K, only inversions of amplitude 8 K or more can be considered as significant. Amplitude, peak and bottom altitudes, and frequency of occurrence of the inversion layer are obtained on a daily basis. Monthly means are obtained by averaging them for the corresponding months over all the years.

5.2.2 Results and Discussion

This study of MTI consists of two sequences of MTIs observed for few days as well as statistical characteristics during 1997-2003. Detailed data analysis techniques have been described in chapter 2.

A lidar observed temperature profile on 30 December 2003 depicting an example of the occurrence of the MTI over Mt. Abu along with CIRA-86 model profile are shown in the Figure 5.10. Very noticeable, strong temperature inversion of about 40 K (as compared to CIRA-86) at height of 70 km is found. The width of the inversion is nearly 6 km. An interesting feature obtained was that, just below the inversion layer, there was cooling of about 12 K (~60-62 km), which is in accordance with mid-latitude study [Hauchecorne et al., 1987].

Figure 5.11 contains few more examples of the MTI, covering different months and years. CIRA-86 model temperature profiles and observed monthly climatological mean (1997-2001) temperature over Mt. Abu are also shown in the figure. Temperature profile on 5 November 1997 (Figure 5.11a) elicits two weak inversions, one at 62 km and other one at about 70 km. Both these inversions are having small scale structures also. An inversion event observed on 02 November 2000 (Figure 5.11b) is having a strong MTI (about 12 K) at 72 km and very noticeable cooling of similar magnitude is found just below the MTI (at about 68 km). A

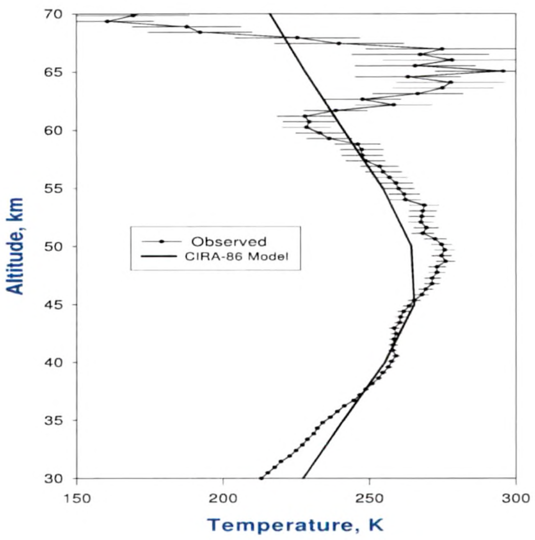

Figure 5.10: *A typical Rayleigh lidar observed altitude profile of temperature showing Mesospheric Temperature Inversion over Mt. Abu on 30 December 2003. CIRA-86 model temperature profile (25°N) is also shown in the figure.*

secondary, weak, little broader signature of inversion is also present in the height range of 60-65 km. Temperature profiles on 5 November 2001 and 25 January 2001, shown in Figure 5.11(c, d) are having very prominent MTI (with inversion amplitude of about 15 K) at about 68 km. It is interesting to note that the signature of cooling, just below MTI is present on 5 November 2001 and also fine structures are present along with a secondary, sharp inversion at 73 km, but these features are missing on 25 January 2001. From above mentioned description it is very clearly discernible that, every MTI event has unique features and characteristics. This shows that their formation mechanism is very complex and amalgamation of various physical, chemical processes is also possible.

5.2.2.1 MTI Event during 8-11 March 2000

A sequence of temperature profiles are shown in Figure 5.12(a-d) for the period 8-11 March 2000. Mean temperature profile of March (short dashed line), along with CIRA-86 model temperature (red line) profiles are also shown in the figure. These nightly mean temperature profiles are exhibiting either well developed MTI or its

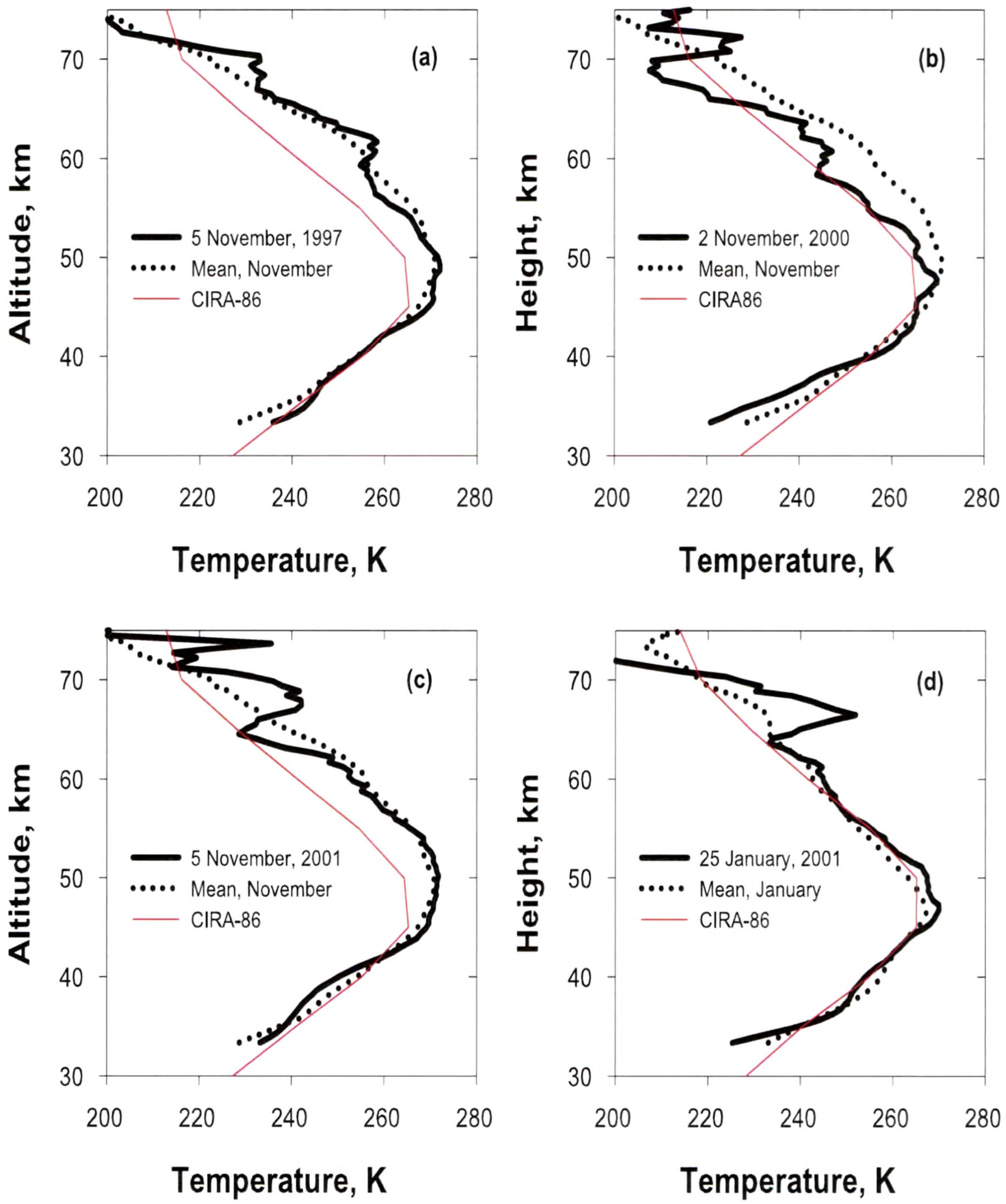

Figure 5.11: *Height profiles of temperature illustrating few typical examples of Mesospheric Temperature Inversions observed over Mt. Abu during different months and years. Monthly climatological mean profile and CIRA-86 model temperature for corresponding months are also given in the figure.*

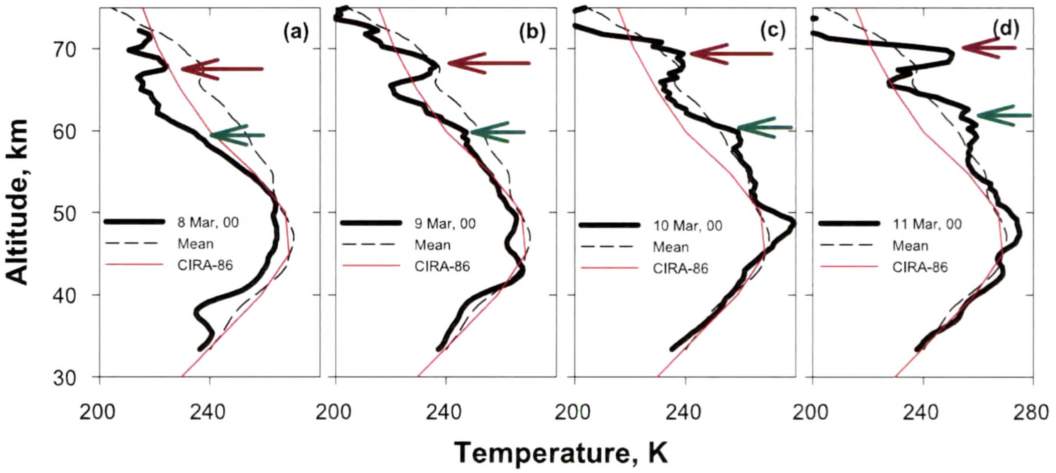

Figure 5.12: *A sequence of nightly mean height profiles of temperature illustrating Mesospheric Temperature Inversions observed over Mt. Abu during 8-11 March 2000. Monthly climatological mean profile of March month and CIRA-86 model temperature profiles are also shown in the figure.*

signature. Red arrow highlights, strong MTI at higher levels (between 68-72 km) and green arrow points, a weaker MTI at lower heights (between 60-64 km).

Following are the important noticeable points that transpire from the sequence of observed MTIs.

(i) Magnitude of upper level (red arrow) MTI increased gradually from 10 to 20 K (from 8-11 March 2000). Magnitude of inversions at lower levels (green arrow) also amplified and became significant during this period.

(ii)There is small but noticeable increase in the occurrence heights of both the MTIs.

(iii) During this episode of MTI, marked signature of cooling is discernable just below MTI.

(iv) MTI at lower heights are associated with the fine structures of the temperature which are not seen in the upper level inversion except on 10 March 2000.

(v) Very interestingly, most of these events also have signatures of the stratospheric sudden warming.

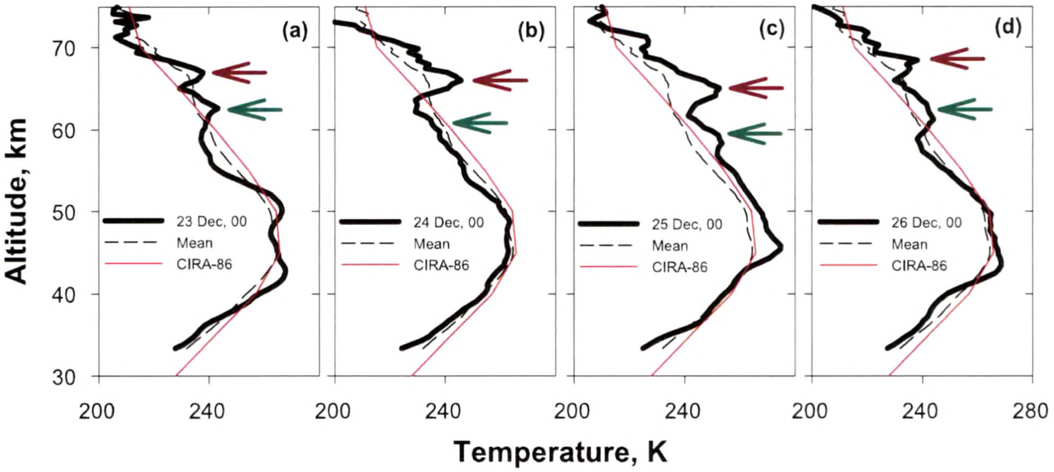

Figure 5.13: A sequence of nightly mean height profiles of temperature illustrating Mesospheric Temperature Inversions observed over Mt. Abu during during 23-26 December, 2000. Monthly mean profile of December months and CIRA-86 model temperature profiles are also shown in the figure.

5.2.2.2 MTI Event during 23-26 December 2000

Figure 5.13(a-d) shows another episode of MTI over Mt. Abu and contains a sequence of temperature profiles from 23 to 26 December 2000. In this figure also, mean temperature profile for the month of December (short dashed line), along with CIRA-86 model temperature (red line) profiles are shown. Again, red arrow highlights strong MTI at higher levels (between 66-70 km) and green arrow points MTI at lower heights (between 60-65 km). In this sequence of MTI, magnitude of upper level (red arrow) of MTI first increased gradually from 5 to 15 K (from 23-25 December) and then decreased on 26 December. Inversion at lower level (green arrow) was seen on 23 December at about 62 km and which then became very weak on the next day. It reappeared again on 25 December and remained on 26 December. Variation in the heights exhibits a similar feature as seen in the upper level MTI.

It is very interesting to note that there are marked differences between these two episodes of MTIs (March and December 2000). During March, heights of the inversions were increasing, whereas during December it first decreased and then

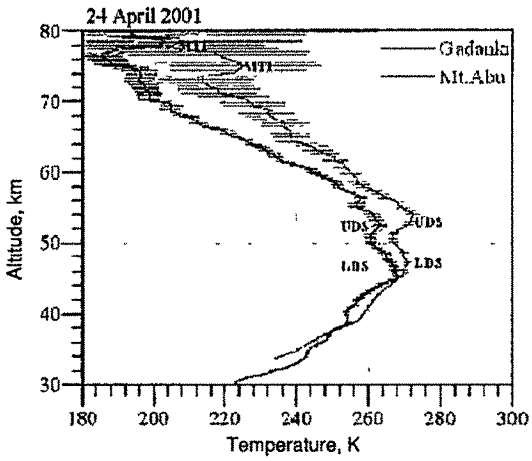

Figure 5.14: Height profiles of temperature illustrating simultaneous occurrence of double stratopause structure and mesospheric temperature inversion over Mt Abu and Gadanki on 24 April 2001.

increased. Very remarkably, the separation between the upper and lower levels of MTIs is more (about 10 km) in March than the observed separation (only about 5 km) during December. The persistent occurrence of MTI over Mt. Abu during extended period of time (4-5 days) during both these events is in accordance with the lidar based, latitude wise observations reported by Hauchecorne et al., [1987] and Leblanc and Hauchecorne, [1997].

An event observed on the night of 24 April 2001 by the lidar over Mt. Abu and Gadanki is shown in Figure 5.14. The figure shows the double stratopause in height region of 45-55 km, and simultaneously MTI over 70-80 km. These profiles provide further credence for the possible association between these phenomena and is possible that the underlying processes behind their formation are similar over sub-tropical and tropical locations. Temperature profiles over Mt. Abu and Mauna Loa for 10 March 2000 are compared and shown in Figure 5.15. Noticeable differences are the presence of SSW and MTI around 48 and 68 km, respectively over Mt. Abu, which are not seen over Mauna Loa on same night.

The dynamics of the middle atmosphere in winter is known to be dominated by planetary waves of large amplitudes. The most important ons are quasi-stationary

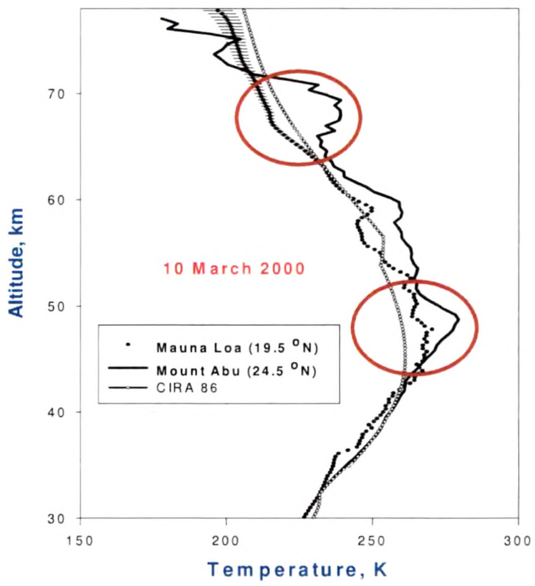

Figure 5.15: *Rayleigh Lidar observed nightly mean temperature profile on 10 March 2000 over Mt. Abu and Mauna Loa. CIRA-86 model temperature is also shown in the plot. Red circles are indicating occurrence of SSW and MTI.*

Rossby waves, which propagate upward from the troposphere and are very strong but quite variable during winter [e.g. Pancheva et al., 2008 and reference therein]. It is known that much of the variability in the mesosphere lower thermosphere (MLT) region is a result of upward propagation of disturbances from the stratosphere, particularly during winter. Therefore, differences observed in the present study may also be attributed to the marked difference in the GW and PW activity during the month of December and, March at Mt. Abu. The observed separation between two layers of MTI over Mt. Abu is shorter than that reported by Meriwether and Gerrard, [2004], on the basis of vertical tidal wavelength (about 25 km). Observed cooling, just below the MTI over Mt. Abu on only few occasions is very much similar to the feature observed at mid- and low- latitude [e.g. Hauchecorne et al., 1987; Sivakumar et al., 2001; Sridharan et al., 2008]. It is also in accordance and feasible through the mechanism proposed by Meriwether and Gerrard, [2004].

5.2.2.3 *Statistical Study of MTIs*

In addition to above described case studies, a climatology of MTIs observed over Mt. Abu using Rayleigh lidar data is also made and important findings are described in this section. These findings are compared with the HALOE (onboard UARS) observations. Figure 5.16(a, b) shows histograms of percentage occurrence of MTI, obtained from lidar observations over Mt. abu and from satellite observations, respectively. It is clearly seen that the magnitude of the temperature inversion is characterized by a broad distribution (analogous to Rayleigh distribution) with a maximum of about 40 K, with the most probable values between 12-18 K. The satellite observed inversions are showing similar distribution pattern, however the magnitude of percentage occurrence is lower than that of lidar observed inversions. The peak of the inversion from satellite is similar to the lidar observed statistics. Strong temperature inversions are missing in the statistics from satellite. Most likely, due to poor vertical resolution (about 3.6 km), sharp, strong MTIs are missed from satellite platforms.

Figure 5.16 shows heights of occurrence of the inversions during different months. Figure 5.17a shows average height of occurrence from January to December; data are not available from July-September due to local monsoon. A peak of the inversion layer is confined to the height range of 74-76 km, with the maximum occurrence around 76 km during June. Occurrence height is less during winter months than during the summer months. From satellite observations also, it is found that the occurrence height is more during summer than during winter and given in Figure 5.17b.

The height variation of the inversion peak over the years is found to be fairly small from satellite observations, with the maximum height of 77 km and the minimum of about 72 km in August and January, respectively. Difference between the lidar and satellite observed MTIs are attributed to the different observation timing and to the satellite passes ($5 \times 5\,^{\circ}$ degree latitude-longitude box centered over Mt. Abu). The lidar and satellite based observations [e.g., Leblanc and Hauchecorne, 1997] also showed that the frequency of occurrence follows an annual cycle with a maximum during the winter months at mid-latitudes and a semiannual cycle with

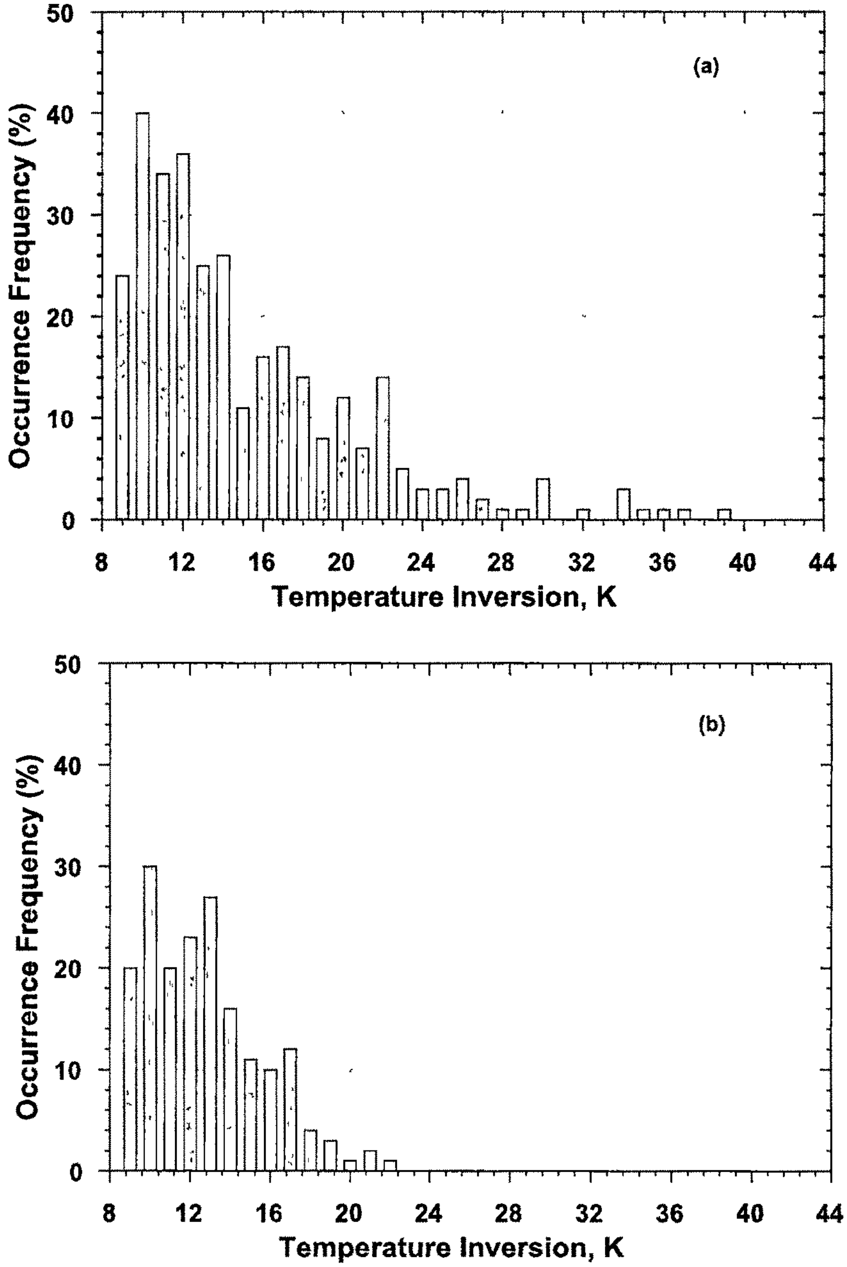

Figure 5.16: Monthly mean occurrence of the MTI during 1997-2003 obtained from (a) lidar and (b) satellite (HALOE onboard UARS) observations over Mt. Abu.

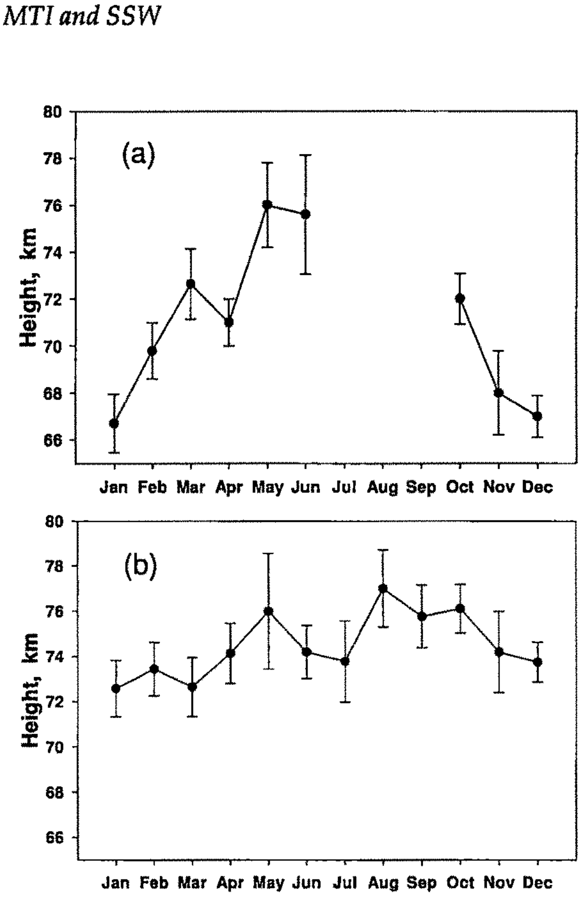

Figure 5.17: Monthly mean height of occurrence of the MTI during 1997-2003 (a) lidar observed and (b) satellite (HALOE on board UARS) observed over Mt. Abu No data is available from July to September due to monsoon.

maxima during the equinoxes at low latitudes.

The seasonal variations of the inversion height and temperature deviations are similar to the one predicted for the altitude of breaking level of GWs [e.g., Lindzen, 1981]. The occurrence pattern of the MTIs is similar to the semiannual variation of GW activity in the upper mesosphere [e.g., Thomas et al., 1984], and this was confirmed by radar observations by Vincent and Fritts, [1987]. Vincent [1984] estimated horizontal winds in the mesosphere using radar measurements, and reported that the rate of wave energy loss to the atmosphere from GW breaking and dissipation would correspond to a heating rate of $\sim$ 12 K/d. Further, partial reflection radar observation during ALOHA-90 campaign showed that the GW activity in the upper mesosphere was very high specially for short period waves, and considerable day-to-day variability was also noted [e.g. Vincent and Lesicar, 1991 and reference therein]. Observed annual cycle in the present study is in agreement with the similar study at mid-latitudes [e.g., Clancy et al., 1994]. Furthermore, the seasonal variation of the altitude of the inversions are very similar to the seasonal variation of the MST radar echoes in the mesosphere shown by Balsely and Garello, [1985] from Poker Flat radar. Kamala et al., [2003] showed that the mesospheric echoes are high during summer months using Indian MST radar. Similar findings have been reported by Chandra et al., [2008]. They consider that the radar echoes are due to turbulent layer generated by the breaking of gravity waves. Rocket borne studies [Sinha, 1992; Das et al., 2009] have also shown the presence of neutral turbulence at mesospheric heights in the Indian low latitude region. Such results seems to indicate that the two phenomena have the same origin and that the temperature inversion is directly related to the breaking of GWs generating turbulence.

The observed mesospheric inversions have largely been interpreted in terms of the mechanisms involving gravity wave breaking, gravity wave-tidal interactions and chemical heating. In spite of the many studies, formation mechanism of MTIs is not understood fully. Possible physical mechanisms proposed for the production of MTIs are diverse. Several interpretations and processes, like chemical heating, associating ozone, dynamical interaction between gravity and tidal wave [e.g., Liu et al., 1998, 2000] were proposed in the past. Mlynczak, [1991], Mlynczak and Solomon [1993] and Meriwether et al., [1995] have reported that heating occurs in the middle atmosphere due to exothermic reactions.

A study of the energy budget of the mesosphere has shown that the wave breaking and turbulent motions are very efficient in the mesosphere and may contribute by few tens of Kelvins per day to the heat budget of the mesosphere. It is then possible to explain how the temperature inversion of about 40 K persists for several days by the continuous breaking of GWs. Further, an impressive fact linking the GW activity to the inversions is the observed difference in the seasonal dependence of the inversions between sub-tropics and mid-latitudes. A comprehensive study of GWs in the middle atmosphere revealed that activity is maximum in winter at high latitudes, and in equinoxes at low latitudes [e.g. Hirota, 1984;

Fritts, 1984]. This seasonal and latitudinal behavior of the gravity wave activity is in agreement with that of the inversion layer.

Mlynczak and Solomon, [1991, 1993] and later Fadnavis and Beig [2004] discussed the conversion of chemical potential energy into molecular translational energy through the release of heat by following exothermic reactions.

$$O + OH \rightarrow O_2 + H \tag{5.3}$$

$$H + O_2 + M \rightarrow HO_2 + M \tag{5.4}$$

$$H + O_3 \rightarrow OH + O_2 \tag{5.5}$$

$$O + HO_2 \rightarrow OH + O_2 \tag{5.6}$$

Heat release in Equations 5.3, 5.4, 5.5 and 5.6 are –16.77, –49.10, –79.90 and –53.27 Kcal/mole, respectively.

Reaction 5.5 is involving ozone and atomic hydrogen and makes the largest contribution to the production of the heat in the upper mesospheric region. Following reactions also make contribution to the heat budget of the mesosphere.

$$O + O_2 + M \rightarrow O_3 + M \tag{5.7}$$

$$O + O + M \rightarrow O_2 + M \tag{5.8}$$

$$O + O_3 + M \rightarrow O_2 + O_2 + M \tag{5.9}$$

Heat release in Equations 5.7, 5.8 and 5.9 are –25.47, –119.40 and –93.65 Kcal/mole, respectively.

It should be noted that all the energy generated in these exothermic reactions is not released in the form of heat. About 20 to 30 % of the energy is transformed into optical emissions (primarily, infrared emissions of OH). Consequently, the maximum heating rate of the mesosphere over the midlatitudes was $\sim$ 12 K/d during nighttime, and decreased by a factor of 2 during day because the ozone concentration is reduced by the solar photolysis of ozone.

Whiteway et al., [1995] estimated the heating rates due to turbulent diffusion with dissipation as high as 15-20 K. One of our recent studies [Das et al., 2009] showed from rocket borne and simultaneous satellite observations over Indian low latitude region that the turbulence can cause heating rates upto about 40 K in this altitude region. Meriwether et al., [1998] suggested that the observed inversions during February 1995 over Utah (39° N, 110° W) are caused by a localized mechanism involving the coupling of GWs to the mesopause tidal structure. The present observations would indicate only the development of the lower inversion layer, with the height coverage limited to about 75 km. The simulation revealed that the lower level inversion could develop to an amplitude of about 10 K. From the above discussion, it can be stated that the dynamics associated with the GWs alone would not be able to account for the observed magnitude of inversions. Observations made over Mt. Abu on consecutive days revealed that an inversion could develop upto a magnitude of 20 K or even more from a condition of non-inversion days. To account for this rate of heating, it may be necessary to supplement the source associated with gravity wave breaking/GW-PW interactions with an additional source which could be the chemical heating [e.g. Meriwether and Mlynczak, 1995; Fadnavis and Beig, 2004]. It should be noted that a 40 K increase in the temperature is associated with about 17% decrease in density. It is also to be noted that the inversion layer persists for few days at nearly same altitude. Furthermore, local density deficiencies and prominent GW structures were observed from reentry data of the US space shuttle at around same altitude [e.g., Champion, 1986].

5.3 Stratospheric Sudden Warming

Stratospheric sudden warming is usually a high latitude process but occasionally it propagates to mid- and low- latitudes through sub-tropics. SSW was described as those few occasions during the late winter months when the subtropical jet stream reaches its maximum intensity, confluence patterns develop between the sub-tropical and polar-front jet streams. This can cause displacement or splitting of the circular pattern of the polar vortex and result in the development of large-amplitude wave trains which precede the occurrence of stratospheric sudden warming events.

SSW events are the clearest and strongest manifestation of the coupling between high- to mid- to low latitude regions and also the coupling of the stratosphere-troposphere system. Recent work has shown that the influence of SSWs on the tropospheric flow can last for many weeks [e.g Baldwin and Dunkerton, 2001; Polvani and Waugh, 2004]. It is, therefore, important to correctly represent stratospheric dynamics, and its coupling to the troposphere in numerical models of the climate system. A useful analogy might be drawn at this point with the atmosphere-ocean system, as understanding and successfully modeling the El Nino-Southern Oscillation is very important for the atmosphere-ocean system. Similarly, understanding and successfully modeling stratospheric sudden warming events is of primary importance for the stratosphere-troposphere system.

SSWs have been mainly classified into major and minor warmings, depending on the amplitude of the temperature perturbations and the state of the zonal circulation [Andrews et al., 1987; Marenco et al., 1997]. Major stratospheric warmings are characterized by large perturbations of temperature, and the reversal of the zonal-mean temperature gradients along with that of the zonal-mean wind at 60°N in the mid-stratosphere. Though, minor warmings are classified by weak temperature perturbations and the reversal of the zonal-mean temperature gradients only. Another classification is based on the synoptic structure of the vortex. According to O'Neill, [2003], one type of SSW is due to vortex displacement and other due to vortex splitting. Recently, Charlton and Polvani, [2007] presented a comprehensive study of these two types of SSWs using NCEP and ERA-40 data.

In the past, SSWs have been observed using lidar at high and mid latitudes by many groups [e.g. Hauchecorne and Chanin, 1983; Whiteway and Carswell, 1994; Donfrancesco et al., 1996; Whiteway et al., 1997; Duck et al., 1998; Walterscheid et al., 2000 and reference therein]. Sivakumar et al., [2004] reported a case study on stratopause warming and Sridharan et al., [2009] presented warming episode during February 2006, using lidar measurements over Gadanki, an Indian low latitude station. Recently, Charyulu et al., [2007] presented very detailed climatological study of the SSW using lidar data of OHP. He also presented a case study of SSW event during December 1998. The cause of these SSWs has been either GW activity as proposed by Whiteway et al., [1997] or enhanced PW activity [Hauchecorne and Chanin, 1983; Marenco et al., 1997]. Another cause may be formation of vortex

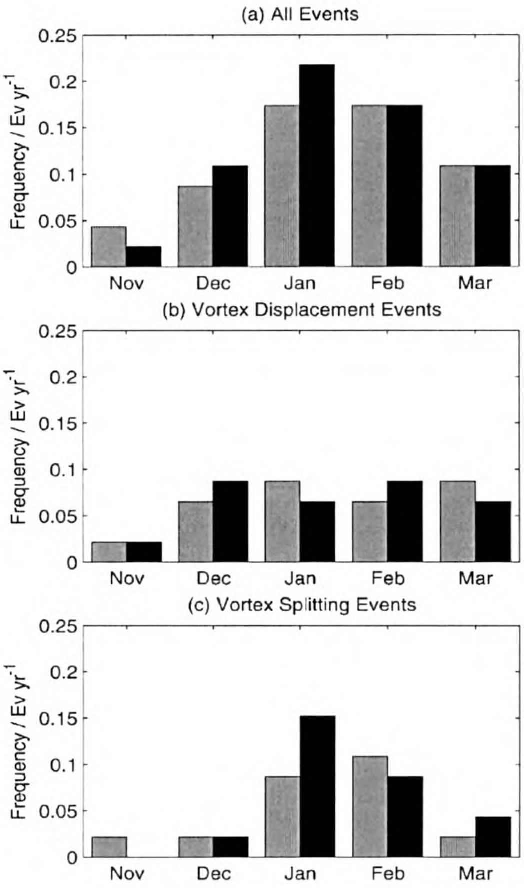

Figure 5.18: *Distribution of stratospheric warmings by month in NCEP–NCAR reanalysis (gray bars) and ERA–40 data sets (black bars): (a) all SSWs, (b) vortex displacements, (c) vortex splits. This figure is based on Charlton and Polvani, [2007].*

core and PW breaking [Labitzke, 1981; Duck et al., 1998; Walterscheid et al., 2000]. In addition to the lidar measurements, rocket and satellite observations based SSW events and modeling of SSW events have also been reported [e.g., Matsuno, 1971; Schoeberl, 1978; Appu, 1984; Randel, 1987; Delisi and Dunkerton, 1988]. Dunkerton et al., [1988] showed that the occurrence of major SSW depends on the phase of Quasi-Biennial Oscillation (QBO) also. They elicited that major SSWs occur only when the QBO phases are westerly.

Characteristically, there are few warming events during every winter, major and/or minor, and these are mostly confined during November to March. Month wise central dates are given in Figure 5.18 [Charlton and Polvani, 2007]. But year 1998 and 1999 was unusually special and had more than one major and minor warming episodes. Furthermore, North Atlantic Oscillation (NAO) Index anomaly was also abnormally high during this year.

Role of sub-tropical region is very crucial as stated above in the definition of SSW. In the current study, two events of SSW observed over Mt. Abu using ground-based lidar measurements during December 1998 and March 1999 are described. The selection of these two events is based on the status of vortex, December 1998 event is due to vortex displacement and a warming episode during March 1999 is associated with vortex splitting. A summary of few different type of events is given in Table 5.2. To support our finding, observations from a different plateform/independent technique, HALOE onboard UARS satellite have also been utilized. Furthermore, the observed SSW events are buttressed in terms of PW and GW activities and dynamical changes in the polar regions.

Table 5.2: SSWs identified in NCEP-NCAR and ERA-40 data sets. 'D' indicates a vortex displacement and 'S' indicates a vortex split. [source, Charlton and Polvani, 2007].

Central date (NCEP)	Central Date (ERA-40)	Type	References
8 Dec 1987	7 Dec 1987	S	Baldwin and Dunkerton,1989
14 Mar 1988	14 Mar 1988	S	
22 Feb 1989	21 Feb 1989	S	Kruger et al., 2005
15 Dec 1998	15 Dec 1998	D	Manney et al., 1999
25 Feb 1999	26 Feb 1999	S	Charlton et al. 2004
20 Mar 2000	20 Mar 2000	D	
11 Feb 2001	11 Feb 2001	S	Jacobi et al., 2003
2 Jan 2002	30 Dec 2002	D	Naujokat et al.,2002

5.3.1 Results and Discussion

Three examples of the observed SSWs over Mt. Abu during different months and years viz., (a) 18 February 1999, (b) 8 March 1999 and (c) 10 March 2000 are shown

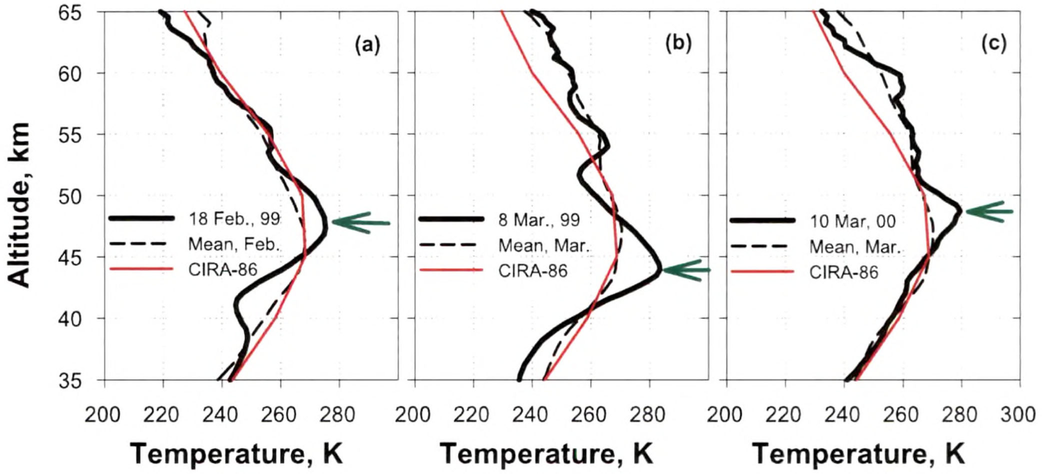

Figure 5.19: *Altitude profiles of temperature illustrating few typical examples of stratospheric sudden warmings observed over Mt. Abu during during different months and years, (a) 18 February 1999, (b) 8 March 1999, and (c) 10 March 2000. All these events are within the range of 10 days from the central date of warming. Green arrows indicate height of the maximum warming. Monthly mean profile of corresponding months and CIRA-86 model temperature profile are also shown in the figure.*

in Figure 5.19. Prominent warming is found in all three events on (a) 18 February 1999, (b) 8 March1999, and (c) 10 March 2000. Climatological mean temperature for the respective months over Mt. Abu along with CIRA-86 model temperature at (25°N) are also shown in the figure. Event of 18 February exhibits warming of about 10 K at altitude of about 47 km. Stronger warming (∼15 K) is noted for 8 March 1999 at lower heights (∼ 44 km) and at rather higher altitude (about 49 km) with magnitude of ∼6 K, on 10 March 2000. Observed features are attributed to the fact that possibly more than one waves is responsible for SSWs. Waves with different characteristics are affecting the general circulation of the stratosphere collectively and facilitate propagation of SSW from high- to low- latitudes.

5.3.1.1 Warming during December 1998

Warming event during December 1998 was associated with displacement of vortex and Figure 5.20 shows lidar observed temperature profile for the night of 17-18 December 1998 (blue and green dots connected by line) along with the standard errors. The mean winter temperature profile derived from the lidar data collected over Mt. Abu from 1997 to 2002 is also displayed (green dashed line). The lidar profile for the night of 17-18 December 1998 clearly shows temperature increasing

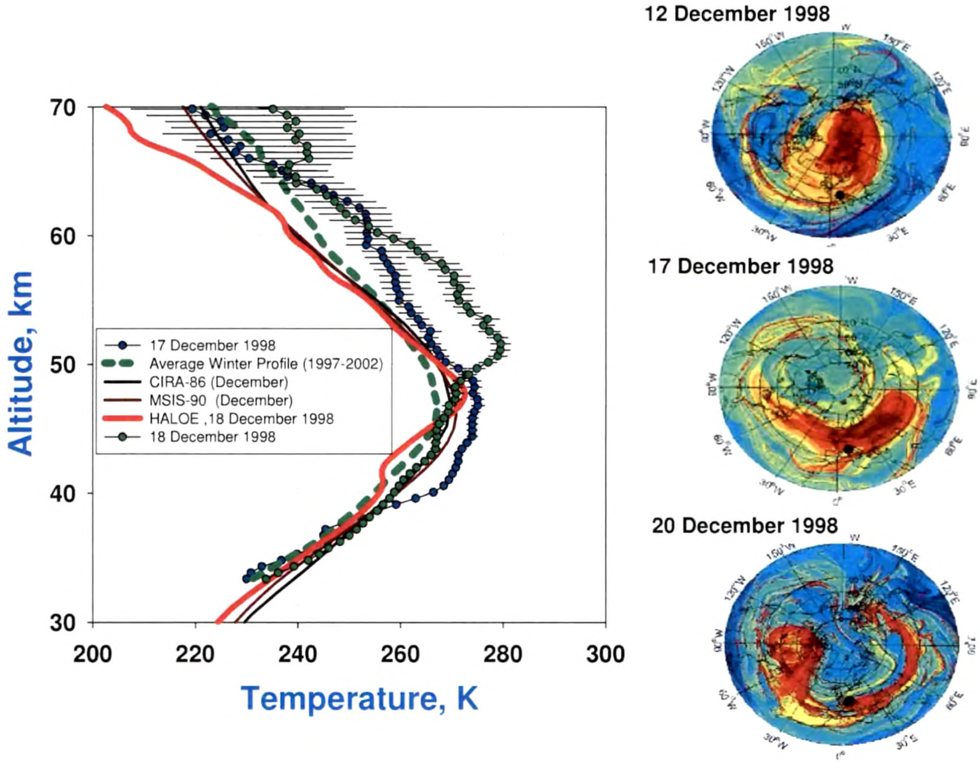

Figure 5.20: Altitude profile of temperature observed over Mt. Abu on 17 December 1998 (in blue) and 18 December 1998 (in green). Thick green dashed line is climatological mean temperature during winter over Mt. Abu. Satellite (HALOE) observed temperature profile on 18 December 1998 over Mt. Abu is shown by thick red line. CIRA-86 and MSISE-90 model temperatures are also shown by black and dark red line for the month of December at 25°N. North Polar stereographic maps of potential vorticity at 950 K provided by MIMOSA simulation for the selected days in December 1998. The outermost circle designates the equator. MIMOSA simulations are reproduced from Charyulu et al., 2007.

in the stratopause and in the lower mesosphere up to a maximum value of 281 K around 52 km. The magnitude of the warming is about fifteen times larger than the standard errors (about 1-2 K at 50 km). Additionally, the HALOE temperature profile measured over the closest location of Mt. Abu is shown in Figure 5.20 (solid red line). HALOE temperature exhibits weak warming (~8 K) than the lidar observed temperature. Nonetheless, it is significantly warmer than the observed winter mean temperature and from CIRA-86 and MSISE-90 model temperatures. Differences between the lidar and HALOE profiles exist and are due to the poorer height resolution of the HALOE measurement (about 3.7 km) in comparison to that of the lidar (about 0.5 km) and also may be due to the different observation timings.

Another interesting feature noted, is very wide stratopause (about 5 km) on 17 December 1998 during the major SSW event. Temperature observed on 18 December 1998 is also significantly higher, (about 15K) in the height range of 50-60 km, than the observed winter mean profile, HALOE temperatures and also CIRA-86, MSISE-90 model temperatures. Right side of the Figure 5.20 contains North polar stereographic maps of potential vorticity at 950 K isentropic level are provided by MIMOSA simulation for the selected days in December 1998. The outermost circle designates the equator. There is a clear indication of the influence of high latitudes phenomena over sub-tropical and tropical latitudes.

The upper mesosphere region (above 65 km), exhibits a cooling of about 2-5 K with respect to the mean profile. It is possibly associated with the stratospheric warming event and, is in accordance with results reported in other studies [Appu, 1984; Delisi and Dunkerton, 1988; Duck et al., 1998; Walterscheid et al., 2000]. The order of magnitude of the stratopause warming observed over Mt. Abu is smaller than that has been reported for mid- and high- latitudes in the northern hemisphere [Hauchecorne and Chanin, 1983; Whiteway and Carswell, 1994; Whiteway et al., 1997; Duck et al., 1998, Charyulu et al., 2007].

5.3.1.2 Warming during March 1999

Figure 5.21 (a-c) shows another warming episode observed over Mt. Abu during 8-10 March 1999. The temperature deviation from climatological mean temperature for different days, are also computed to get better quantitative outlook and, are shown in Figure 5.21 (d-f). To further characterize the operative processes, a stereographic view of potential vorticities on given days are also shown in Figure 5.21 (g-i). On 8 March 1999, maximum warming (about 15 K) is noted at about 45 km

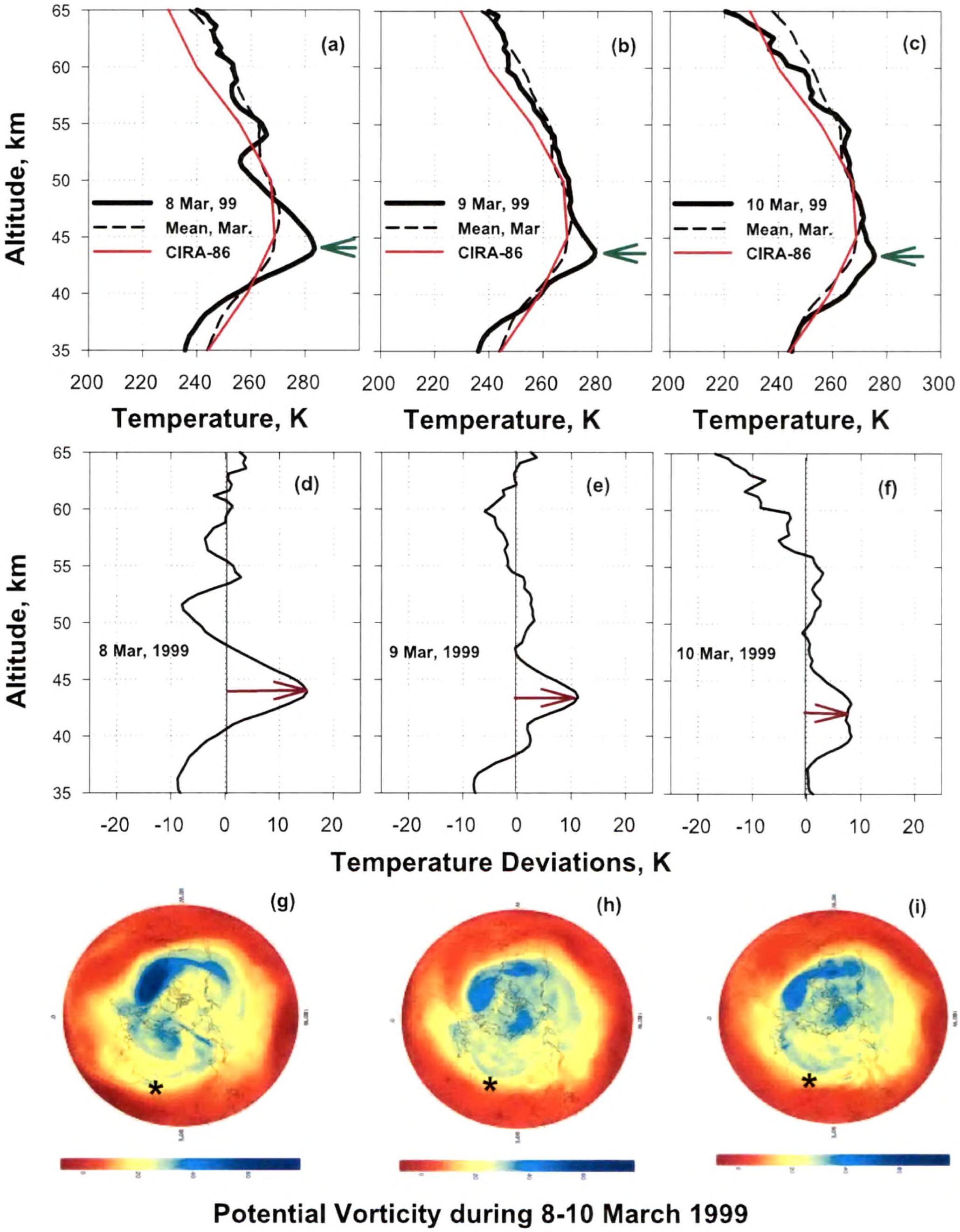

__Figure 5.21:__ A sequence of nightly mean height profiles of temperature illustrating stratospheric sudden warming episode over Mt. Abu during 8-10 March 1999 shown in (a), (b) and (c). Monthly mean profile of March 1999 and CIRA-86 model temperature profiles are also shown in the figure. Green and red arrows indicate height and strength of the maximum warming. Stereographic view of potential vorticity during 8-10 March 1999 is also given in the figure (g), (h) and (i), respectively. Location of Mt. Abu is indicated by a black star.

and progressively the magnitude of warming decreased. The height of the maximum warming also decreased during these three days. And interestingly, warming became broader on 10 March 1999, accompanied with a signature of double stratopause. Furthermore, a strong wave feature is found in the altitude profile of the temperature with vertical wavelength (about 12 km) on 8 March 1999, which further substantiates the fact that waves are playing a very vital role in the SSW episodes.

To further characterize SSW and to unravel the atmospheric dynamics (associated with PW) during the SSW events, isentropic maps of potential vorticity have been used. Similar, approach has been followed elsewhere and is used to study SSW in connection with the breaking of planetary waves [Dunkerton and Delisi, 1986 and reference therein]. This hypothesis suggests that large-scale wave breaking leads to polar-vortex distortion and erosion, and may induce stratospheric warming. In getting the signature of SSWs in the sub-tropical and tropical latitudes, the size/strength and displacement/splitting of the vortex determines the range of latitudes over which planetary and Rossby waves are able to propagate.

The status of various physical parameters in the polar region are shown in Figure 5.22. Area weighted (90°N-50°N) polar cap temperature at 10 hPa is shown in Figure 5.22a and very prominent peaks during December 1998 and Feb-March 1999 are present. Average zonal wind at 10 hPa also decreased and even reversed from its normal values as shown in Figure 5.22b. Fluxes associated with different waves are also shown in Figure 5.22c. Significant meridional heat flux anomalies (given in Figure 5.22d) were present during this period. It is clear from Figure 5.22, that the above described parameters are anomalous for relatively longer duration during warming episode of Feb-March 1999 than during December 1998 It is expected, as these episodes are associated with different state of polar vortex; December 1998, due to vortex displacement and February-March 2000, due to vortex splitting.

Another tool to decipher and characterize the variations in the strength of the polar vortex are annular modes, which are hemispheric-scale patterns characterized by synchronous fluctuations in pressure of one sign over the polar caps and of opposite sign at lower latitudes [Baldwin and Dunkerton, 2001] and within the stratosphere, annular mode are a measure of the strength of the polar vortex, which

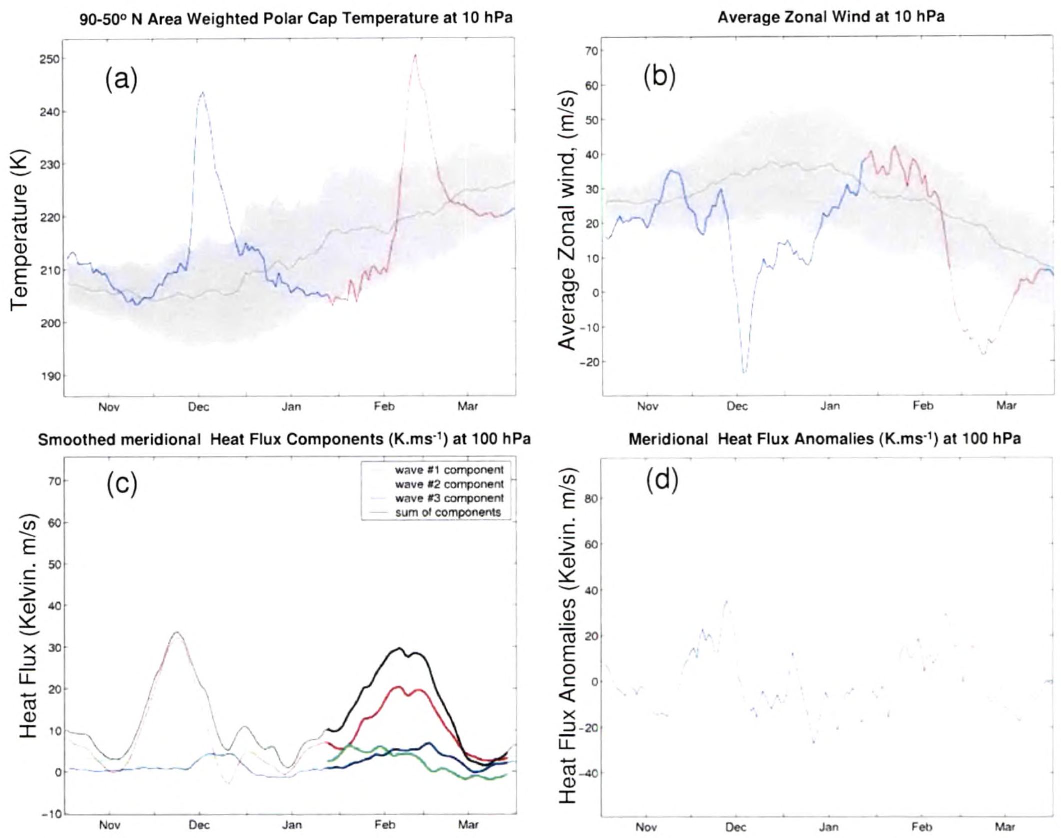

Figure 5.22: *The status of polar (a) temperature, (b) winds and (c) the components of heat fluxes. Anomalies in heat fluxes are also given in (d). This figure is generated using ERA-40 data set*

is recognized as the North Atlantic Oscillation (NAO) [e.g., Hurrel, 1995] over the Atlantic sector. Figure 5.23 [based on Baldwin and Dunkerton, 2001] illustrates the time-height development of the annular mode, with daily resolution in northern hemisphere winter of 1998-1999. In the stratosphere the time scale is relatively long, illustrating periods when the polar vortex was warm and weak (red), beginning in December to late February, and periods when the polar vortex was cold and strong (blue). This again strengthens the view that the SSWs during December 1998 and March 1999 were due to long range transport from polar- to mid- to sub-tropical latitudes. Calculations of Elisan-Palm flux, indicative of strength of PW activity and dynamics, during December 1998 event [Charyulu et al., 2007]

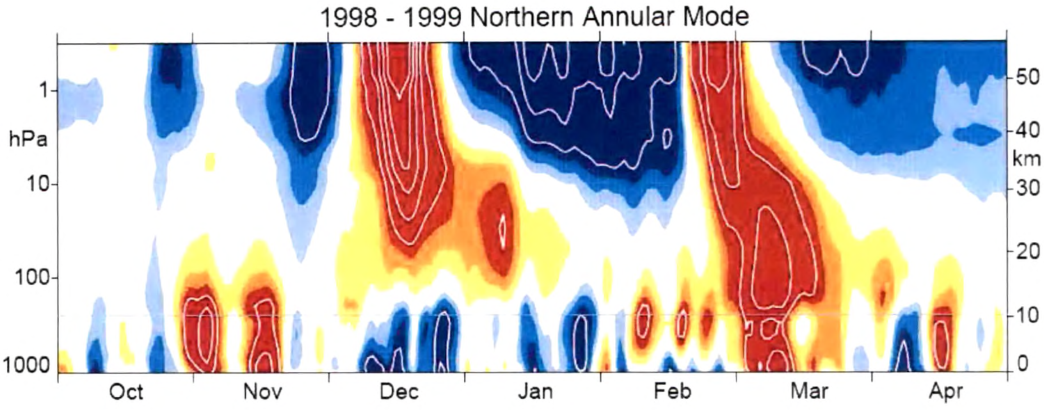

Figure 5.23: *Time-height development of the northern annular mode during the winter of 1998-1999. The indices have daily resolution and are non-dimensional. Blue corresponds to positive values (strong polar vortex), and red corresponds to negative values (weak polar vortex). The contour interval is 0.5, with values between 20.5 and 0.5 unshaded. The thin horizontal line indicates the approximate boundary between the troposphere and the stratosphere. This figure is based on Baldwin and Dunkerton, 2001.*

have also revealed enhanced PW activity, which are another major driver for the occurrence and propagation of SSW to the lower latitudes.

Recently, it is has been demonstrated that SSWs have imprint on the different distant spheres also. Chau et al., [2009] revealed that the equatorial vertical E $\times$ B drifts exhibit a unique and distinctive daytime pattern during a minor SSW event. They proposed that both events might be related through the global effects of planetary waves. Another interesting study by Osprey et al., [2009] showed that the rate of high energy cosmic ray muons, as measured underground, is strongly correlated with SSW events.

5.4 Summary

Specific features of middle atmospheric temperature profiles viz., double stratopause, mesospheric temperature inversion, and stratospheric sudden warming have been studied over Mt. Abu.

Lidar based climatological study of double stratopause is presented from three different stations in the northern hemisphere viz., OHP, Mt. Abu and Gadanki, representing mid-, sub- tropical and low- latitude stations, respectively. Detailed study of the double stratopause from these stations ascertains that the structure exists over the globe with significant seasonal and latitudinal variations. It is also found that the occurrence characteristics over Mt. Abu and OHP are very similar, possibly due to more influence of the mid-latitude processes over Mt. Abu and also could be due to similar topography at both these locations. The high and low correlation coefficients obtained for the UDS and LDS heights of occurrence, respectively and their corresponding mean potential energy illustrates that GW is one of the most probable generative mechanisms for UDS layer. Similarly, the extracted PWs display low and high amplitudes for the UDS and LDS height regions and suggest the major role of PWs in generating LDS. This is in agreement with wave propagation in the middle atmosphere. PWs propagate upward and equator-ward with decreasing amplitudes toward tropics, while GWs propagate vertically with exponentially increasing amplitudes. Additionally, GW breaking and associated turbulence nearby the stratopause region could also contribute to the observed cooling at the stratopause height and thereby generating double stratopause.

Present study of the MTIs over Mt. Abu from two different, independent techniques, lidar and satellite, revealed very interesting features of the MTIs. The sequence of continuous observations revealed that the inversions lasts for few nights, which is similar to the observed feature over mid-latitudes. The seasonal dependence of the inversion is found to be similar for sub-tropical and mid-latitudes. Further, present study revealed that the occurrence frequency of MTI is maximum during winter and following an annual cycle, similar to the mid-latitude stations. In spite of significant latitudinal separation, inversions over sub-tropical location closely resemble those reported for mid-latitudes [e.g. Hauchecorne et al., 1987]. The seasonal variation of the altitude of the inversion is very similar to the seasonal variation of the MST radar echoes in the mesosphere. Rocket borne studies also revealed the presence of neutral turbulence at mesospheric heights in the Indian low latitudes region. These results indicate that these two phenomena could have the same origin. Possibility of a rapport between temperature inversions and turbulence due to breaking of GWs cannot be ruled out.

SSWs are mostly observed over high- and mid-latitudes, however, a lidar study over Mt. Abu demonstrated that depending upon their strength and background atmospheric conditions, these events/episodes are affecting sub-tropical locations also. Two events associated with different vortex conditions, December 1998 and March 1999, were studied. It is found that the events associated with vortex splitting are having stronger impact for longer durations than the vortex displacement associated warmings. High latitude processes also have been studied to corroborate these warming episodes. It is clearly brought out that the SSW events are affecting the sub-tropical latitudes. These events are the clear and strong manifestation of the latitudinal coupling as well as coupling of the stratosphere-troposphere system.

CHAPTER 6

Long Term Temperature Trends over Mt. Abu

In the last few decades there has been a great concern for long term changes in the Earth's atmosphere, mainly due to increased anthropogenic activities globally. Temperature trends in the stratosphere are an important component of global change. These trends provide evidence of the roles of natural and anthropogenic climate change mechanisms; the imprint of distinct tropospheric warming and stratospheric-mesospheric cooling provides information on the consequences of these mechanisms [e.g., Intergovernmental Panel on Climate Change (IPCC), 2001, 2007].

Roble and Dickinson [1989] were the first to report that due to increased concentration of CO_2 and CH_4, in addition to the warming of the troposphere, there is an associated cooling in the stratosphere and mesosphere. In recent years, there have been significant scientific efforts in obtaining the middle atmospheric temperature trends both by way of observation and through development/improvement of models.

Over longer timescales and even in 11 year solar cycle, various atmospheric responses were obtained, varying from slightly positive to negative [e.g., Mohankumar, 1995; Hauchecorne et al., 1991; Ramaswamy et al., 2001, Labitzke et al., 2002;

Beig et al., 2003]. Recently, Bencherif et al., [2006] calculated temperature trends in the Upper Troposphere and Lower Stratosphere (UTLS) region in the southern hemisphere using radiosonde data from Durban, South Africa (30.0°S, 30.9°E) over the period 1980 to 2001 (22 years). They studies a mean temperature climatology and trends and reported that temperature is one of the most important indicators of changes in dynamical and radiative processes in the atmosphere. A trend analysis revealed a cooling trend at almost all heights in the UTLS region, with a maximum cooling rate of 1.09 ± 0.41 K/decade, at 70 hPa. They reported that cooling rates were higher in summer than in winter.

Studies of trend investigations and evolution of stratospheric temperature [Ramaswamy et al., 2006; Schwarzkopf and Ramaswamy 2008] reported that in the tropical upper stratosphere there was a positive response of $\sim$1 K in accordance with photochemical theory, whilst in mid- and high-latitudes, a large negative signal was clearly observed.

Analysis of simulated temperature trends is now a standard diagnostic tool for evaluating stratospheric climate model performance [e.g., Eyring et al., 2007]. The recent assessments concluded that between 1980 and 2000, in the global mean, the lower stratosphere was cooling at a rate of around 0.5-1 K/decade, cooling less rapidly (about 0.5 K/decade) in the mid-stratosphere, and cooling at more than 2 K/decade in the upper stratosphere and lower mesosphere [Ramaswamy et al., 2001; Shine et al., 2003]. The magnitude of trends is large compared to trend in the global mean surface temperature, which is about 0.2 K/decade over the same period [e.g., IPCC, 2007]. A study based on model inter-comparisons [Shine et al., 2003], reported on the causes of the stratospheric cooling and concluded that the upper stratospheric trends were driven by ozone depletion and increase in carbon dioxide. It also revealed that the degree of agreement between model and observations was not very good. At the same time it was found that the models could not account for the apparent minimum in the cooling trend in the mid-stratosphere.

A major impediment in developing a comprehensive middle atmospheric temperature trends is uncertainty regarding the homogeneity of observational data. Most of the instruments have been designed and operated primarily to provide information for weather forecasting or were focused on short-term research (due to several non scientific issues viz., lack of logistical, financial, manpower support etc.), rather than for the detection of long-term trends, and hence continuity of record has not been a main concern.

The longest data series from radiosondes which extends back to the late 1950s. However, radiosonde observation are limited by height up to $\sim$ 35-40 km and there have been many changes in instrumentation over the period of last $\sim$50 years. Hence the radiosonde data contains significant inhomogeneities [e.g., Gaffen, 1994; Lanzante et al., 2003a, 2003b; Seidel et al., 2004].

Satellites provide nearly global observations of middle atmospheric temperatures and this era started few decades ago, with the series of observations (beginning in the late 1970s) from the TIROS Operational Vertical Sounder (TOVS) instruments on the NOAA operational satellites. These instruments provide data up to the upper stratosphere in the height range of $\sim$ 25-50 km. They are the main source of temperature information over multi-decadal periods. These also could not serve appropriately for trend detection due to several reasons viz., instrument packages were relatively short-lived, data from 13 different satellites have been used since 1979, each instrument package has slightly different characteristics, the orbits differ between satellites and drift for individual satellites, the overlap period between different satellites, etc.

Other important sources of data on temperature trends in the stratosphere and the mesosphere include the rocketsonde measurements. But these also could not provide long term temperature data due to high cost of rockets, payloads, several strict logistic requirements, etc. severely constrained frequency and spatial distribution of rocket launches [Free and Seidel, 2005].

One of the most important sources of continuous long term temperature records in the atmosphere is the Rayleigh lidar measurements (covering altitudes 30-80 km) [e.g., Chanin et al., 1987; Keckhut et al., 1999, 2004 and reference therein]. One of the major strengths of the lidar is that, no adjustment or external calibration needed and studies suggest that individual profiles can be derived with an accuracy of better than $\sim$1 K in the height range of about 30-60 km [e.g., Keckhut et al, 2004]. Several lidars were deployed within the Network for the Detection of Stratospheric Change (NDSC) [Kurylo and Solomon, 1990], and are currently part of the Network for the Detection of Atmospheric Composition Change (NDACC). Time series of these data span from one to more than two decades. These records are available only for a small number of stations. Though, lidar provides valuable corroborative information on the middle atmospheric thermal structure, its spatial coverage is too limited to permit reliable calculation of global trends. As stated earlier, these studies were mainly concentrated in the mid- and high-latitudes regions. There in no such study of the long term temperature trends from sub-tropical Indian location. Keckhut et al., [1995] presented a study on the prediction of data length for significant trends detection and showed that minimum length of data should be more than two solar cycles for significant trends estimation. In present study, an attempt is made to examine the last 11 years Rayleigh lidar data for possible long term temperature trend over Mt Abu.

6.1 Data Sets and Method of Analysis

The longest temperature data series in the upper stratosphere and mesosphere in India have been provided by routine Rayleigh lidar observations over Mt. Abu, from 1997 to 2007. The data have been collected regularly throughout the year except during local monsoon months of June to August. The temperature data series in the upper stratosphere and mesosphere, covers a complete solar cycle with $\sim$500 nights of lidar observations. Out of these observations, $\sim$400 nights data (when signal is good up to $\sim$75 km) have been used. Prior to the estimation of temperature trend, short term variabilities were removed. For overcoming day to day variations, monthly mean profiles were obtained and to filter out seasonal variation, each monthly profile was taken individually for every year. For removing interannual variation the temperature deviations were calculated from climatological mean for each month [Funatsu et al., 2008]. It is important to mention that during the last $\sim$ 11 years of the observations no major changes were made in the PRL's Rayleigh lidar system which warrants the data quality due to instrumental drifts. Furthermore, these observations over Mt. Abu were conducted by the same team of scientific and engineering staff. In addition to the lidar data, satellite data from HALOE (onboard UARS) from 1991-2005 have also been used in this study.

Temperature trends were estimated by simple linear regression for the period 1997-2007. The time series of the temperatures at fixed altitudes for different months were constructed and similar plots were created from the deviations obtained from climatological mean for each month.

6.2 Results

Temperature trends over Mt. Abu were estimated using Rayleigh lidar data from 1997-2007 and HALOE (onboard UARS) data from 1991 to 2005.

Figure 6.1 shows an annual time series of the monthly mean temperatures from lidar (1998-2007) and HALOE (1992-2005) for the month of January (a representative of local winter) at different height levels. Temperatures at 35 km, 45 km and 55 km represent stratosphere, near stratopause and the lower mesosphere, respectively. Simple linear regression fits are also given in Figure 6.1. There is a decreasing temperature trend at 35 km, 45 km and very week negative trend at 55 km from lidar. However, from satellite observations, a decreasing trend at 35 km, very week trend at 45 km and a increasing trend at 55 km is obtained. Decreasing temperature trend is strongest at 35 km from both, lidar and satellite temperatures during January.

Similar plots are shown for the month of April in Figure 6.2 at heights 35 km, 45 km and 55 km. During April also, a decreasing trend is revealed from both techniques (lidar and satellite) at these three altitude levels representing different regions of the middle atmosphere. During April decreasing trend is weaker than the January, except at 55 km, whereas during January a weak trend is revealed by lidar and increasing trend is shown by satellite.

Figure 6.3 shows the temperature deviations (ΔT) from the mean temperature at altitudes 55 km, 45 km and 35 km, respectively for the month of January and April from 1997 to 2007. Temperature trends, estimated by simple linear regression, were -0.55 $\pm$ 0.10 K/year, at 35 km, -0.49 $\pm$ 0.19 K/year at 45 km and -0.05 $\pm$ 0.21 K/year at 55 km in the month of January and are shown in Figure 6.3. Due to large scatter in temperature values at 55 km, trend estimation errors are high, considering the errors in the estimation, the trend at this level may not be statistically

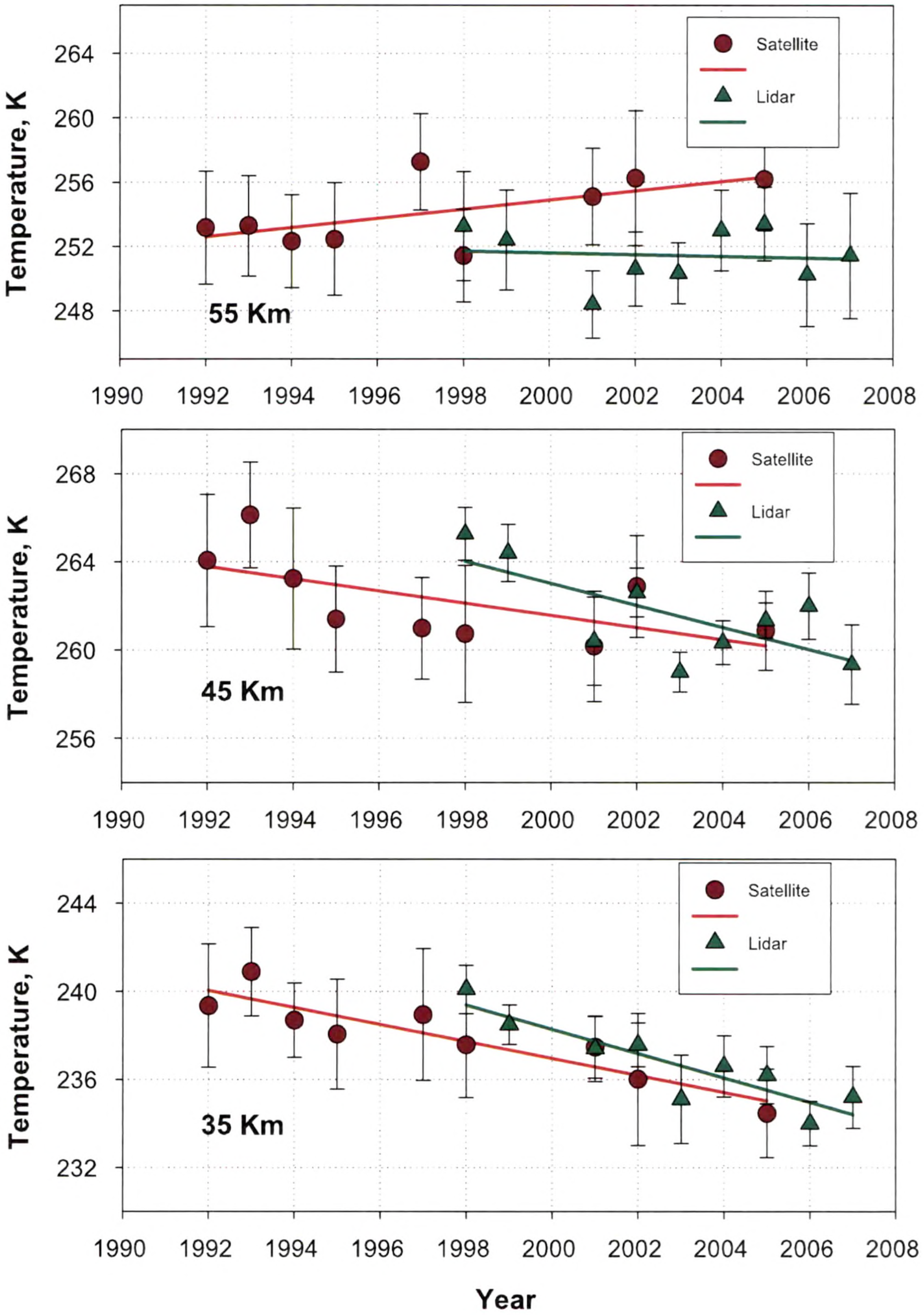

Figure 6.1: *Variation of the mean temperature during January over Mt. Abu from 1998-2007 (from lidar) and 1992-2005 (from satellite) at different heights 55 km, 45 km and 35 km. Simple linear regression best fits are also shown for lidar (green line) and satellite (red line) temperatures.*

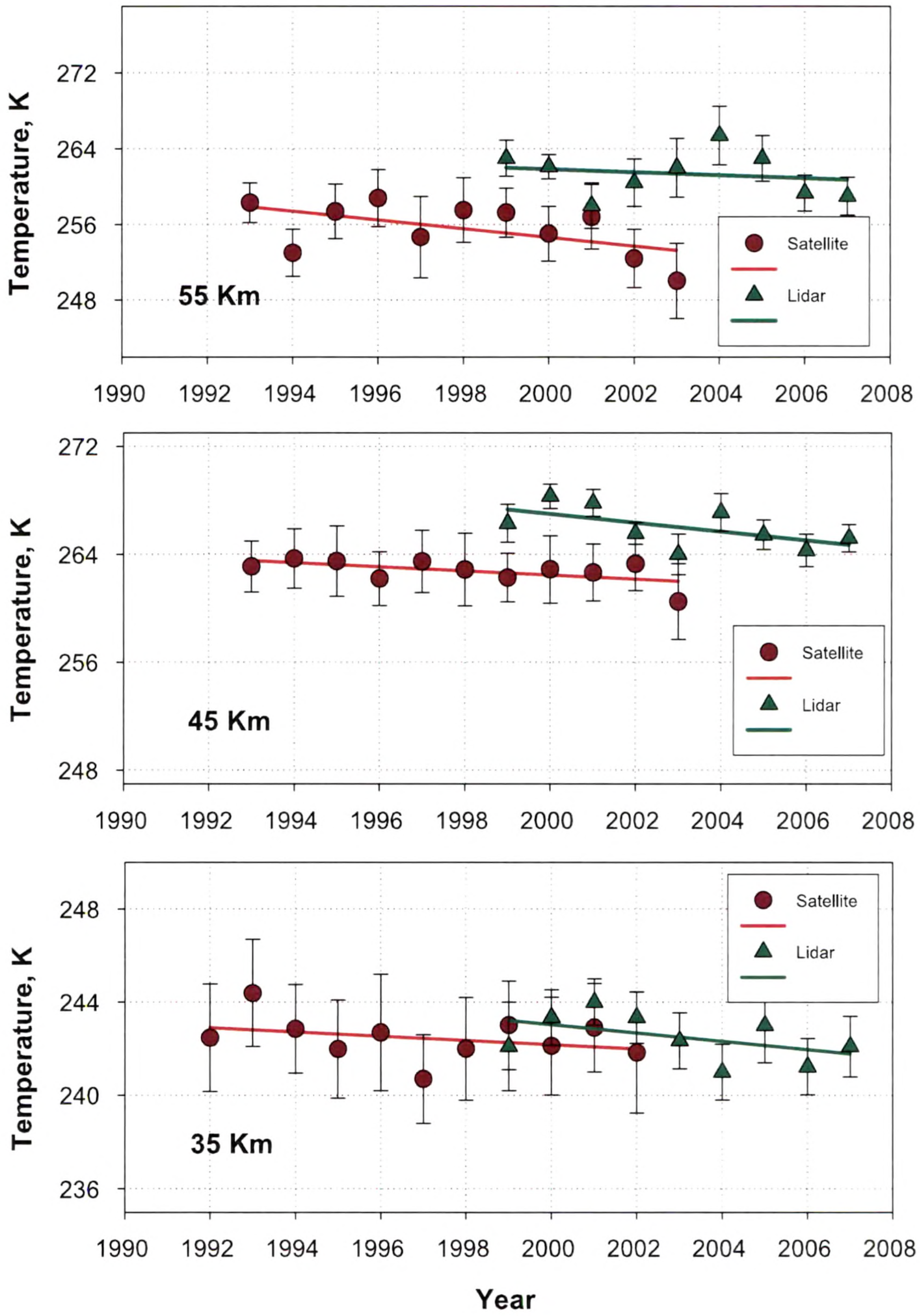

Figure 6.2: *Same as Figure 6.1 but for the month of April (lidar temperatures are from 1999-2007).*

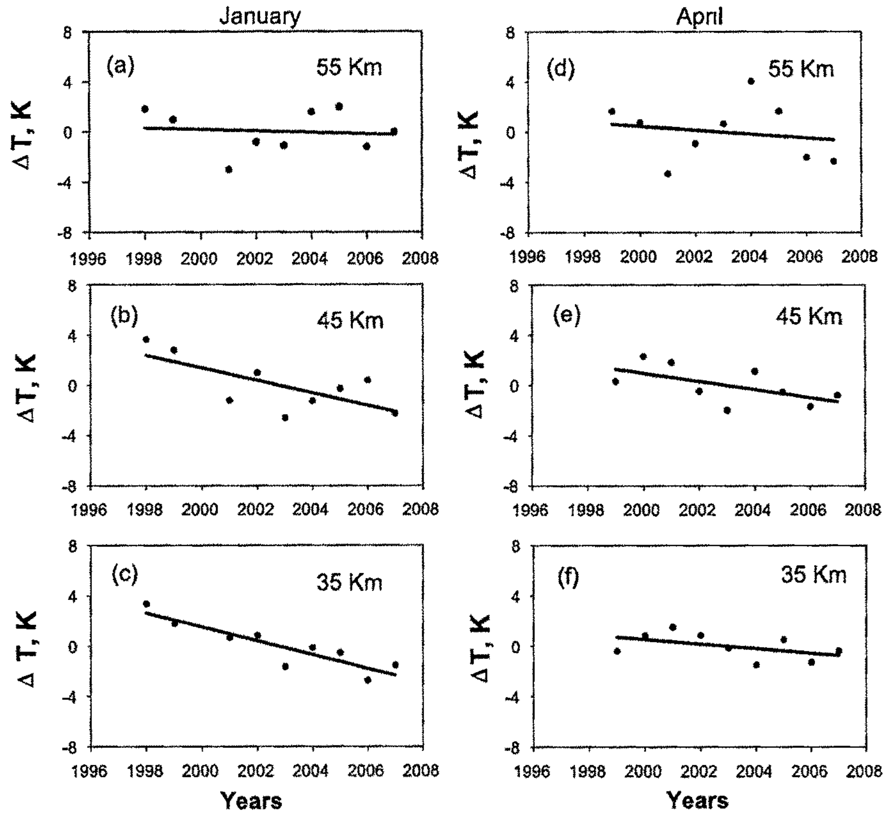

Figure 6.3: Temperature deviations from climatological mean temperature for the month of January (1998-2007) and April (1999-2007) over Mt. Abu. Simple linear regression fits are also shown.

significant. At 35 km and 45 km estimation errors are not very large so at these levels trends are significant. It should be noted that these are only temperature trends and not temperature trends, which require longer data length.

Similarly, temperature deviations were estimated for the month of April and shown in Figure 6.3(d-f). Observed temperature trend is the strongest (-0.33 $\pm$ 0.16 K/year) at stratopause level (45 km) and the weakest (-0.15 $\pm$ 0.32 K/year) at 55 km during April. The temperature trend is -0.17 $\pm$ 0.12 K/year at 35 km, but at this altitude estimation errors are also high due to large scatter in the temperature in these height region.

From the study of deviations for the month of January and April, it is found that the decreasing temperature trends in the stratosphere are weaker in April than in

January. Though, in the lower mesosphere these are not significant as the errors are of similar magnitude as trends.

Seasonally stronger temperature trends are found during winter -4.2 ± 2.5, -4.8 ± 2.4 and -2.0 ± 2.1 K/decade at 35, 45 and 55 km, respectively. The temperature trends during summer months are -2.1 ± 2.0, -2.6 ± 1.8 and -2.3 ± 2.7 K/decade at 35, 45 and 55 km, respectively. Observed temperature trends are lower in summer than during winter months. Stronger decreasing trend in temperature during winter months is possibly due to decreased ozone number density in the sub-tropics [Leblanc et al., 2000; Randel and Wu, 2007]. A long term temperature trend study in the UTLS region of the southern hemisphere reveled a stronger trend during summer than in winter [Bencherif et al., 2006]. Considering hemispheric seasonal differences, observed stronger stratospheric trends in winter over Mt. Abu are in agreement with the trends in the sub-tropics of the southern hemisphere.

6.2.1 Possible Influence of Natural Forcing

Solar variability and volcanic eruptions are two major components of natural forcings, which can influence the middle atmospheric temperature structure. The 11-year solar cycle plays an important role in the middle atmospheric temperature [Chandra, 1985]. Quantifying solar effects in the stratosphere-mesosphere is important for understanding forcing mechanisms and coupling with the troposphere [e.g., Haigh, 1994], and for comparison with model simulations [e.g., Austin et al., 2007, 2008]. The data used in this study covers almost one recent solar cycle (1997-2007), which is not influenced by any large volcanic signal.

A recent study by Randel et al. [2009], demonstrated that the solar cycle signature (solar maximum to solar minimum) in the temperature trends is of the order of 0.2 K/decade over sub-tropical region. Therefore, the effect of the solar cycle variation is not looked into detail as the data series covers only one solar cycle, from a solar minimum (1997-98) to the next solar minimum (2007). A plot of the sunspot variation (proxy of the solar activity) is given in Figure 6.4. Keckhut et al., [1999] explored the tidal effects also and found that their impact on trends are minor as measurements are mainly obtained in the first half of the night over Ob-

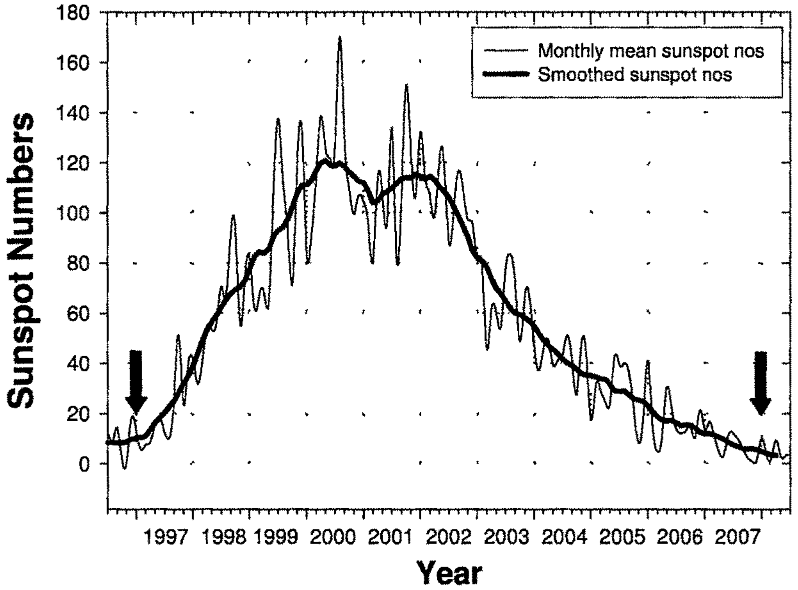

Figure 6.4: Variation of the monthly mean sunspot numbers during 1997–2007. Smoothed sunspot numbers are also shown by thick red line. Blue arrows indicate the beginning (1997) and end (2007) of the lidar data used in present study

servatoire de Haute-Provence (OHP). Over Mt. Abu also most of the observations were made during first half of the night. As demonstrated in Chapters 4 and 5, Mt. Abu and OHP temperature structures are very similar hence, over Mt. Abu also, there may be very minor or negligible effect of tidal forcing on the estimated temperature trend.

6.2.2 Comparison with Trends/Tendencies over Other Locations

Observed temperature trends over Mt. Abu are compared with the trends and trends over other locations from lidar and other techniques in different regions of the Earth's atmosphere and are summarized in Table 6.1. In general temperature trends are showing decreasing temperatures in the middle atmosphere. Observed temperature trend over Mt. Abu is in reasonable agreement with the observed trend over OHP, a mid-latitude station [Funatsu et al., 2008].

***Table 6.1:** Comparison of observed temperature trends over Mt. Abu with the temperature trends over other locations.*

Location and Height	Study Period	Technique	Temp. Trend (K/decade)	References
44°N (60-70 km)	1978-1989	Lidar	- 0.4	Hauchecorne, et al., [1991]
10°N to 90°N (26-35 km)	1973-1985	Rocket	-0.5	Labitzke and van Loon [1995]
44°N, 47°N (55-75 km)	1979-1991	Lidar	> - 0.4	Keckhut et al., [1995]
44°N, 6°E	2001-2007	Lidar		Funatsu et al., [2008]
32 km			-2.5 ± 2.6	
36 km			-4.4 ± 3.2	
40 km			-5.0 ± 3.2	
24.5°N, 72.7°E	1997-2007	Lidar		Present study
35 km			-3.2 ± 2.3	
45 km			-3.7 ± 2.1	
55 km			-2.2 ± 2.4	

6.3 Discussion and Summary

The analysis of Rayleigh lidar data (1997-2007) over Mt. Abu, revealed a decreasing temperature trends in the upper stratosphere and in the lower mesosphere. Observed temperature trends could be due to the following major geophysical processes - ozone plays a vital role in the stratospheric and mesospheric processes. Stratospheric temperature is mostly governed by ozone while temperature impacts ozone concentrations due to heat sensitive chemical kinematics. Another important factor responsible for the stratospheric and mesospheric cooling is the increased concentration of CO_2, mostly due to increased anthropogenic activities.

Kokin et al., [1990] reported a cooling trend in the mesosphere using Soviet rocket data base. However, trends were highly variable (6-12 K/decade) in the five different sites located over the high latitudes. Another study based on rocket by Kokin and Lysenko, [1994] revealed reasonable agreement with Mt. Abu which presents a cooling of 0.4 K/year in the summer.

On comparing with model predictions, 2-D numerical models show a maximum of cooling around 45 km, which is in good agreement with lidar observed trend over Mt. Abu. Considering decrease in temperature due to both, the doubling of equivalent CO_2 and the decrease in ozone, simulations by Brasseur et al., [1990] predicted a maximum cooling at north pole of 23 K. Further, including heterogenous chemistry, there is a positive feedback on the ozone destruction [Pitari et al., 1992], leading to the extension of this cooling to mid latitudes. They showed that, at the present rates of increase in greenhouse gas, temperature could decrease in the stratosphere by about 0.10 to 0.20 K/year, which is in reasonable agrement with our observations over Mt. Abu.

Golitsyn et al., [1996] presented a long term temperature trend study in the middle atmosphere based on rocket flights from high- mid- and low-latitudes. They used temperature data from weekly rocket temperature soundings at polar (Heiss Island, 80.6°N and Molodezlmaya, 67.7°S), temperate (Volgograd, 48.7°N and Balk-hash, 46.8°N) and tropical (Thumba, 8.5°N) latitudes and found a significant cooling, of the order of a few Kelvin at 30-40 km, $\sim$10 K at 50 km and $\sim$20 K at 60-70 km. Ramaswamy et al., [2001] showed a decreasing temperature

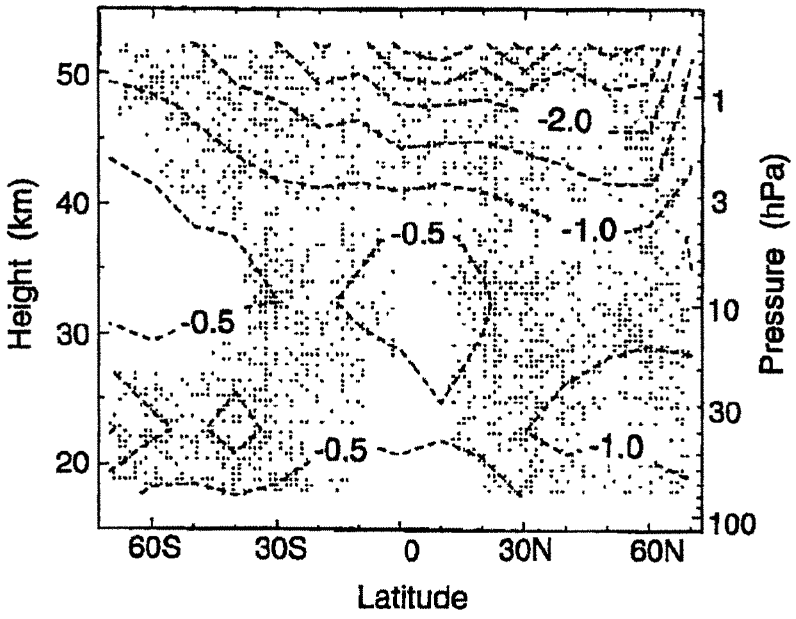

Figure 6.5: Zonal, annual-mean decadal temperature trends versus altitude for the 1979-1994 period, as obtained from the satellite (using MSU and SSU channels) retrievals Contour interval is -0.5 K/decade. Shaded areas denote significance at the 2σ level. (Source, Ramaswamy et al., [2001]).

trend in the middle atmosphere based on observations from satellite platforms. Figure 6.5 shows a zonal, annual-mean decadal temperature trends versus altitude for the 1979-1994 period. Contours in the figure are at interval of -0.5 K/decade and shaded areas denote significance at the 2σ level. There is a significant decreasing temperature trend in the middle atmosphere (-0.5 - 2.0 K/decade) of the sub-tropical region. Over Mt. Abu, though similar cooling trend is observed in the stratosphere, above 45 km, there is stronger cooling reported by Ramaswamy et al., [2001], which is not found over Mt. Abu. This may be due to different observing platforms and stronger influence of local dynamical features, which are stronger over Mt. Abu due to its location in the hilly terrain. The length of the data also could be a possible source of these differences.

A review of long term temperature trends in the mesosphere and lower thermosphere was presented by Beig et al., [2003, 2008], who found that a majority of studies indicate negative trends in the lower and middle mesosphere with an amplitude of a few degrees (2-3 K)/decade. Furthermore, it was reported that the solar signatures were much smaller in the trends and in some cases, no significant solar signature was noted.

A review of ozone and lidar temperature validations brought out a positive association between ozone and temperatures in the stratosphere [Keckhut et al., 2004], which is in agreement with the present study over Mt. Abu. Further, Keckhut et al., [2005], analyzed three independent temperature data sets (US rocketsondes, the OHP lidar, and the global temperature database made by the successive SSU on the NOAA satellites) for quantifying the influence of the 11-year solar cycle modulation of the UV radiation. Measurements covered the upper stratosphere and the mesosphere, where the direct photochemical effect is expected. The impact of the 11-year solar cycle on temperature trends was found to be location dependent and variable. In the tropics, a 1-2 K positive response in the mid and upper stratosphere has been found and at mid-latitudes, negative responses of several Kelvin have been observed, during winters. Manzini et al., [2003] developed a new interactive chemistry-climate model for the study of sensitivity of the middle atmosphere to ozone depletion and increase in greenhouse gases. They also found an association between ozone depletion and recent stratospheric cooling. Recently, Pawson et al., [2008] explored link between the stratospheric thermal structure and the ozone distribution in the Goddard Earth Observing System chemistry-climate model (CCM). They validated ozone and temperature fields using estimates based on observations. Their ozone-change experiments revealed that the thermal structures of the general circulation model (GCM) and CCM respond in a similar manner to ozone differences between 1980 and 2000, with a peak ozone-induced temperature change of about 1.5 K (over 20 years) near the stratopause. Furthermore, they reported that greenhouse gas-induced cooling increases with altitude and, near the stratopause, contributes an additional 1.3 K to the cooling near 1 hPa between 1980 and 2000.

The altitude range covered in the present study (except the lower mesosphere) corresponds to a region where the direct photochemical and radiative effects on ozone are expected. On the 11-year time scale, ozone responds qualitatively as predicted by photochemical models [e.g., McCormack and Hood, 1996], however,

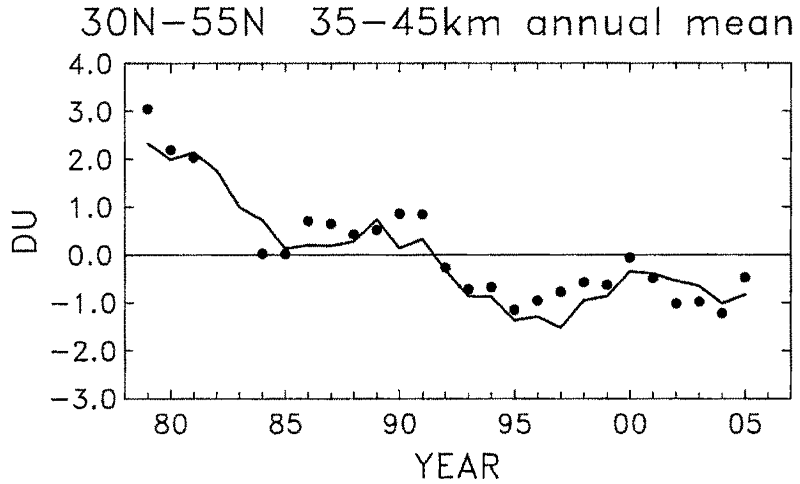

Figure 6.6: *Time series of annual average ozone anomalies from SAGE I and II data, averaged over 35-45 km and 30° - 55°N. Regression fit is also shown in figure. (Source, Randel et al., [2007]).*

some differences in magnitude do exist. In the tropical region, response showing a maximum at around 40 km of 1-2 K and extending from 30 to 50 km is reported by both SSU and US rocketsonde data series. Randel et al., [2007] presented ozone trends in the region 30-55°N from the last 25 years (1979-2005) and a graph reproduced from their study is shown in Figure 6.6. A strong decreasing trend in ozone is seen up to 1995 and later, though trend is weak, it continues to be negative. Recently, Observed decreasing temperature trend could be due to decreasing ozone trends in the sub-tropical region. Another very important aspect that needs to be looked for temperature trends in the middle atmosphere is the dynamics (due to presence of gravity and planetary waves). These could be a major source for the uncertainty in the temperature trends. Tropospheric and sea surface temperatures are also affecting middle atmosphere on longer time scales and their features could be incorporated in the model studies.

Recently, Randel et al., [2009] up-dated the scenario of the observed stratospheric temperature trends using satellite, radiosonde, and lidar observations. In their study, satellite data include measurements from the series of NOAA operational instruments, including the Microwave Sounding Unit covering 1979-2007 and the Stratospheric Sounding Unit (SSU) covering 1979-2005. They found a cooling of ∼-0.5 K/decade in the lower stratosphere over the globe for 1979-2007. Trends in the middle and upper stratosphere showed cooling of about 0.5-1.5 K per decade during 1979-2005, with the greatest cooling in the upper stratosphere near 40-50 km which is again in agreement with our findings at Mt. Abu.

Long term temperature study over Mt. Abu shows that there is a decreasing trend in the temperatures in the middle atmosphere. Maximum decrease in temperature is noted during the winter months. During summer months, though overall trend is negative, the scatter in temperature is large and trends are weaker than trends during winter months. To further ascertain the findings from lidar observations over Mt. Abu, these temperature trends are compared with the satellite observations. Though, general agreement was found in the temperature trends obtained from the two different platforms, results from lidar are more precise. Observed temperature trends, may not be statistically very significant, but are an indicator of the temperature trend over a sub-tropical location. Observed temperature trends are attributed to the increased concentration of the CO_2 in the middle atmosphere due to increased anthropogenic activities and also due to the possible depletion of ozone over the sub-tropical region. Observed trends qualitatively agree with model predictions by Ramaswamy et al. [2006] and with satellite observed temperature trend in the middle atmosphere.

There are many implications of temperature changes in the middle atmosphere, such as, long term temperature changes may have a great impact on the important geophysical processes (dynamical, radiative and chemical) in the middle atmosphere and scenario of ozone depletion or recovery may also get affected due to temperature dependent chemical kinematics of the middle atmosphere. In view of growing evidence of the stratosphere-troposphere coupling [Baldwin et al., 2007], the weather and climate in the troposphere may also show an imprint of these changes. A longer data series will bring out more clear and quantitatively significant middle atmospheric temperature trends over Mt. Abu in future studies.

CHAPTER 7

Summary and Scope for Future Work

Thermal structure of the middle atmosphere over a sub-tropical station, Mt. Abu has been studies using a Rayleigh lidar, operated during 1997–2007.

A comprehensive temperature climatology has been established for this site. It is observed that the day to day variability is less than ~5 K for altitudes below 50 km and up to ~10 K around 70 km. The variability is least around 40–50 km. Mean values of the stratopause height and temperature are found to be 48 km and 271 K, respectively. Both the stratopause height and temperature are the lowest during winter months. Significant differences in winter and summer temperatures are found. Winter temperatures are ~12 K cooler than the summer temperatures in the height range of 45–65 km. Seasonal variation shows equinoctial maxima with a winter minimum. A cold winter pool is found in the altitude region of about 45–60 km. A very sharp negative temperature change of about 16 K from October to December and a positive temperature change of about 14 K from March to April are observed from March to April. Significant correlation of total columnar ozone with stratospheric temperature is found over Mt. Abu. The observed winter cold temperature is in corroboration with the observed low ozone concentration over another sub-tropical location, Mauna Loa, using DIAL [Leblanc et al., 1997].

A comparative study of the observed temperatures over Mt. Abu with empirical models, satellite observations and with similar observations at other locations in the northern and southern hemispheres has been conducted. In the height range of 65–75 km, model temperatures are colder (~10 K) than the lidar observed temperatures. Similar behavior has been observed over mid-latitudes. [e.g., Hauchecorne et al., 1991; Gobbi et al., 1995]. Notwithstanding the observed differences, lidar measurements are found to be closer to the MSISE-90 model than the CIRA-86 and the Indian low latitude model. Temperature profiles obtained from lidar and satellite (HALOE onboard UARS) are qualitatively in agreement, but the dynamical features obtained from lidar measurements are not found in HALOE observations, possibly because these were smoothed out in the HALOE data due to poor vertical resolution. It is found that the temperature morphology over Mt. Abu is very similar to the mid-latitude station OHP. Various middle atmospheric features pertaining to mid-latitudes are also found in the temperature structures over Mt. Abu. It is to be noted that the features are significantly different from those observed over low latitudes. This is the first lidar based study over Mt. Abu, comparing a large database from several stations and using different techniques which brings out above mentioned facts very clearly.

Specific features of the middle atmospheric temperature profiles viz., double stratopause, mesospheric temperature inversion and stratospheric sudden warming have been studied over Mt. Abu. Lidar based climatological study of double stratopause is presented for three stations in the northern hemisphere viz., OHP, Mt. Abu and Gadanki, representing mid-, sub-tropical and low- latitudes, respectively. Observation of the double stratopause at these stations ascertains that this is a global feature with significant seasonal and latitudinal variations. The overall percentage of occurrence shows that it is maximum for Gadanki (63%) followed by OHP (44%) and Mt. Abu (42%). It is found that the occurrence and their characteristics over Mt. Abu and OHP are very similar, possibly due to the influence of the mid-latitude processes over Mt. Abu and also due to similar topography (which plays an important role in inducing waves of similar characteristics) at both locations. The study of potential energy illustrates that gravity waves are the probable generation mechanism for upper double stratopause layer, and planetary waves play a major role in generating lower double stratopause.

The present study of the mesospheric temperature inversions (MTI) over Mt. Abu using two independent techniques viz., lidar and satellite, revealed that the occurrence frequency of MTI has an annual cycle with a maximum during winter, as observed over mid-latitudes. Another interesting feature obtained is the persistence of MTI for several days, which is also similar to the mid-latitude observations [Leblanc et al., 1995]

Few events of stratospheric sudden warmings (SSW) have been observed over Mt. Abu. Though these are mostly observed in high- and mid-latitudes, few could influences tropical and sub-tropical middle atmosphere, depending upon their strength and background atmospheric conditions. Two events associated with different vortex conditions during December 1998 and March 1999, have been studied. It is found that the events associated with vortex splitting have a stronger impact for a longer duration than the vortex displacement associated warmings. It is clearly brought out that the effect of SSW events can be felt upto the sub-tropical latitudes. These events are the clearest and strongest manifestations of the latitudinal coupling as well as coupling of the stratosphere-troposphere system.

The last 11 year's lidar data recorded over Mt. Abu were analyzed and it is found that there is a decreasing trend in the temperature of the stratosphere and the mesosphere. Seasonally, stronger temperature trends of -4.2 $\pm$ 2.5, -4.8 $\pm$ 2.4 and -2.0 $\pm$ 2.1 K/decade at 35, 45 and 55 km, respectively, were observed during winter months. During summer months, though overall trend is negative, the scatter in temperature is large and trends are weaker than the trends during winter months. It should be noted that these results are only indicative of the temperature trends over Mt. Abu, as these trends quantitatively may not be very significant considering the possible errors in the temperature estimation. To further ascertain the findings from the lidar observations over Mt. Abu, temperature trends are compared with the satellite observations. Observed trends qualitatively agree with model predictions also [Ramaswamy et al., 2006]. These temperature trends may have great impact on the overall dynamics of this region and scenario of ozone recovery and/or loss.

It is very well established that lidar is a versatile tool to study various atmospheric processes in the lower and middle atmosphere with very good spatial resolution. The present study is focussed on the middle atmospheric thermal structure between ~30–75 km. The atmosphere below ~30 km is equally important and its thermal structure plays a vital role in deciphering issues closer to the climate and weather.

Changes in the thermodynamics of the stratosphere and the mesosphere region have implications for the atmosphere at lower altitudes and vice-versa. A more comprehensive picture of the spatial extent of these changes, the underlying physics, and future implications need to be addressed using concurrent observations in the lower atmosphere [McDermid et al., 1995; Leblanc et al., 1998, Alpers et al., 2004]. Due to the presence of aerosols and other pollutants, it is not possible to derive atmospheric temperature below 30 km using a Rayleigh lidar. For obtaining temperature in 1 to 25 km region, Raman lidar is one of the prime ground based instruments. By combining profiles from Raman and Rayleigh lidar, the complete thermal structure of the neutral atmosphere can be obtained. There is a strong coupling between the troposphere and stratosphere as they affect each other on short and large time scales [Baldwin et al., 2003, Sigmond et al., 2008]. In the coupling of troposphere and stratosphere, waves and winds play a vital role. So there is an urgent need to study the lower atmospheric temperature structure that has manifestations of the overall dynamics of this region and it will be very useful in addressing issues related to dynamical coupling (through GWs and PWs) in the lower and middle atmosphere. Various less understood and unresolved issues pertinent to wave generation, propagation, saturation and breaking at different levels can be addressed in the future through such studies.

Event based phenomena viz., double stratopause, mesospheric temperature inversion and stratospheric sudden warming play a substantial role in the middle atmospheric dynamics. Therefore, a further study including a wider database from various platforms viz., rockets, satellite etc., in conjunction with strong modeling of middle atmospheric processes is very important and will shed more light on their formation mechanism and impact on the general circulation of the middle atmosphere.

In view of the recent concern over global change due to increased anthropogenic activities, long term temperature change in the atmosphere is an issue of paramount importance. Therefore, in future studies, the consequences of the long term temperature trends should be addressed more comprehensively by integrating its impact on the dynamical features (PWs and GWs) and by studying the role of important chemical species viz., carbon dioxide, ozone etc., in the middle atmosphere.

References

Acharya, Y. B., Som Sharma and H. Chandra, Effect of Signal Induced Noıse from PMT ın Lidar Systems, *Measurements*, vol. 35, p 269–276, 2004.

Achatz, U., The prımary nonlinear dynamics of modal and non modal perturbations of monochromatic inertia-gravity waves, *J. Atmos. Scı.*, 64 (1), 74-95, doi:10.1175/JAS3827.1., 2007.

Alexander, M. J , and T. J. Dunkerton, A spectral parameterızations of mean flow forcing due to breaking gravity waves, *J. Atmos. Sci.*, 56 (24), 4167-4182, doı.10.1175/1520, 1999.

Allen, D. R , Stanford, J. L., Elson, L. S., Fishbein, E. F., Froidevaux, L., and Waters, J. W.. The 4-day wave as observed from the Upper Atmosphere Research Satellıte Mıcrowave Limb Sounder, *J. Atmos Sci.*, 54, 420-434, 1997.

Alpers, M., R. Eixmann, C. Fricke-Begemann, M. Gerdıng, and J. Hoffner, Temperature lıdar measurements from 1 to 105 km altitude using resonance, Rayleıgh and Rotational Raman scattering, *Atmos. Chem. Phys.*, 4, 793-800, 2004.

Andrews, D G., J.R. Holton and C.B Leovy, *Middle Atmosphere Dynamics*, International Geophysics Serıes, vol. 40, 489 pp., Academic Press Inc., Orlando, USA, ISBN:0-120-58576-6, 1987.

Ainsworth, J , D. Fox, and H Lagow, Upper-Atmosphere Structure Measurement Made with the Pitot-Static Tube, *J. Geophys. Res.*, 66(10), 3191-3212, 1961

Appu, K. S., On Perturbations in the Thermal structure of Tropical stratosphere and Mesosphere in Winter, *Ind. J. of Rad. and Space Phys*, 13, 35-41, 1984.

Austin, J., L. L. Hood, and B. E. Soukharev, Solar cycle variations of stratospheric ozone and temperature in simulations of a coupled chemistry-climate model, *Atmos. Chem. Phys.*, 7, 1693-1706, 2007.

Austin, J., et al. , Coupled chemistry climate model simulations of the solar cycle in ozone and temperature, *J Geophys. Res.*, 113, D11306, doi:10.1029/ 2007JD009391, 2008.

Baldwin, M. P., and T J Dunkerton, Stratospheric harbingers of anomalous weather regimes, *Science*, 294, 581-584, 2001.

Baldwin, M. P , D. W J. Thompson, E. F. Shuckburgh, W. A. Norton and N. P. Gillett, Weather from the stratosphere, *Science*, 301 (5631), 317-319, 2003.

Baldwin, M. P., Martin D, T. G. Shepherd, How Will the Stratosphere Affect Climate Change ?, *Science*, vol 316, 1576-77, 2007.

Ballard, H. N. and B Rofe, Stratospheric circulation, Ed. by Webb W L., *Academic Press*, p 141, 1969.

Balsley, B.B. and K. S. Gage, The MST radar techniques: potential for middle atmospheric studies, *Pure Appl. Geophys*, 118, 452-493, 1980.

Balsley, B.B. and R Garello, The kinetic energy density in the troposphere, stratosphere and mesosphere: a preliminary study using the Poker Flat M.S.T. radar in Alaska, *Radio Science*, 20, 1355-1361, 1985.

Barnett, J J., and M Corney, Middle atmosphere reference model derived from satellite data, *Handbook for Middle Atmosphere Program*, 16, 47-137, 1985.

Barnett, J. J. and Labitzke, K. Climatological distribution of planetary waves 5 in the middle atmosphere, Adv. Space Res , 10, (12), 6391, 1990.

Becker, E , and D. C Fntts, Enhanced gravity-wave actıvity and interhemispheric coupling durmg the MaCWAVE/MIDAS northern summer program 2002, *Ann. Geophys.*, 24 (4), 1175-1188, 2006.

Beig, G., et al., Review of mesospheric temperature trends, *Rev. Geophys.*, 41(4), 1015, doi:10.1029/2002RG000121, 2003.

Beig, G., J. Scheer, M. G. Mlynczak, and P. Keckhut, Overvıew of the temperature response in the mesosphere and lower thermosphere to solar activity, *Rev. Geophys.*, 46, RG3002, doi:10.1029/2007RG000236, 2008.

Bencherıf, H., Leveau, J., Porteneuve, J., Keckhut, P., Hauchecorne, A.,M egıe, G., Fassina, F., Bessa, M ,. Lidar developments and observatıons over Reunion Island (20:8.S; 55:5.E). In: Ansmann, A , Neuber, R., Rairoux, P., Wandınger, U. (Eds.), *Advances ın Atmospherıc Remote Sensıng with Lıdar* Springer, Berlin, 1996

Bencherif, H , B. Morel, A. Moorgawa, M Mıchaelıs, J. Leveau, J. Porteneuve, A. Hauchecorne, and D. Faduilhe, Observation and first validation of stratospherıc temperature profiles obtained by a Rayleigh-Mie LIDAR over Durban, South Africa, *South Afrıcan J. Scı.*, 96, 487-492, 2000.

Bencherıf, H., R D. Diab, T. Portafaıx, B. Morel, P. Keckhut, and A. Moorgawa, Temperature climatology and trend estımates ın the UTLS region as observed over a southern subtropical sıte, Durban, South Afrıca, *Atmos. Chem. Phys.*, 6, 51215128, 2006.

Branstator, G., The relationship between zonal mean flow and quasıstatıonary waves in the mid-troposphere, *J. Atmos. Scı.*, 41, 2163- 2178, 1984.

Brasseur, G., and S. Solomon, Aeronomy of the mıddle atmosphere, 2 ed., 452 pp., *D. Reidel Publishing Company*, Dordrecht, The Netherlands, ISBN·90-277-2343-5, 1986.

Brasseur, G. et al., An interactive chemical dynamical radıatıve two dimensional model of the middle atmosphere, *J. Geophys Res.*, 95, 5639-5655, 1990

Burris, J., Wm. Heaps, B. Gary, W. Hoegy, L. Laıt, T McGee, M. Gross, and U. Singh, Lıdar Temperature Measurements during the TOTE/VOTE Mıssion, *J. Geophys. Res* ,103, 3505-3510, 1998.

Cagnazzo, C., C. Claud, and S. Hare, Aspects of stratospheric longterm changes induced by ozone depletion, *Clim. Dyn.*, doi:10.1007/s00382-006-0120-1, 2006.

Cerny, T. and C.F. Sechrist Jr., Calibration of the Urbana lidar system, *Aeronomy Report No. 94, University of Illinois, Urbana*, 1980.

Chakrabarty, D. K., et al., Balloon measurement of stratospheric ion conductivities over the tropics, em J. Atmos Terr. Phys., vol. 56, no. 9, pp. 1107-1115, 1994

Champion, K. S.W., Middle atmospheric model and comparision with the Shuttle reentry density data, *Adv. in Space Research*, 6, 1986.

Chandra, H., Som Sharma, Y. B. Acharya and A. Jayaraman, Rayleigh Lidar Studies of Thermal Structure over Mt. Abu, *J. Ind. Geophys. Union*, Vol. 9, pp 279-298, 2005.

Chandra, H, H S S Sinha, Uma Das, R N Misra, S R Das, Jayati Dutta, S C Chakravarty, A K Patra, N Venketswara Rao and D Narayana Rao, First mesospheric turbulence study made using coordinated rocket and MST radar measurements over Indian low latitude region, *Ann. Geophys.*, 26, 2725-2738, 2008

Chandra, S., The solar-induced oscillations in the stratosphere: a myth or reality, *J. Geophys. Res.* 90, 2331-2339, 1985.

Chanin, M.L. and A. Hauchecorne, Lidar observations of gravity and tidal waves in the stratosphere and mesosphere, *J. Geophys. Res.*, 86, no c10, 9715-9721, 1981.

Chanin, M.L. and A. Hauchecorne, Lidar studies of temperature and density using Rayleigh scattering, *MAP Handbook*, 13, 87-98, 1984.

Chanin, M.L , A. Hauchecorne, and N. Smires, Contribution to the CIRA model from Ground based lidar, *Handb. MAP*, 16, 305-314, 1985.

Chanin, M L., N. Smirs, and A. Hauchecorne, Long-term variation of the temperature of the middle atmosphere at mid latitude: Dynamical and radiative causes, *J. Geophys. Res.*, 92(D9), 10,93310,941, 1987.

Charyulu, D. V., V. Sivakumar, H. Bencherif, G. Kirgis A. Hauchecorne, P. Keckhut, and D. Narayana Rao, 20-year LiDAR observations of stratospheric sudden warming over a mid-latitude site, Observatoire de Haute Provence (OHP; 44°N, 6°E)· case study and statistical characteristics, *Atmos. Chem. Phys. Discuss* , 7, 15739-15779, 2007.

Charlton, A.J. and L.M Polvani, A new look at Stratospheric Sudden Warming events: Part I. Climatology and Modelling Benchmarks, *Journal of Climate*, 20, 449-469, 2007.

Chau J. L., B. G. Fejer, L. P. Goncharenko, Quiet variability of equatorial E X B drifts during a sudden stratospheric warming event, *Geophys Res. Lett.*, 36, L05101, doi 10.1029 / 2008GL036785, 2009.

Chen, S., Z. Hu, M A. White, H. Chen, D. A. Krueger, and C. Y. She, Lidar observations of seasonal variation of diurnal mean temperature in the mesopause region over Fort Collins, Colorado (41N, 105W), *J. Geophys Res*, 105, 12, 371-380, 2000.

Chen, W., H.-F. Graf, and M. Takahashi, Observed interannual oscillations of planetary wave forcing in the Northern Hemisphere winter, *Geophys. Res. Lett.*, 29(22), 2073, doi.10.1029/2002GL016062, 2002.

Chen, W., and T. Li, Modulation of northern hemisphere wintertime stationary planetary wave activity: East Asian climate relationships by the Quasi-Biennial Oscillation, *J. Geophys Res*, 112, D20120, doi·10.1029/2007JD008611, 2007.

Christopher, J M., M. G. Mlynczak, R R Garcia and R. W. Portmann, A detailed evaluation of the stratospheric heat budget 1. Radiation transfer, *J. Geophys. Res.*, 104, No D6 ,6021-6038, 1999.

Clancy, R. T. and D. W. Rusch, Climatology and trends of mesospheric(58-90 km) temperature based upon 1982-1986 SME limb scattering profiles, *J . Geophys. Res.*, 94, 3377-3393, 1989.

Clancy, R.T , D.W. Rusch, and M T. Callan, Temperature minima in the average thermal structure of the middle atmosphere (70-80 km) from analysis of 40- to 92-km SME global temperature profiles, *J. Geophys. Res.*, 99, 19,001-19,020, 1994.

Clemesha B. R., in Handbook for *MAP*, Vol 13, ed. by R. A. Vincent, 1984.

Collis, R T.H. and P.B. Russell, Lidar measurements of Particles and Gases by Elastic Backscattering and Differential Absorption, in Laser Monitoring of the Atmosphere (ed E.D Hinkley), 71-151, 1976.

Curtis, P. D., J. T. Houghton, G. D. Peskett and C D Rodgers, The pressure modulator radiometer for Nimbus F, *Proc. R Soc. London Set. A*, 337, 135-150, 1974

Cutler, L.J., R.L.Collins, K. Mizutani, and T. Itabe, Rayleigh lidar observations of Mesospheric Inversion Layers at Poker Flat, Alaska (65°N, 147°W), *Geophys. Res. Lett.*, 28, 1467-1470, 2001

Das, Uma, H. S. S. Sinha, Som Sharma, H. Chandra and Sanat K. Das, Fine Structure of the Low Latitude Mesospheric Turbulence, doi:10.1029/2008JD011307, *J. Geophys Res.* 2009, (in press)

Delisi, D. P. and Dunkerton, T. J.: Seasonal variation of the semiannual oscillation, *J. Atmos. Sci*, 45, 2772-2787, 1988.

Donfrancesco, G. D., Adriani, A., Gobbi, G. P., and Congeduti, F., Lidar observations of stratospheric temperature above McMurdo Station, Antartica, *J. Atmos. Terr. Phys.*, 58, 1391-1399, 1996.

Drummond, J. R., J. T. Houghton, G. D. Peskett, C. D. Rodgers, M. J Wale, J. Whitney and E J. Williamson, The stratospheric and mesospheric sounder on Nimbus 7, *Philos. Trans. R. Soc. London. Ser. A*, 296, 219-241, 1980.

Dubin, M., A. R. Hull and K. S. W Champion (Eds.), U.S. Standard Atmosphere 1976, 227 pp., NOAA, NASA, USAF, Washington, USA, 1976.

Duck, T J., J.A. Whiteway, and A.I Carswell, Lidar observations of gravity wave activity and Arctic stratospheric vortex core warming, *Geophys Res. Lett.*, 25, 2813–2816, 1998.

Duck, T J, J. A. Whiteway and A. I Carswell, A detailed record of High Arctic middle atmospheric temperatures, J. Geophys. Res., 105 (D18), 22,909-22,918, doi:10.1029/2000JD900367, 2000.

Dudhia, A., S E. Smith, A R. Wood, and F. W. Taylor, Diurnal and semi-diurnal temperature variability of the middle atmosphere as observed by ISAMS, Geophys. Res. Lett, 20, 1251-1254, 1993.

Dunkerton, T. J. and Delisi, D. P.: Evolution of potential Vorticity in the winter stratosphere of January-February 1979, J. Geophys. Res., 91, 1199-1208, 1986.

Dunkerton, T. J., Delisi, D. P., and Baldwin, M. P.: Distribution of Major Stratospheric warmings in relation to the Quasi-Biennial Oscillation, Geophys. Res. Lett , 15, 136-139, 1988.

Ellis, P., G. Holah, J. T. Hougton, T. S. Jones, G. Peckham, G. D. Peskett, R Pick, C D. Rodgers, H. Roscoe, R. Sandwell, Remote sounding of atmospheric from satellites. IV: The selective chopper radiometer for Nimbus 5, *Proc. R. Soc. London. Ser. A*, 334, 149-170, 1973.

Elterman, L., UV, Visible, and IR Attenuation for Altitudes to 50 km, Enviromental Research Papers no 285, Air Force Cambridge Research Laboratories, Bedford, Massachusetts, USA, 1968.

Evans, R. D., The Atomic Nucleus, *McGraw-Hill Book Company*, pp 7, 1955.

Eyring, V., et al., Multimodel projections of stratospheric ozone in the 21st century, *J. Geophys Res.*, 112, D16303, doi:10.1029/ 2006JD008332, 2007.

Fadnavis, S. and G. Beig, Mesospheric temperature inversions over the Indian tropical region, *Ann Geophys* , 22, 3375-3382, 2004.

Fadnavis, S , D. Siingh, G. Beig, and R. P Singh, Seasonal variation of the mesospheric inversion layer, thunderstorms, and mesospheric ozone over India, *J. Geophys. Res.*, 112, D15305, doi:10.1029/2006JD008379, 2007.

Ferrare, R. A., McGee, T.J., Whiteman, D., Burris, J., Owens, M., Butler, J., Barnes, R.A , Schmidlin, F., Komhyr, W , Wang, P H., McCormick, M.P. and Moller, A.J., Lidar measurements of stratospheric temperature during STOIC, *J Geophys Res.*, 100, 9303-9312, 1995.

Fiocco, G. and L.D. Smullin, Detection of scattering layers in the upper atmosphere (60-140 km) by optical radar, *Nature*, 199, 1275-1276, 1963.

Fishbein, R. E., et al., Validation of UARS MLS temperature and pressure measurements, *J Geophys. Res.*, 101, 9983 - 10,016, special issue on UARS Data Validation, 1996.

Fleming, E. L., S. Chandra, J. Barnette, and M. Corney, Zonal mean temperature, pressure, zonal wind and geopotential height as functions of latitude,*Adv. Space. Res* , 10, 1211 -1259, 1990.

Fortuin, J.P.F. and H Kelder, An ozone climatology based on ozonesonde and satellite measurements, *J. Geophys. Res.*, 103, 31709-31734, 1998.

Free, M. and D. J. Seidel, Causes of dıfferıng temperature trends in radıosonde upper air datasets, *J. Geophys. Res.*, 110, D07101, doi:10.1029/2004JD005481, 2005.

Fritts, D. C., Gravity wave saturation in the middle atmosphere: A review of theory and observations, *Rev. Geophys. Space Phys.*, 22 (3), 275-308, 1984.

Fritts, D. C., and P. K. Rastogi, Convectıve and dynamical ınstabilities due to gravity wave motions in the lower and mıddle atmosphere - Theory and observations, *Radıo Scı.*, 20 (6), 1247-1277, 1985

Fritts, D.C. and R.A. Vincent, Mesospheric momentum flux studies at Adelaıde, Australıa· Observatıons and a gravıty wave/tidal interactıon model, *J. Atmos. Sci.*, 44, 605-619, 1987.

Fritts, D.C., and T.E. vanZandt, Spectral estimates of gravıty wave energy and momentum fluxes, Energy dissipation, acceleration, and constraints, *J. Atmos. Sci.*, 50, 3685-3694, 1993.

Frıtts, D. C., and M. J. Alexander, Gravıty wave dynamics and effects ın the middle atmosphere, *Rev. Geophys.*, 41 (1), 1003, doi·10.1029/2001RG000106, 2003.

Fritts, D. C., S. L. Vadas, K. Wan and J. A Werne, Mean and variable forcing of the middle atmosphere by gravity waves, *J. Atmos. Solar-Terr. Phys.*, 68 (3-5), 247-2652, 2006.

Funatsu, B. M., C. Claud, P. Keckhut, and A. Hauchecorne, Cross-validatıon of Advanced Mıcrowave Sounding Unıt and lıdar for long-term upper-stratospheric temperature monitorıng, *J. Geophys. Res.*, 113, D23108, doı:10.1029/2008JD010743, 2008.

Gaffen, D. J , Temporal ınhomogeinities in radıosonde temperature records, *J. Geophys. Res.*, 99, 3667- 3676, 1994.

Garcia, R. R., et al., Clımatology of the semiannual oscıllation of the tropical mıddle atmosphere, *J. Geophys. Res.*, vol. 102, no. D22, 26,019-26,032, 1997.

Gardner, C. S., G. C. Papen, X. Chu, and W. Pan, Fırst Lidar Observations of Mıddle Atmosphere Temperatures, Fe Densıtıes, and Polar Mesospherıc Clouds Over the North and South Poles, Geophys Res Lett , 28, 1199-1202, 2001

Geller, M.A , Dynamıcs of the mıddle atmosphere, *Space Science Reviews*, 34, 359-375, 1983.

Geller, M.A., Coupling processes in the lower and mıddle atmosphere, *edıted by Eivind V. Thrane, Tom A. Blix and David C. Fritts*, pp 95-123, printed by Kluwer Academic Press, The Netherlands, 1992.

Gill, A.E., Atmosphere-Ocean Dynamıcs, Academic Press, 1982.

Gille, J C., J. M. Russell III, P. L. Baıley, L. L. Gordley, E. E. Remsberg, J. H. Lıenesch, V. W. G. Planet, F. B. House, L. V. Lyȷak and S. A. Beck, Validation of temperature retrievals obtaıned by the Lılb Infrared Monitor of the Stratosphere (LIMS) experıment on NIMBUS 7, *J. Geophys. Res.*, 89, 5147-5160, 1984

Gılle, J. C., et al., Accuracy and precısıon of cryogenic limb array etalon spectrometer (CLAES) temperature retrıevals, *J. Geophys. Res.*, 101, 9583- 9602, specıal issue on UARS Data Validation, 1996.

Gırolamo, P, R. Marchese, D. N. Whıteman, and B. B. Demoz, Rotatıonal Raman lidar measurements of atmospherıc temperature in the UV, Geophys. Res. Lett., 31, L01106, doi:10 1029/2003GL018342, 2004.

Gobbı, G P., T Deshler, A. Adriani, and D J. Hofmann, Evidence for denitrification in the 1990 Antarctıc sprıng Stratosphere· I, Lıdar and temperature measurements, Geophys. Res. Lett., 18, 1995-1998, 1991.

Gobbı, G.P., Lidar observatıons of mıddle atmospheric temperature varıability, *Ann. Geophys* , 13, 648–655, 1995.

Golitsyn, G. S. et al., Long term temperature trends ın the mıddle and upper atmosphere, *Geophys Res. Lett.*, 23, 1741–1744, 1996

Grant, W. B., M. A Fenn, E. V Browell, T. J. McGee, U. N. Singh, M. R. Gross, I. S. McDermid, L. Froidevaux, and P-H. Wang, Correlatıve stratospherıc ozone measurements with the airborne UV DIAL system during TOTE/VOTE, Geophys. Res. Lett., 25, 623-626, 1998.

Gross, M. R., T. J McGee, R. A. Ferrare, U. Singh, and P. Kımvılıkani, Temperature Measurements Made with a Combmed Rayleigh-Mie/Raman Lidar, Applıed Optıcs, 24, 5987-5995, 1997.

Gupta, R. K , Mohan, B., and Vernekar, K G., Thermal structure features of double stratopause over Thumba, *India Journal Radio and Space Phys.*, 7, 277–286, 1978.

Gupta, S. P., Solar Cycle variation of stratospheric conductivity over low latitude, *Adv Space Res.*, vol. 26. no. 8, pp 1225–1229, 2000.

Hagan, M.E., Forbes, J.M., Vial, F., On modelling migrating solar tides *Geophys. Res. Lett.* 22, 893–896, 1995.

Haigh, J D., The role of stratospheric ozone in modulating the solar radiative forcing of climate, *Nature* 370, 544–546, 1994.

Hare, S. H. E., L. J Gray, W. A. Lahoz, A. O Neill, and L. Steenman-Clark, Can stratospheric temperature trends be attributed to ozone depletion ?, *J Geophys. Res.*, 109, D05111, doi.10.1029/2003JD003897, 2004.

Hauchecorne, A. and Chanin, M. L.: Density and temperature profiles obtained by lidar between 35 and 70 km, *Geophys Res. Lett.*, 8, 565–568, 1980.

Hauchecorne, A. and Chanin, M. L.: Mid latitude observations of planetary waves in the middle atmosphere during the winter over 1981-1982, J. Geophys. Res., 88, 3843-3849, 1983.

Hauchecorne, A. M.L. Chanin, and R. Wilson, Mesospheric temperature inversion and gravity wave breaking, *Geophys. Res. Lett.*, 14, 933-936, 1987

Hauchecorne, A., and A Maillard, A 2-D dynamical model of mesospheric inversion in winter, *Geophys. Res. Lett.*, 17, 2197-2200, 1990.

Hauchecorne, A , M L. Chanin, and P. Keckhut, Climatology and trends of the middle atmospheric temperature (33-87 km) as seen by Rayleigh lidar over the south of France, *J. Geophys Res.*, 15, 297-303, 1991.

Hauchecorne, A., M.L. Chanin, P. Keckhut, and D Nedeljkovic, Lidar monitoring of the temperature in the middle and lower atmosphere, *Appl. Phys.*, B 54, 2573-2579, 1992

Heaps, W.S. and T.J. McGee, Balloon-borne lidar measurements of stratospheric hydroxyl radical, *J. Geophys. Res* , 88, 5281-5289, 1983.

Heaps, W.S. and T.J. McGee, Progress in stratospheric hydroxl measurement by balloon-borne lidar, *J Geophys. Res.*, 90, 7913-7921, 1985.

Heath, D. F., et al , Developments in Atmospheric Science 1, Ed. by Verniani F., p131, 1974.

Hedin, A. E. Extension of the MSIS thermosphere model into the lower atmosphere, *J. Geophys. Res.*, 96, 11591172, 1991.

Hervig, et al., Validation of temperature measurements from the Halogen Occultation Experiment,*J. Geophys. Res* , 101, 10,277-10,285, 1996.

Hines, C. O., Internal atmospheric gravity waves at ionospheric heights, *Can. J. Phys.*, 38, 1441-1481, 1960.

Hinkley, E.D (ed), Laser Monitoring of the Atmosphere, Springer-Verlag, 1976.

Hirota, I., Climatology of gravity waves in the middle atmosphere, *J. Atmos. Terr. Phys.*, 46, 767-773, 1984.

Holton, J R., The role of gravity wave induced drag and diffusion in the momentum budget of the mesosphere, *J Atmos Sci* , 39, 791-799, 1982.

Holton, J.R., The influence of gravity wave breaking on the general circulation of the middle atmosphere, *J. Atmos. Sci.*, 40, 2497-2507, 1983.

Hood, L.L., Coupled stratospheric ozone and temperature responses to short-term changes in solar ultraviolet flux: an analysis of Nimbus 7 SBUV and SAMS data, *J. Geophys. Res.* 91, 5264-5276, 1986.

Hood, L., R. McPeters, J. McCormack, L. Flynn, S. Hollandsworth, and J. Gleason, Altitude Dependence of Stratospheric Ozone Trends Based on Nimbus 7 SBUV Data, *Geophys. Res. Lett.*, 20(23), 2667-2670, 1993.

Huang, F. T., H. G. Mayr, and C. A. Reber, Intra-seasonal Oscillations (ISO) of zonal-mean meridional winds and temperatures as measured by UARS, *Annales Geophysicae*, 23, 1131-1137, 2005.

Hurrell, J. W., Decadal Trends in the North Atlantic Oscillation: Regional Temperatures and Precipitation, *Science*, 269, 676-679, 1995.

Inaba, H., Detection of atoms and molecules by Raman scattering and resonance fluorescence, in Laser Monitoring of the Atmosphere (ed. E.D. Hinkley), 153-236, 1976.

Innis, J.L , Klekociuk, A.R., Planetary wave and gravity wave influence on the occurrence of polar stratospheric clouds over Davis Station, Antarctica, seen in lidar and radiosonde observations, *J. Geophys. Res.*, 111, D22102, doi:10.1029 / 2006JD007629, 2006.

Intergovernmental Panel on Climate Change (IPCC), *Climate Change 2001: The Scientific Basis: Contribution of Working Group I to the Third Assessment Report of the Intergovernmental Panel on Climate Change*, edited by J. T Houghton et al , Cambridge Univ. Press, New York, 2001.

Intergovernmental Panel on Climate Change (IPCC), *Climate Change 2007: The Physical Science Basis: Contribution of Working Group I to the Fourth Assessment Report of the Intergovernmental Panel on Climate Change*, edited by S. Solomon et al., Cambridge Univ. Press, New York., 2007.

Jayaraman A., Y. B. Acharya, B. H. Subbaraya,B.H. and Chandra, H., Nd:YAG backscatter lidar at Ahmedabad (23°N, 72.5°E) for tropical middle atmospheric studies *Appl. Optics*, 34, 6937, 1995a

Jayaraman A., S. Ramchandran, Y. B. Acharya and B. H. Subbaraya, Pinatubo volcanic aerosol layer observed at Ahmedabad (23°N), India, using neodymium: yttrium /aluminium/ garnet backscatter lidar, *J. Geophys. Res.*, 100, 23209–23214, 1995b.

Jayaraman A., Y. B. Acharya,Y.B., H. Chandra, B H. Subbaraya, S. Ramchandran, and S Ramaswamy, Laser radar study of the middle atmosphere over Ahmedabad, *Ind. J. Radio and Space Phys.*, 25, 318–327, 1996.

Jenkins, D B , D.P. Wareing, L. Thomas and G. Vaughan, Upper stratospheric and mesospheric temperatures derived from lidar observations at Aberystwyth, *J. Atmos. Terr. Phys.*, 49, 287-298, 1987.

Kallberg, P., A. Simmons, S. Uppala, and M. Fuentes, The ERA-40 archive *ERA-40 Project Report Series*, No. 17, ECMWF, 31 pp., 2004.

Kamla S., D. Narayna Rao, S. C. Chakravarty, J. Dutta and B S N Prasad, Vertical structure of mesospheric echoes from the Indian MST radar, *J. Atmos. Terr. Phys.*, 65, 71-83, 2003.

Karoly, D. J., Ozone and Climate Change, *Science*, vol. 302, p 236-237, 2003.

Keckhut P., M.L. Chanin and A. Hauchecorne, Stratosphere temperature measurement using raman lidar, *Appl. Opt*, 29, 5182-5186, 1990.

Keckhut, P., A. Hauchecorne, and M. L. Chanin, Mid-latitude long-term variability of the middle atmosphere trends, and cyclic and episodic changes, *J. Geophys Res.*, 100, 18,887- 18,897, 1995.

Keckhut, P., et al , Semi-diurnal and diurnal temperature tides (30- 55 km): Climatology and effect on UARS-lidar data comparisons, *J. Geophys. Res.*, 101, 10,299-10,310, special issue on UARS Data Validation, 1996

Keckhut, P., M.E. Gelman, J.D Wild, F. Tissot, A.J. Miller, A. Hauchecorne, M.L. Chanin, E.F. Fishbein, J. Gille, J.M. Russell III and F.W. Taylor, Semidiurnal and diurnal temperature tides (30-55 km): climatology and effect on UARS-LIDAR data comparisons, *J. Geophys. Res.*, 101, 10299-10310, 1996.

Keckhut, P., F. J. Schmidlin, A. Hauchecorne, and M. L. Chanin, Stratospheric and mesospheric cooling trend estimates from US rocketsondes at low latitude stations (8 degrees S- 34 degrees N), taking into account instrumental changes and natural variability, *J. Atmos. Sol. Terr. Phys.*, 61, 447- 459, 1999.

Keckhut, P., J. Wild, M Gelman, A. J. Miller, and A. Hauchecorne, Investigations on long-term temperature changes in the upper stratosphere using lidar data and NCEP analyses, *J Geophys. Res.*, 106, 7937- 7944, 2001.

Keckhut, P., et al., Review of ozone and temperature lidar validations performed within the framework of the Network for the Detection of Stratospheric Change, *J Environ. Monit.*, 6, 721 - 733, 2004

Keckhut, P, C. Cagnazzo, M.-L. Chanin, C. Claud, and A. Hauchecorne, The 11-year solar-cycle effects on the temperature in the upper-stratosphere and mesosphere, part I: Assessment of observations, *J Atmos. Sol. Terr. Phys.*, 67, 940- 947, 2005.

Kent, G S and R W.H. Wright, A review of laser radar measurements of atmospheric properties, *J. Atmos. Terr. Phys.*, 32, 917-943, 1970.

Kerker, M., The Scattering of light and other electromagnetic radiation, Academic Press, New York, U.S A., 1969.

Kim, Y.-J , S D Eckermann and H -Y. Chun, An overview of the past, present and future of gravity wave drag parameterization for numerical climate and weather prediction models, Atmosphere-Ocean, 41 (1), 65-98, 2003

Kishore Kumar, G., M. Venkat Ratnam, A. K. Patra, S. Vijaya Bhaskara Rao, and J. Russell, Mean thermal structure of the low-latitude middle atmosphere studied using Gadanki Rayleigh lidar, Rocket, and SABER/TIMED observations, J. Geophys. Res., 113, D23106, doi:10.1029/ 2008JD010511, 2008.

Kistler, R., and Coauthors, The NCEP-NCAR 50-Year Reanalysis: Monthly means CD-ROM and documentation. Bull. Amer. Meteor Soc., 82, 247-267, 2001.

Klckouciuk, A. R., M. M. Lambert, R. A Vincent, First year of Rayleigh lidar measurements of middle atmospheric temperatures above Davis, Antarctica, *Adv. Space Res.*, 32(5), 771–776, 2003.

Kokin, G. A. et al., temperature changes in the stratosphere and mesosphere during 1964-1988 based on rocket sounding data, *Phys. Atmos. Okeana*, 26, 702-710, 1990.

Kokin, G. A and E. V Lysenko, On the temperature trends of the atmosphere from rocket and radiosonde data, *J. Atmos. Solar-Terr Phys* , 56, 1035-1040, 1994

Kurylo, M. J , and S. Solomon, Network for the detection of stratospheric change: A status and implementation report, in NASA Upper Atmosphere Research Program and NOAA Climate and Global Change Program (NASA), *NASA Technical Report*, Washington, D C., 1990.

Labitzke, K , Climatology of the stratosphere and mesosphere, *Phil Trans. R. Soc. London Ser. A*, 296, 7–17, 1980.

Labitzke, K.: Stratospheric-mesospheric midwinter disturbances: a summary of observed characteristics, J. Geophys Res., 86, 9665–9678, 1981.

Labitzke, K., and H. van Loon, A note on the dıstrıbutıon of trends below 10 hPa: The extratropical Northern Hemisphere, *J. Meteorol. Soc. Jpn.*, 73, 883–889, 1995.

Labitzke, K., J. Austin, N. Butchart, J. Knıght, M. Takahashi,M. Nakamoto, T. Nagashima, J. Haigh, V. Williams, The global signal of the 11-year solar cycle in the stratosphere: observatıons and models, *J. of Atmospherıc and Solar-Terrestrial Physics* 64, 203-210, 2002.

Lal, S , Subbaraya, B.H and Narayanan, V,.Equatorıal stratospheric and mesospherıc structural variatıons durıng the years 1971-74, em Space Res., Vol 19, p.147, 1979

Lal, S., Studies in equatorial neutral atmosphere, Ph D. thesis, *Gujarat Unıversıty*, 1981.

Lal, S , Borchers, R. Fabıan, P. and Krueger, B.C. The vertical dıstribution of CH4, N2O, CFC-12 and CFC-11 in the middle atmosphere at mid-latitudes *J. Atm. and Terr. Physıcs*, Vol 51, p 81, 1989.

Lal, S , Borchers, R., Fabian, P., Patra, P.K. and Subbaraya, B.H Vertıcal distributıon of methyl bromide over Hyderabad, Indıa *Tellus*, 1994, Vol. 46B, p.373, 1994.

Lambeth, J.D., and Callis, L.B., Temperature varıations in the middle and upper stratosphere, 1979-1992, *J. Geophys. Res.*, 99, 20,701-20,712, 1994.

Langematz, U , M. Kunze, K. Kruger, K. Labitzke, and G. L. Roff, Thermal and dynamical changes of the stratosphere since 1979 and their lınk to ozone and CO2 changes, *J. Geophys. Res.*, 108(D1), 4027, doi:10 1029/2002JD002069, 2003.

Lanzante, J., S. Klein, and D. J. Seıdel, Temporal homogenızation of monthly radiosonde temperature data. Part I: Methodology, *J. Clim.*, 16, 224 - 240, 2003a.

Lanzante, J., S. Klein, and D. J. Seıdel , Temporal homogenizatıon of monthly radiosonde temperature data. Part II: Trends, sensitivitıes and MSU comparisons, *J. Clim.*, 16, 241 – 262, 2003b.

Lawrence, B., and W. Randel, Varıabılity in the mesosphere observed by the Nımbus 6 pressure modulator radiometer, *J. Geophys. Res.*, 101(D18), 23475-23489, 1996.

Leblanc, T., A Hauchecorne, M-L. Chanın, C. D Rodgers, F. W. Taylor, and N. J. Lıvesey, Mesospheric Temperature inversıons as seen by ISAMS in December 1991, *Geophys. Res. Lett.*, 22, 1485-1488, 1995.

Leblanc,T , and A. Hauchecorne, Recent observations of mesospheric temperature inversions, *J. Geophys. Res.*, 102, 19, 471-19,482, 1997.

Leblanc, T., I. S. McDermid, P. Keckhut, A. Hauchecorne, C. She, and D. A. Krueger, Temperature climatology of the middle atmosphere from long-term lidar measurements at middle and low latitudes, *J. Geophys. Res.*, 103, 17,191-17,204, 1998.

Leblanc, T., and I.S. Mcdermid, A. Hauchecorne, and P. Keehut, Evaluation and optimization of lidar temperature analysis algorithms using simulated lidar data, *J. Geophys. Res.*, 103, 6177- 6187, 1998

Leblanc, T, and I. Stuart McDermid, Stratospheric ozone climatology from lidar measurements at Table Mountain (34.4° N, 117.7° W) and Mauna Loa (19.5°N, 155.6°W),*J. Geophys. Res.*, 105, 14,613-14,623, 2000.

Leblanc, T., and I. S. McDermid, Quasi-biennial Oscillation Signatures in Ozone and Temperature Observed by Lidar at Mauna Loa, Hawaii, (19.5°N, 155.6°W), *J. Geophysical Research*, 106, 14,869-14,874, 2001.

Li, T , T. Leblanc, and I. S. McDermid, Interannual variations of middle atmospheric temperature as measured by the JPL lidar at Mauna Loa Observatory, Hawaii (19.5°N, 155.6°W), *J Geophys. Res.*, 113, D14109, doi:10.1029/ 2007JD009764, 2008.

Limpasuvan, V., Thompson , D. W. J., and Hartmann, D. L., The life cycle of Northern Hemisphere sudden stratospheric warmings, *J. Climate*, 17, 25842596, 2004.

Lindzen, R.S., Turbulence and stress owing to gravity wave and tidal breakdown, *J. Geophys Res.*, 86, 9707-9714, 1981.

Lindzen R.S., and J. Forbes, Turbulence originating from convectively stable internal waves, *J. Geophys Res* , 88, 6549-6553, 1983.

Liou, K N., An Introduction to Atmospheric Radiation, Academic Press, 1980.

Liou, K N, An Introduction to Atmospheric Radiation Second Edition This is Volume 84 in the INTERNATIONAL GEOPHYSICS SERIES, second edition Ackademic press, Elsevier Science (USA), 2002.

Liu, H.L., and M.E. Hagan, Local heating/cooling of the mesosphere due to gravity wave and tidal coupling, Geophys. Res. Lett., 25, 941-944, 1998.

Lıu, H.-L., M. E. Hagan, and R. G. Roble, Local mean state changes due to gravity wave breakıng modulated by the diurnal tide, *J. Geophys. Res.*, 105, 12,381 12,396, 2000.

Liu, H.-L., and J. W. Meriwether, Analysis of a temperature mversion event in the lower mesosphere, *J. Geophys. Res.*, 109, D02S07, doi:10.1029/2002JD003026, 2004

Maiman, T.H., Stimulated optical radiatıon ın Ruby, *Nature*, 187, 493-494, 1960.

Malinga, S B. and Poole, L. M. G , The 16-day variation in the mean flow at Grahamstown (33°S, 26.5°E),*Ann. Geophysicae.*, 20, 20272031, 2002

Manzını, E., B. Steil, C. Bruehl, M. A. Giorgetta, and K. Krueger, A new ınteractıve chemıstry-clımate model, 2: Sensıtivity of the mıddle atmosphere to ozone depletion and increase in greenhouse gases and implications for recent stratospherıc cooling, *J. Geophys. Res.*, 108(D14), 4429, doi·10 1029/2002JD002977, 2003

MAP 86, Draft Reference Mıddle Atmosphere in the Handbook for the Middle Atmosphere Program, 16, 1985.

Marenco, F., di Sarra, A., Cacciani, M., Fiocco, G, and Fua, D.: Thermal structure of the winter middle atmosphere observed by lidar at Thule, Greenland, durıng 1993-1994, *J Atmos. Solar. Terr. Phys.*, 59, 151-158, 1997

Matsuno, T.: A dynamical model of the stratospheric sudden warming, J. Atmos. Scı., 28, 1479-1494, 1971.

McCormack, J.P., L. L. Hood, Apparent solar cycle variations of upper stratospheric ozone and temperature: latıtudinal and seasonal dependences *J. Geophys. Res.* 101, 20933-20944, 1996.

McDermid, I. S., T. D. Walsh, A. Deslis, and M. White, Optical systems desıgn for a stratospheric lıdar system, *Appl Opt.*, 34, 6201- 6210, 1995a.

McDermid, I. S., S M. Godin, and T. D. Walsh, Results from the Jet Propulsion Laboratory stratospheric ozone lidar during STOIC 1989, *J. Geophys. Res.*, 100, 9263-9272, 1995b.

Measures, R.M., Laser Remote Sensing: Fundamentals and Applications, Wıley & Sons, 1984.

Megie, G. and J. Pelon, Measurements of the ozone vertical distribution (0–25 km): comparison of various instruments, GAP-observatoire de Haute Provence, *Planet. Space Sci*, 39, 791-799, 1983.

Melfi, K. D. Evans, J. Li, D. Whiteman, R. Ferrare, and G. Schwemmer, Observation of Raman scattering by cloud droplets in the atmosphere, *Appl. Opt.*, 36, 3551-3559, 1997.

Meriwether, J. W. and Mlynczak, M. G.: Is chemical heating a major cause of the mesosphere inversion layer ?, J. Geophys. Res., 100, 1379-1387, 1995.

Meriwether, J. W., Gao, X., Wickwar, V. B., Wilkerson, T., Beissner, K., Collins, S., and Hagan, M. E.: Observed coupling of the mesosphere inversion layer to the thermal tidal structure, Geophys. Res. Lett., 25, 1479-1482, 1998.

Meriwether, J. W. and Gardner, C. S.: A review of the mesosphere inversion layer phenomenon, *J. Geophys. Res.*, 105, 12 405- 12 416, 2000.

Meriwether, J. W. and Gerrard, A. J.: Mesosphere inversion layers and stratosphere temperature enhancements, Rev. Geophys, 42, RG3003, doi:10.1029/ 2003RG000133, 2004.

Michelson, H. A., G. L. Manney, M. R. Gunson and R. Zander, Correlations of stratospheric abundances of NO_y, O_3, N_2O, and CH_4 derived from ATMOS measurments, *J Geophys. Res.*, 103, 28347-28359, 1998

Miller, D. E., J. L. Brownscombe, G. P. Carruthers, D. R. Pick and K. H. Stewart, Operational temperature sounding of the stratosphere, *Philos. Trans. R. Soc. London. Ser. A*, 296, 65-71, 1980.

Mitev, V., Lidar measurements of the atmospheric temperature by rotational Raman scattering, *Acta Physica Polonica*, 66, 311-322, 1984.

Mlynczak, M. ,Nonlocal thermodynamic equilibrium processes in ozone: Implications for the energy budget of the mesosphere and lower thermosphere, *J. Geophys. Res.*, 96(D9), 17217-17228, 1991

Mlynczak, M. G., and S. Solomon, A detailed evaluation of the heating efficiency in the middle atmosphere, *J. Geophys Res.*, 98(D6), 10,51710,541, 1993.

Mohankumar, K., Temperature variabilıty over the tropical middle atmosphere, *Ann. Geophys.*, 12, 448- 496, 1994

Mohankumar, K., Solar actıvıty forcing of the middle atmosphere, *Ann. Geophys.*, 13, 879-885, 1995.

Nagpal, O P, Dynamical processes ın the tropical middle atmosphere, *Ind. J Rad. and Sapce. Phy.*, 17, pp 232–251, 1988.

Naja, M. and Lal, S. Changes m surface ozone amount and its diurnal and seasonal patterns from 1954–55 to 1991 93 measured at Ahmedabad (23N), India., *Geophys. Res. Let.*, Vol. 23, p.81, 1996.

Namboothiri, S. P., T. Tsuda, M. Tsutsumi, T. Nakamura, C. Nagasawa, and M. Abo, Simultaneous observatıons of mesospherıc gravity waves with the MU radar and a sodium lıdar, *J. Geophys Res.*, 101, 40574063, 1996.

Namboothiri, S. P., N. Sugimoto, H. Nakane, I. Matsuı, and Y. Murayama, Rayleigh lidar observations of temperature over Tsukuba, winter thermal structure and comparıson studies, *Earth Planets Space*, 51, 825832, 1999

Nash, J. D., and J. N. Moum, Rıver plumes as a source of large–amplitude ınternal waves in the coastal ocean, *Nature*, 437, 400–403, 2005.

Nee, J B. et al., Middle atmospheric temperature structure over two tropıcal locations, Chung–Li (25°N, 121°E) and Gadanki(13.5°N,79.2°E), *J. Atoms. Solar Terrestrial Phys*, 64, 1311–1319, 2002.

ONeill, A., Stratospheric Sudden Warmıngs, *Encyclopedia of Atmospherıc Scıences*, 134220 1353, 2003.

Osprey S., et al., Sudden stratospherıc warmings seen in MINOS deep underground muon data, *Geophys. Res Lett.*, 36, L05809, doi·10.1029/2008GL036359, 2009

Pancheva, D , et al., Planetary waves in couplıng the stratosphere and mesosphere during the major stratospheric warmıng ın 2003/2004, *J. Geophys. Res.*, 113, D12105, doi:10.1029/2007JD009011, 2008.

Parameswaran, K., et al., Altıtude profiles of temperature from 4 –80 km over the tropics from MST radar and lıdar, *J. Atmos. Sol. Terr. Phys*, 62, 1327–1337, 2000.

Patra, P. K., S. Lal, S. Venkataramanı, and D. Chand, Halogen Occultation Experıment (HALOE) and balloon–borne in sıtu measurements of methane in stratosphere and theır relation to the quasi–biennial oscillation (QBO), *Atmos. Chem Phys.*, vol. 3, 1051–1062, 2003

Patra, P.K., Lal, S , Sheel, V , Subbaraya, B.H., C. Bruehl, R. B. Borchers, and Fabıan, P., Chlorine partitioning in the stratosphere based on in–sıtu measurements *Tellus*, Vol. 52B, p 934–946, 2000.

Pawson, S., R. S. Stolarski, A. R. Douglass, P. A. Newman, J. E. Nıelsen, S. M. Frıth, and M. L. Gupta, Goddard Earth Observing System chemistry–climate model sımulatıons of stratospherıc ozone–temperature couplıng between 1950 and 2005, *J. Geophys. Res.*, 113, D12103, doı·10.1029/2007JD009511, 2008.

Pettifer, R.E.W., Signal ınduced noıse ın lidar experiments, *J. Atmos Terr Phys* , 37, 669–673, 1975.

Pitarı, G., et al., Ozone response to the CO_2: Result from a stratospheric circulation model with heterogenous chemıstry, *J. Geophys. Res.*, 97, 5953–5962, 1992

Polvanı, L. M., and D. W. Waugh, Upward wave actıvıty flux as precursor to extreme stratospheric events and subsequent anomalous surface weather regımes *J. Climate*, 17, 35483554, 2004

Raghavarao, R, R Suhasini, R. Srıdharan, B V Krıshnamurthy and O P Nagpal, Vertical structure and characteristics of 23–60 day (zonal) oscillation over the tropical latitudes during the wınter months of 1986– Results of equatorıal wave campaign–II, *Proc. Ind Acad Scı (Earth Planet. Sci.)*, vol 99, no. 3, pp 413–423, 1990.

Ramaswamy, V, M. L. Chanin, J. A. ngell, J. Barnett, D. Gaffen, M. Gelman, P Keckhut, Y. Koshelkov, K. Labitzke, J. J. R. Lin, A. O'Neıll, J. Nash, W. Randel, R. Rood, K. Shine, M Shiotani, and R. Swınbank, Stratospheric temperature trends: Observatıon and model sımulations, *Rev of Geophys*, 39, 71– 122, 2001.

Ramaswamy, V., M. Schwarzkopf, W. J. Randel, B D. Santer, B. J. Soden, and G. L. Stenchikov , Anthropogenic and natural influences in the evolution of lower stratospheric cooling, *Science*, 311, 11381141, Science, 2006.

Randel, W. J. and B A Boville, Observations of Major Stratospheric Warming during December 1964, *J. Atmos. Sci.*, 44, 21792186, 1987.

Randel, W. J., Wu F., Russell J.M., Waters J.W., Froidevaux L., Ozone and temperature–changes in the stratosphere following the eruption of Mount–Pinatubo, *J. Geophys. Res* , 100, 16753–16764, 1995.

Randel, W., Udelhofen, P., Fleming, E., Geller, M., Gelman, M., Hamilton, K., Karoly, D , Ortland, D., Pawson, S., Swinbank, R., Wu, F., Baldwin, M., Chanin, M. L., Keckhut, P., Labitzke, K., Remsberg, E., Simmons, A., and Wu, D., The SPARC intercomparison of middle atmospheric climatologies, *J. Clim.* 17, 986–1003, 2004

Randel, W. J., and F. Wu, A stratospheric ozone profile data set for 1979–2005: Variability, trends, and comparisons with column ozone data, *J. Geophys. Res.*, 112, D06313, doi:10.1029/2006JD007339, 2007

Randel, W., et al., An update of observed stratospheric temperature trends, *J. Geophys. Res.*, 114, D02107, doi:10.1029/2008JD010421, 2009

Rawcliff, R. D. et al., *J. Geophys. Res.* 68, 6425, 1963.

Rayleigh, Lord, On the Electromagnetic Theory of Light, *Phil. Mag.*, 12, 81, 1881.

Rayleigh, Lord, On the Light from the Sky, Its Polarization and Colour, *Phil. Mag* , 41, 107274, 1871.

Reber, C. A., C. E. Trevathan, R. J. McNeal, and M. R. Luther, The Upper Atmosphere Research Satellite (UARS) Mission,*J. Geophys. Res.* 98, D6, 10643–10647, 1993.

Remsberg, E. E., et al., An Assessment of the Quality of HALOE Temperature Profiles in the Mesosphere with Rayleigh Backscatter Lidar and Inflatable Falling Sphere Measurements,*J. Geophys. Res.*, 107(D19), 10.129/2001jD001521, 2002.

Revathy, K., S.R. Prabhakaran Nair, and B.V. Krishna Murthy, Deduction of temperature profile from MST radar observations of vertical wind, *Geo. Phys. Res.*, 23, 295–288, 1996

Roble R . G., and Dickinson R E., How will changes in carbondioxide and methane modify the mean structure of the mesosphere and thermosphere, *Geophys. Res Lett.*, 16, 1441–1444, 1989.

Robock A, Stratospheric control of climate, *Science*, 272, 972–73, 1996.

Russell, J. M., et al , The Halogen Occulation Experiment, *J. Geophys Res* , 98, 10 77710 979, 1993.

Sahu, L. K. and S. Lal, Changes in the levels of surface ozone due to convective downdrafts over the Bay of Bengal, *Geophys Res. Let* , 33, doi·10.1029/2006GL025994, 2006

Sası, M N and K. Sengupta, A model equatorıal atmosphere over the Indıan zone from 0 to 80 km, Scientific report ISRO–VSSC–SR–19, 1979.

Sası, M N., and K. Sen Gupta, A reference atmosphere for Indian equatorıal zone from surface to 80 km – 1985, SPL : SR : 006:85, Space Physics Laboratory, Vikram Sarabai Space Centre, Trivandrum, India, 1986.

Sası, M.N , A reference atmosphere for the Indian equatorial zone, *Indian J. Radıo and Space Phys.*, 23, 299–312, 1994

Schmıdlin, F. J., Temperature ınversıon near 75 km, *Geophys Res. Lett.*, 3, 173–176, 1976.

Schmidlin F. J., Repeatabılty and measurement uncertainty of United States meteorological rocketsonde, *J. Geophys. Res.*, 86, 9599–9603, 1981.

Schoch, A., G. Baumgarten, and J. Fıedler, Polar middle atmosphere temperature clımatology from Rayleigh lidar measurements at ALOMAR (69°N), *Ann. Geophys.*, 26, 1681–1698, 2008

Schoeberl, M. R., Stratospherıc warmıngs· observatıons and theory, *Rev. Geophys. Space Phys.*, 16, 521–538, 1978.

Schotland, R. M., Some observation of the vertıcal profile of water vapour by a laser optical radar, *Proc. 4th Symp. on Remote Sensing of the Env. 12-14 Aprıl 1966*, Unıversity of Michıgan, Ann Arbour, 273–283, 1966.

Scinocca J F , Haynes P. H., Dynamical forcing of planetary waves by troposphenc baroclinic eddies, *J Atmos Sci* 55, 2361–92, 1998.

Scorer, R. S., Theory of waves in lee of mountains, *Quart. J. Roy. Meteorol. Soc.*, 75, 4156., 1949.

Seıdel, D. J , et al., Uncertainty in signals of large–scale climate variations ın radıosonde and satellite upper–air temperature data sets,*J. Clim.*, 17, 2225–2240, 2004.

Shardanand and A.D. Prasad Rao, Absolute Rayleigh scattering cross–sectıons of gases and freons of stratospheric interest in the visible and ultraviolet regions, *NASA TN 0–8442*, 1977.

Sharma, Som, V. Sivakumar, H. Chandra and P. B. Rao, A Comprehensive study on middle atmospherıc thermal structure over a Low and near Mid–Latitude Stations, *Advances Space Res.*, Vol. 37, pp 2278–2283, 2006.

She, C. Y., J. Sherman, T. Yuan, B. P. Williams, K. Arnold, T. D. Kawahara, T. Li, L. F. Xu, J. D. Vance, P. Acott, and D. A. Krueger, The first 80–hour continous lıdar campaign for simultaneous observation of mesopause regıon temperature and wınd, em Geophys. Res Lett , 108, 1319, doi:10.1029/2002GL016412, 2003

Shepherd, T G , Large–scale atmospheric dynamics for atmospheric chemists, *Chemıstry Revıews*, 103, 4509–4531, 2003.

Shine, K. P., A comparison of model simulated trend in stratospheric temperature, *Q J R. Meteorol Soc* , 129, 1569– 1588, 2003.

Sıca, R. J , Thayaparan, T., Argall, P. S., Russell, A. T., and Hockıng, W. K , Modulatıon of upper mesospheric temperature inversıons due to tidal–gravıty wave interactıons, *J. Atmos. Sol. Terr Phys* , 64, 915–922, 2002

Sıca, R. J., P. S Argall, T. G.Shepherd, and Koshyk, J. N., Model–measurement comparison of mesospheric temperature ınversions, and a simple theory for theır occurrence,*Geophys. Res Lett* , 34, L23806, doı·10 1029/2007GL030627, 2007.

Sıca, R. J. et al, Valıdatıon of the Atmospheric Chemistry Experiment (ACE) Versıon 2.2 Temperature Usıng Ground–based and Space–borne Measurements, *Atmospherıc Chemıstry and Physics*, 8, 35–62, 2008.

Sıgmond, M , J. F. Scinocca, and P. J Kushner, Impact of the stratosphere on tropospheric climate change,*Geophys. Res. Lett.*, 35, L12706, doi.10.1029 / 2008GL033573, 2008.

Singh, U. N., P. Keckhut, T. J. McGee, M. R. Gross, A. Hauchecorne, E F. Fıshbeın, J. W. Waters, J. C. Gılle, A. E. Roche, and J M. Russell III, Stratospheric temperature measurements by two collocated NDSC lidars at OHP during UARS validation campaign, *J. Geophys. Res.*, 101, 10,287– 10,298,1996 special issue on UARS Data Validation.

Sinha, H. S. S , Plasma. density irregularities in the equatorial D–region produced by neutral turbulence *J. Atmos. Sol Terr. Phys* , 54, 49–61, 1992

Sivakumar, V., Y. Bhavani Kumar, K. Raghunath, P. B. Rao, M Krishnaiah, K. Mizutani, T. Aoki, M. Yasui, and T. Itabe, Lidar measurements of mesospheric temperature inversion at a low latitude *Ann. Geophys* , 19, 1039–1044, 2001

Sivakumar, V., P. B. Rao, and M. Krishnaiah, Lidar measurements of stratosphere–mesosphere thermal structure at a low latitude: Comparison with satellite data and models, *J. Geophys. Res.*, 108(D11), 4342, doi:10 1029/2002JD003029, 2003.

Sivakumar, V., B. Morell, H. Bencherif, J. L. Baray, S. Baldy, A. Hauchecorne, and P.B. Rao, Atmos. Rayleigh lidar observation of a warm stratopause over a tropical site, Gadanki (13.5° N; 79.2° E), *Atmos Chem. Phys.*, 4, 1989–1996, 2004.

Sivakumar, V., P.B. Rao and H. Bencherif, Lidar observations of middle atmospheric gravity wave activity over a low–latitude site (13.5°N; 79.2°E), *Ann. Geophys* , 24, 112, 2006

Sridharan, S., S. Sathishkumar, and S. Gurubaran, Influence of gravity waves and tides on mesospheric temperature inversion layers: simultaneous Rayleigh lidar and MF radar observations,*Ann. Geophys.*, 26, 3731–3739, 2008

Sridharan, S., S. Sathishkumar, and K Raghunath1, Rayleigh lidar observations of enhanced stratopause temperature over Gadanki (13.5 N, 79.2 E) during major stratospheric warming in 2006, *Ann. Geophys* , 27, 373–379, 2009.

Steinbrecht, W.; Hassler, B ; Claude, H.; Winkler, P.; Stolarski, R.S.: Global distribution of total ozone and Lower stratospheric temperature variations, *Atmospheric Chemistry and Physics*, 3, 1421, 2003.

Stratton, J.A., Electromagnetic Theory, McGraw–Hill, New York, U.S.A., 1941.

Subbaraya, B.H and S. Lal, The structure of the equatorial mesosphere at Thumba, *Pure Appl. Geophys.*, Vol. 118, p 581, 1980.

Subbaraya, B.H. and S. Lal, Rocket measurements of ozone concentrations in the stratosphere and mesosphere over Thumba, *Proc. Indian Acad. Sci. (Earth and Planet. Sci),* Vol. 90, p.173, 1981.

Synge, E.H., A method of investigating the higher atmosphere, *Phil. Mag.*, 9, 1014–1020, 1930.

Thomas, L. and S.K. Battacharyya, in *Proc 5th Rocket and Balloon Programs and Related Research*, ESA SP–152, 49–50, 1980.

Thomas, L., D.P. Wareing and D.B. Jenkins, Observation of a thin layer of material in the upper stratosphere, *Nature*, London, 312, 627–628, 1984.

Thomas, L., Laser radar observations of middle atmosphere structure and composition, *Phil. Trans. R. Soc. London*, 597–609, 1987.

Thomas L., A K P Marsh,, D P Wareing,, I Astin, and H. Chandra, VHF echoes from the midlatitude mesosphere and thermal structure observed by lidar, *J. Geophys Res.*, 101, 12867–12877, 1996.

Ting, M., M. P. Hoerling, T. Xu, and A. Kumar, Northern Hemisphere teleconnection patterns during extreme phases of the zonal–mean circulation,*J Clim.*, 9, 2615–2633, 1996.

Uppala, S. M., et al., The ERA–40 reanalysis, *Q. J. R. Meteorol. Soc* , 131, 2961–3012, 2005.

Venkateswaran, S., J. Moore, and A. Krueger, Determination of the Vertical Distribution of Ozone by Satellite Photometry, *J. Geophys. Res* , 66(6), 1751–1771, 1961

Vincent, R.A., Gravity wave motions in the mesosphere, *J. Atmos. Terr Phys* , 46, 119–128, 1984.

Vincent, R.A , and D.C. Fritts, A morphology of gravity waves in the mesosphere and lower thermosphere over Adelaide, Australia, *J. Atmos. Sci.*, 44, 748–760, 1987

Vincent, R.A., Gravity waves in the southern hemisphere middle atmosphere. a review of theory and observations, in Dynamics, transport and photochemistry in the middle atmosphere of the southern hemisphere, A O'Neill, (ed), Kluwer Academic Publishers, 159–170, 1990.

Vincent, R. A., and D. Lesicar, Dynamics of the equatorial mesosphere: First results with a new generation partial reflection radar, *Geophys. Res. Lett*, 18, 825– 828, doi.10.1029/91GL00768, 1991

Volland, H., Atmospheric Tidal and Planetary Waves, *Kluwer Academic Publishers*, Boston, MA., 1988.

Walterschied, R. A., Sivjee, G. G, and Roble, R. G.: Mesospheric and lower thermosphere manifestations of a stratospheric warming event over Eureka, Canada (80° N), *Geophys. Res. Lett.*, 27, 2897–2900, 2000.

Wang, P.–H., M. P. McCormick, W P. Chu, J Lenoble, R. M. Nagatani, M.–L. Chanin, R. A. Barnes, F. Schmidlin, and M Rowland, SAGE II stratospheric density and temperature retrieval experiment,*J. Geophys, Res.*, 97, 843– 863, 1992.

Wayne Richard P, Chemistry of Atmosphere, third edition, Oxford university press, 2000.

Whiteman, D. N., S. H. Melfi, and R. A. Ferrare, Raman lidar system for the measurement of water vapor and aerosols in the Earth's atmosphere, *Appl Opt.*, 31, 3068– 3082, 1992.

Whiteman and S. H. Melfi, Cloud liquid water, mean droplet radius, and number density measurements using a Raman lidar, *J. Geophys. Res.*, 104, 31411–31419, 1999.

Whiteway, J. A. and A. I. Carswell, Rayleigh lidar observations of thermal structure and gravity wave activity in the high arctic during a stratospheric warming, *J. Atmos. Sci.*, 51, 3122–3136, 1994.

Whiteway, J., A I Carlswell and W E Ward, Mesospheric temperature inversions with overlying nearly adiabatic lapse rate: An indication of well mixed turbulent layer, *Geophys. Res Lett.*, 22, 1201–1204, 1995.

Whiteway, J A., T. J.Duck, D P. Donovan, J, C Bird, S. R. Pal, and A. I. Carswell, Measurements of gravity wave activity within and around the Arctic stratospheric vortex, *Geophys Res. Lett.*, 24, 1387–1390, 1997

Wickwar, V.B., K.C. Beissner, T.D. Wilkerson, S.C. Collins, J.M Maloney, J.W. Meriwether, Jr., and X. Gao, Climatology of mesospheric temperature profiles observed with the Consortium Rayleigh–scatter lidar at Logan, Utah,* in Advances in Atmospheric

Remote Sensing with Lidar, edited by A. Ansmann, R. Neuber, P. Rairoux, and U. Wandinger, pp. 557–560, Springer Verlag, Berlin, 1997.

Wiegand, R. C., and E. C. Carmack, The climatology of internal waves in a deep temperate lake, *J Geophys. Res.*, 91, 3951–3958, 1986

Wild, J.D , et al., Comparison of stratospheric temperature from several lidars, using NMC and MLS data as transfer reference, *J Geophys. Res.* 100, 11,105-11,111, 1995.

Wilson, R., A. Hauchecorne, and M L Chanin, Gravity wave spectra in the middle atmosphere as observed by Rayleigh lidar, *Geophys. Res. Lett.*, 17, 1585–1588, 1990

Wilson, R., M.L. Chanin and A. Hauchecorne, Gravity waves in the middle atmosphere as observed by Rayleigh lidar I: case studies, *J. Geophys. Res.*, 96, 5153–5167, 1991a.

Wilson, R., M.L. Chanin, and A. Hauchecorne, Gravity waves in the middle atmosphere as observed by Rayleigh lidar II· climatology, *J. Geophys Res.*, 96, 5169–5183, 1991b.

Woodman, R. F. and A Guillen, Radar observations of winds and turbulence in stratosphere and mesosphere, *J Atmos. Sci* 31, 493–505, 1974.

Wright, J. B., Stratospheric circulation, Ed by Webb W. L., *Academic Press*, p 115, 1969.

Zeng, G, and J . A. Pyle, Changes in tropospheric ozone between 2000 and 2100 modelled in a chemistry–climate model,*Geophys. Res. Lett.*, 30, no 1392, 2003

Zink, F., and R. A Vincent, Some inferences on turbulence generation by gravity waves, *J Geophys. Res.*, 109 (D11), D11109, doi·10.1029/2003JD003992, 2004.

List of Publications

Publications in Peer Reviewed Journals

1. Acharya, Y. B. **Som Sharma** and H. Chandra, "Effect of Signal Induced Noise from PMT in Lidar Systems", Measurements, Vol. 35, p 269-276, 2004.

2. **Sharma, Som** and H. S. S. Sinha "Atmospheric Soundings from Mt. Abu" Bull. Astro. Soc. of India, Vol. 33, pp 259-264, 2005.

3. Chandra, H. **Som Sharma**, Y. B. Acharya and A. Jayaraman "Rayleigh Lidar Studies of Thermal Structure over Mt. Abu" JIGU, Vol. 9, pp 279-298, 2005.

4. **Sharma, Som**, V. Sivakumar, H. Chandra and P. B. Rao, "A Comprehensive study on middle atmospheric thermal structure over a Low and near Mid-Latitude Stations", Advances Space Res., Vol. 37, pp 2278-2283, 2006.

5. Sivakumar V., Benchrif H., Fudilhe D., Hauchecorne A., Rao D. N., **Som Sharma**, Chandra H., Jayaraman A. and Rao P. B., "Rayleigh Lidar observations of double stratopause structure over three different northern hemisphere stations",Atmos. chem. phys. Discuss., Vol. 6, P 6933-6956, 2006.

6. Das, Uma, H. S. S. Sinha, **Som Sharma**, H. Chandra and Sanat K. Das, "Fine Structure of the Low Latitude Mesospheric Turbulence", doi:10.1029/2008JD011307, J. Geophys. Res. (in press).

7. **Sharma, Som** , S. Lal, Y. B. Acharya and H. Chandra, "MTI over a sub-tropical location using lidar and satellite observation" Annals Geophys. (communicated).

8. **Sharma, Som**, S. Lal, Y. B. Acharya and H. Chandra "Stratospheric-mesospheric thermal structure and long term temperature trends over a sub-tropical station Mt. Abu (24.5°N, 72.7°E)." (in preparation).

9. **Sharma, Som**, S. Lal, Y. B. Acharya and H. Chandra, "Rayleigh Lidar observed stratospheric sudden warming over Mt. Abu: An evidence of interaction between planetary wave and stratospheric circulation (in preparation).

Publications in Conference Proceedings

1. H. Chandra, **Som Sharma**, Y. B. Acharya and A. Jayaraman, Rayleigh Lidar studies of Temperature structure over Mt. Abu, Proc. of Dynamics Coupling in Equatorial Atmosphere Ionosphere System (DYCEAIS-2002), ISRO-HQ-SR-51-2003, pp 31-35, 2003.

2. **Sharma, Som**, S. Lal, A. Jayaraman, Y. B. Acharya and H. Chandra, Rayleigh Lidar study of middle atmospheric thermal structure over a high altitude sub-tropical station (Mt. Abu, 24.5°N, 72.7°E), Proceedings of Reunion Island International Symposium (RIIS-2007), November 2007, Reunion, France (under printing).

Papers Presented in Conferences/Symposia and Workshops

1. Chnadra, H. **Som Sharma**, A. Jayarman and Y. B. Acharya, "Rayleigh Lidar Study of over Mt. Abu, NSSS, February 2004, Kotayam, India.

2. **Sharma, Som**, H. Chandra and A. Jayaraman and Y. B. Acharya, "A Comprehensive study on middle atmospheric thermal structure over a sub-tropical station" IAGA/ICMA workshop, August 2004, Bath, U.K.

3. **Sharma, Som**, A. Jayaraman, Y. B. Acharya and H. Chandra, D. Narayana Rao and Y. Bhavani Kumar, Simultaneous study of middle atmospheric thermal structure using Rayleigh Lidar observations at Mt. Abu and at Gadanki,

Eleventh International Workshop on Technical and Scientific Aspects of MST Radar (MST-11) December 10-15, 2006, Gadanki/Tirupati, India.

4. **Sharma, Som**, V. Sivakumar, H. Chandra and P. B. Rao, A Comprehensive study on middle atmospheric thermal structure over a Low and near Mid-Latitude Stations, 35^{th} Scientific Assembly of COSPAR, 18-25 July 2004, Paris, France.

5. Sivkumar V., H. Bencherif, D.V. Charaulu, P. B. Rao, A. Hauchecorne, D. N. Rao, **Som Sharma**, H. Chandra, A. Jayaraman, Rayleigh lidar investigation of sudden stratospheric warming observed over NH and SH stations, Western Pacific Geophysics Meeting (WPGM), 24-27 July, 2006, Beijing, China (Invited paper).

6. **Sharma, Som**, A. Jayaraman, Y. B. Acharya and H. Chandra, D. Narayana Rao, Y. Bhavanikumar, V. Sivakumar, "Lidar Investigation of Differences in Middle Atmospheric Thermal Structure between Tropical and Sub-tropical Sites" Remote sensing of the atmosphere and clouds (SPIE), 13-16 November, 2006, Goa, India.

7. **Sharma, Som**, S. Lal, A. Jayaraman, Y. B. Acharya and H. Chandra "Rayleigh Lidar study of middle atmospheric thermal structure over a high altitude sub-tropical station (Mt. Abu, 24.5°N, 72.7°E)", RIIS-2007, 5-9 November 2007, Reunion, France.

8. **Sharma, Som**, A. Jayaraman, S. L al, Y. B. Acharya and H. Chandra, "Study of Middle Atmospheric Thermal Structure Over a Sub-tropical Station, Mount Abu" ACLINT-2007, November 2007, Ahmedabad, India.

9. **Sharma, Som**, S. Lal, A. Jayaraman, Y. B. Acharya and H. Chandra, "Lidar study of Stratospheric Sudden Warming (SSW) over Mt. Abu" National Space Science Symposium (NSSS-2008), 26-29 February 2008, Ooty, India.

10. **Sharma, Som**, S. Lal, Y. B. Acharya and H. Chandra "Lidar study of stratospheric thermal structure and long term trends over a sub-tropical station

Mount Abu (24.5°N, 72.7°E)" 4^{th} SPARC GA, August-September 2008, Bologna, Italy.

11. **Sharma, Som,** S. Lal, Y. B. Acharya and H. Chandra, "Rayleigh Lidar observed Stratospheric Sudden Warming (SSW) over Mt. Abu: An evidence of interaction between planetary wave and stratospheric circulation" 4^{th} SPARC GA, August-September 2008, Bologna, Italy.

12. **Sharma, Som** "Imprint of Greenhouse cooling in Lidar observed stratospheric thermal structure over a sub-tropical station Mount Abu (24.5°N, 72.7°E, MSL height 1.7 Km), at University of Bresia, September 2008, Bresia, Italy. (Invited)